UNIVERSITY OF OKLAHOMA

GRADUATE COLLEGE

TRANSLATION AND DEVELOPMENT OF NOVEL ANNEXIN A5 – PROTEIN DRUG CONJUGATES FOR THE TREATMENT OF TRIPLE-NEGATIVE BREAST CANCER

A DISSERTATION

SUMBITTED TO THE GRADUATE FACULTY

in partial fulfillment of the requirements for the

Degree of

DOCTOR OF PHILOSOPHY

By

ALEXIS WOODWARD

Norman, Oklahoma

2022

TRANSLATION AND DEVELOPMENT OF NOVEL ANNEXIN A5 – PROTEIN DRUG CONJUGATES FOR THE TREATMENT OF TRIPLE-NEGATIVE BREAST CANCER

A DISSERTATION APPROVED FOR THE

STEPHENSON SCHOOL OF BIOMEDICAL ENGINEERING

BY THE COMMITTEE CONSISTING OF

Dr. Roger Harrison, Chair

Dr. Wei Chen

Dr. Edgar O'Rear

Dr. Vassilios Sikavitsas

Dr. Barbra Safiejk-Mroczka

Acknowledgments

As a I compete the chapters in this book, I realize this chapter of my life could not have been possible without the support of many people. First and foremost, I would like to thank my committee members, Dr. Roger Harrison, Dr. Wei Chen, Dr. Edgar O'Rear, Dr. Vassilios Sikavitsas, and Dr. Barbra Safiejk-Mroczka for their constant support and guidance throughout my course work and projects. I would like to especially thank Dr. Harrison for your mentorship, patience, and sharing your desire to create new medicines to help individuals suffering from cancer and infectious diseases. Your commitment to science and developing the next generation of scientist is truly inspiring.

I would like to thank Gabriela FN Faria. It has been an honor to watch you grow as a scientist, and I am lucky enough to call you a friend as well. I know you are going to go on to do great things, and I am excited to see where the future takes you. I could not ask for a better person to complete my Ph.D. alongside. To my lab mates, Dr. Patrick McKernan, Charles Bagarie, Benjamin Southard, Adam Aissanou, Clement Kach, and Parker Bryant, thank you for challenging me and aiding in my technical development in lab. I would also like to thank the office personnel of the CMBE department, Madena McGinnis, Terri Colliver, and Nicole Palmeter. Your work in the office made me graduate journey so much smoother and saved my sanity during this time. I would also like to thank you for the constant support and midday conversations that provided me a break from my studies.

This degree could not have been completed without my family. To my mom Suzette, thank you for being a constant support by being just a phone call away. Your selflessness, humor, and love are a large reason this degree has been made a reality. To my siblings, Kallie, Will, Mariah, Kevin and Shannon thank you for being a source of fun, optimism, and a weekend trip when

needed. To my dad Kevin and Susan, thank you for being constant cheerleaders, this degree would not be possible without you as well. To my friends in the biomedical engineering department and OU community thank you for your comradery. Especially Meredith Jones, David Nedrelow, Nathan Donahue, Michael “Rue” Felder, Sabrina Gardner, and Melissa Sadir thank you for being amazing friends, a source of support, and humor during this journey. To my friends from Nebraska, Maggie Blanchard, Abby Cleary, Devon Fox, Claire “Clondon” London, Ashton Parks, Rachel Pettid, Anna Whaley, Abby Jameson, Jessica Carter, Connor McManigal, and Grant Zebold, thank you for being lifelong friends and a source of constant support.

To the ladies of Tennis Time and all my tennis women’s and mixed doubles teams, thank you for welcoming me into the community with open arms and providing constant support during my journey. To Elizabeth Elliott and Beau Lanier thank you for your friendship, life advice, constant fun on and off the court. Finally, I want to thank Shane Rider, Winn Carroll, James Bland, and David San Martin for being the best trivia team on this side of the Mississippi. May Tequila Mockingbird’s reign never end.

Sources of Financial Support

We thank the Oklahoma Center of Advancement of Science and Technology (OCAST), The Jean Wheeler Sparks and Baxter Abbott Sparks Breast Cancer Research Fund at The University of Oklahoma Foundation, and the Universidad Nacional de San Agustín – Arequipa. Mass Analysis was completed in collaboration with the University of Texas-Medical Branch at Galveston. The Mass Spectrometry Facility is supported in part by Cancer Prevention Research Institute of Texas (CPRIT) grant number RP190682.

Graduate Student financial support was generously provided by the Stephenson School of Biomedical Engineering Department, the Douglas and Hilda Bourne Engineering Scholarship, OU Graduate Student Senate Travel and Conference grants, and the Robberson Travel and Research Grant. This research could not have been completed without the generous support of the funding agencies listed above.

Table of Contents

List of Figures

List of Tables

Abstract

Triple-negative breast cancer (TNBC) is the most aggressive breast cancer subset with limited targeted chemotherapies. TNBC is defined by the absence of the estrogen, progesterone, and HER2 hormonal receptors on the cell surface, and targeted hormonal-based therapies are ineffective. The current standard of care for these patients remains untargeted systemic chemotherapy that does not discriminate between healthy and cancerous tissue, resulting in severe dose limiting side effects. Identifying a novel biomarker for this disease remains a top priority in targeted cancer therapy.

Extracellular exposure of phosphatidylserine (PS) is tightly regulated in healthy cells. Typically confined to the inner cytosolic leaflet, once extracellularly exposed, it acts as an "eat me" signal for macrophage phagocytosis. However, cancer (especially TNBC) cells have high externalized PS, but do not undergo apoptosis, making PS a promising biomarker for TNBC therapy. Annexin A5 (ANXA5) is the native binding partner to PS and can be used to actively target and deliver chemotherapeutic agents to the tumor microenvironment via PS externalization.

While many advancements have been made in developing targeted chemotherapeutics, protein-drug conjugates have changed how cancer is treated. Protein-drug conjugates consist of a protein linked to a drug, and depending on the conjugation method, a linker that connects the protein and drug together. The protein acts as a delivery vehicle to localize a drug to cancer cells and vasculature through a cancer biomarker. By targeting and localizing the drug to the tumor, less drug is needed to induce cell death, resulting in fewer side effects.

This dissertation will focus on translating two ANXA5 protein drug conjugates and developing one ANXA5-protein drug conjugate for the treatment of TNBC. ANXA5 has proven to be an invaluable delivery vehicle with high specificity to externalized PS. A microtubule inhibitor, a DNA alkylating agent, and a histone deacetylase inhibitor have all been linked to

ANXA5, and all three ANXA5 drug conjugates have shown better anticancer activity than their respective free drug *in vitro*. ANXA5 protein drug conjugates provide a novel avenue to treat an untargeted cancer.

Chapter 1: Introduction

Biomarker cancer therapy

Cancer is one of the leading causes of death worldwide. By the year 2040, it is estimated that 28.4 million new cancer cases will be diagnosed worldwide, an increase of 47% compared to 2020 [1]. The standard of care for many patients includes conventional untargeted chemotherapy, radiation, and/or surgery. Conventional chemotherapeutic drugs are administered systemically, are nonselective, have rapid body clearance, and have a wide biodistribution [2, 3]. Consequently, high doses of chemotherapy are needed to achieve sufficient accumulation in the tumor. However, higher doses induce systemic toxicity and death of healthy tissues, which results in severe side effects, and a higher dose can induce drug resistance, generating a more aggressive phenotype [2, 3]. To increase therapeutic efficiency and decrease side effects, researchers have engineered drug delivery systems to passively or actively target tumors.

Passive and active targeting are two of the largest fields of drug delivery. Passive targeting exploits the enhanced permeability and retention (EPR) effect to deliver drugs and nanoparticles to tumors. However, the EPR effect is heavily debated and extremely heterogeneous among cancer types, leading to low drug uptake [3]. It is estimated that only 1% of passive targeted chemotherapies reach the tumor; however, the therapeutic efficiency increases by 10 times when using an active targeting method [4]. Active targeting relies on the overexpression of biomarkers in tumor cells and tumor vasculature as docking stations for monoclonal antibodies, proteins, and/or peptides to increase the accumulation and therapeutic effects of chemotherapies and nanotechnology. Although active targeting and engineered nanotechnology have increased the efficacy of drug delivery, protein corona formation changes the surface properties of nanoparticles

and can bury the targeting agent, leading to off-target unloading [5]. Additionally, the heterogeneity of biomarkers plays a confounding role in the fight against cancer.

Biomarkers can be used to diagnose cancers or select treatment options. More importantly, biomarkers can act as a magnet to actively target a cancer treatment to tumor cells and tumor vasculature. To date, the FDA has approved targeted treatments for 33 different cancers; however, each disease typically requires a unique biomarker, and there is a need for novel and translational biomarkers across cancer types [6-8]. A universal targeting strategy is a top priority in cancer therapy. Phosphatidylserine is an excellent translational biomarker candidate for all cancer types.

Phosphatidylserine (PS) is restricted to the inner leaflet of the plasma membrane in healthy cells; however, as cells become apoptotic, PS is flipped to the outer leaflet, promoting phagocytic removal [9]. Although PS is constantly exposed at elevated levels in cancer cells, they do not undergo apoptosis and the tumor survives. This increase in external PS makes it an attractive biomarker for targeted cancer treatment. The protein annexin A5 (ANXA5), which binds to PS, can be used to deliver targeted treatments to the primary tumor, tumor vasculature, and metastases.

Phosphatidylserine

The asymmetric phospholipid composition of plasma membranes is tightly regulated and provides insights into cellular health. In healthy cells, the outer leaflet is mainly composed of phosphatidylcholine and sphingomyelin, whereas the inner leaflet is composed of phosphatidylinositol, phosphatidylethanolamine, and phosphatidylserine (PS) [10]. While PS constitutes a small fraction of the membrane (3–10%), it is the only anionic phospholipid in the bilayer and plays a major role in regulating cell death and removal [9, 11]. Its negative charge

contributes to the regulation of many cellular functions both internally and externally, but this dissertation will focus on the extracellular expression of PS as a biomarker target.

The expression of PS in the cytosolic leaflet maintains cellular homeostasis. This asymmetry is maintained by two calcium-dependent transporters, flippase and scramblase (**Figure 1**) [12]. Flippase is an adenosine triphosphate (ATP)-dependent transporter that exclusively transports anionic phospholipids to the cytosolic membrane against their concentration gradient. Scramblase is ATP-independent and randomly moves phospholipids bidirectionally across the plasma membrane. Together, these transporters regulate PS expression (**Figure 1**). While the regulation of PS in healthy cells is widely accepted, PS regulation in cancer is not fully known.

The increased externalization of PS in many cancer types make it a potential biomarker for cancer therapy. Compared to healthy cells, tumor cells and tumor vasculature alter their total phospholipid concentration, have more PS in the plasma membrane, and have up to seven times more externalized PS [13-19]. PS is highly externalized in metastatic triple-negative breast cancer, glioblastoma, and astrocytoma, suggesting that high PS exposure on the outer leaflet is associated with aggressive and metastatic tumors [14]. Although upregulated PS externalization in cancer is widely accepted, the exact mechanism remains elusive [20]. It is suggested that Brac-1 germline mutations [21-23], intracellular calcium levels [14], intracellular and extracellular pH levels [24, 25], phosphorylation of PS transporters [26-30], and protein expression of the PS transporters [31] all impact externalization of PS on cancer cells. Additionally, PS aids in the metastatic potential of cancer cells [32-36] and induces an immunosuppressive tumor microenvironment mainly through macrophage interactions [37-41]. Because of these compounding factors, targeting PS with its native binding partner annexin A5 is an attractive option for targeted cancer therapy.

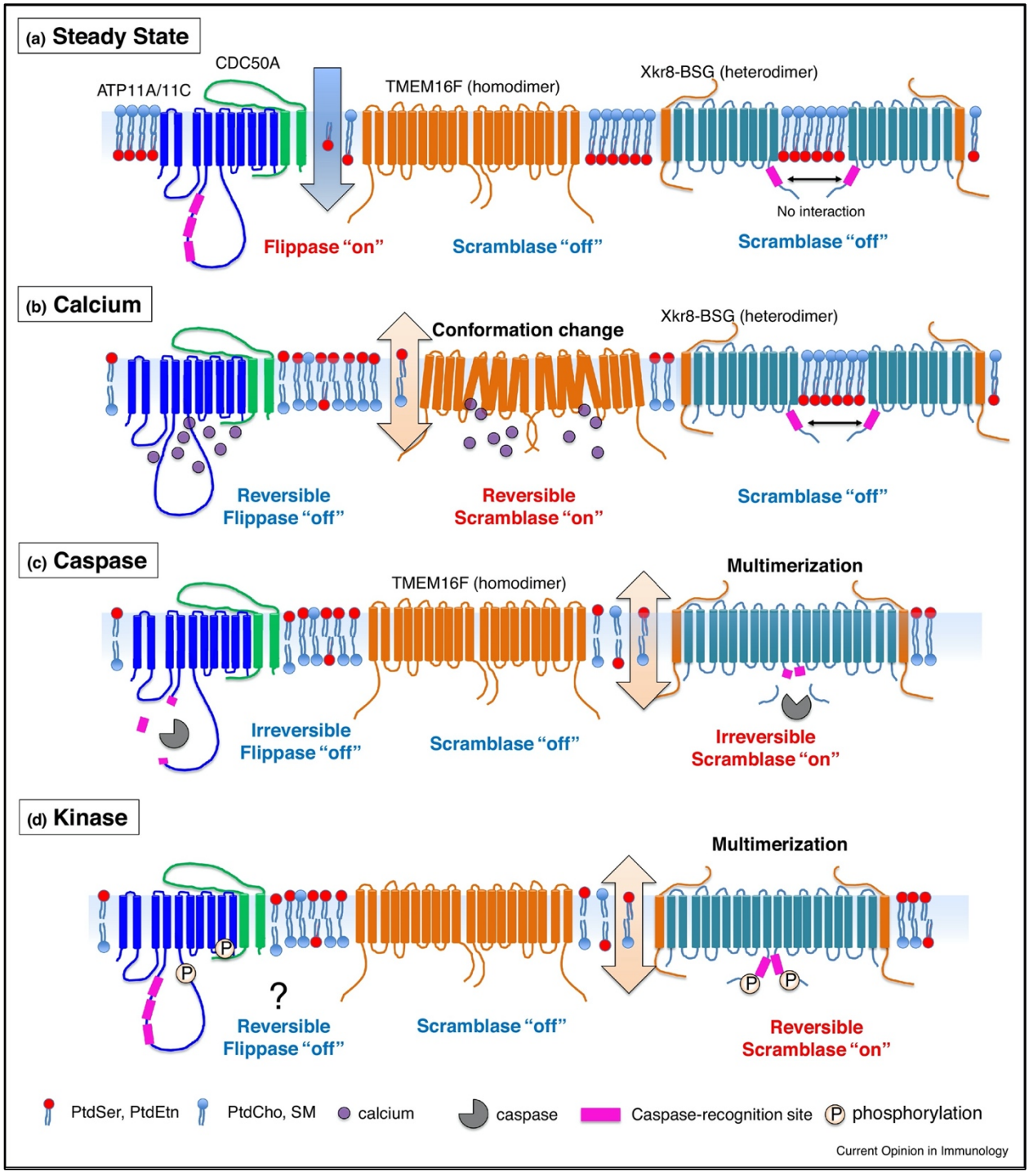

Figure 1: Flippase and scramblase activity based on cell state

a) At steady state, PS is sequestered to the inner leaflet. ATP11A/C is turned on, while TMEM16F and Xkr8 are turned off. b) During cellular stress, mitochondria release calcium into the cytosol. The calcium

then binds to ATP11A/C, turning it off and preventing PS from being returned to the inner leaflet. TMEM16F is turned on, randomly switching PS to the inner and outer leaflet. During this time, Xkr8 is off. c) If cellular stress persists, the mitochondria release caspases to activate apoptosis. Caspase cleaves the long cytosolic loops of ATP11ATP/C, irreversibly turning it off. Caspases also cleave Xkr8, resulting in constitutive activation and random expression of PS. During this time, TMEM16F is off. d) Phosphorylation reversibly turns on Xkr8, and potentially turns off ATP11A/C. Scramblase remains off during this time [12].

Annexin A5 (ANXA5)

The non-apoptotic externalization of PS in cancer cells can be targeted via ANXA5 to deliver chemotherapeutic agents to the tumor [42]. ANXA5 is a member of the annexin protein family and is the native binding partner to PS in the body. The annexin family is characterized by its ability to bind negatively charged phospholipids in the presence of calcium. Additionally, annexins must possess structurally conserved sequences of approximately 70 amino acid residues that comprise the annexin core domain [43, 44]. There are 12 ANXA genes in humans, all of which have 4 annexin core domains (except ANXA6, which has 8), in addition to the C-terminal and N-terminal domains. Each core domain consists of 5 alpha helices (A, B, C, D, and E) that contain binding sites for both calcium and negatively charged phospholipids. ANXA5 was the first member of the ANXA family to be crystallized and imaged, illustrating the bent-disk shape of the protein (**Figure 2**).

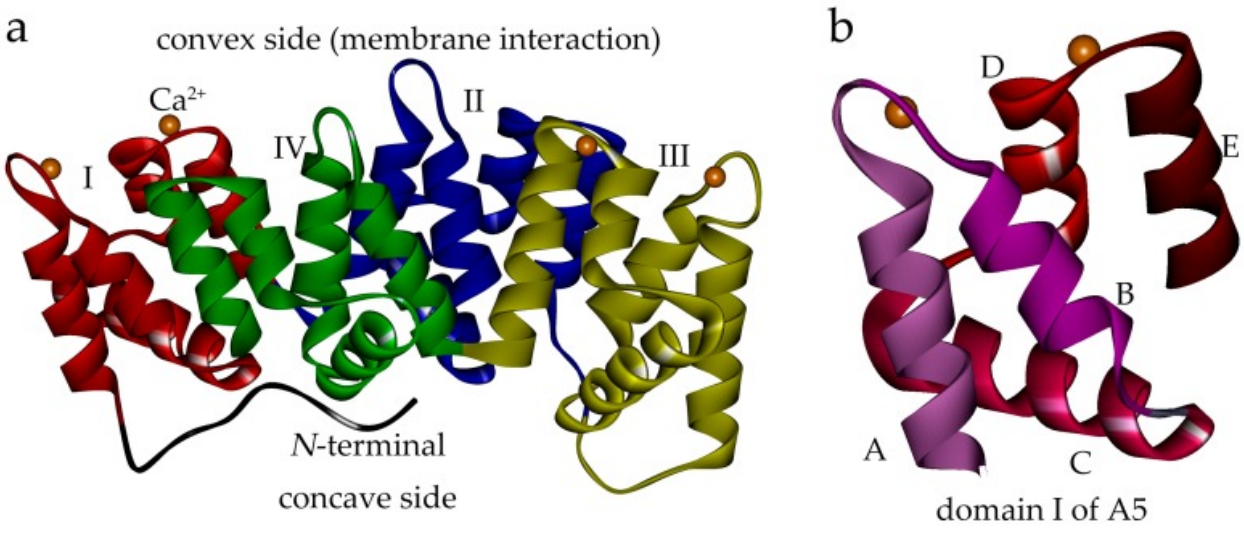

Figure 2: Ribbon structures of ANXA5 and repeated domains

a) The C-terminal domains consist of four structurally conserved domains (I: red, II: blue, III: yellow, IV: green). Calcium binding sites are indicated by orange balls. Membrane binding occurs on the convex side, and the protein does not undergo conformational changes after binding. The N-terminal domain is indicated in black. b) Domain I represents the repeated domains consisting of five alpha helices (A, B, C, D, and E) [45].

ANXA5 (~36 kDa) is an extracellular protein that reversibly binds PS. ANXA5 was first discovered as an anticoagulant protein and soon gained traction as a novel biomarker for apoptosis due to its high binding affinity for PS (dissociation constant K_d = 15 nM) in the presence of calcium [46]. The binding of ANXA5 to PS is regulated by calcium-binding sites on the protein, and domain IV is critical for both calcium and PS membrane binding [45]. Each ANXA5 core has three different calcium-binding sites between the AB loop (type II calcium binding), which is necessary for PS binding, whereas the DE loop and B site (type III calcium binding) increase the

binding affinity of the protein to the membrane [43]. Twelve molecules of calcium can be bound, and the specific binding orientation promotes ANXA5 trimerization while maintaining the membrane in the liquid-crystal phase [43, 47]. A unique feature of ANXA5 is that it does not undergo conformational changes and retains its concave-bent shape after binding and trimer formation, which assists in cell internalization [48]. The ANXA5 trimers self-assemble into an ordered 2D lattice, increasing the surface tension and concaving the plasma membrane inward (**Figure 3**) [49-51]. This indicates that internalization is non-receptor-mediated and solely driven by ANXA5 binding/trimerization, which is advantageous because internal cell signaling is not required for entry. Once internalized, the endosome containing ANXA5 fuses with a lysosome. and the protein is degraded. ANXA5 has a circulation half-life of 4 min but has high PS-mediated tumor uptake in mice [52]. Because the EPR effect is beneficial for molecules over 40 kDa, it is unlikely that the passive EPR effect is a major contributor to ANXA5 localization in the tumor; it is therefore likely that active targeting of PS drives ANXA5 tumor uptake [53].

Due to the high binding affinity and nonreceptor-mediated endocytosis of ANXA5, it is an attractive option to actively target the exposure of PS on tumor cells and tumor vasculature. To date, the use of ANXA5 to target and treat melanoma, lymphoma, neuroblastoma, and pancreatic, lung, breast, prostate, ovarian, colon, and non-small cell cancers has been investigated, demonstrating it as a useful delivery vehicle for many types of cancer therapy [54]. The work presented in this dissertation will focus on targeting triple-negative breast cancer.

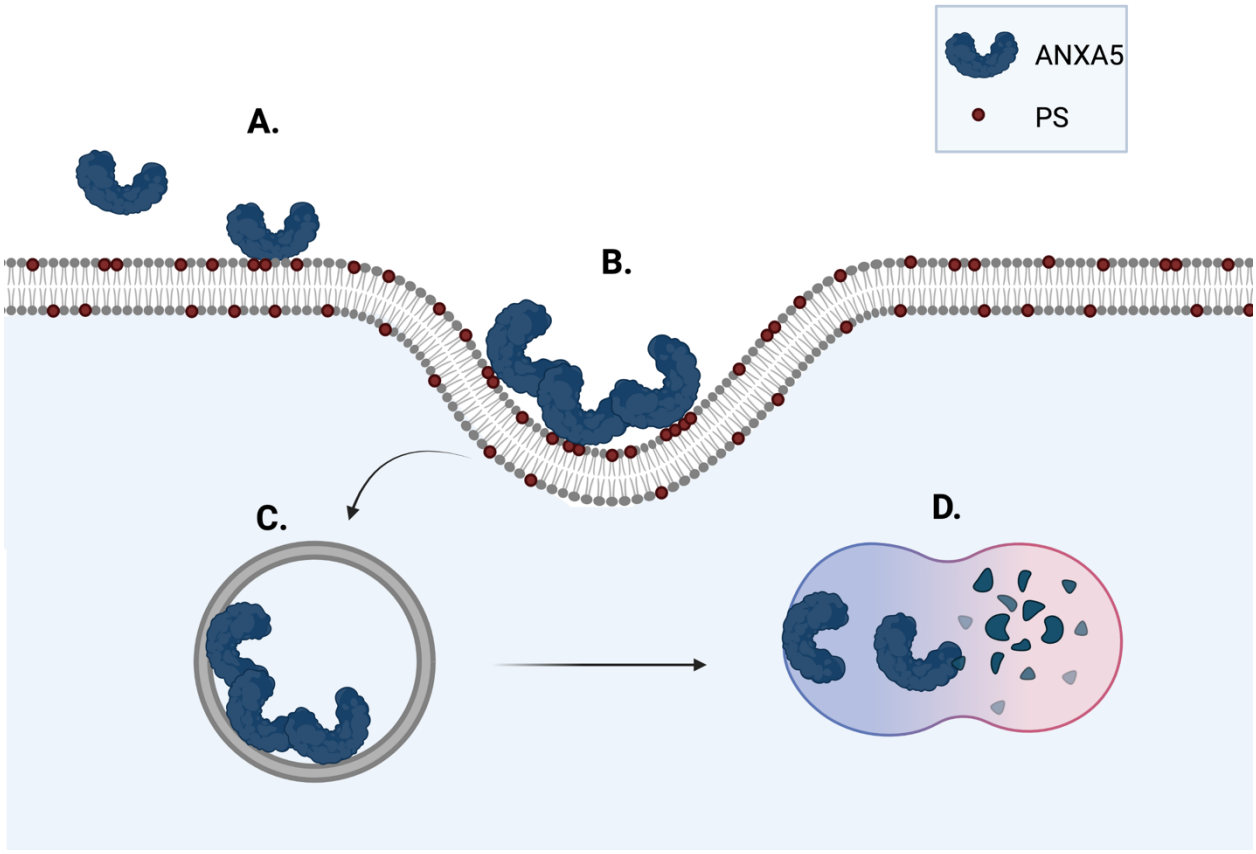

Figure 3: Internalization of ANXA5 into cells is nonreceptor-mediated

A) ANXA5 binds to upregulated and externalized PS in cancer cells. B) After binding, ANXA5 does not undergo conformational changes, which induces trimerization. Formation of the trimer increases the surface tension on the plasma membrane and concaves the membrane inward. C) An endosome containing the ANXA5 trimer is formed. D) The ANXA5 endosome fuses with a lysosome, and the protein is degraded. Figure created using Biorender.com.

Why triple negative breast cancer?

While PS is a translational biomarker across cancer types, this dissertation will focus on treating breast cancer, more specifically triple-negative breast cancer through ANXA5-PS mediated protein drug conjugates.

For women worldwide, breast cancer is the most diagnosed and deadly cancer type and does not discriminate against developed or developing countries (**Figure 4**) [55]. When focusing on the United States of America, breast cancer rates have been increasing at approximately 0.5% per year since the mid 2000s (**Figure 5**). In 2022 alone, nearly one-third of all cancer diagnoses in women will be a breast cancer diagnosis [6]. While breast cancer is widespread, it is heterogeneous and is defined by the hormonal receptor status on the cell surface.

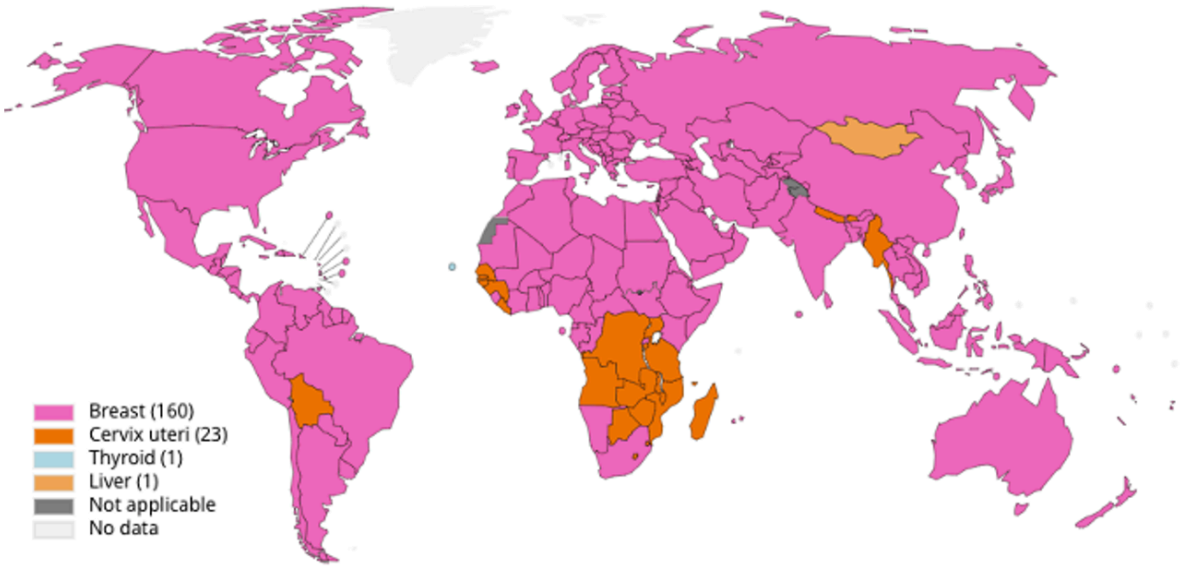

Figure 4: Breast cancer is the most common cancer site for females worldwide

[55] © CP. Wild, E. Weiderpass, BW Stewart. Creative Commons Attribution (CC BY) license (http:// https://creativecommons.org/licenses/by-nc-nd/3.0/igo/).

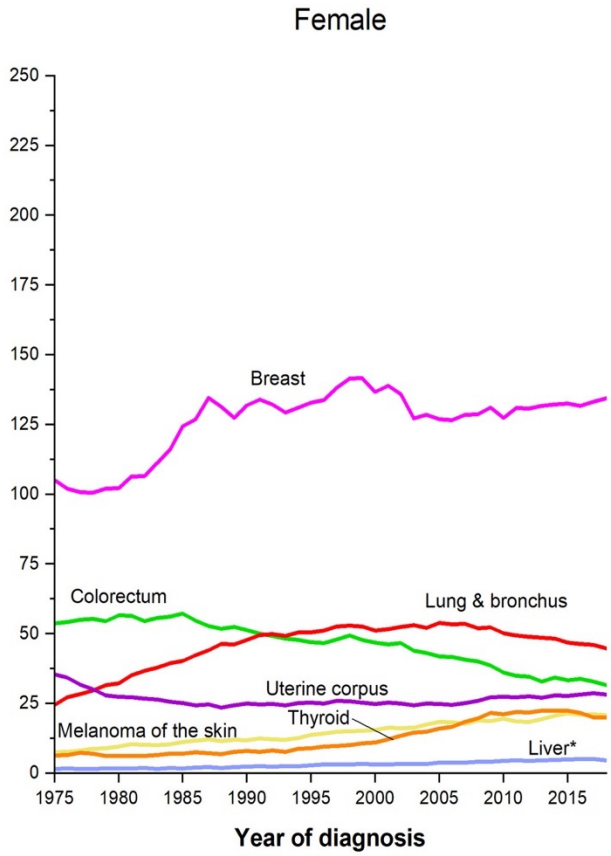

Figure 5: Breast cancer has been the most diagnosed cancer in in the United States of America from 1975 to 2018.

[6] © RL Siegel, KD. Miller, HE Fuchs, A. Jemal. Creative Commons Attribution (CC BY) license (http://creativecommons.org/licenses/by/4.0/).

The three hormonal receptors that categorize breast cancer subtypes are estrogen receptor (ER), progesterone receptor (PR), and human epidermal growth factor 2 receptor (HER2). When cancers are ER, PR, and/or HER2 positive, patients tend to have a positive response rate to targeted endocrine-based therapies, have lower cell proliferation rates, lower tumor grades, and often have a good prognosis (**Figure 6**) [56]. Unlike ER, PR, and HER2 positive breast cancer subtypes, triple- negative breast cancer (TNBC) is defined by the absence of all three hormonal receptors rendering the triple negative phenotype.

To be categorized as TNBC, less than 1% of the tumor cells must stain positive for ER and PR and must have a staining score of 0 to +1 for HER2 as determined by immunohistochemistry [57]. Although molecular cell staining defines this breast cancer subtype, TNBC is the most heterogenous breast cancer subtype and is further categorized into four different transcriptional subtypes or six different molecular subtypes. TNBC is the most aggressive breast cancer and has a high proliferation index (**Figure 6**) [56, 58]. The aggressive nature of this disease results in high rates of metastasis to the bone, brain, liver, and lungs resulting in poor survival [56, 59, 60].

TNBC makes up 15-20% of all breast cancer cases in the United States of America and has the lowest 5-year survival rate of all breast cancers [56, 60, 61]. According to the National Institutes of Health Surveillance, Epidemiology, and End Results Program (SEER) (https://seer.cancer.gov), TNBC 5-year survival is only 77.1% in comparison to hormonal positive breast cancer which has a 5-year survival rate of 89.9%. Once TNBC regionally or distantly metastasizes, the 5-year survival rates drop to 65.8% and 12.0% respectively [56, 60].

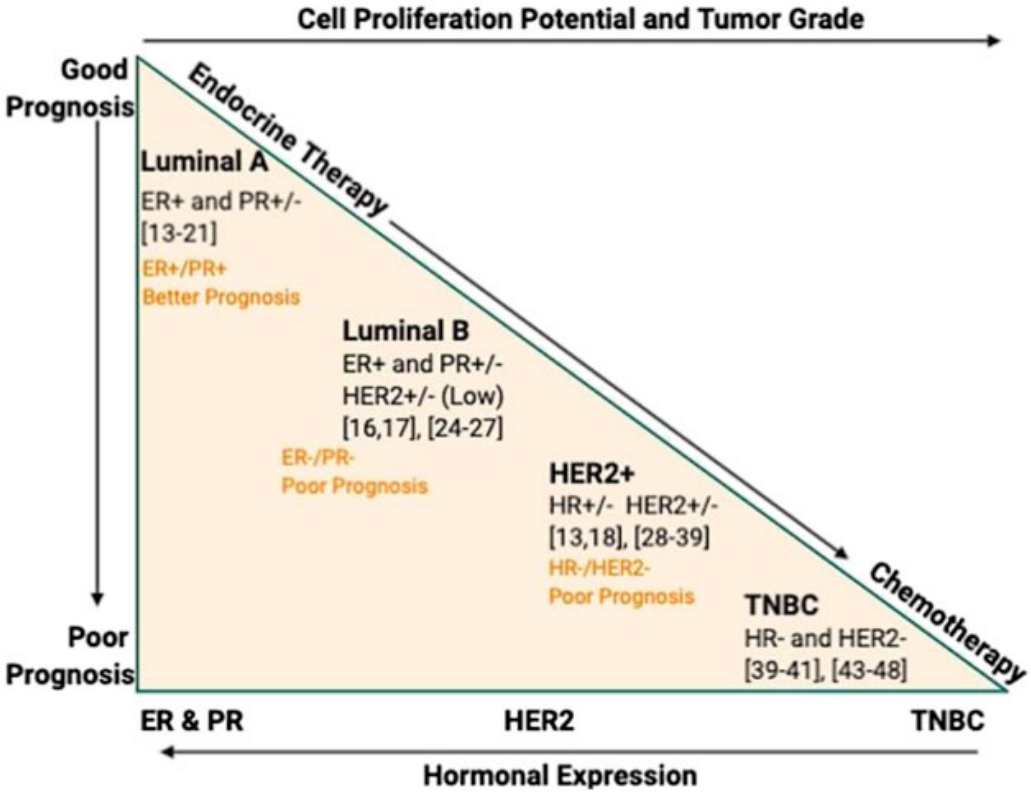

Figure 6: Breast cancer hormonal receptor status in correlation to prognosis, therapy response, and cell proliferation rate.

When breast cancer cells ER, PR, or HER2 positive patients tend to have a better prognosis, better response to endocrine-based therapies, and have lower proliferation index and tumor grade. TNBC cells are negative for all three receptors and tend to have a poor prognosis, poor response to endocrine-based therapies, and have high cell proliferation and tumor grade [56].

Because TNBC is defined by the lack of hormonal receptors (ER, PR, and HER2) on the cell surface, targeted endocrine-based therapies are ineffective (**Figure 6**). TNBC has been coined an orphan disease because of limited success in developing targeted treatments, and the standard of care for TNBC patients remains untargeted-conventional chemotherapy, radiation, and/or surgery [57, 62]. TNBC is treated with a wide range of chemotherapeutic drugs (topoisomerase II inhibitors, DNA alkylating agents, microtubule targeting taxanes, anti-metabolites, and/or platinum agents), but the drugs are nonselective and induce dose-limiting side effects all over the body (e.g. hair loss, nausea, vomiting, fatigue, hearing loss, weight loss, bone loss, reproductive damage, nephrotoxicity, hepatotoxicity, cardiotoxicity, and/or neurotoxicity) [63-66]. On top of dose-limiting side effects, heterogenous tumor barriers such as multi-drug exporters, cancer stem cells, hypoxia, and aberrant signaling pathways all promote singular- and multi-drug resistance [66, 67]. These compounding factors severely limit the therapeutic options for this disease.

Current Targeted Treatments for TNBC

It has only been in the last four years that the FDA has approved targeted poly(ADP-ribose) polymerase (PARP) inhibitors, checkpoint inhibitors, and an antibody-drug conjugate for TNBC [57, 68-71]. PARP inhibitors target the genetic instability of cancer and inhibit the repair of single-strand DNA breaks through PARP enzymes. While PARP inhibitors have been advantageous in treating TNBC with germline BRAC mutations, they have been met with challenges in the clinic. PARP inhibitors have high rates of drug resistance, are only effective for the 20% of TNBC patients with BRCA mutations, and increase the overall risk of serious adverse events when compared to traditional chemotherapy [68, 72-74]. Checkpoint inhibitors also provide a targeted treatment for TNBC.

Checkpoint inhibitors provide a long-lasting anticancer response in patients, and TNBC has been categorized as a tumor with a high density of tumor-infiltrating lymphocytes, especially $CD8^+$ T-cells [75, 76]. However, less than 20% of TNBC patients respond to an immune checkpoint blockade therapy, suggesting that there are compounding factors in the TME that prevent an adaptive antitumor response [77, 78]. TNBC patients have benefited from adding checkpoint inhibitors to their standard-of-care chemotherapy regimens, but when a checkpoint inhibitor is added, 100% of patients experience treatment-related adverse events [69]. The adverse events can be severe and impact the remaining quality of life for patients (e.g., hepatitis, arthralgia, hyper/hypothyroidism, blurred vision, and type 1 diabetes mellitus) [69, 76, 79]. Lastly, only one antibody-drug conjugate has been approved for TNBC.

Sacituzumab-govitecan (SG) is a trophoblast cell-surface antigen 2 (Trop-2) targeted humanized antibody linked to the topoisomerase-I inhibitor, SN-38, with a hydrolysable linker. Trop-2 is overexpressed in many cancer types including TNBC and aids in tumorigenesis and anchorage dependent cell growth [80]. SN-38 is the active from of the prodrug, irinotecan, and is linked to the antibody with a property linker that allows for pH-mediated release of the drug in the tumor cell and the tumor microenvironment (TME) [80-82]. While pH-mediated drug release takes advantage of the pH difference between the plasma (pH = 7.4) and the TME (pH = 4.0-5.0), the spontaneous hydrolysis of the linker results in unloading of SN38 systemically [83, 84]. Additionally, the internalization of the antibody is only 2-fold higher than the control, indicating its cellular internalization maybe inefficient [83]. This suggests the SG antibody drug conjugate may not be acting as a traditional targeting antibody, but more as an SN-38 prodrug to localize the drug to the tumor microenvironment [83]. In the Phase III ASCENT clinical trial, SG side effects for TNBC patients included neutropenia, leukopenia, diarrhea, anemia, febrile neutropenia,

alopecia, and fatigue [85]. When comparing the SG treatment group to traditional chemotherapy, the SG treatment group had side effects that occurred more frequency and presented more severely [85].

Although PARP inhibitors, checkpoint inhibitors, and SG have provided targeted treatments for TNBC, their therapeutic benefit is constrained by dose-limiting side effects, drug resistance, off target drug unloading, and lack of biomarkers to successfully treat TNBC. There is still a need to develop TNBC targeted therapies to decrease systemic side effects and increase the therapeutic impact of the therapy. Like many other cancer cells, TNBC has an increase in PS externalization, but the cells do not undergo apoptosis [14]. PS externalization has been correlated to tumor malignancy, and because TNBC is an innately aggressive tumor, TNBC is an ideal disease to focus ANXA5-PS based therapies [15].

ANXA5 Protein Drug Conjugates

This dissertation focuses on translating and developing novel ANXA5 protein drug conjugates for the treatment of TNBC. Protein-drug conjugates consist of a protein linked to a drug. A linker may be needed to join the protein and drug together depending on the functional groups available for conjugation (**Figure 7**).

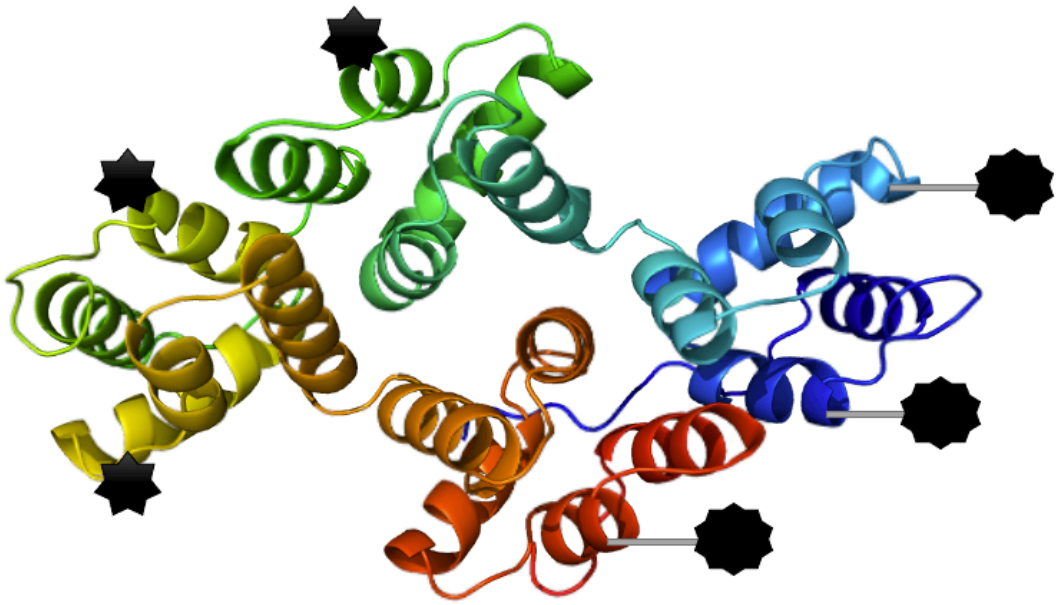

Figure 7: Composition of protein drug conjugates

Depending on functional groups found on the drug molecule and protein, drugs can be directly linked to the protein (as indicated by the black seven-point star) or linked to a protein with a small linker (as indicated by the black 9-point start with a small gray rectangular linker).

The ANXA5 protein-drug conjugates fill a unique space in the fight against cancer. First, ANXA5 acts as a delivery vehicle to localize a drug to cancer cells and vasculature through cancer's natural PS externalization. Second, by targeting and localizing the drug to the tumor, less drug is needed to induce cell death, resulting in fewer side effects. Third, the ANXA5-drug conjugates are cost-effective and easy to produce. ANXA5 is easily produced in *Escherichia coli (E. coli)* because ANXA5 does not require post-translational modifications like some monoclonal antibodies. *E. coli* also provides fast-growth kinetics and high cell densities increasing protein

production [86]. Additionally, by needing fewer drug, the overall cost remains lower. Fourth, ANXA5 is biologically compatible. ANXA5 is a human protein and does not require any other species' DNA or protein fragments for protein formation, unlike chimeric or humanized antibodies [87]. Finally, the simple design consisting of the protein, drug, and if applicable, linker, makes it an elegant platform to treat cancer. The simple design of antibody-drug conjugates (as seen with our ANXA5-drug conjugates) also has been advantageous in obtaining FDA approval for cancer therapy, indicating the ANXA5-drug conjugates could be easily translated into a clinical trial [88]. The three ANXA5-drug conjugates explored in this dissertation are ANXA5-mertansine (ANXA5-DM1), ANXA5- chlorambucil (ANXA5-CMB), and ANXA5-valproic acid (ANXA5-VPA).

ANXA5-DM1

History of DM1

Mertansine (DM1) a derivative of maytansine has shown to be a powerful anticancer agent and has a rich history dating back 50 years. In 1972, Maytansine was isolated from the *Maytenus serrata* plant, and the class of drugs now referred to as "maytansinoids" was born [89]. DM1 and the four other maytansinoid derivatives displayed profound anticancer activity against both liquid (leukemia: P388 and KB) and solid (melanoma: B16 and lung carcinoma) tumors [89, 90]. In 1977, Maytansine was discovered to be a competitive inhibitor for the vinblastine binding sites on tubulin and was 200-1000 fold more toxic than the vinca alkaloids [91]. This indicated that maytansinoids induce cell death by microtubule inhibition. By 1978, the first phase I clinical trials for both solid and liquid tumors began [92-95]. Although some patients benefited from the anticancer activity of maytansine, dose-limiting side effects were observed at doses as low as 0.5-2 mg/m^2 [92-95]. Maytansine caused central nervous and gastrointestinal system toxicity, and nearly every patient experienced severe tiredness, weakness, nausea, vomiting, and diarrhea. The side effects were so

severe some patients refused to finish the maytansine treatment, indicating the free drug is too toxic for systemic use, and this limited the therapeutic potential of the drug in the clinic [92-95]. Because of the severe side effects, it would take another decade before maytansinoids would be utilized as a chemotherapeutic agent.

The invention of monoclonal antibodies revived maytansinoids as anticancer agents. ImmunoGen's goal was to link maytansine to a monoclonal antibody to maintain the cytotoxic action but simultaneously decrease the systemic side effects. However, maytansine did not contain any functional groups suitable for cross linking [96, 97]. The team developed a synthetic derivate of maytansine that contained a lone sulfhydryl that would enable the team to link the molecule to the monoclonal antibody via a disulfide bond [96, 97]. The synthetic maytansine derivative was coined "drug maytansinoid 1" or DM1 (**Figure 8**) [98]. DM1 was 3-10 fold more toxic than maytansine and was successfully linked to several antibodies [97]. By linking DM1 to the humanized anti-CanAg antibody (Cantuzumab-DM1), the maximum tolerated dose of DM1 increased to 235 mg/m^2 for intravenous administration every 3 weeks, or 115 mg/m^2 for weekly intravenous administration [97, 99]. The addition of the antibody increased the maximum tolerated dose by 470 and 230 times more than the 0.5 mg/m^2 dose observed with free maytansine [97]. It would take another decade before the first and only DM1 based antibody drug conjugate would be approved by the FDA. In 2013, the FDA approved trastuzumab-emtansine (T-DM1) for HER2 positive metastatic breast cancer, and in 2019, T-DM1's approval was expanded for early-stage HER2 positive breast cancer [100, 101]. By linking DM1 to an antibody the drug's mechanism of action does not change.

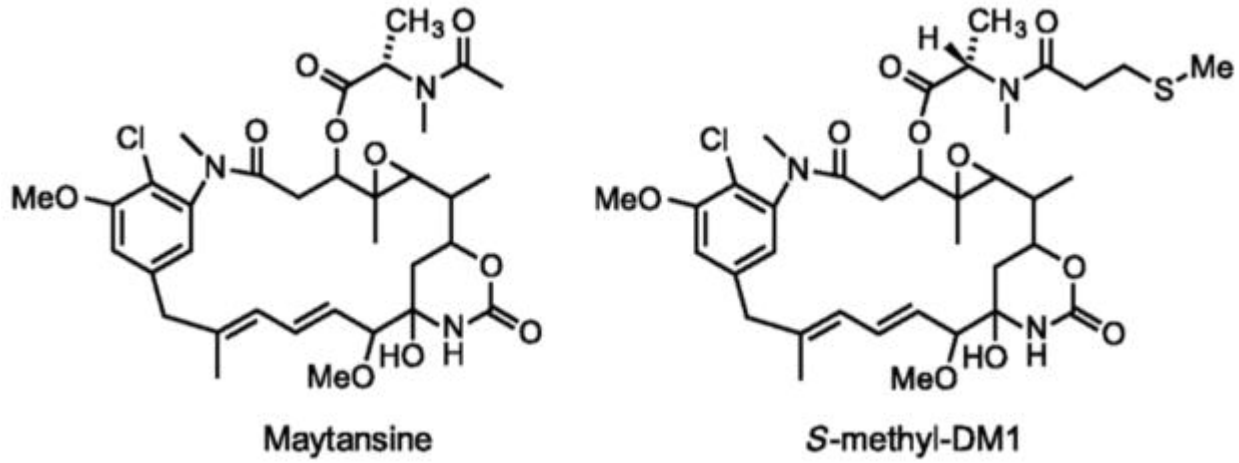

Figure 8: Maytansine and DM1 molecular structures

DM1 contains a lone sulfhydryl group which provides a chemical group suitable for cross linking. [11].

DM1 mechanism of action

DM1 is a potent anticancer drug that inhibits microtubule formation. Microtubules are small hollow tubes used for intracellular trafficking, cell movement, and provide structural support for dividing cells. Microtubules are composed of α/β tubulin heterodimers held together by noncovalent bonds [102]. Originally, it was thought that maytansine binds to the same binding site as vinca alkaloids, but it is now known that vinca alkaloids and maytansinoids bind to different sites on the β tubulin subunit [103]. Maytansinoids bind to β tubulin and inhibit the longitudinal polymerization by either blocking the addition of new tubulin subunits or forming drug-tubulin complexes that cannot be added to the growing microtubules [104]. In contrast, the vinca alkaloids act as a wedge between the α/β tubulin heterodimers and block the conformational change

necessary to form the microtubules [104]. By inhibiting microtubule formation, DM1 causes mitotic catastrophe by preventing the kinetochores (proteins that connect chromosomes to microtubules during mitosis) to connect to the microtubules (because DM1 inhibits microtubule formation), forcing the cell into apoptosis during metaphase, ultimately inhibiting mitosis [105]. On top physically inducing cell death by blocking microtubule formation, DM1 has also been shown to alter the type of cell death from apoptosis to an immunogenic cell death.

Immunogenic cell death

Harnessing the body's immune system is the next frontier in cancer therapy. The goal of immunotherapy is to maintain or restore our bodies innate and adaptive antitumor response to eliminate primary and metastatic lesions. Although immunotherapies have shown to be an invaluable addition to some cancers, it is not effective for all cancers because of the complex nature of the TME [106].

Cancer is a parasite composed of the body and will trick the body into believing it is a healthy group of cells. This phenomenon even occurs when the tumor has a high concentration of infiltrating lymphocytes. Although this is not a comprehensive list, tumors modulate the immune system to promote tumor survival in various ways. First, tumors have an extremely heterogeneous expression and often will lose major histocompatibility (MHC) class I/II molecules to prevent recognition of the cells by T cell receptors (TcR) and evade immune destruction [107, 108]. Second, high PS externalization promotes immune tolerance mainly through the Tryro3, Axl, and Mertk (TAM) receptors on macrophages. TAM signaling is essential for the phagocytosis of apoptotic cells. The TAM ligands (Gas6 and Pros1) act as a bridge to link PS and TAM receptors together to enhance phagocytosis by macrophages and promote anti-inflammatory cytokine release through suppression of nuclear factor-κB (NF-κB) and STAT-1 to limit the adaptive immune

response to cells with extracellular PS exposure [37, 38]. Phagocytosis increases the secretion of the immunosuppressive cytokines IL-10, TGF-β, and IL-4, restricting dendritic cell maturation and natural killer cell activation [38, 39]. Third, tumors upregulate immune checkpoint-inhibiting ligands (e.g., PD-L1) that inactivate $CD8^+$ T-cells. When PD-L1 binds to PD-1, this interaction blocks the downstream signaling caused by the TcR engagement with MHC I/II molecules [109]. The PD-L1 and PD-1 interaction causes an impaired T-cell activation and IL-2 production, ultimately protecting the tumor cell from immune destruction [109]. Additionally, PD-L1/PD-1 expression decreases T-cell homing to the tumor, and PD-L1 protects the tumor cells from cytotoxic lymphocyte-mediated cell lysis [110, 111]. Lastly, hypoxia also has negative impacts on immune regulation in the TME.

TNBC is an extremely heterogeneous disease, but a hypoxic tumor microenvironment and low response rates to immune checkpoint inhibitors remain an interlinked and underlying thread of this disease. TNBC is a fast-growing cancer, and hypoxia is more prevalent in TNBC than other breast cancer subtypes [112]. As the tumor cells divide, the distance between the cells and existing vasculature increases, generating an oxygen and nutrient gradient [113]. When the oxygen concentration remains low, the cancer cells adapt and alter downstream gene expression, mainly through hypoxia-inducible factor one-alpha (HIF1-α) to promote survival. Under normal oxygen concentration (~ 9% O_2) HIF1-α is hydroxylated by the prolyl hydroxylase domain-containing enzymes (PDH) at conserved proline residues for proteasomal degradation, but under hypoxic concentrations (~ 1-2% O_2), the PDH activity is diminished and HIF1-α becomes stabilized [114]. Once stabilized, HIF1-α enters the nucleus, forms a heterodimer with HIF-1β, and complexes with p300/CBP. The entire complex (HIF1-α- HIF-1β- p300/CBP) then binds hypoxia response element on DNA which activates hundreds of genes that regulate angiogenesis, metastasis,

epithelial to mesenchymal transition, cancer stemness, metabolic reprogramming, and immune modulation [115, 116]. Of particular importance to cancer therapy is the negative effects hypoxia has on immune modulation.

Although TNBC is the most immunogenic breast cancer subtype, only 18.5% of patients respond to an immune checkpoint blockade therapy [77, 78]. One explanation for poor antitumor immune response is the presence of hypoxic pockets in the TME that activates HIF1-α expression in both cancer and immune cells.

While HIF1-α regulation is complex and involves multiple signaling pathways, the phosphoinositide 3-kinase/protein kinase B/mammalian target of rapamycin (PI3K/AKT/mTOR) signaling pathways provides an upstream target to regulate hypoxia and subsequent HIF1-α expression. The PI3K/AKT/mTOR is one of the most dysregulated signaling pathways for solid cancers, with nearly 70% of all cancer having an abnormal expression [117, 118]. The mTOR protein expression is upregulated in TNBC, making mTOR a targetable molecule to regulate HIF1-α [119].

When the TME remains hypoxic, PI3K phosphorylates AKT which indirectly activates mTOR [118]. mTOR is a catalytic subunit for the mTOR complex 1 (mTORC1) and mTOR complex 2 (mTORC2), but only mTORC1 is sensitive to rapamycin treatments. mTORC1 regulates many key processes necessary for cell growth and proliferation based on nutrient, energy, and oxygen status [116]. In contrast, mTORC2 regulates AKT phosphorylation to regulate cell survival and metabolism [116]. Once activated, mTORC1 regulates transcription of HIF1-α expression through STAT3 and regulates transcription of HIF1-α expression through 4E-BP1/eIF4E and S6K1 [120]. Hypoxia and HIF1-α also regulate the adaptive immune response.

Hypoxia in the spleen and lymph nodes most likely plays a protective role, where the low oxygen concentration promotes the expression of HIF1-α to prevent the activation of $CD8^+$ T-cells and TcR mediated signaling [121]. In the tumor, hypoxia causes effector cell suppression by downregulating the transcriptional and translational expression of IFN-γ, TNF-α, and granzyme B in $CD8^+$ T-cells which characterizes T-cell exhaustion [112]. Hypoxia also induces HIF1-α dependent epigenetic inactivation of $CD8^+$ T-cells and natural killer cells through interactions with HDAC1 [112]. More importantly, hypoxia and HIF1-α also upregulate PD-1 on T-cells and PD-L1 on tumor cells, dendritic cells, tumor-infiltrating macrophages, and myeloid-derived suppressor cells promoting tumor immunity [121]. While many factors decrease immune activation in the TME, the type of cell death caused by chemotherapy can also impact immune activation.

Classical apoptosis is the body's elegant way of removing sick or dying cells with the innate immune system, mainly through macrophage phagocytosis. While inducing classical apoptosis can be beneficial in decreasing tumor burden, it does not take advantage of the adaptive immune system. Recently, immunogenic cell death (ICD) has been characterized as a unique pathway to activate the adaptive immune system against cancer.

The Nomenclature Committee of Cell Death (NCCD) defines ICD as "a form of regulated cell death that is sufficient to activate an adaptive immune response in an immunocompetent host" (**Figure 9**) [122]. For a chemotherapeutic agent to be considered an ICD inducer, the dying cells must externalize or secrete damage-associated molecular patterns (DAMPs) after treatment with the drug [123]. After the release of the DAMPs, they must bind to their cognate receptors on antigen-presenting cells that promote the recruitment, activation, and maturation of the antigen-presenting cells [123, 124]. Additionally, the antigen-presenting cells must migrate to the tumor-draining lymph nodes where they can train cytotoxic T-cells for the destruction of cancer [123].

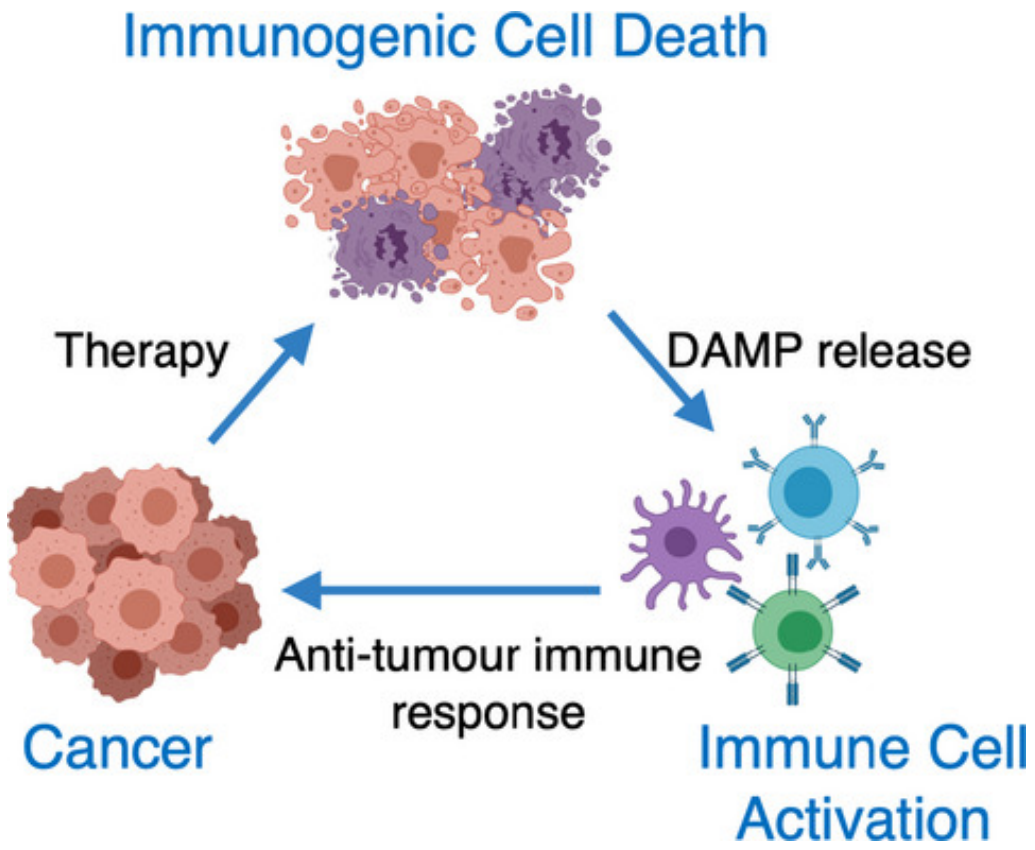

Figure 9: Immunogenic cell death

Immunogenic cell death is a regulated form of cell death that elicits an adaptive antitumor immune response. [124] © A. Ahmen and S. WG. Tait. Creative Commons Attribution (CC BY) license (http://creativecommons.org/licenses/by/4.0/)

Immunogenic cell death damage-associated molecular patterns

ICD is characterized by the release of three hallmark DAMPs: extracellular release of ATP, extracellular expression calreticulin, and extracellular release of high mobility group box 1 (HMGB1) [123, 125]. Unlike apoptosis, the ICD hallmarks cause spatiotemporal activation of the adaptive immune responses through the recruitment of antigen-presenting cells and tumor-specific cytotoxic lymphocytes to eliminate the tumor (**Figure 10**) [125]. The DAMPs all work together to increase the activation of the adaptive immune response.

Extracellular ATP release is a "find me" signal for antigen-presenting cells and increases dendric cell activation through the P2RX7 receptor [123, 126]. The binding of ATP to P2RX7 activates the NLRP3 inflammasome and promotes IL-1β section, which is necessary for dendric cells activation and cross-presentation to tumor-specific cytotoxic T-cells [123, 126]. Calreticulin is a protein confined to the lumen of the endoplasmic reticulum where it aids in calcium regulation in the cell, production of MHC molecules, and aids in antigen loading onto MHC molecules [123]. Upon ICD, calreticulin translocates to the extracellular plasma membrane before caspase 3-mediated PS exposure [123]. Extracellular calreticulin binds to the CD91 receptor on dendritic cells prompting the release of TNF-α and IL-6 [127]. Because calreticulin is exposed before apoptosis-mediated PS expression, calreticulin shifts the dying cell recognition from macrophages, which promote immune tolerance, to dendritic cells, which prime cytotoxic T-cells for antitumor immunity. The calreticulin-mediated phagocytosis increases the release of proinflammatory cytokines and aids in the priming of T-helper cells [123, 128]. HMGB1 is a nuclear-non-histone chromatin-associated protein that aids in DNA organization and transcriptional regulation. Once HMGB1 is extracellularly released, it acts as an inflammatory cytokine in the late stage of ICD after both the nuclear and plasma membrane have been permeabilized [123, 129]. Once HMGB1

binds to its receptors (RAGE, TLR2/4/9, CXCR4, or TIM-3) on antigen-presenting cells, it encourages the recruitment and maturation of dendritic cells for T-cell priming [130].

When linked to an antibody, DM1 has induced immunogenic cell death both *in vitro* and *in vivo* [131, 132]. *In vitro*, DM1 has increased the extracellular release of ATP and HMBG1 and increased the extracellular exposure of calreticulin [131]. *In vivo*, DM1 promoted tumor lymphocyte infiltration, increased INF-γ production, enhanced antigen uptake, and activated cytotoxic lymphocytes in the tumor-draining lymph nodes [132]. Because hypoxia is an intrinsic property of TNBC that increases PD-1/PD-L1 checkpoint molecules, targeting HIF1-α through mTOR-mediated signaling with rapamycin, in tandem with an anti-PD-l monoclonal antibody, is a logical choice to pair with ANXA5-DM1 for cancer therapy.

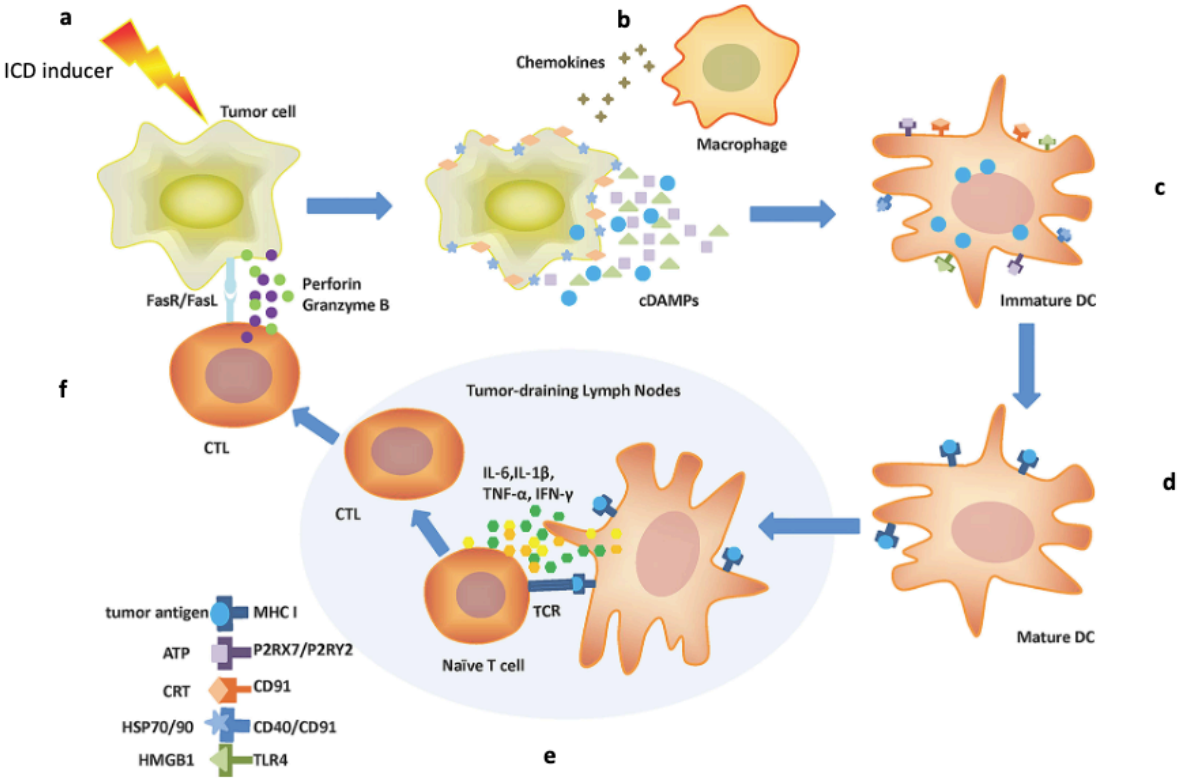

Figure 10: Spaciotemporal adaptive immune system activation by immunogenic cell death

a) ICD-inducing agent kills the cell ultimately causing the b) release of ICD DAMPs to recruit dendritic cells into the TME. c) ICD DAMPs bind to their respective receptors and promote tumor antigen uptake by on immature dendric cells d) causing dendritic cell maturation. e) Mature dendritic cells migrate to the tumor-draining lymph nodes, where they present tumor antigens to naïve T cells and release IL-6, IL-1β, TNF-α, and INF-γ to aid in T cell differentiation. f) Cytotoxic T cells migrate from the tumor-draining lymph node to the TME and kill tumor cells through the stimulation of the FasR/FasL pathway to release perforin and Granzyme B. Image adaptive from [127].

ANXA5-DM1 conjugate

The ANXA5-DM1 conjugate was previously designed in our lab by Ben Southard [133]. This work optimized the conjugation of ANXA5 and DM1 together through a two-step reaction utilizing sulfosuccinimidyl 4-(N-maleimidomethyl) cyclohexane-1-carboxylate (Sulfo-SMCC) crosslinking (**Figure 11**). Sulfo-SMCC contains both an amine-reactive N-hydroxysuccinminde (NHS ester), and a sulfhydryl-reactive maleimide group. First, the NHS ester reacts with the primary amines (lysine resides) on ANXA5 creating a stable amide bond between the two molecules. Second, DM1 is introduced, and the maleimide on ANXA5-sulfo-SMCC reacts with the lone sulfhydryl group on DM1 creating a non-cleavable thioester bond. The thioester bond reduces random drug unloaded outside the tumor microenvironment [134, 135]. Another advantage of the thioester bond is that it requires internalization and lysosomal breakdown of the protein for the drug to be released (**Figure 12**) [136]. The lysosomal breakdown produces two main drug metabolites, S-Methyl-DM1 and Lysine-SMCC-DM1, which are both as effective as the parent DM1 molecule [137].

ANXA5 and DM1 are both excellent candidates for sulfo-SMCC crosslinking. ANXA5 has 22 primary lysine residues and up to 22 molecules of DM1 molecule can be loaded onto one ANXA5 molecule. ANXA5 only contains one sulfhydryl molecule (cysteine residue) on the N-terminal domain, limiting the ANXA5-ANXA5 byproduct formation. DM1 does not have any primary amines and therefore is unable to react with sulfo-SMCC. This means DM1-DM1 byproducts are not formed.

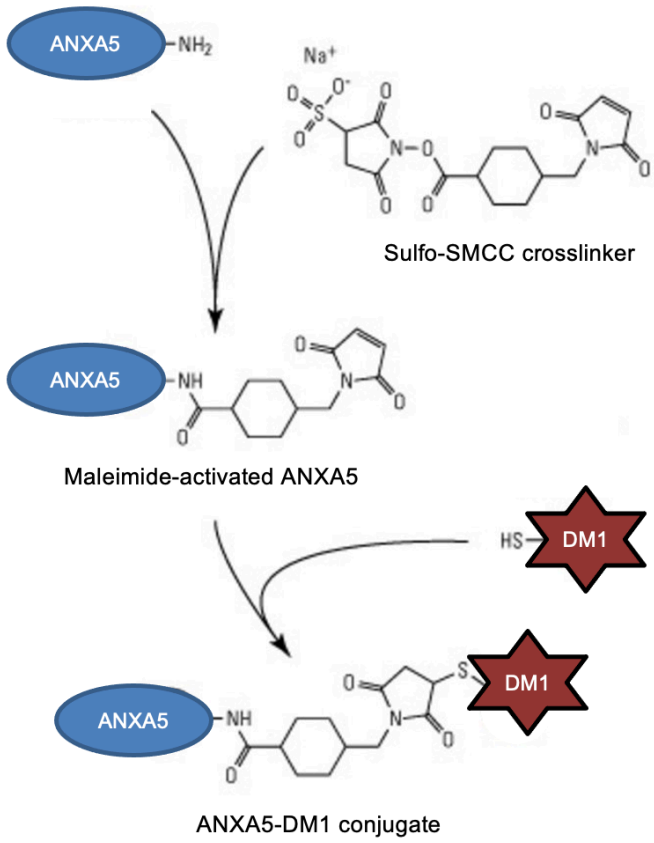

Figure 11: ANXA5-DM1 crosslinking scheme

DM-1 is linked to ANXA5 in a two-step reaction. First, the lysine residues on ANXA5 are activated with sulfosuccinimidyl 4-(N-maleimidomethyl) cyclohexane-1-carboxylate (Sulfo-SMCC). Second, DM1 is introduced and the maleimide on ANXA5-sulfo-SMCC reacts with the lone sulfhydryl group on DM1. Image adapted from: https://www.thermofisher.com/order/catalog/product/22322.

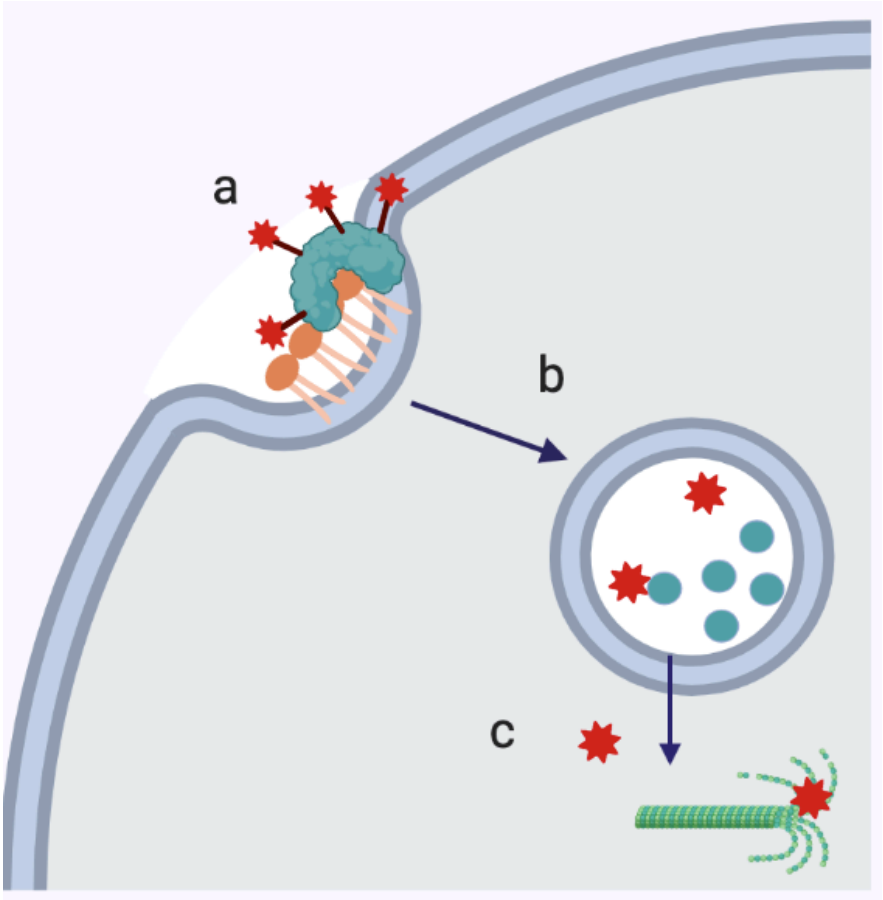

Figure 12: ANXA5-DM1 mechanism of action

a) ANXA5-DM1 binds to PS expressing cancer cells. b) ANXA5-DM1 is internalized and ANXA5 is broken down in the lysosome. c) Free DM1 diffuses out of the lysosome and causes mitotic catastrophe. Image created with Biorender.com.

ANXA5-CMB

History of CMB

Chlorambucil (CMB) is one of the world's oldest chemotherapeutic drugs and is on the World Health Organization's List of Essentials Medicines [138, 139]. While CMB has proven to be a lifesaving drug, its discovery resulted from chemical warfare. During World War I, mustard gas was used as a chemical weapon and caused severe-blistering chemical burns on the skin, eye, and respiratory tract [140]. Although mustard gas killed fewer than 5% of individuals who received care after exposure, the debilitating effects were enough to make Allied forces offer governmental funding for a mustard gas antidote in the following years [140, 141]. Mustard gas was shown to induce severe leukopenia and bone marrow toxicity, as early as 1919, but it would not be until an accident during World War II that the chemotherapeutic potential of mustard gas was brought to light [142, 143].

Off the shore of Bari Italy, a ship containing 100 tons of mustard gas was attacked during an air strike and nearly 1000 men died of mustard gas inhalation and leukopenia [141]. This accident prompted American scientists to develop mustard gas derivatives that were safer, but just as toxic as the sulfur-based mustard gas for cancer therapy. In 1942, Dr. Gilman Goodman, developed the first nitrogen-based mustard gas derivative, chlormethine [144]. Chlormethine had promising results in an animal model but could only be injected intravenously because it was too reactive to be administered orally. By introducing an electron-withdrawing aromatic ring next to the nitrogen atom, the aromatic ring in the center of CMB delocalizes electrons away from the nitrogen atom and decreases aziridinium ion formation. This modification made CMB less reactive than its aliphatic progenitor and could be taken orally (**Figure 13**) [145]. CMB was approved by

the FDA in 1957 and has been used for over 65 years for the treatment of hematopoietic malignancies such as chronic lymphocytic leukemia, lymphoma, and myeloma [146-149].

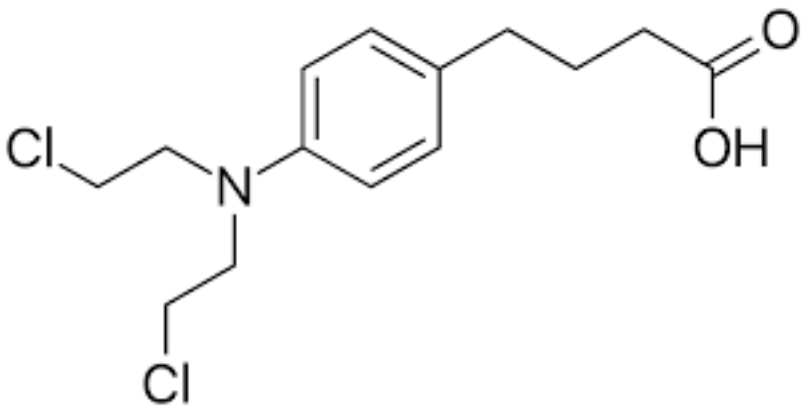

Figure 13: Molecular structure of CMB

CMB Mechanism of Action

CMB is an aromatic mustard gas derivative and induces cell death through DNA alkylation. The two electrophilic chlorine atoms typically react with the N7 on guanine in DNA and RNA generating covalent adducts [145, 146, 150]. The adduct then reacts with a neighboring base generating an intrastrand and/or opposite strand crosslink [146]. Once cross-linked the DNA and RNA cannot be opened for translation/transcription, and the cell undergoes apoptosis. While CMB has proven to be an excellent anti-cancer agent, it is untargeted and common side effects are nausea, vomiting, sores/ulcers in the mouth, swollen glands, low white cell count, unusual bleeding/bruising, overall tired/weakness, and changes in menstruation [151]. By utilizing the terminal carboxylic acid moiety on CMB, it can be linked to ANXA5, and a targeted treatment of CMB is created.

ANXA5-CMB conjugate

The ANXA5-CMB conjugate was previously designed in our lab by Dr. Patrick McKernan and Charles Bagarie [152, 153]. This work optimized the conjugation of ANXA5 and CMB together through carbodiimide crosslinking chemistry. 1-ethyl-3-(3-dimethylamino)propylcarbodiimide hydrochloride (EDC) is a zero-length carboxy to amine crosslinker (**Figure 14**). First, EDC activates the carboxylic acid on CMB creating the unstable o-acylisourea active ester. Next, ANXA5 is introduced, and the primary amines (lysine residues) displace the EDC crosslinker generating a stable amide bond between ANXA5 and CMB. By linking CMB to ANXA5, a targeted delivery of CMB has been created (**Figure 15**).

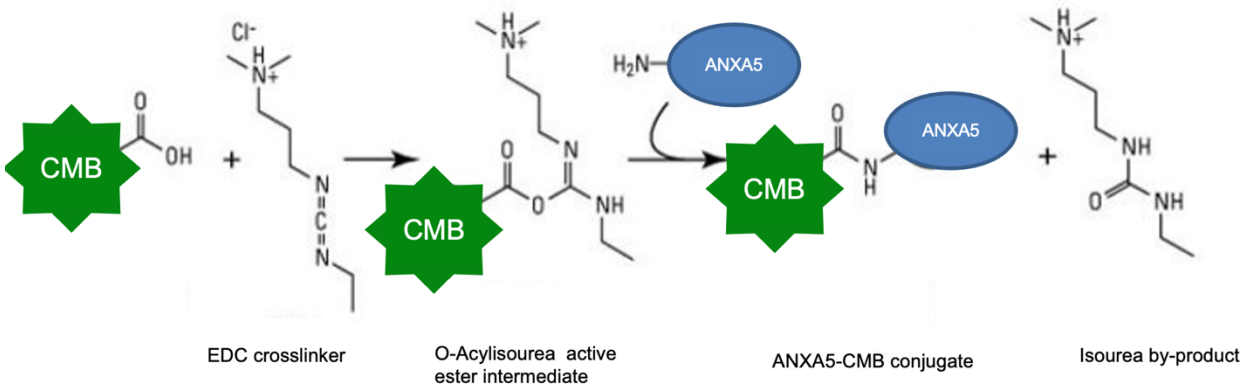

Figure 14: ANAX5-CMB crosslinking scheme

First, CMB is activated with EDC. The CMB-EDC reaction generates a reactive O-acylisourea ester intermediate. Next, a primary amine (lysine reside) on ANXA5 is introduced, and the EDC is displaced generating an sourea by-product and the ANXA5-CMB conjugate. Image adapted from https://www.thermofisher.com/order/catalog/product/22980.

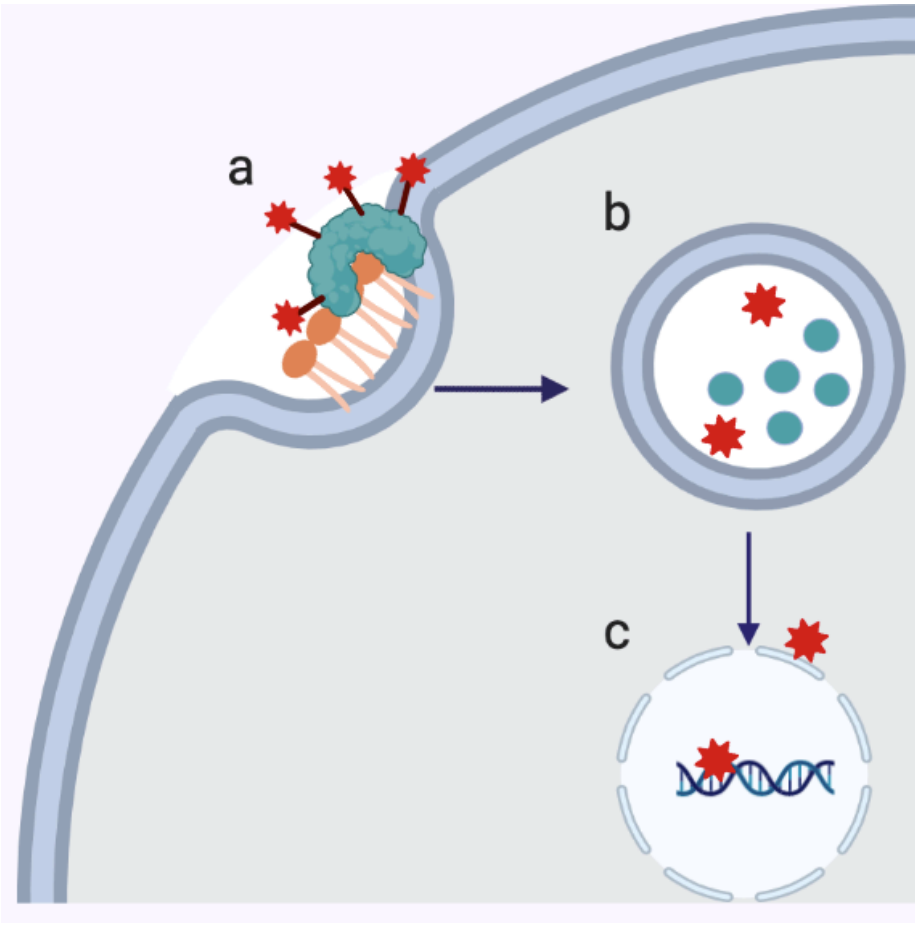

Figure 15: ANXA5-CMB mechanism of action

a) ANXA5-CMB binds to PS-expressing cancer cells. b) ANXA5-CMB is internalized, and ANXA5 is broken down in the lysosome. c) Free CMB diffuses out of the lysosome and enters the nucleus, where it crosslinks DNA and induces apoptosis. Image created with Biorender.com.

ANXA5-Valproic Acid

Valproic Acid History

The last drug of interest for this dissertation is valproic acid (VPA). VPA is a short-chain fatty acid that was first synthesized in 1882 when exploring new organic solvents [154]. In 1963, VPA was discovered as an antiepileptic agent, and in 1978, VPA was granted FDA approval for seizures and is well tolerated in patients [155]. The lifesaving antiepileptic mechanism of action has gained VPA a spot on the World Health Organizations List of Essential Medicine [156]. However, VPA's anticancer activity was just discovered over the past 21 years [157]. VPA has been classified as an histone deacetylase inhibitor (HDACi) and has displayed anticancer activity in many cancer types. As a HDACi, VPA helps to reset the epigenetic modifications that play a confounding role in cancer onset, progression, and underlie all 10 hallmarks of cancer (**Figure 16**) [158-160].

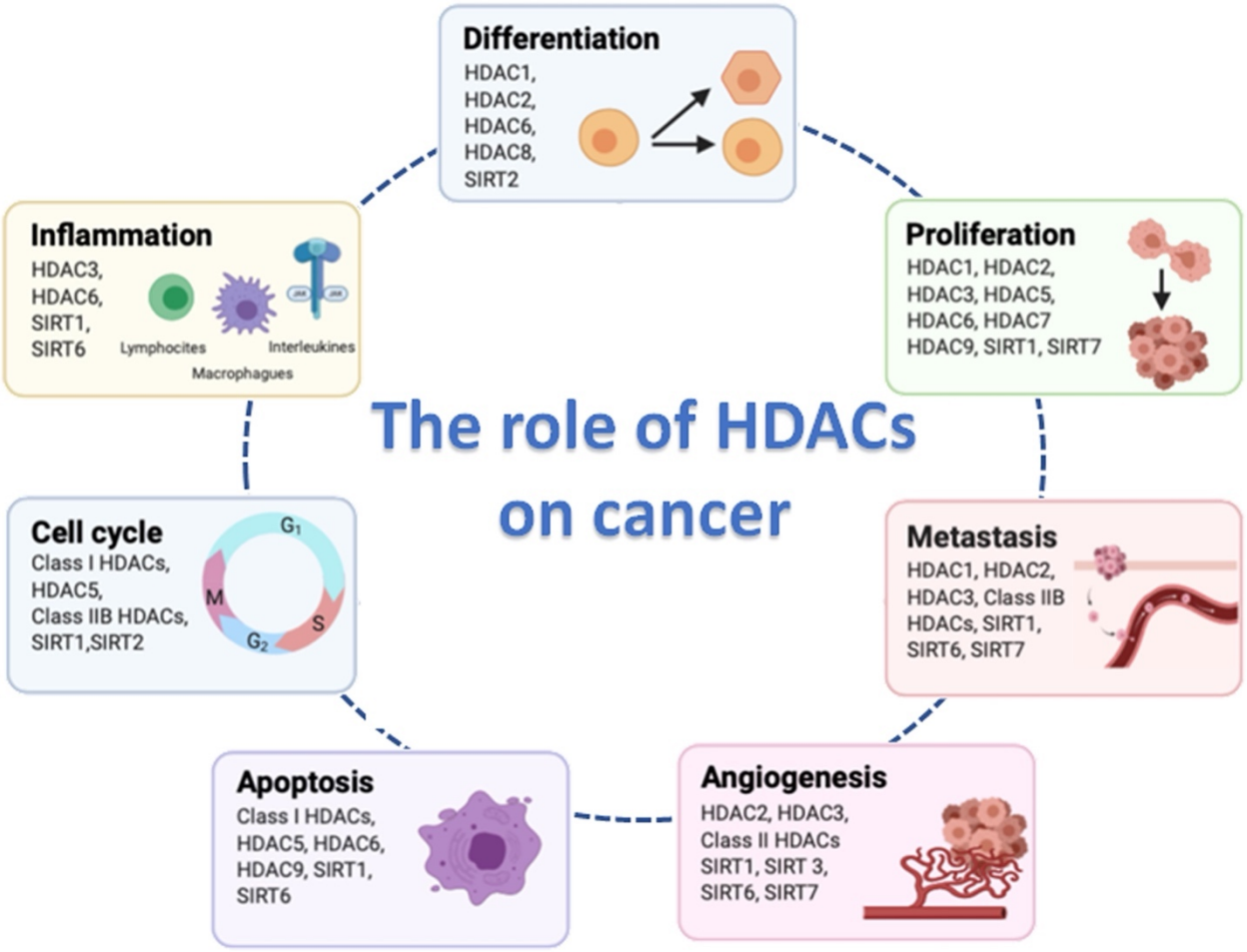

Figure 16: Role of HDAC on the hallmarks of cancer

[160] © L. Hontecilla-Prieto, R. Flores-Campos, A. Silver, E. de Alava, N. Hajji, and D. J. Garcia-Dominguez. Creative Commons Attribution (CC BY) license (http://creativecommons.org/licenses/by/4.0/).

Histone Acetylation

Epigenetic modifications are "tags" placed on DNA or histones which promote the opening or closing of the chromatin structure, which regulates transcription and gene expression within a cell without altering the sequence of the DNA. Of particular interest for cancer is histone acylation. Histone acetylation is a reversible epigenetic modification and is regulated by histone acylase transferases (HAT) and histone deacetylases (HDAC) (**Figure 17**) [161]. HATs transfer an acetyl group from acetyl-CoA to the amino groups of N-terminal lysine residues on histones [162, 163]. The addition of the acetyl group removes the positive change of the lysine residue, disrupts the electrostatic interaction with the negatively charged DNA, and opens the chromatin structure promoting transcription (**Figure 18**) [162-164]. However, HDACs remove the acetyl group via hydrolysis. The removal of the acetyl group re-establishes the electrostatic interaction between the positively charged lysine and negatively charged DNA and closes the chromatin structure repressing transcription.

In many cancer types, including TNBC, HDACs are overexpressed and cause a global downregulation of histone H3 and H4 acetylation, shifting the chromatin structure to a closed position (**Figure 19**) [163, 165]. The closed chromatin structure decreases the transcription of tumor suppressor genes and increases oncogenes transcription that promotes growth/proliferation, differentiation/metastasis, angiogenesis, and inflammation. This overexpression of HDACs makes them an attractive target to regulate cancer growth, but treating solid cancers with HDACi have been met with limitations.

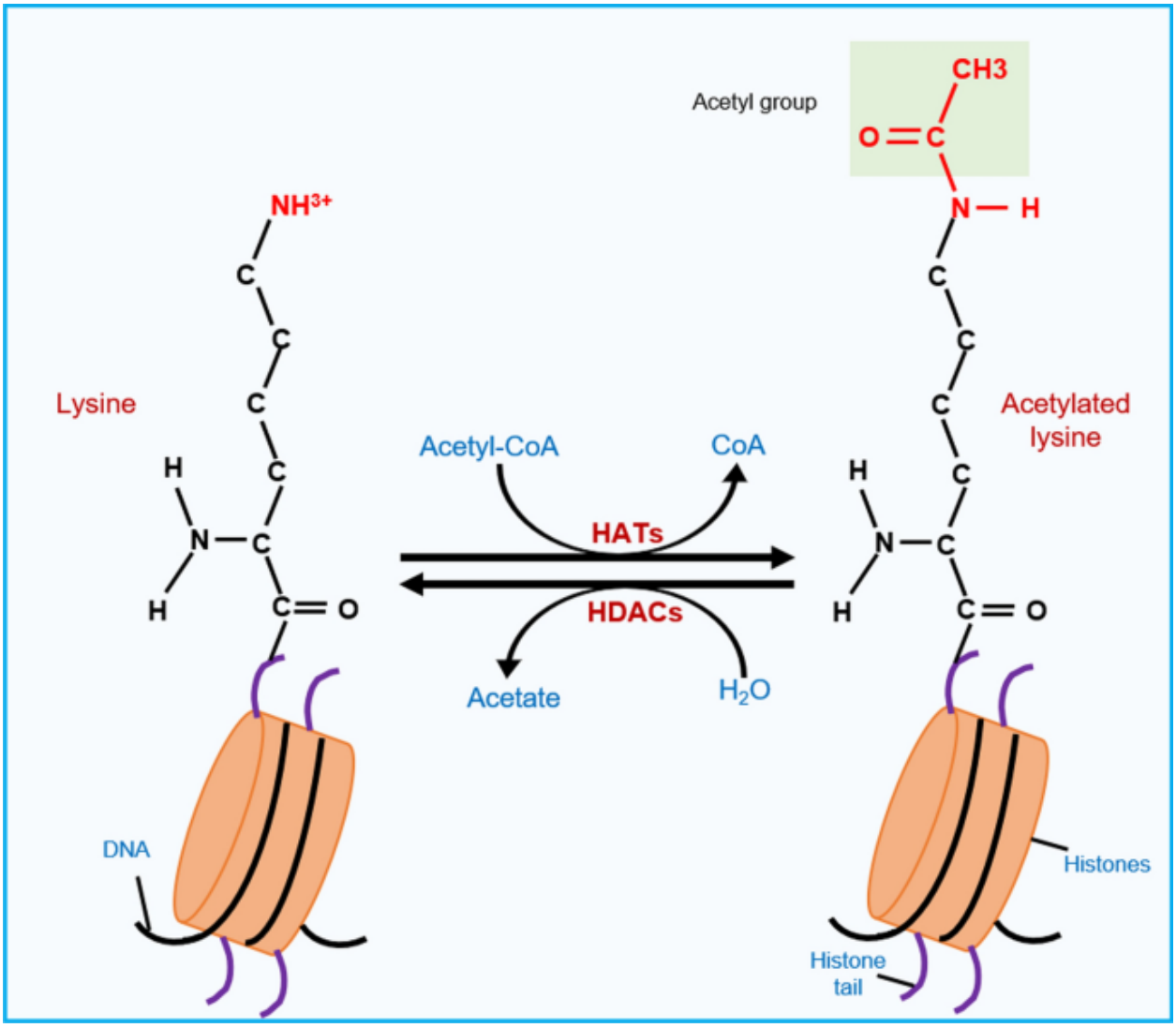

Figure 17: Acetylation of histones is regulated by HAT and HDAC

HATs transfer an acetyl group from acetyl-CoA to the amino groups of N-terminal lysine resides. In contrast, HDACs remove the acetyl group from the N-terminal lysine residues [161]. Reprinted with permission from Springer © 2021.

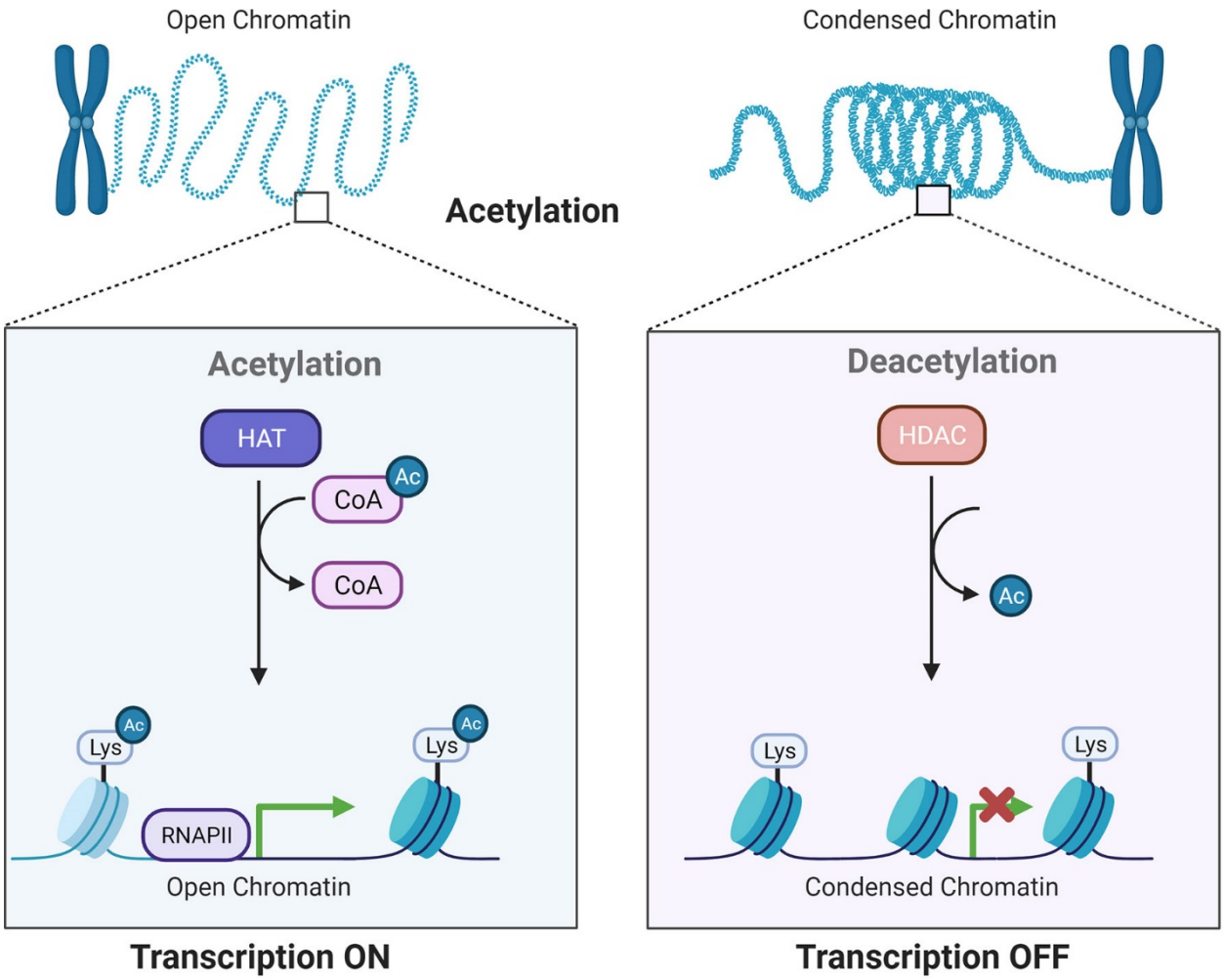

Figure 18: Acetylation regulates transcription

HATs transfer an acetyl group from acetyl-CoA to the amino groups of N-terminal lysine resides, disrupting the electrostatic interaction between the DNA and histones, ultimately opening the chromatin structure to promote transcription. HDACs remove the acetyl group from the N-terminal lysine residues re-establishing the electrostatic interaction between the DNA and histones and ultimately closing the chromatin structure. [164] © R. Hai, L. He, G. Shu. Creative Commons Attribution (CC BY) license (http://creativecommons.org/licenses/by/4.0/).

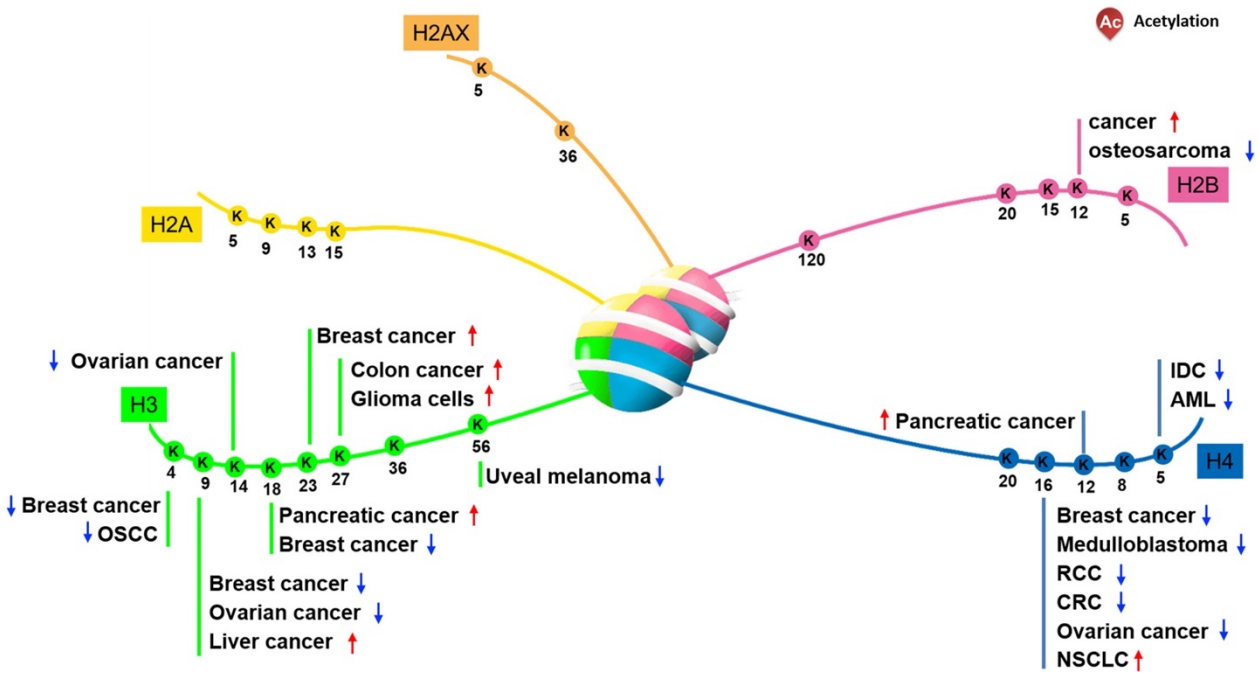

Figure 19: Aberrant histone acetylation patterns for cancer

For breast cancer, there is an apparent global downregulation of histone acetylation on histones 3 and 4. [162] © D. Wu, Y. Qie, Y. Jiao, X. Qui, and D. Liu. Creative Commons Attribution (CC BY) license (http://creativecommons.org/licenses/by/4.0/).

To date, the FDA has approved four HDACi (vorinostat, panobinostat, belinostat, and romidepsin), but they are only approved for hematological cancers. As single agents, the FDA-approved HDACi have limited therapeutic benefits for solid cancers [166]. This is most likely due to the poor pharmacokinetic profiles the HDACi have in the body because of low water solubility and cell permeability [167]. To overcome these issues, four different HDACi-antibody-drug conjugates have been created. The first is vorinostat linked to cetuximab, the second is vorinostat linked to trastuzumab, the third is ST8176AA1 linked to trastuzumab, and the fourth is

ST8176AA1 linked to cetuximab [168-170]. Like other ADC, the antibodies are only targeted to cancers expressing HER2 (trastuzumab) or epidermal growth factor receptor (cetuximab), meaning these therapies can only be used on cancers expressing these receptors. Because vorinostat and ST8176AA1 do not possess any primary amines, alcohols, or phenols, the drugs must undergo multistep reactions before they can be linked to the antibody [168, 170]. By increasing the complexity of the chemistry needed to link the antibody and drugs together, the yield decreases while simultaneously increasing the cost of production. There is a need to develop a novel targeted HDACi for cancer therapy, that requires simple chemistry to maximize the yield while maintaining a low cost. VPA is an excellent candidate for the simple EDC crosslinking mechanism due to the single carboxylic acid moiety on the molecule (**Figure 20**).

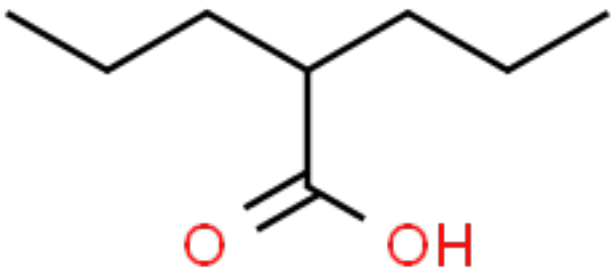

Figure 20: Valproic acid molecular structure

Valproic Acid Mechanism of Action

VPA is a class I and class IIa HDACi that leads to hyperacetylation of histones H3 and H4 with favorability at the lysine 9 residue of histone H3 and lysine 8 residue of histone H4 [171-174]. VPA blocks HDAC activity by binding to the catalytic site [175]. More specifically, the carboxylic acid on VPA complexes with the zinc ion in the active site of the HDAC preventing substrate access into the catalytic site [176, 177]. As a free drug, VPA is a potent regulator of gene expression. In cervical cancer, VPA induced a two-fold upregulation of over 1,000 genes, which include genes that regulate cell cycle control, apoptosis, and tumor suppressors. Additionally, a two-fold downregulation of over 500 genes was also observed, which include genes that regulate tumor survival [174, 178].

As for breast cancer, VPA has a wide range of anticancer effects. VPA has been shown to regulate apoptosis by upregulation of P21, Bak, and M30 protein expression, caspase 3 and 7 activations, downregulation of Bcl-2 protein, as well as, halt cycle progression at the G0/G1 phase [179-182]. Additionally, VPA has been shown to turn TNBC cells ER-α positive and re-sensitize drug-resistant tumors [183-187]. While VPA is an excellent candidate as an anticancer drug, it requires high doses (1-10 mM after 72 hours) to be effective *in vitro* [187-191]. Additionally, VPA is associated with high liver, heart, and brain metabolism. Additionally, when VPA is in blood, it is bound to albumin, limiting clinical translation for cancer therapy [187-191]. Because HDAC are overexpressed enzymes that contribute to almost every aspect of cancer growth and progression, creating a targeted treatment of ANXA5-VPA to reset the acetylation homeostasis in TNBC will create the first HDAC-targeted treatment for this orphan disease (**Figure 21**).

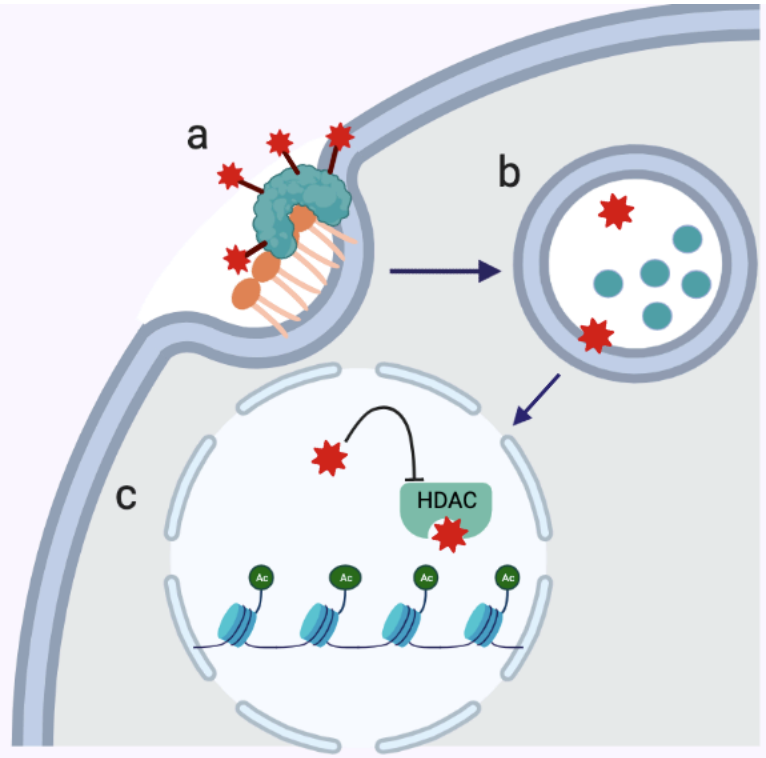

Figure 21: ANXA5-VPA mechanism of action

a) ANXA5-VPA binds to PS-expressing cancer cells. b) ANXA5-VPA is internalized, and ANXA5 is broken down in the lysosome. c) Free VPA diffuses out of the lysosome and enters the nucleus, where it inhibits HDAC activity resetting the acetylation homeostasis. Image created with Biorender.com.

Scope of Dissertation

TNBC remains an untargeted disease burdened by a lack of targeted biomarkers on the cell surface. Patients are forced to rely on high doses of untargeted and nonselective chemotherapy resulting in severe dose-limiting side effects. This dissertation will focus on exploiting TNBC's upregulated extracellular PS exposure as a targetable biomarker for cancer therapy. The unifying theme of this dissertation is utilizing three different ANXA5-based protein drug conjugates for the treatment of TNBC. This dissertation will primarily focus on expanding existing *in vitro* and *in vivo* knowledge about two ANXA5-protein drug conjugates and developing one ANXA5-protein drug conjugate for the treatment of TNBC:

1. ANXA5-DM1
    a. Characterize the protein-to-drug ratio through mass analysis
    b. *In vitro* characterization of ANXA5-DM1 binding to TNBC and healthy vasculature and mammary epithelium
    c. *In vitro* quantification of ANXA5-DM1 cytotoxicity on TNBC and healthy vasculature and mammary epithelium and assess ANXA5-DM1 as an ICD inducer
    d. *In vivo* translation in an immunocompetent mouse model to assess ANXA5-DM1 as a free agent or in combination with an mTOR inhibitor and checkpoint-inhibiting antibody.
2. ANXA5-CMB
    a. *In vitro* quantification of ANXA5-DM1 cytotoxicity on healthy vasculature and mammary epithelium

b. *In vivo* translation in an immunocompetent mouse model to assess ANXA5-DM1 as a mouse model and dosage optimization

3. ANXA5-VPA
    a. Create ANXA5-VPA conjugate and characterize the drug-to-protein ratio
    b. *In vitro* quantification of ANXA5-DM1 cytotoxicity on TNBC

Publications

Chapter 1 has material from a peer-reviewed review article in *Cancer Letters,* of which I was the first author [54]. The *in vitro* work in Chapter 3 has been submitted to *Molecular Biomedicine* and is currently being revised. I will be a co-first author for this publication. The *in vivo* work will also be submitted to a peer-reviewed journal, and I will be the first author of this publication. Chapter 5 has been submitted to the University of Oklahoma's Office of Technology Commercialization as an invention disclosure with the hope of obtaining a patent. Dr. Harrison and I have co-authored the invention disclosure. This work will ultimately be submitted to a peer-reviewed journal for publication, where I will be the first author.

While outside the scope of this dissertation, I have also assisted in the development of an ANXA5-ampicillin conjugate for the treatment of infectious diseases [192]. I was a co-author for this publication. This further illustrates the translational application of ANXA5, as well as, the expertise I have gained in bioconjugation. Additionally, I have provided ANXA5 for a collaboration with Dr. Wilhelm's group, where I was a co-author on a publication in *Nano Letters* [193]. Finally, I will be a co-author on at least 2 other publications with Gabriela Faria's work utilizing an ANXA5-single-walled carbon nanotube conjugate in combination with photothermal therapy and immune stimulation for the treatment of TNBC.

Chapter 2: Materials and Methods

ANXA5 production

ANXA5 expression

Recombinant ANXA5 was produced in BL21(DE3) *Escherichia coli (E. coli)* transfected with a pET-30 Ek/LIC/ANXA5 plasmid. *E. coli* was first grown in 10 ml and expanded to 1 L. *E. coli* were grown in Terrific Broth (TB) medium containing 35 ug/ml kanamycin (Fisher Scientific, Pittsburgh, PA, USA) 37 °C and shaking at 220 rpm to an optical density (OD) of 1.2. To stimulate ANXA5 expression, 0.4 mM isopropyl β-D-thiogalactopyranoside (IPTG) (Fisher Scientific, Pittsburgh, PA, USA) was added to the culture. ANXA5 protein expression occurred for 19 hours at 25 °C and shaking at 200 rpm. *E. coli* containing ANXA5 protein was harvested via centrifugation at 3500 x g for 5 minutes and stored at -20 °C overnight. *E. coli* was lysed via sonication, and the cell suspension was centrifuged at 3500 x g for 2 hours. The supernatant was retained for purification.

ANXA5 immobilized metal affinity chromatography purification

ANXA5 was purified via immobilized metal affinity chromatography (IMAC). The supernatant was loaded into a 5 ml HisTrap HP column (Cytiva, Marlborough, MA, USA) with 500 mM NaCl (VWR, Randor, PA, USA) and 40 mM imidazole (Sigma-Aldrich, St. Louis, MO, USA) to reduce non-specific protein binding. Once ANXA5 was loaded into the column, the column was washed with 50 ml of wash buffer 1 (20 mM sodium phosphate buffer (Fisher Scientific, Pittsburgh, PA, USA) containing 500 mM NaCl, and 40 mM imidazole, pH 7.4). Next, the column was washed with 300 ml of wash buffer 2 (20 mM sodium phosphate buffer containing 500 mM NaCl, 40 mM imidazole, and 1.0% Triton X-114 (Sigma-Alrich, St. Louis, MO, USA), pH 7.4) to remove

endotoxins. ANXA5 was eluted with an elution buffer (20 mM sodium phosphate buffer containing 500 mM NaCl, 500 mM imidazole, pH 7.0). After elution, ANXA5 was dialyzed into 20 mM sodium phosphate buffer, pH 7.4, to remove excess imidazole and salt for His-tag cleavage. His-Tag was cleaved via an engineered HRV 3C protease (Sino Biologics, Wayne, PA, USA) cleavage site that cleaves the sequence LEVLFQ↓GP removing the polyhistidine-tag according to the manufacturer's instructions. Cleaved ANXA5 was dialyzed in 20 mM sodium phosphate buffer containing 100 mM NaCl at pH 7.4. A Bradford assay (Bio-Rad, Hercules, CA, USA) was used to determine protein concentration (**Appendix A, Figure 74**). The ANXA5 protein solution was flash frozen in liquid nitrogen and stored at -80 °C.

ANXA5-DM1 Bioconjugation

ANXA5 and DM1 (MedChemExpress, Monmouth Junction, NY, USA) were linked together through sulfosuccinimidyl-4-(N-maleimidomethyl)cyclohexane-1-carboxylate (sulfo-SMCC) (TCI, Portland, OR, USA) crosslinking chemistry. First, 13.76 mM (6 mg/ml) of sulfo-SMCC is dissolved in DI water. If the sulfo-SMCC does not fully dissolve, gently heat the sulfo-SMCC mixture to 40-50 °C. Allow the solution to cool to room temperature before the addition of the protein. Next, add 200 μL of the sulfo-SMCC solution to 1 ml of 27.77 μM (1 mg/ml) ANXA5 and allow to react for 1 hour at 4°C on an orbital shaker. The maleimide moiety of the sulfo-SMCC linker readily captures the only thiol functional group in DM1. Dissolve 9.03 mM (6.66 mg/ml) DM1 in DMSO (Fisher Scientific, Pittsburgh, PA, USA). Add 150 μL of DM1 mixture to ANXA5-sulfo-SMCC solution and allow to react for 2 hours at 4°C on an orbital shaker. The resulting ANXA5-DM1 biconjugate is then purified from excess free DM1 with an 8-hour dialysis in 2 L of 30 mM sodium phosphate buffer at pH 7.4 with a regenerated cellulose dialysis membrane of

MWCO 12-14 kDa (Fisher Scientific, Pittsburgh, PA, USA) at 4 °C. Dialysate is changed at least once to ensure removal of unreacted molecules.

ANXA5-CMB Bioconjugation

The ANAX5-CMB bioconjugate was synthesized by linking CMB (TCI America, Portland, OR, USA) to ANXA5 via 1-ethyl-3(3-dimethylaminopropyl)carbodiimide (EDC) crosslinking chemistry. CMB (6.5 mM) is dissolved in 50 µL of an acid alcohol solution of 3% HCl and 95 % EtOH v/v (VWR Inc., Radnor, PA, USA). A working solution is prepared by diluting this acid alcohol solution in 1 mL of 30 mM PBS (Mallinckrodt Chemicals, Phillipsburg, NJ, USA) at pH 4.5. The carboxylic acid moiety of CMB is then activated with 65 mM EDC, forming an unstable O-acylisourea intermediate for 30 minutes. Excess reactive EDC is quenched with 2 mM β-mercaptoethanol (Sigma-Aldrich, St. Louis, MO, USA), preventing the formation of crosslinked byproducts downstream. The resulting solution of CMB-EDC is added to 2 mL of 27.77 µM (1 mg/ml) ANXA5 in 30 mM PBS, where the activated CMB reacts readily with the primary amines of ANXA5 lysine residues for 12 h at 4 °C [194]. At this point, excess CMB forms a visible precipitate in neutral pH solution and is removed by centrifuging at 10,000 rcf for 1 h at 4 °C. The supernatant is collected, and the resulting ANXA5-CMB bioconjugate is further purified from excess free CMB with an 8-hour dialysis in 2 L of 30 mM sodium phosphate buffer at pH 7.4 with a regenerated cellulose dialysis membrane of MWCO 12-14 kDa (Fisher Scientific, Pittsburgh, PA, USA) at 4 °C. Dialysate is changed at least once to ensure removal of unreacted molecules.

ANXA5-VPA Bioconjugation

The ANAX5-VPA bioconjugate was synthesized by linking valproic acid, sodium salt (Cayman Chemicals, Ann Arbor, MI, USA) to ANXA5 via 1-ethyl-3(3-dimethylaminopropyl)carbodiimide

(EDC) crosslinking chemistry. VPA at a concentration of 69.5 mM (10 mg/ml) was dissolved in PBS (pH 7.4). The carboxylic acid moiety of VPA is then activated with 851.6 mM (132 mg/ml) EDC forming an unstable O-acylisourea intermediate for 30 minutes. Excess reactive EDC is quenched with 2 mM β-mercaptoethanol (Sigma-Aldrich, St. Louis, MO, USA), preventing the formation of crosslinked byproducts downstream. The resulting solution of VPA-EDC is added to 1 mL of 27.77 μM (1 mg/ml) ANXA5 in 30 mM PBS, where the activated VPA reacts readily with the primary amines of ANXA5 lysine residues for 2 hours at 25 °C. The resulting ANXA5-VPA biconjugate is then purified from excess free VPA with an 8-hour dialysis in 2 L of 30 mM sodium phosphate buffer at pH 7.4 with a regenerated cellulose dialysis membrane of MWCO 12-14 kDa (Fisher Scientific, Pittsburgh, PA, USA) at 4 °C. Dialysate is changed at least once to ensure removal of unreacted molecules.

ANXA5-Drug Conjugate SDS-PAGE Quantification

Drug loading was confirmed via SDS-PAGE. ANXA5 and ANXA5-DM1, ANXA5-CMB, or ANXA5-VPA were denatured in 2x Laemelli sample buffer (Bio-Rad, Hercules, CA, USA) and heated to 100 °C for 5 minutes. Samples were transferred to 4-20% mini-protean TGX precast 10-well gradient gels (Bio-Rad, Hercules, CA, USA). The samples were run at 200 V for 30 minutes in 1% tris-glycine-SDS running buffer (Bio-Rad, Hercules, CA, USA) stained with Imperial stain (Thermo Fisher, Waltham, MA, USA) and destained with DI water overnight. DI water was changed at least once, and to decrease destaining time a paper towel was added.

Denaturing Intact Mass Analysis

Denaturing intact mass analysis mass analysis on ANXA5 and ANXA5-drug conjugates was performed by Dr. Aaron Bailey, at The University of Texas Medical Branch in Galveston, Texas using the following procedure: Samples containing purified ANXA5-DM1 and ANXA5-CMB (0.14 mg/mL final concentration) were analyzed using size exclusion chromatography (SEC) coupled directly to mass spectrometry. Sample injection (1 µL) and on-line SEC-desalting was accomplished using an organic/acidic mobile phase (30% acetonitrile, 0.1% formic acid, 0.02% trifluoroacetic acid) pumped with a Vanquish Horizon UHPLC system (Thermo Scientific) through a SEC UHPLC column (BEH200 SEC 4.6 x 50 mm, Waters), at a flow rate of 20 µL/min. The LC flow path was connected in line with an Orbitrap Eclipse Tribrid mass spectrometer (Thermo Scientific) via a heated electrospray ionization (HESI-II) ion source (Thermo Scientific). The ion source was operated with 3500 V spray voltage, sheath gas setting of 40 units, auxiliary gas setting of 10 units, and vaporizer temperature of 75˚C. The MS capillary temperature was set to 325˚C. Intact mass spectra were generated by using an RF Lens setting of 50 V to desolvate protein ions, isolating a mass range of m/z 500-450, and reacting isolated ions with proton transfer charge reduction for 6 ms, followed by scanning for charge reduced intact protein product ions using a mass range of m/z 500 – 8000. Intact protein ions were detected in the Orbitrap, scanning at a resolution setting of 50,000 (at m/z 200). Raw LC-MS data were analyzed using BioPharma Finder (Thermo Scientific) software. LC-MS spectra representing intact ANXA5-DM1 profiles were deconvoluted using the ReSpect and Sliding Window algorithms with a ReSpect mass tolerance of 20 ppm, a Sliding Window mass tolerance of 20 ppm, and a deconvolution mass range of 35 – 45kDa [195]. Intact mass assignments of individual ANXA5-DM1(n) conjugate isoforms

were based on tolerance of 100 ppm. Drug-to-protein ratio was calculated as a weighted average of the ReSpect-Sliding Window abundances for each of the ANXA5-DM1(n) isoforms detected.

Cell lines and Culture Conditions

All cell lines and cell media were purchased from American Type Culture Collection (ATCC, Manassas, VA, USA) except HAAE-1, which was purchased from Corielle Institute (Camden, NJ, USA). EMT6 murine breast carcinoma cells were cultivated with Waymouth's MB 752/1 medium (Gibco [Thermo Fisher], Waltham, MA, USA) supplemented with 2 mM glutamine, 15% FBS, and 1% antibiotic-antimitotic (10,000 IU penicillin, 10,000 μg/ml streptomycin, and 25 μg/ml amphotericin B, Corning, Kennebunk, MA, USA). 4T1 murine breast cancer cells were cultivated with Roswell Park Memorial Institute 1640 medium (RPMI-1640) supplemented with 10% FBS and 1% antibiotic-antimitotic. Human umbilical vein endothelial cells (HUVEC) were cultured in vascular cell basal medium supplemented with endothelial cell growth kit BBE (0.2% bovine brain extract, 5 ng/ml rh EGF, 10 mM L-glutamine, 0.75 Units/ml heparin sulfate, 1 μg/ml hydrocortisone, 50 μg/ml ascorbic acid, 2% FBS, ATCC) and 1% antibiotic-antimycotic. Human abdominal aorta endothelial (HAAE-1) cells were cultured in Hams F-12 medium supplemented with 30 μg/ml endothelial cell growth supplement (15 mg/500 ml media), 17.5 U/ml heparin (8750 U/500 mL or 17.5 mg heparin / 500 ml), 10% FBS, and 1% antibiotic-antimycotic. MCF10A nontumorigenic human breast epithelial cells were cultured in mammary epithelial growth medium (MEGM) with MEGM bullet kit (Lonza, Greenwood, SC, USA) (2 mL BPE, 0.5 ml hEGF, 0.5 ml insulin, 0.5 ml hydrocortisone, 0.5 ml GA), the GA-1000 was omitted due to ATCC recommendations. Additionally, ATCC recommends 100 ng/ml cholera toxin (Sigma-Aldrich, St. Louis, MO, USA), which was added to the MCF10A cell culture medium as well as 1% antibiotic-antimycotic.

All adherent cells were passaged using 0.25 % (w/v) trypsin in 0.53 mM EDTA (Thermo Fisher Scientific, Waltham, MA, USA) except MCF10A, which used soybean trypsin inhibitor for trypsin neutralization. All cell lines were cultured under a 5% CO_2 supplemented atmosphere at a temperature of 37 °C and 100% relative humidity. Medium was refreshed every 48 h. Adherent cancer cell cultures were grown to less than 75% confluence, and healthy cell lines cells were grown to confluency because they decrease PS expression upon confluency. Cell type description can be found in **Appendix B5**.

In Vitro Binding Studies

Colorimetric adherent cell binding strength

Binding strength was analyzed via a modified indirect ELISA. Cells (50,000 cells/well) were grown onto 24 well plates and fixed with 0.025% glutaraldehyde once cancer cells were 70-80% confluent. Cancer cells were blocked with 0.5% bovine serum albumin (BSA) for 1 hour at 37 °C. Cells were incubated with 0-20 nM of biotinylated ANXA5 for 2 hours at 37 °C and 5% CO_2. ANXA5 was biotinylated with ROCHE biotin protein labeling kit (ROCHE, Basel, Switzerland) and the level of biotinylating was quantified with Pierce Biotin Quantification kit (Pierce Biotechnology, Walham, MA, USA) per manufacturer's instructions (see appendix B6 and B7). Cells were washed four times with 0.5% BSA to removed unbound ANXA5. Cells were then seeded with 2 μg/ml streptavidin-horseradish peroxidase (Strep-HRP) for 1 hour at room temperature. Cells were washed four times with 0.5% BSA to remove unbound Strep-HRP and the chromogenic substrate O-phenylenediamine (OPD) and 30% hydrogen peroxide were added to each well to induce a yellow color change. Cells were incubated at room temperature in the dark. Supernatant was collected, and the absorbance was read at 450 nm on a BioTek Synergy HT

microtiter plate reader (Winooski, VT). For each concentration of biotinylated ANXA5, the specific binding was obtained by subtracting non-specific binding, when no calcium was present (biotinylated ANXA5 with 5 mM of EDTA), from the total binding (biotinylated ANXA5 with 2 mM $CaCl_2$). The dissociation constant was determined using the nonlinear regression one site total and nonspecific binding model in GraphPad Prism version 9 software (Graph Pad, San Diego California, USA).

Flow cytometry analysis of ANXA5 calcium dependence

To validate ANXA5 calcium dependence, flow cytometry was utilized. For all flow cytometry studies ANXA5-FITC (Abcam Cambridge, MA, USA) was utilized per manufacturer's recommendations. Briefly, 50,000 cells/well were seeded onto 24 well plates and treated 24 hours later. Cells were lifted from the plate with standard trypsinization methods. Cells were collected at 1-5 x 10^5 cells via centrifugation and resuspended in 500 µL of binding buffer supplied by manufacturer. To chelate the calcium in the binding buffer, 5 mM of EDTA was added. Next, 5 µL of FITC-ANXA5 was added incubated for 15 minutes in the dark at room temperature. After incubation, cells were analyzed on a BD Biosciences Accuri C6 flow cytometer (Franklin Lakes, NJ, USA), with excitation at 488 nm and a 533/30 band pass filter, which was used to capture 5,000 gated events per sample. Data was collected and analyzed with BD C6 Accuri software. All experiments were conducted in triplicate.

Fluorescent analysis of ANXA5 binding in suspension

To compare ANXA5 binding between 4T1, EMT6, and MCF10A cells, a fluorescent in suspension assay was utilized. ANXA5-FITC (Abcam Cambridge, MA, USA) was utilized per manufacturer's recommendations. Briefly, cells were grown in T-75 plates until 70-80% confluent

for TNBC cells and 90-100% confluent for healthy cells. Cells were lifted from the plate with standard trypsinization methods. Cells were collected at 5 x 10^5 cells via centrifugation and resuspended in 100 μL of the binding buffer supplied by manufacturer. Next, 1 μL of ANXA5-FITC was added and incubated on an orbital shaker 5 minutes at room temperature in the dark. After incubation, cells were centrifuged at 500 x g for 5 minutes to remove unbound ANXA5-FITC. Cells were resuspended in 100 μL of binding buffer and transferred to an opaque black 96 well plate. Fluorescence (ex/em 486/528, sensitivity 100) was read on a BioTek Synergy HT microtiter plate reader. All experiments were conducted with a sample size of 6-9.

ANXA5 binding stability

Cells were grown in 24 well plates to 70-80% confluence and incubated with 100 nM of biotinylated ANXA5-HRP for 2 h then washed. On days 0, 1, and 2, separate sets of cells. Quantification of bound ANXA5 protein was performed using a chromogenic assay as described for evaluating binding strength.

Flow cytometry analysis of confluency effects on ANXA5 binding

To determine the effects confluency has on both cancerous and healthy cell ANXA5 binding, flow cytometry was utilized. For all cell types, cells were grown to 50-70% confluency (non-confluent) or 90-100% confluency (confluent). Cells were lifted from the plate with standard trypsinization methods. Cells were collected at 1-5 x 10^5 cells via centrifugation and resuspended in 500 μL of binding buffer supplied by manufacturer. Next, 5 μL of FITC-ANXA5 was added and incubated for 15 minutes in the dark at room temperature. After incubation, cells were analyzed on BD Biosciences Accuri C6 (Franklin Lakes, New Jersey, USA), with excitation at 488 nm and a 533/30 band pass filter, which was used to capture 5,000 gated events per sample. Data was collected and analyzed with BD C6 Accuri software. All experiments were conducted in triplicate.

In vitro cytotoxicity studies

ANXA5 cytotoxicity

Cell viability was assayed by a resazurin assay (n = 3-5). Cancer cells were seeded at 5,000 cells/well in 96 well plates and treated 24 hours after seeding. Healthy cells were seeded at 10,000 cells per well in 96 well plates and treated once cells reached 90-100% confluency. Cells were treated with 0-0.7 μM of ANXA5 in fully supplemented growth medium supplemented with 2 mM calcium to promote ANXA5 binding. After 72 hours, the cell medium was removed, and 100 μl fresh medium containing 10% Alamar Blue (Bio-Rad Laboratories, Hercules, CA, USA) was added to each well. Cells were placed back into the incubator for 2-6 hours to allow cells to reduce the resazurin dye and induce a color change to assess viability. Media (100 μl) was transferred to opaque black plates, and fluorescence (ex/em 530/590, sensitivity 50) was read on a BioTek Synergy HT microtiter plate reader. Percent viability was determined by comparing treatment groups to the untreated control (0 μM).

ANXA5-DM1 cytotoxicity validation

Cell viability was assayed by a resazurin assay (n = 3). EMT6 cells were seeded at 5,000 cells/well in 96 well plates and treated 24 hours after seeding. Cells were treated with 0-1000 nM of DM1 in the ANXA5-DM1 conjugate in growth medium fully supplemented with 2mM of calcium to promote ANXA5 binding. After 72 hours, an Alamar Blue assay was utilized to determine viability. Percent viability was determined by comparing treatment groups to the untreated control (0 μM).

ANXA5-DM1 healthy cell cytotoxicity

Cell viability was assayed by a resazurin assay (n = 3-6). HAAE-1, HUVEC, and MCF10A cells were seeded at 10,000 cells per well in 96 well plates and treated once cells reached 90-100% confluency. Cells were treated with 0-10 μM of DM in the ANXA5-DM1 conjugate or free DM1 in growth media fully supplemented with 2 mM calcium to promote ANXA5 binding. After 72 hours, an Alamar Blue assay was utilized to determine viability. Percent viability was determined by comparing treatment groups to the untreated control (0 μM).

ANXA5-DM1 seeding density effects on cytotoxicity

To explore seeding density effects on ANXA5-DM1 cytotoxic effects, cells were seeded at 5,000 or 10,000 cells per well in 96 well plates and treated 24 hours later. Cells were seeded with 0-10 nM of ANXA5-DM1 or free DM1 for 24 hours in growth media fully supplemented with 2 mM calcium to promote ANXA5 binding. After 72 hours, an Alamar Blue assay was utilized to determine viability. Percent viability was determined by comparing treatment groups to the untreated control (0 μM).

ANXA5-CMB healthy cell cytotoxicity

Cell viability was assayed by a resazurin assay (n = 3-6). HUVEC and MCF10A cells were seeded at 10,000 cells per well in 96 well plates and treated once cells reached 90-100% confluency. Cells were treated with 0-100 μM of CMB in the ANXA5-CMB conjugate in growth media fully supplemented with 2 mM calcium to promote ANXA5 binding. After 72 hours, an Alamar Blue assay was utilized to determine viability. Percent viability was determined by comparing treatment groups to the untreated control (0 μM).

ANXA5-VPA TNBC cytotoxicity

Cell viability was assayed by a resazurin assay (n = 3). EMT6 and 4T1 cells were seeded at 5,000 cells/well in 96 well plates and treated 48 hours after seeding. Cells were treated with 0-100 mM of VPA in the ANXA5-VPA conjugate or free VPA growth medium fully supplemented with 2mM of calcium to promote ANXA5 binding. After 72 hours, an Alamar Blue assay was utilized to determine viability. Percent viability was determined by comparing treatment groups to the untreated control (0 μM).

Immunogenic cell death studies

ATP release

To determine if ANXA5-DM1 induces ATP release from cells after treatment, an ATP luminescence kit (Molecular Probes, Eugene, OR, USA) was utilized according to manufacture's instructions. Briefly, EMT6 and 4T1 cells were seeded at 5,000 cells/well in 96 well plates and treated 24 hours after seeding. Cells were treated with 0 or 10 nM of DM1 in the ANXA5-DM1 conjugate or free DM1 for 24 hours. After 24 hours, 10 μL of cell media was added to 90 μL of standard reaction solution in a white plate. Luminesce reading was obtained from the plate reader, and ATP concentration was calculated by comparing luminescence reading to a standard curve (**Appendix B12 and Figure 77**).

Calreticulin externalization

To determine if ANXA5-DM1 induces calreticulin surface expression, flow cytometry was utilized. EMT6 and 4T1 cells were seeded at 25,000 cells/well in 24 well plates and treated 24 hours after seeding. Cells were treated with 0 or 10 nM of DM1 in the ANXA5-DM1 conjugate or

free DM1 for 24 hours. After 24 hours, media was collected into microcentrifuge tubes to collect dead cells. To ensure there would be enough cells, three wells were combined to be one sample. Cells in the plates were then washed with PBS, and 100 µL of trypsin was added to each well. Once, 90% of cells were removed from the plate (2-5 minutes), cells were added to the microcentrifuge tubes, and centrifuged at 500 x g for 5 minutes. Cells were resuspended in 200 µl. of 0.5% BSA-PBS and counted to have at least 100,000 cells per sample. Cells were then fixed with 4% PFA (Thermo Fisher Scientific, Waltham MA, USA) for 20 minutes at 4 °C. Cells were then washed two times with 500 µl of 0.5% BSA-PBS at 500 x g for 5 minutes. After the second wash, cells were resuspended in 100 µl of 0.5% BSA-PBS, and 1 µl of CD16/CD32 Fc Block (eBioscience, San Diego, CA, USA) was added. Cells were then incubated for 20 minutes at 4 °C. Finally, 1 µl of FITC labeled calreticulin (Novus Biologicals, Centennial, CO, USA) was added. Cells were incubated for another 30 minutes at 4 °C in the dark. After incubation, cells were analyzed on BD Biosciences Accuri C6 (Franklin Lakes, New Jersey, USA) with excitation at 488 nm, and a 533/30 band pass filter was used to capture 10,000 gated events per sample. Data was collected and analyzed with BD C6 Accuri software. One sample composed of three wells, and each sample was analyzed 3 times. All experiments were conducted in triplicate.

In Vivo Tumor Models

All animal studies were performed in accordance with the protocols approved by the Institutional Animal Care and Use committee (IACUC) at the University of Oklahoma. Animals were housed in a pathogen-free facility at the University of Oklahoma and monitored daily.

4T1 Tumor Implantation in BALB/cJ Mice

Six-week-old BALB/cJ mice (Jackson Laboratory; 000651) were injected with $1x10^5$ 4T1 cells in the fourth mammary fat. Tumor cell implantation were performed with 30-gauge needle with 50% matrigel (Corning, Corning, NY, USA) and 50% PBS in 100 μL.

EMT6 Tumor Implantation in BALB/cJ Mice

Six-week-old BALB/cJ mice (Jackson Laboratory; 000651) were injected with $1x10^6$ cells in the fourth mammary fat. Tumor cell implantation were performed with 30-gauge needle in with cells suspended in 100 μL PBS.

Mice Mass and Tumor Volume

Mice mass and tumor volumes were measured every 3-7 days during each study. Tumor volumes were measured using caliper measurements, and volume was determined though the modified ellipsoid formula $V = \frac{L*W^2}{2}$, where length is the longest diameter of the tumor and the perpendicular diameter is the width [196, 197].

ANXA5-DM1 Preliminary Dosing

Mice were implanted with 4T1 cells on day 0. Once tumors reached 3-5 mm in diameter, treatment began. Mice were treated with 0-0.25 mg/kg of DM1 intraperitonially (IP) in the ANXA5-DM1 conjugate once every 7 days for 21 days. Tumor volumes and survival were monitored.

ANXA5-DM1 Holistic Treatment

Mice were implanted with EMT6 or 4T1 cells on day 0. Once tumors reached 3-5 mm in diameter, treatment began. Mice were treated IP with 0.025 mg/kg ANXA5-DM1 once every 7 days, 5

mg/kg, rapamycin daily, and/or 5 mg/kg anti-PD1 on days 1, 5, 9 of treatment (**Figure 22**) Mice were treated for 21 days, and survival was monitored.

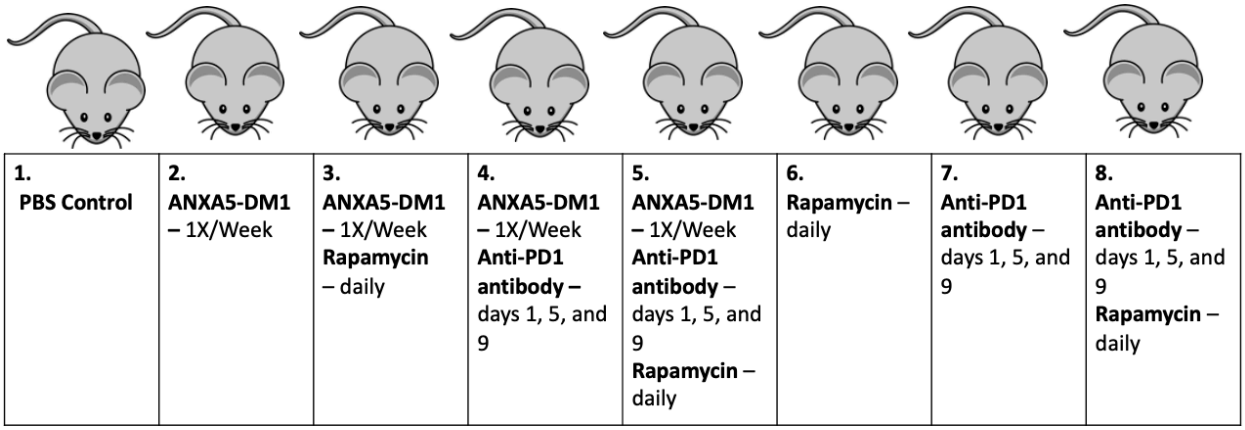

1. PBS Control	2. ANXA5-DM1 – 1X/Week	3. ANXA5-DM1 – 1X/Week Rapamycin – daily	4. ANXA5-DM1 – 1X/Week Anti-PD1 antibody – days 1, 5, and 9	5. ANXA5-DM1 – 1X/Week Anti-PD1 antibody – days 1, 5, and 9 Rapamycin – daily	6. Rapamycin – daily	7. Anti-PD1 antibody – days 1, 5, and 9	8. Anti-PD1 antibody – days 1, 5, and 9 Rapamycin – daily

Figure 22: Treatment groups and dosing schedule for holistic dosing treatment

ANXA5-DM1 Intratumoral Treatment

Mice were implanted with EMT6 cells on day 0. Once tumors reached 3-5 mm in diameter, treatment began. Mice were treated with 0-0.25 mg/kg of DM1 intratumorally (IT) in the ANXA5-DM1 conjugate daily for 21 days, and tumor volumes and survival were monitored.

ANXA5 immunogenicity

Protein specific antibody titers were analyzed as previously described [198]. Briefly, 3 mg/kg of ANXA5 was administered daily for 21 days. One mouse was euthanized at day 0, 10, and 21 of treatment, and blood was collected via a cardiac puncture. Blood was allowed to coagulate at room temperature for 30 minutes, then centrifuged at 3,500 x g for 10 minutes, retaining the supernatant and stored at – 80 °C. A sandwich ELISA assay was performed to determine protein specific

antibody titers. A 0.1 M carbonate coating buffer and 20 μg/mL ANXA5 were incubated overnight at 4°C on high binding capacity ELISA 96 well plates (VWR; Ranor, PA, USA). Plates were then washed and blocked with fetal bovine serum, and plasma dilutions were incubated overnight at 4°C. Following additional washes, goat anti-mouse IgG and IgM conjugated to HRP (Jackson ImmunoResearch Laboratories, Inc., West Grove, PA; 315-035-044) was used to develop OPD as described in the *in vitro* binding assays. Antibody titers are presented as the greatest dilution that produces a positive result. ELISA absorbance cut off values were determined by the mean of the negative controls + 3 SD, so any absorbance value above this value was considered positive [199].

ANXA5-CMB Dosing

Mice were implanted with 4T1 cells on day 0. Once tumors reached 3-5 mm in diameter, treatment began. Mice were treated with 0-5 mg/kg of ANXA5-CMB or free CMB IP daily or on a 5 day on 2 days off dosing cycle that continued for 21 days. Tumor volume and survival were monitored.

Statistics

All statistical analysis was performed with GraphPad Prism 9 version 4.1. A student's T-test was performed for ANXA5-calcium dependence binding, confluency effects for ANXA5 binding, and dose specific cytotoxicity studies that utilized two groups. A one-way analysis of variance (ANOVA) was performed for the in-suspension binding, ANXA5 cytotoxicity, ATP release, calreticulin surface expression, mice mass, and tumor volumes studies that utilized 3 or more groups. Tukey's multiple comparison post hoc analysis was utilized to determine statistical significance between the groups. A log-rank Cox-Mantel test was preformed to analyze survival. A cut off value of $p < 0.05$ indicated significance for all studies.

Chapter 3: ANXA5-DM1 Results and Discussion

E. coli Growth Buffer Optimization

The effects of *Escherichia coli (E. coli)* growth medium on ANXA5 production is summarized in **Figure 23**. Previously, ANXA5 has been transformed and produced in *E. coli* [200]. *E. coli* is a cheap, fast, and efficient way to amplify plasmids to produce recombinant proteins, but the growth media can impact production yield. All *E. coli* growth media contain yeast extract as a source of vitamins and minerals and tryptone as a nitrogen source for nucleic acid and amino acid production [201]. However, the amount of yeast extract, tryptone, glycerol, and the addition of a buffer can affect bacterial cell growth and ultimately protein yield [201, 202].

Previously, *E. coli* containing the ANXA5 vector was grown in Luria broth (LB) medium and had an average yield of approximately 35 mg of purified ANXA5 per liter of medium [152, 198]. While 35 mg of ANXA5 is a high yield when compared to other ANXA5 productions in literature, further optimization of the *E. coli* growth buffer could increase the overall yield [203, 204]. LB medium is the most common growth medium for *E. coli,* but the acidification of the medium from glucose metabolism can limit cell density and viability [86, 201]. Terrific broth (TB) medium is a "richer" broth and contains nearly five times more yeast extract than the LB medium and includes glycerol and a potassium phosphate buffer [201, 202]. The addition of glycerol provides an additional energy source for the bacterial cells allowing for faster growth but also increases the survival of bacteria [201, 202]. The addition of the phosphate buffer prevents TB acidification, increasing viability [201]. TB can hold five times more biomass than LB, making TB an ideal medium to increase ANXA5 production yield [205]. When *E. coli* bearing the ANXA5 vector is grown in TB media, the protein production yield significantly increases. The average

yield was approximately 130 mg of purified ANXA5 per liter of medium. By switching the *E. coli* growth medium to TB, 3.6 times more ANXA5 can be produced.

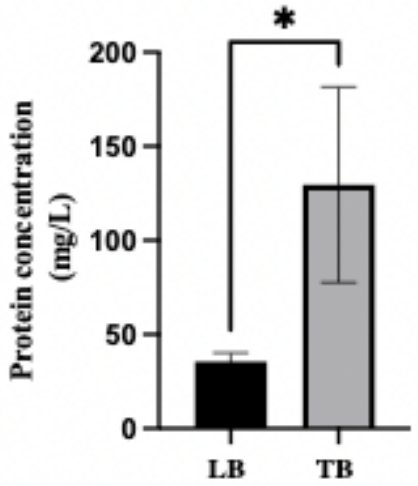

Figure 23: E. coli growth medium effects on ANXA5 production.

TB media significantly increased ANXA5 production from 35 mg/L with LB media to 130 mg/L with TB media. Statistical significance was performed with a student's T-test. Data is represented as mean ± SD. Statistical significance is denoted by *($p < 0.05$).

ANXA5-DM1 Characterization

ANXA5-DM1 was characterized via SDS-PAGE, absorbance, and intact denaturing mass spectroscopic analysis. Previously, Ben Southard characterized the ANXA5-DM1 conjugate through SDS-PAGE and absorbance at 288 nm [206]. Through SDS-PAGE size quantification and absorption of DM1 at 288 nM (**Appendix B2**), the drug-to-protein ratio was 6 ± 3 molecules of DM1 to 1 molecule of ANXA5 (**Figure 24**). The sulfo-SMCC crosslinking chemistry makes the ANXA5-DM1 conjugate readily reproducible as shown by two separate conjugations in lanes 6

and 7, with an unconjugated ANXA5 control in lane 5. A majority of the conjugate exists as a monomer ranging from 37-44 kDa, but a small amount of the conjugate exists at approximately 72 kDa, indicating protein-protein crosslinking. While protein-protein crosslinking is not the desired outcome of the conjugation, ANXA5 requires trimer formation for internalization, and this small portion of dimerized ANXA5 may aid in protein internalization into the cell.

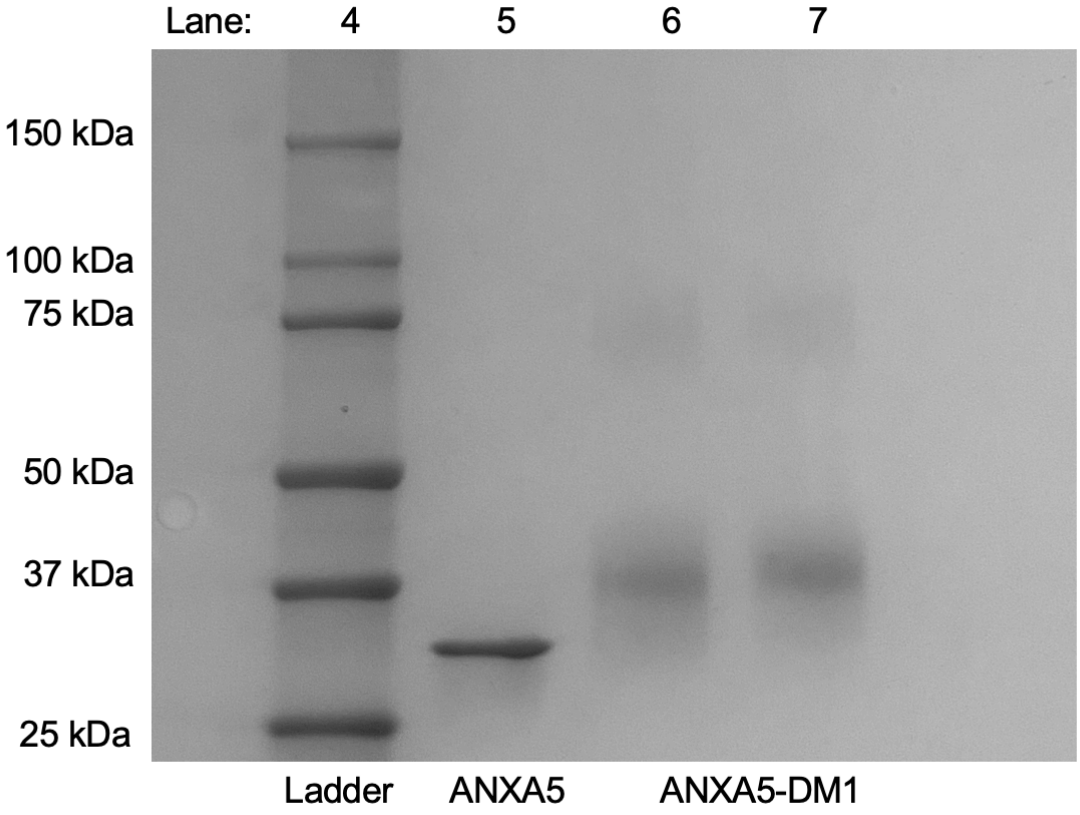

Figure 24: SDS page of ANXA5-DM1 conjugate

ANXA5-DM1 shows a mass increase consistent with 6 ± 3 molecules of DM1 added to each protein in lanes 6 and 7. Lane 5 has unconjugated ANXA5 as a control.

Denaturing intact mass analysis further confirmed drug loading. Denaturing intact mass analysis was completed by Dr. Aaron Bailey at the University of Texas Medical Branch. The mass analysis of ANXA5 showed the protein ANXA5 exists as isobaric isomers, meaning the protein has two distinct species with the same nominal mass but different exact masses as determined by the retention time. The isomer's retention time differs by 1.6 minutes (**Appendix A, Figure 68**), and the mass only differs by 21.07 Da. Additionally, our ANXA5 protein differs from the NCBI protein database (accession number NP_001145.1) by 21 Da (**Figure 25**). This mass change is most likely due to a substitution of histidine (H) to asparagine (N) and a loss of another H. H-to-N substitutions are one of the most common mutations of wild-type amino acids [207]. Additionally, when examining H to N substitutions at the structural level, this substitution typically does not impact the secondary structure, especially alpha-helices [207]. The ANXA5 family is defined by the ANXA5 core domain which consists of five alpha helices, meaning this mutation probably does not impact the structure and function of the ANXA5 protein [43, 44].

By deconvoluting the ANXA5-DM1 conjugate in the mass range of 35-45 kDa, a left-shifted bell curve distribution of ANXA5-DM1 is observed (**Figure 26**). Each linker and drug add 975 Da to the weight of the protein, and the ANXA5-DM1 conjugate had a range of 1 to 8 linker(s) and drug(s) added. The weighted average of the drug-to-protein ratio was obtained using ReSpect and sliding windows algorithms. The weighted average of the conjugate was 3.9 molecules of DM1 to 1 molecule of ANXA5, which is within the range previously found with SDS-PAGE. The intact mass analysis further verified the makeup of the ANXA5-DM1 conjugate and confirms the conjugate is readily reproducible.

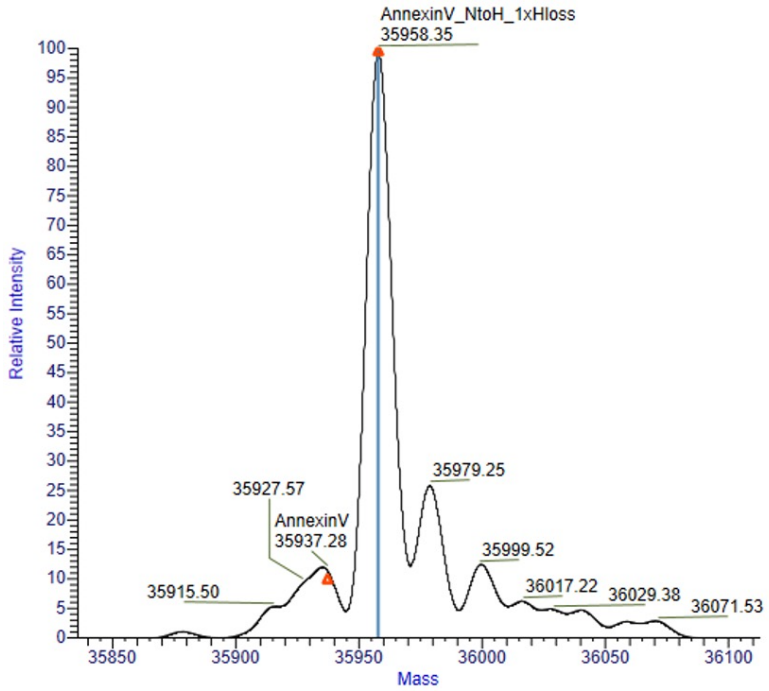

Figure 25: ANXA5 mass intensity

ANXA5 exists as two isobaric isomers and differ by 21.07 Da.

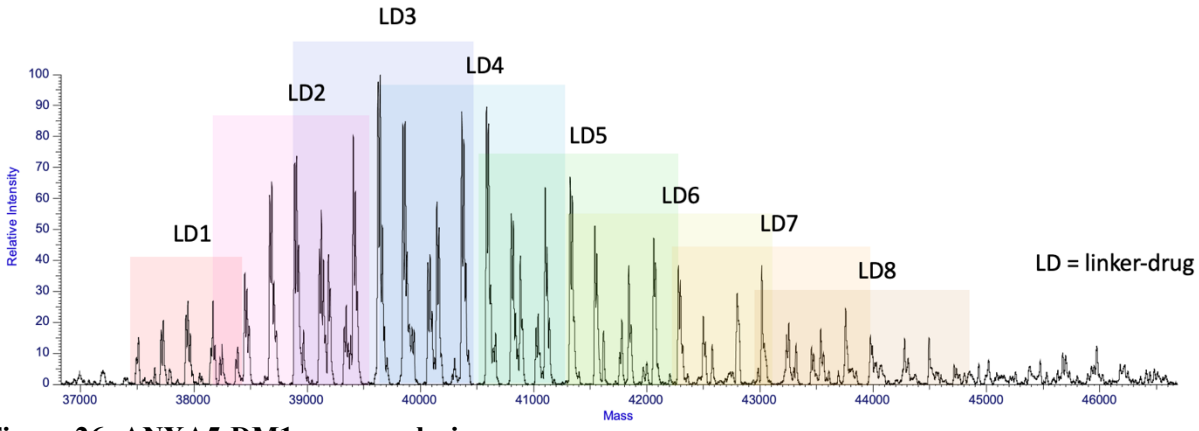

Figure 26: ANXA5-DM1 mass analysis

Drug to protein ratio was calculated as weighted average of deconvoluted spectra using ReSpect and sliding windows algorithms. Each linker-drug adds 957 Da indicated by the pastel boxes. Weighted average of ANXA5-DM1 was 3.8 molecules of DM1 to 1 molecule of ANXA5.

ANXA5 Binding

Colorimetric binding

To confirm the ability of the ANXA5 to bind to PS on the surface of TNBC cells, equilibrium binding experiments with increasing concentrations of biotinylated ANXA5 were used. Initially, biotinylation of the ANXA5-DM1 was attempted but, a low biotinylation level of the protein was observed. Because biotinylation of the protein also utilizes the primary amines (lysine residues), biotin loading was hindered by the previous addition of the drug. To overcome this, ANXA5 was labeled with biotin, and DM1 was omitted for binding studies. Although DM1 was omitted from binding studies, biotin acts as a placeholder for the drug because it utilizes the same residues for conjugation and confirms that the lysine resides are not necessary for protein binding. For all binding studies, 4-7 molecules of biotin were loaded onto 1 ANXA5 protein, which is equivalent to the loading of DM1 onto ANXA5.

Cells were treated with 0-20 nM of ANXA5, and total, non-specific, and specific binding were obtained. Total binding was obtained by supplementing 0.5% BSA with 2 mM Ca^{2+} to promote ANXA5 binding. Non-specific binding was obtained by supplementing 0.5% BSA with 5 mM EDTA, a calcium-chelating agent. The EDTA removes excess calcium and inhibits ANXA5 binding. Specific binding was obtained by subtracting non-specific binding from total binding. The dissociation constant (K_d) was obtained using GraphPad Prism 9 software using nonlinear regression of binding saturation of one site.

After subtracting out 0 nM ANXA5 background absorbance, the non-specific binding was essentially 0, meaning ANXA5 was not binding to the EMT6 and 4T1 cells (**Figure 27 a/b**). The

total and specific binding were nearly identical indicating the binding of ANXA5 to PS is calcium-dependent (**Figure 27 a/b**). The dissociation constants are given in **Table 1**. The K_d is an equilibrium constant that measures when 50% of the binding sites (PS) are occupied by the protein (ANXA5). The smaller the K_d, the less protein is needed to occupy the binding sites and indicates a high affinity for the ligand. In the case of cancer treatment, it is beneficial to have antibody/protein drug conjugates with high affinity and specificity to the cancer cells while sparing healthy cells.

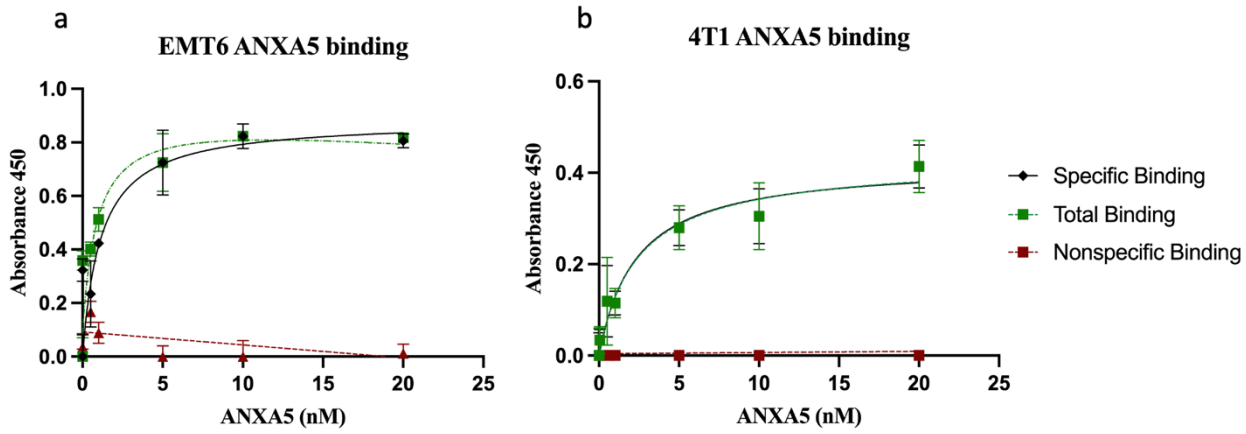

Figure 27: Binding strength of ANXA5 on TNBC with PS externalization

a) EMT6 and b) 4T1 cells were incubated with 0-20 nM of ANXA5. Total binding (green square with dot-dash line) was measured with the addition of 2 mM Ca^{2+} to promote ANXA5 binding. Nonspecific binding (red triangle with dashed line) was measured with the addition of EDTA to chelate residual Ca^{2+}, inhibiting ANXA5 binding. Specific binding (black square with solid line) was obtained by subtracting nonspecific binding from total binding. The dissociation constant of the specific binding was 1.14 nM for EMT6 cells and 2.31 nM for 4T1 cells. Data presented as mean ± SD (n = 3).

Table 1: ANXA5 dissociation constants on 4T1 and EMT6 cell lines

Cell line	Dissociation Constant (K_d)
4T1	2.31 nM
EMT6	1.14 nM

Flow cytometry calcium dependence

To further validate ANXA5-PS calcium dependence, flow cytometry was utilized. Flow cytometry analysis was conducted on EMT6 and 4T1 with 13 nM of ANXA5-FITC, in the presence of calcium (to promote binding) or EDTA (to inhibit binding). The concentration of 13 nM of ANXA5 is a PS-saturating amount as established by our colorimetric binding assays. The presence of calcium significantly increased ANXA5-FITC binding to EMT6 and 4T1 cells as indicated by median fluorescent intensity when compared to EDTA-treated cells (**Figure 28**). The presence of calcium increased binding by 2 to 4.7 times for EMT6 and 4T1 cells, respectively. Additionally, the presence of calcium shifts the ANXA5-FITC histogram to the left in comparison to the unstained and EDTA curves (Appendix A**, Figures 69 and 70**). In comparison to our colorimetric binding assay which allows for 2 hours for binding, this flow cytometry protocol limited binding to 15 minutes. While binding time was decreased by 8 times, there is still a significant increase in ANXA5-FITC binding to the surface of the cell. This indicates the binding of ANXA5 to external PS is fast and specific when calcium is present.

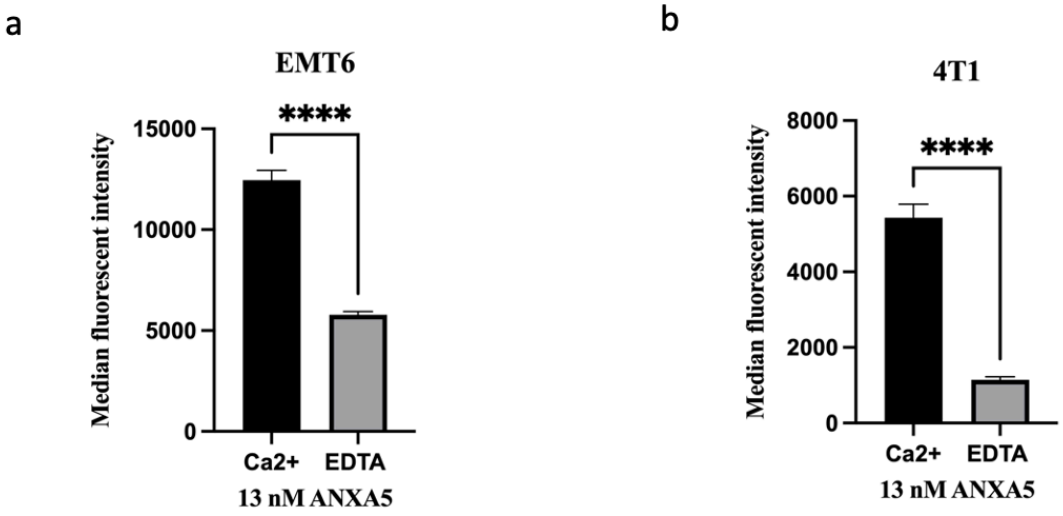

Figure 28: Flow cytometry analysis of the effects of calcium of ANXA5-PS binding

The binding of ANXA5 to PS on a) EMT6 and b) 4T1 cell membranes is calcium-dependent. TNBC cells were incubated with ANXA5-FITC (13 nM) for 15 minutes at room temperature and then analyzed via flow cytometry. When calcium is chelated with EDTA, ANXA5 binding is significantly decreased. Statistical analysis was performed with a student's T-test with data represented as mean ± SD (n = 3). Statistical significance is denoted by ****($p < 0.0001$).

ANXA5 binding in suspension

To compare ANXA5-PS binding on cancerous cells to healthy cells, a fluorescent in suspension binding assay was conducted. EMT6, 4T1, and MCF10A healthy mammary cells were incubated with 13 nM of ANXA5 for 5 minutes in the presence of calcium to promote binding. While both cancer cells had an increase in relative fluorescent intensity, 4T1 cells had significantly more ANXA5 binding than both EMT6, and MCF10A cells (**Figure 29**). Because high PS extracellular exposure on cancer cells has been associated with more aggressive and metastatic tumors, it is unsurprising that the most metastatic and aggressive tumor model had the highest ANXA5 binding

[14]. It is also important to note that the ANXA5 binding studies utilize a human ANXA5 protein on both human and murine cell lines, indicating the human ANXA5 binds to PS on murine cells in an extremely fast and specific manner in addition to human cells.

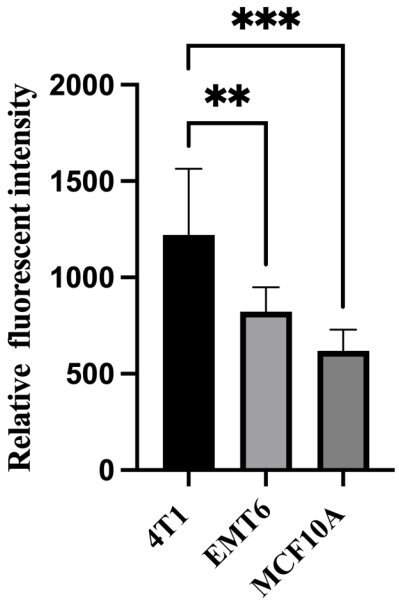

Figure 29: ANXA5-PS binding comparison for murine TNBC and MCF10A healthy human mammary cells

4T1 cells have significantly more ANXA5 binding than EMT6 and MCF10A cells. TNBC and MCF10A cells were incubated with ANXA5-FITC (13 nM) for 5 minutes at room temperature and then analyzed in suspension for relative fluorescent intensity. Statistical analysis was performed with a one-way ANOVA with Tukey's multiple comparisons with data represented as mean ± SD (n = 6-9). Statistical significance is denoted by **($p < 0.0021$) and ***($p < 0.0002$).

Binding Stability

The binding stability of ANXA5 was determined in the presence of calcium over two days (**Figure 30**) [208]. EMT6 displayed excellent stability on day 1. The cells had 100% more protein bound on day 1 in compared to day 0, but a steep drop off was observed on day 2 with less than 20% of the original ANXA5 protein present. For 4T1 cells, ANXA5 binding was more consistent with a small drop off to 50% on day 1 and followed by an increase back to 100% on day 2. This data suggests that a higher amount of ANXA5 is needed for internalization on EMT6 than in comparison to 4T1 cells. However, both cells had ANXA5 present after 48 hours of incubation, indicating ANXA5 can remain in solution or bound to cells for an extended duration of time.

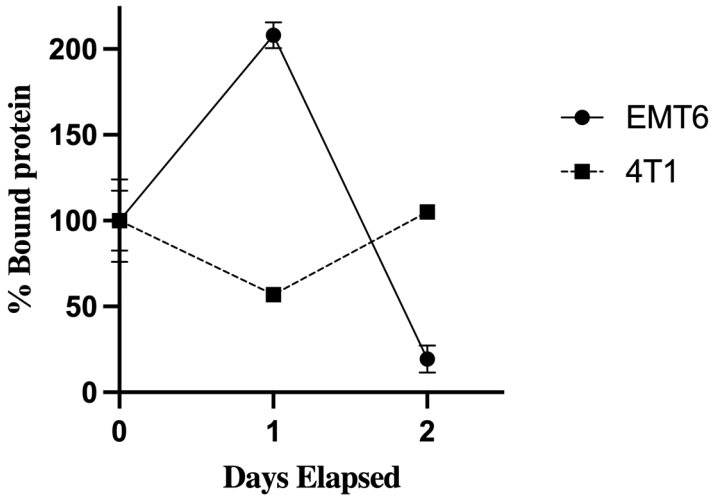

Figure 30: Binding stability of ANXA5 over 2 days for EMT6 and 4T1 cell lines

Cells were seeded with 100 nM of ANXA5 for 0-2 days. At each day ANXA5 binding was quantified by absorbance and day 0 was normalized to 100%. EMT6 cells had a 100% increase in ANXA5 binding on day 1 followed by a steep drop off by day 2. 4T1 cells had a small drop off to 50% on day 1 and by day 2 ANXA5 binding returned to 100% (n = 6).

Flow cytometry analysis for confluency mediated PS exposure

The next goal was to determine how to model healthy cell PS exposure *in vitro*. Previous work by Brent Van Rite and John Krais has determined that when healthy vascular cells (HAAE-1) are grown to 100% confluency, PS externalization is decreased which mimics healthy vasculature [209, 210]. To validate this finding, flow cytometry was used to measure the median fluorescent intensity of ANXA5-FITC binding to confluent and non-confluent HAAE-1, MCF10A, and EMT6 cells. The median fluorescent intensity was calculated by subtracting the median fluorescent intensity of unstained cells from the median fluorescent intensity of ANXA5-FITC stained cells in the presence of calcium. Cells were stained with 13 nM of ANXA5-FITC to saturate external PS on the cell surface as established by the colorimetric binding assay.

For the TNBC cell line EMT6, confluency did not impact ANXA5-FITC binding to exposed PS (**Figure 31a**). However, confluency did impact healthy vascular and mammary cells ANXA5-PS binding. When HAAE-1 and MCF10A cells are non-confluent, ANXA5-FITC binding is 1.4 and 4.3 times more as determined by the median fluorescent intensity in comparison to confluent cells (**Figure 31 b and c**). This finding suggests PS externalization on healthy vascular and mammary cells is contact-dependent. The confluent HAAE-1 and MCF10A cells mimic healthy vasculature and mammary epithelium by decreasing PS externalization. This provides a model for both healthy and cancerous vasculature and epithelium to test the cytotoxicity of the conjugate. Moving forward, all healthy cell cytotoxicity studies will have cells grown to confluency to mimic PS exposure *in vivo.*

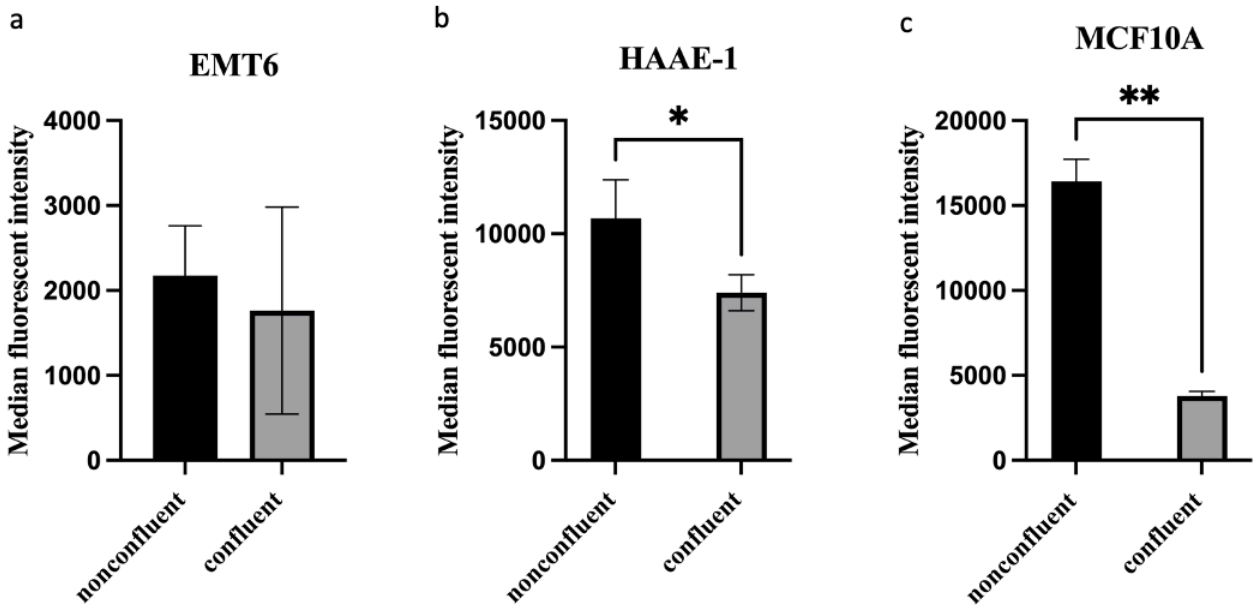

Figure 31: Confluency effects of ANXA5-PS binding to TNBC and healthy cells

a) Confluency does not impact ANXA5 binding to TNBC EMT6 cells. Confluent healthy cells b) HAAE-1 and c) MCF10A cells have significantly less ANXA5 binding to the cell surface. Cells were grown to 50-70% confluency (nonconfluent) or 90-100% confluency (confluent) and incubated with 13 nM of FITC-labeled ANXA5 for 15 minutes at room temperature and then analyzed via flow cytometry. Statistical analysis was performed with a student's T-test with data represented as mean ± SD (n = 2-3). Statistical significance is denoted by *($p < 0.033$) and ** ($p < 0.0021$).

ANXA5 *In Vitro* Cytotoxicity

To ensure DM1 is causing the cytotoxic action of the conjugate, cytotoxicity studies of ANXA5 were carried out on TNBC cells (EMT6 and 4T1), as well as, healthy vascular (HUVEC and HAAE-1) and mammary (MCF10A) cells. Cells were treated with 0-0.7 μM of ANXA5. Cells were treated on day 1 and incubated with the conjugate for 72 hours. After 72 hours, cell viability was analyzed via a fluorescent Alamar Blue assay. Percent viability was determined by

normalizing the control (0 μM ANXA5) to 100% and comparing each treatment group to the control (n = 3-5).

The cytotoxic effects of ANXA5 against five different cell lines are shown in **Figure 32**. The presence of ANXA5 on two TNBC and three healthy cell lines did not significantly impact viability with doses up to 0.7 μM. The inhibitory concentration of 50 percent (IC50) protein equivalent for ANXA5 in the ANXA5-DM1 conjugate is 0.052 nM [133]. The highest dose of 0.7 μM ANXA5, is nearly 13,460 times more protein than found in the ANXA5-DM1 concentration that induces 50% cell death for TNBC cells. These findings are not surprising given the fact that ANXA5 has a protection function for both healthy and cancerous cells.

Umbilical cells have high ANXA5 protein content, and the presence of ANXA5 is necessary for forming the maternal-fetal interface during pregnancy [211, 212]. ANXA5 also binds to syncytiotrophoblasts (human placenta cells) to prevent coagulation, maintains blood flow to the placenta, and aids in membrane resealing of trophoblasts [212-214]. Additionally, ANXA5 is an anticoagulant protein that competes with the prothrombin complex and prevents it from binding to PS, ultimately preventing coagulation and decreasing vascular inflammation [212, 215]. ANXA5 has a protective function on umbilical cells, placental cells, developing trophoblasts, and vascular cells and explains why healthy vascular cell viability was not impacted by increasing ANXA5 concentration. On the other hand, ANXA5 is overexpressed in breast cancer, cervical colorectal cancer, hepatocellular carcinoma, non-small cell lung cancer, and renal cell carcinoma and aids in tumorigenesis, metastasis, progression, and survival [216-221]. This suggests ANXA5 may act as an oncogenic protein, and the TNBC cells were not impacted by increasing ANXA5 concentration. These findings also suggest that ANXA5 is a nontoxic protein, and the cytotoxic action of the ANXA5-DM1 conjugate is a result of the addition of the drug to the protein and not ANXA5 alone.

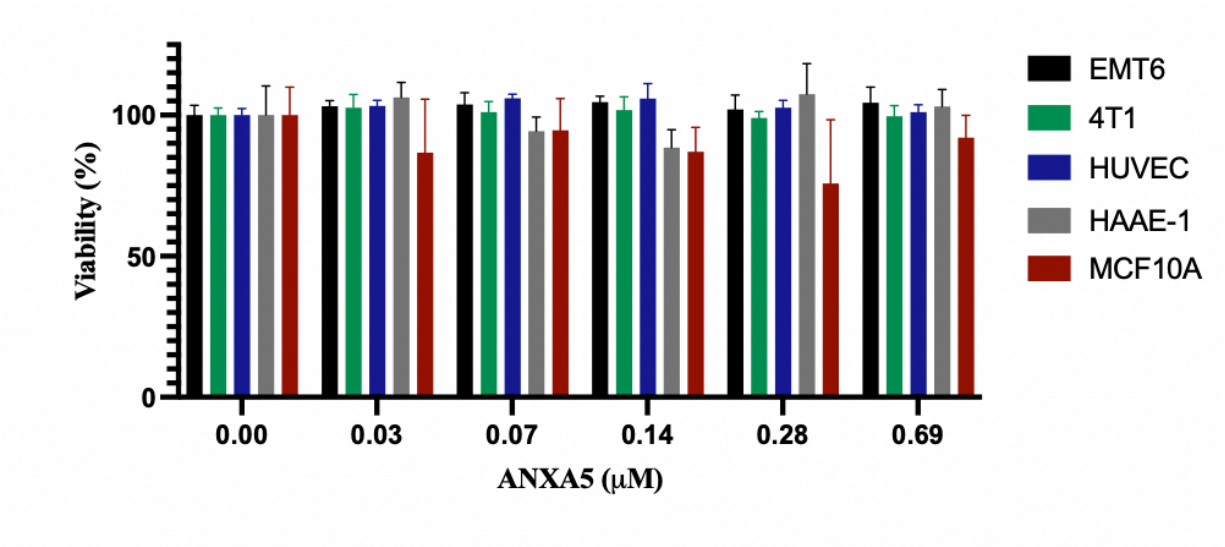

Figure 32: 72-hour cytotoxic effects of ANXA5 on cancerous and healthy cell lines

EMT6, 4T1, HUVEC, HAAE-1, and MCF10A cells were incubated with 0-0.7 μM of ANXA5 for 72 hours. Viability was determined by an Alamar Blue assay, and each sample was represented as a percentage of the untreated control (0 μM). Data represented as mean ± SD (n = 3-5).

ANXA5-DM1 TNBC Cytotoxicity Validation

Previously, Ben Southard established the ANXA5-DM1 conjugate to have an IC50 value of 0.21 nM for EMT6 cells [133]. To validate this finding, EMT6 cells were treated with 0 to 100 nM of DM1 in the ANXA5-DM1 conjugate. Cells were treated on day 0 and incubated with the conjugate for 72 hours. After 72 hours, cell viability was analyzed via a fluorescent Alamar Blue assay. Percent viability was determined by normalizing the control (0 uM DM1) to 100% and comparing each treatment group to the control (n = 3).

ANXA5-DM1 has significant cytotoxic effects on EMT6 cells at doses below 1 nM after 72 hours of treatment (**Figure 33**). When comparing two determinations of the IC50 to that obtained by Ben Southard, both readily reproduce an IC50 value below 1 nM as shown in **Table 2**. ANXA5-DM1 has very similar IC50 values to the antibody-drug conjugate consisting of trastuzumab, a HER2-targeting antibody, linked to DM1 (T-DM1). T-DM1 displayed high cytotoxicity against HER2+ amplified cell lines (SK-BR-3 and BT-474) with IC50 values of 0.22 nM and 4.26 nM after 72 hours [222]. However, an IC50 value could not be obtained for MCF7 cells which have normal HER2 expression, indicating T-DM1 treatment is only beneficial for cancer cells with an over-expression of HER2.

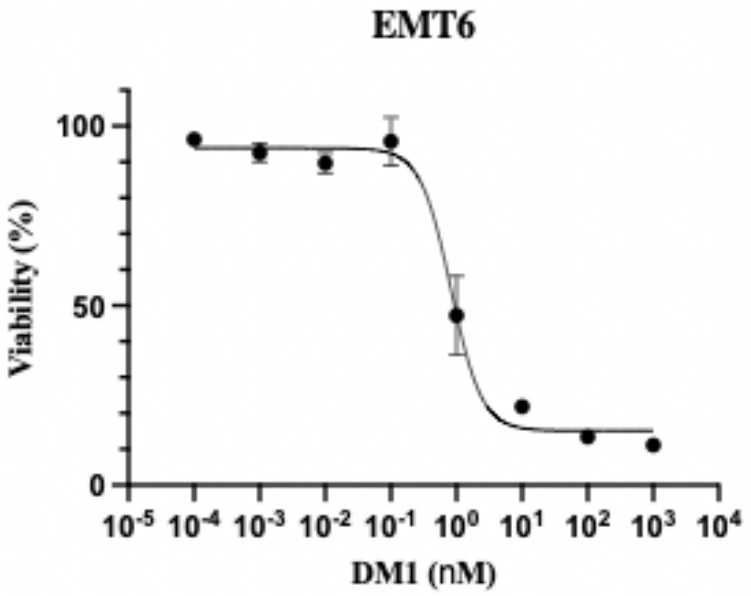

Figure 33: Validation of ANXA5-DM1 cytotoxicity on EMT6 cells

The IC50 concentration of ANXA5-DM1 for EMT6 cells is 0.41 nM. Cells were treated on day 0 and incubated with free ANXA5 in fully supplemented growth medium with 2 mM of calcium for 72 hours. Viability was determined by the Alamar Blue assay, and each sample was represented as a percentage of the untreated control. Data is represented as mean ± SD (n = 3).

Table 2: IC50 values of ANXA5-DM1

ANXA5-DM1 sample	IC50
1 (Ben Southard)	0.21 nM
2	0.82 nM
3	0.20 nM
Average	0.41 ± 0.35 nM

T-DM1 induces cell death in two ways, first by antibody-mediated effects and second by drug-mediated effects. Trastuzumab targets the HER2 receptor to prevent HER2-HER2 dimerization and ultimately inhibits the activation of the intracellular tyrosine kinase and downstream signaling of phosphatidylinositol 3-kinase (PI3K)–AKT–mammalian target of rapamycin (mTOR) and RAS–mitogen-activated protein kinase (MAPK) signaling pathways, decreasing proliferation, cell mobility, invasiveness, and cell survival [105, 223]. After Trastuzumab binds to HER2, the antibody-drug conjugate is internalized through receptor-mediated endocytosis. The endosome fuses with a lysosome, causing lysosome degradation of the antibody and allowing active transport of DM1 into the cytoplasm, where it inhibits microtubule polymerization and the cell undergoes apoptosis [105]. Although T-DM1 significantly improves patient outcomes, nearly every patient treated with T-DM1 develops resistance over time through reduced HER2 expression, T-DM1 recycling, and/or an increase in drug efflux transporters [105, 224].

ANXA5 may be a better delivery vehicle than Trastuzumab because ANXA5 does not impact cell viability or signaling and has a direct degradation route. Trastuzumab and T-DM1 induce the same amount of antibody-dependent cell-mediated cytotoxicity for HER2-expressing

cells [225]. ANXA5 does not induce cell death, and a more predictable drug-mediated cell death can be observed. ANXA5 also does not impact cell signaling, which limits the cancer cell's ability to dysregulate or mutate signaling pathways to promote cancer-specific survival. ANXA5 internalization is non-receptor mediated, and the protein will not be salvaged or recycled.

ANXA5 does not possess an Fc domain like antibodies, so it cannot interact with an Fc receptor (FcRn). When antibodies are bound to the FcRn, the antibody is salvaged and recycled. The antibody will not undergo lysosomal degradation, and the drug will not be released into the cell [226]. However, when molecules are not bound to an FcRn, the unbound molecules, like ANXA5, are transported to the lysosome for lysosomal degradation, ultimately releasing the drug to induce apoptosis [226]. ANXA5 solely acts as a delivery vehicle and helps to restrict the ability of cancer to mutate as opposed to Trastuzumab.

Seeding Density Effects on ANXA5-DM1 Cytotoxicity

ANXA5-DM1 has proven to be a reliable anticancer agent that induces significant cell death under 1 nM after 72 hours, but the effects of cell seeding density and ANXA5-DM1 have yet to be explored. EMT6 cells were seeded at either 5,000 or 10,000 cells per well and treated with 0 to 10 nM of DM1 in the ANXA5-DM1 conjugate for 24 hours. Cells were treated on day 0 and incubated with the conjugate for 24 hours. After 24 hours, cell viability was analyzed via a fluorescent Alamar Blue assay. Percent viability was determined by normalizing the control (0 nM DM1) to 100% and comparing each treatment group to the control (n = 3).

ANXA5-DM1 induced significantly more cell death at doses of 0.1-10 nM for cells seeded at 5,000 cells per well versus 10,000 cells per well (**Figure 34**). The IC50 value for 5,000 cells per well was 0.033 nM and the IC50 for 10,000 cells per well was 0.15 nM. When cells are seeded at 12,000 cells per well, an IC50 value for ANXA5-DM1 could not be obtained after 24 hours of

treatment, but after 72 hours of treatment, the IC50 was found to be 0.21 nM [133]. The cells seeded at 5,000 cells per well needed 4.5 times less drug to induce 50% cell death than cells seeded at 10,000 cells per well, suggesting cell density impacts the cytotoxic action of the ANXA5-DM1 conjugate. Similar trends for free DM1 were observed, but the IC50 value for the free drugs could not be obtained at these doses (**Appendix A, Figure 72**).

Although the loss of contact inhibition is a hallmark of cancer, higher cell density alters cell signaling, growth, and metastasis. For TNBC, when cells are seeded at a high density, the invasion of cancer into an epithelial monolayer *in vitro* and lung metastases *in vivo* is decreased [227-229]. Cell aggregation proportionally increases as with cell density [230]. Cell aggregation provides a "dilution effect", where one cell may act as a sink for the chemotherapy to spare the entire population, or the entire cell aggregation will absorb a small amount of the chemotherapy, keeping the drug concentration to a sublethal amount [231]. Additionally with more cells present, the demand for resources also increases. Higher seeding density causes nutrient depletion, and chemotherapeutic drugs have been shown to induce autophagic protein and lysosomal enzymes in as little as 48 hours after initial seeding [232, 233]. Interestingly, autophagic activity decreases during mitosis [234]. When cells are seeded at higher seeding densities, the cells are not actively dividing. Because DM1 is a microtubule inhibitor, it will only induce cell death in cells that are actively dividing. While higher seeding densities may 1) impact cell invasion/metastases, 2) provide dilution effects, and 3) induce autophagy, there are very few studies that compare starting cell density to growth characterization of the cells, so more work in this area is needed to fully understand how seeding densities effect targeted chemotherapy [235]. However, this may indicate that the ANXA5-DM1 conjugate would be better suited for early-stage intervention when tumors are not as burdened by nutrient and space depletion.

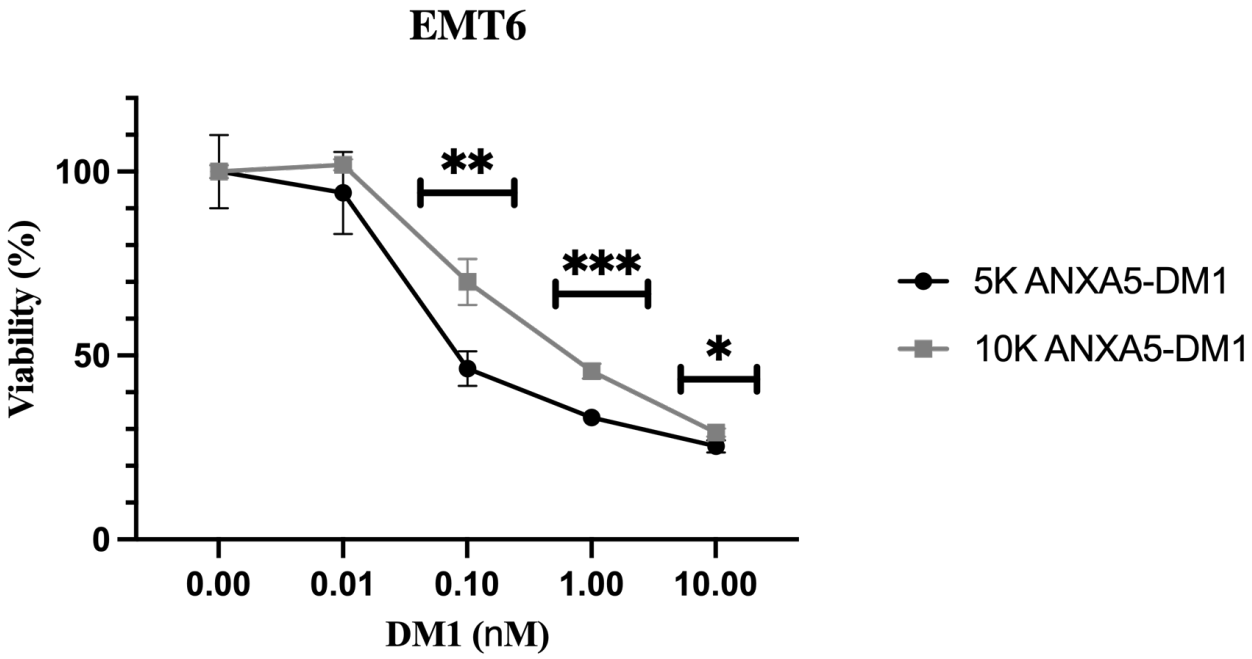

Figure 34: 24 hour Seeding density effect for ANXA5-DM1 on EMT6 cytotoxicity

The IC50 for cells seeded with 5k cells per well was 0.033 nM, and the IC50 for cells seeded at 10k cells per well was 0.15 nM. EMT6 cells were seeded at 5k or 10k cells per well and treated with 0-10 nM DM1 in the ANXA5-DM1 conjugate in fully supplemented growth medium with 2 mM calcium. Cell viability was measured via an Alamar Blue assay, and each sample was represented as a percentage compared to the untreated control (0 nM) after 24 hours. Statistical analysis at each dose was performed with a student's T-test with data represented as mean ± SD (n = 3). Statistical significance is denoted by *($p < 0.033$), **($p < 0.0021$), and *** ($p < 0.0002$).

ANXA5-DM1 Healthy Cell Cytotoxicity

Previously, Ben Southard established the ANXA5-DM1 conjugate to have enhanced cytotoxicity against murine TNBC cells when compared to free DM1. The IC50 values of the TNBC cells are summarized in **Table 3**. By conjugating DM1 to ANXA5, the conjugate was 130 to 377 times more effective at inducing cell death than the free drug after 72 hours [133]. While the cytotoxic activity of the ANXA5-DM1 conjugate is excellent against TNBC cells, the cytotoxicity of the conjugate must be quantified for healthy mammary and vasculature cells.

Table 3: ANXA5-DM1 and DM1 IC50 values for 4T1 and EMT6 cells.

Cell line	ANXA5- DM1 IC50	DM1 IC50	IC50 Ratio
4T1	0.85 nM	320 nM	377
EMT6	0.21 nM	28 nM	130

ANXA5-DM1 cytotoxicity studies were carried out on confluent healthy vascular (HAAE-1 and HUVEC) and mammary (MCF10A) cells with varying concentrations of ANXA5-DM1. Cells were grown to confluency because they mimic PS expression *in vivo* (**Figure 31**). Cells were treated with 0-10 μM of DM1 in the ANXA5-DM1 conjugate or free DM1. Cells were treated on day 0 and incubated with the conjugate for 72 hours. After 72 hours, cell viability was analyzed via a fluorescent Alamar Blue assay. Percent viability was determined by normalizing the control (0 μM DM1) to 100% and comparing each treatment group to the control (n = 3-6).

The cytotoxicity of MCF10A, HAAE-1, and HUVEC cells are shown in **Figures 35-37**. The ANXA5-DM1 conjugate exhibited 100% cytotoxicity at 1 μM for TNBC cells [133]. When healthy cells are treated with 10 times more drug in the conjugate (10 μM) complete cell death is

not observed. Ten micromolar rendered nearly 20-35% more viability for all healthy cell lines. More importantly, when comparing the IC50 for the TNBC cell lines and the healthy cell lines it takes 5 to 190 times more ANXA5-DM1 conjugate to induce the same amount of death (**Figure 38 and Table 4**), indicating ANXA5-DM1 uptake is limited in the healthy cell lines and less cytotoxicity is observed.

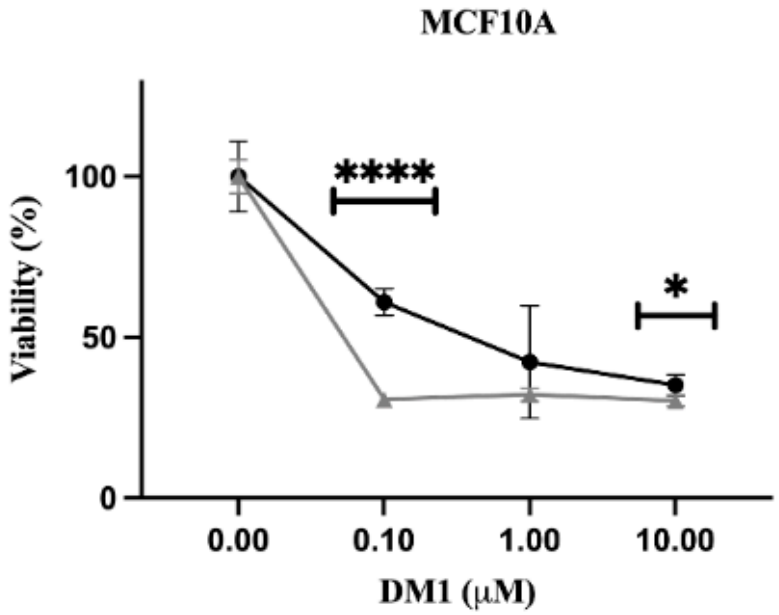

Figure 35: 72-hour effects of ANXA5-DM1 and free DM1 on MCF10A

The IC50 concentration for ANXA5-DM1 was 77.7 nM and the IC50 concentration of free DM1 was 29.8 nM. MCF10A cells were treated with 0-10 μM DM1 in the ANXA5-DM1 conjugate or free DM1 in fully supplemented growth medium for 72 hours. Cells were grown to 90-100% confluency. Cell viability was measured via an Alamar Blue assay, and each sample was represented as a percentage compared to the untreated control (0 μM) after 72 hours. Statistical analysis at each dose was performed with a student's T-test with data represented as mean ± SD (n = 3). Statistical significance is denoted by *($p < 0.033$) and **** ($p < 0.0001$).

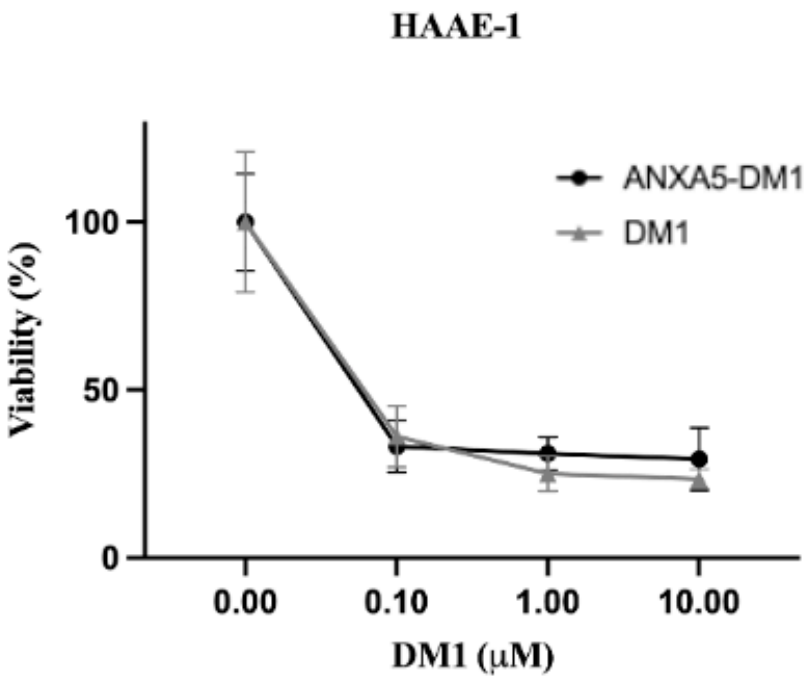

Figure 36: 72-hour effects of ANXA5-DM1 and free DM1 on HAAE-1 viability.

The IC50 concentration for ANXA5-DM1 was 33.9 nM and the IC50 concentration of free DM1 was 44.7 nM. HAAE-1 cells were treated with 0-10 μM DM1 in the ANXA5-DM1 conjugate or free DM1 in fully supplemented growth medium for 72 hours. Cells were grown to 90-100% confluency. Cell viability was measured via an Alamar Blue assay, and each sample was represented as a percentage of the untreated control (0 nM) and viability was compared to the control (0 μM) after 72 hours (n = 3). No statistical significance between ANXA5-DM1 and free DM1 was observed.

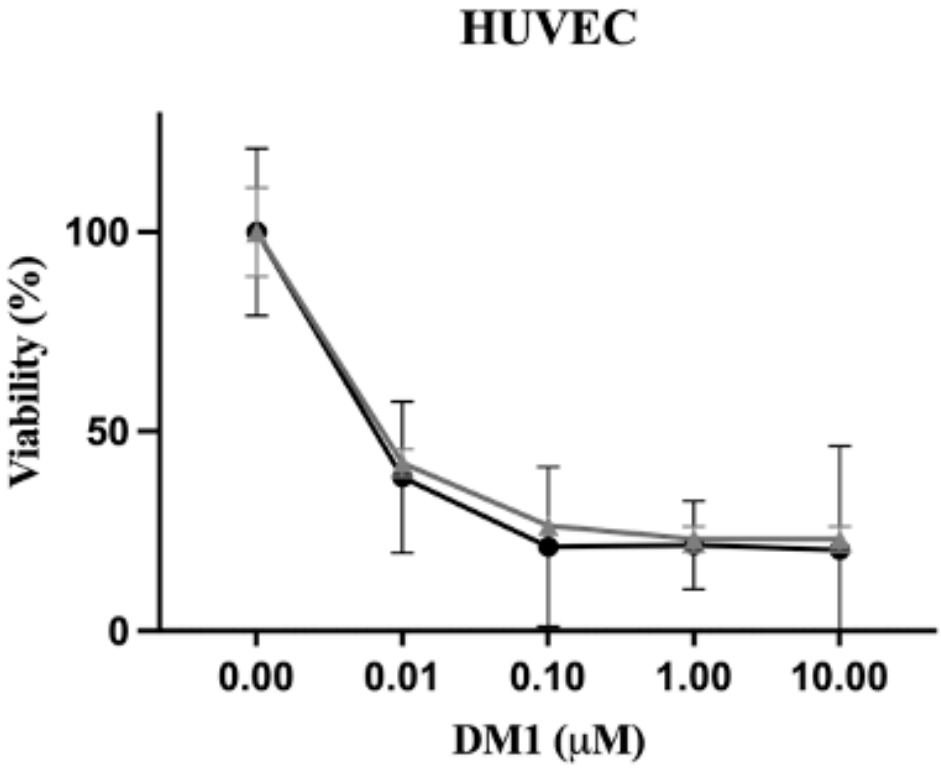

Figure 37: 72-hour effects of ANXA5-DM1 on HUVEC viability

The IC50 is 4.0 nM for ANXA5-DM1 and 5 nM for free DM1. HUVEC cells were treated with 0-10 M DM1 in the ANXA5-DM1 conjugate or free DM1 in fully supplemented growth medium. Cells were grown to 90-100% confluency. Cell viability was measured via an Alamar Blue assay and viability was compared to the control (0 μM) after 72 hours. Data represented as mean ± SD (n = 3). No statistical significance was observed.

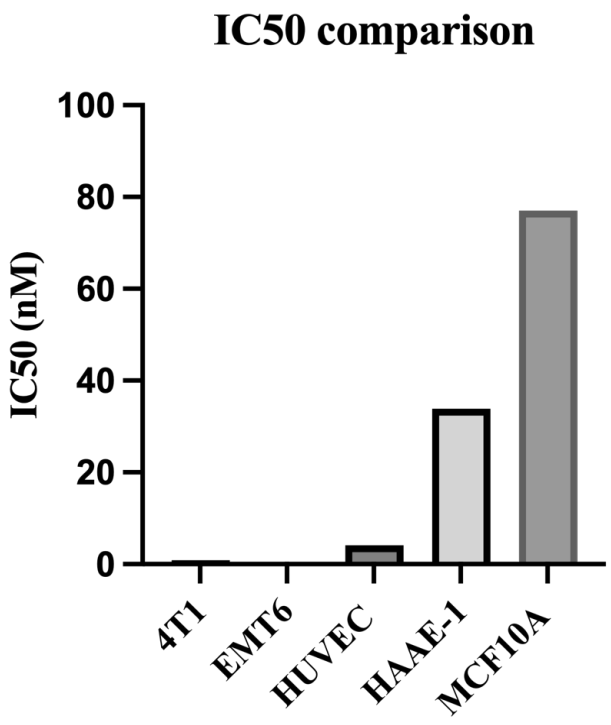

Figure 38: IC50 comparison for TNBC and healthy cells.

The IC50 value of the TNBC cells are 5 to 190 times less than the healthy cell lines.

Table 4: Summary of ANXA5-DM1 cytotoxicity for TNBC and healthy vascular and mammary cells.

Cell line	Cell type	IC50 (nM)
4T1	Murine TNBC	0.85
EMT6	Murine TNBC	0.41
HUVEC	Healthy Human Umbilical Venule Epithelium	4.1
HAAE-1	Healthy Human Aorta	33.9
MCF10A	Healthy Human Mammary Epithelium	77.7

While it was not expected to observe cell death in the healthy cell lines, the cell death observed by the ANXA5-DM1 conjugate is most likely a result of a low PS expression and a positive stress feedback loop. PS is almost exclusively found on the inner cytosolic leaflet of healthy cells, but there is still minimal PS extracellular exposure. The binding of ANXA5 to PS is very rapid, but more importantly, once bound to the surface of PS-expressing cells, the ANXA5-PS bond is stable for up to 2 days (**Figure 30**) [209]. Once bound, ANXA5 is internalized, which brings DM1 into the cell, where it can induce cell stress. When cells become stressed, more PS becomes externalized which allows for the recruitment of more ANXA5-DM1 into the cell to induce cell death, rendering a positive feedback loop [192].

ANXA5-DM1 Immunogenic Cell Death

It is well known that DM1 induces apoptosis through mitotic catastrophe, but recently, antibody-drug conjugates containing maytansinoids have shown to be a powerful immune modulator by inducing immunogenic cell death (ICD) [131]. To assess ANXA5-DM1 as an ICD inducer, ATP release and calreticulin surface expression were analyzed for EMT6 cells. An Alamar Blue assay was run in tandem with the ICD assays to quantify cytotoxicity alongside ICD (**Figure 39**). EMT6 cells were treated with 10 nM of DM1 in the ANXA5-DM1 conjugate or free DM1 for 24 hours. After 24 hours, ATP release was analyzed through a luminescent luciferin/luciferin assay, and surface calreticulin expression was quantified via flow cytometry.

At 10 nM, ANXA5-DM1 significantly increased ATP release and calreticulin surface expression (**Figure 39 a/b**). ANXA5-DM1 caused nearly 10 times more ATP released than free DM1 (**Figure 39 a**). Cancer cells require large stores of ATP to undergo constant division, protein production, and cell signaling, so it is unsurprising that the untreated control had essentially 0 ATP

in the extracellular space. Incubation with ANXA5-DM1 also significantly increased calreticulin surface expression in comparison to the untreated control as determined by median fluorescent intensity (**Figure 39 b**). Although both ANXA5-DM1 and free DM1 significantly increased cell death (**Figure 39 c**), free DM1 only increased ATP release but had no effect on calreticulin surface expression. ANXA5-DM1 significantly increased cell death in comparison to free DM1.

When comparing 10 nM of ANXA5-DM1 to 100 nM of a HER2-maytansine antibody-drug conjugate, ANXA5-DM1 was able to significantly increase ATP release by nearly 20 times more and 40 hours sooner with 10 times less drug [131]. It is also important to note, that the HER2-maytansine antibody-drug conjugate caused less ATP release than free maytansine, but the ANXA5-DM1 drug conjugate had the opposite effect. The HER2-maytansine antibody-drug conjugate, only had a loading of 1.8 molecules of maytansine per molecule of antibody, while ANXA5 is loading twice as many drugs per protein. Additionally, ANXA5-DM1 shows superiority in cytotoxicity to both the free drug and the HER2-maytansine antibody-drug conjugate. The HER2-maytansine antibody-drug conjugate requires five days to induce an IC50 value below 1 nM and has an almost identical IC50 value to the free drug. Taken all together, this suggests ANXA5 provides a better vehicle to deliver maytansinoid drugs into the cell, where it can induce cell death by mitotic catastrophe and induce the release of ICD DAMPs.

Ideally, we would have tested for the release of HMGB1 as well, but the price of HMGB1 and related kits were too expensive and hindered testing this ICD DAMP. However, by testing two of the three main DAMPS (ATP release and surface calreticulin expression), it has provided insight into the different stages of ICD. Calreticulin is exposed in the early stages of ICD before apoptotic-mediated PS exposure [123, 236]. In contrast, ATP and HMGB1 are released when the nuclear

and plasma membrane begin to bleb after apoptosis has commenced [123, 237]. All this indicates the ICD by ANXA5-DM1 is quick and efficient.

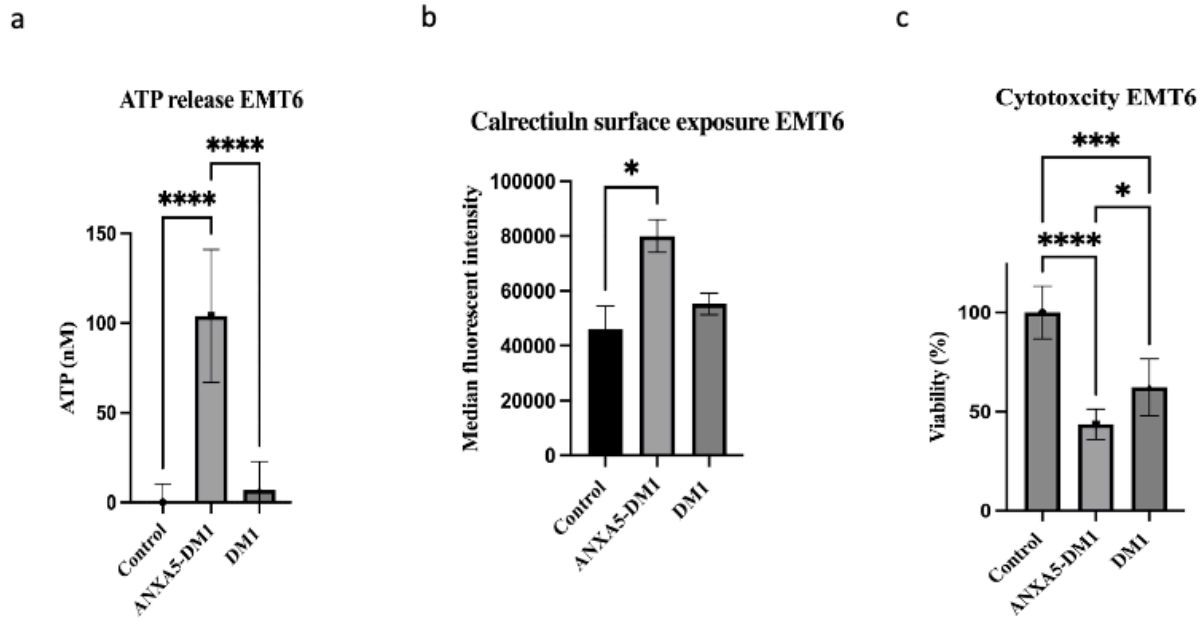

Figure 39: Immunogenic cell death activity of 10 nM ANXA5-DM1 and DM1

EMT6 cells were seeded at 5k per well and treated with 10 nM DM1 in the ANXA5-DM1 conjugate or free DM1 in fully supplemented growth medium for 24 hours. a) 10 nM of ANXA5-DM1 significantly increased ATP release into media in comparison to 0 nM control and free DM1 (n = 6). ATP release was quantified by luminescence, and the amount of ATP present was compared to the standard curve prepared. b) 10 nM of ANXA5-DM1 significantly increased calreticulin surface expression in comparison to the control. Calreticulin surface expression was quantified by flow cytometry with 10,000 gated events (n = 2 with each sample run in triplicate). c) 10 nM of ANXA5-DM1 significantly increased cell death in comparison to free DM1 (n = 3). All statistical analysis was performed with a one-way ANOVA with Tukey multiple comparisons. Data presented as mean ± SD. Statistical significance is denoted by *($p < 0.0332$), **($p < 0.0021$), ***($p < 0.0002$), and **** ($p < 0.0001$).

ANXA5-DM1 Preliminary Dosing

Because ANXA5-DM1 displayed cancer-specific binding and cytotoxicity *in vitro*, ANXA5-DM1 was expanded into a syngeneic mouse model using 4T1 TNBC orthotopic tumors. Mice were treated with intraperitoneal (IP) injections of 0, 0.0025, 0.025, or 0.25 mg/kg of DM1 in the ANXA5-DM1 conjugate once every 7 days for 21 days after tumors reached 3-5 mm in diameter to ensure the tumor was vascularized. The free DM1 controls were omitted because DM1 is extremely toxic and can only be administered when linked to a protein or antibody.

While no treatment significantly increased survival, the treatment had good tumor control (**Figures 40 and 41**). The 0.025 mg/kg dosage had the best tumor control and maintained tumor volume under 150 mm^3 only after two doses (day 22) and resulted in a tumor volume nearly two times smaller than the control. Additionally, this dosage maintained tumor volume under 500 mm^3 throughout the entire treatment. Because only one mouse remained in the control group on day 22, it is impossible to obtain statistical significance for tumor volumes. Interestingly, the highest dose of 0.25 mg/kg, had a steep increase in tumor volume after 2 doses (day 22). This treatment had minimal effect on mouse weight (**Figure 42**).

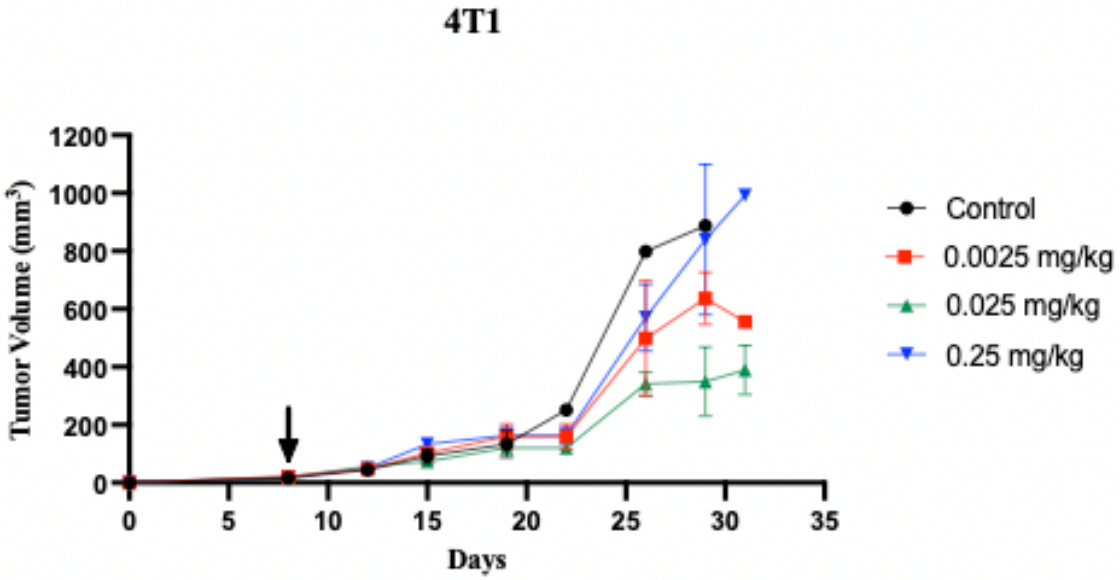

Figure 40: Effect of ANXA5-DM1 on tumor volume for BALB/cJ mice bearing 4T1 tumors

Treatment began on day 7 (indicated by arrow) when mice tumors were 3-5 mm in diameter. Mice were treated IP with 0-0.25 mg/kg of DM1 of the ANXA5-DM1 conjugate once every 7 days for 21 days. No statistical significance was observed due to high standard deviation and uneven sample sizes (n = 4-6).

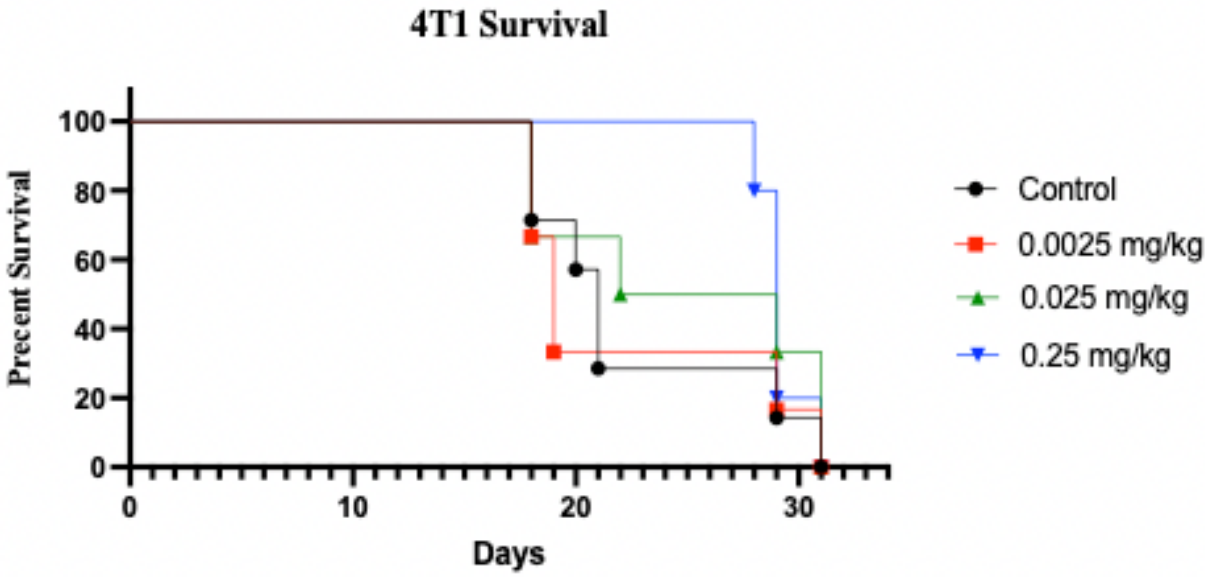

Figure 41: Effect of ANXA5-DM1 on survival for BALB /cJ mice bearing 4T1 tumors

Treatment began on day 7 (indicated by arrow) when mice tumors were 3-5 mm in diameter. Mice were treated IP with 0-0.25 mg/kg of DM1 of the ANXA5-DM1 conjugate once every 7 days for 21 days. Overall survival was the same for all groups, no statistical significance observed (n = 4-6).

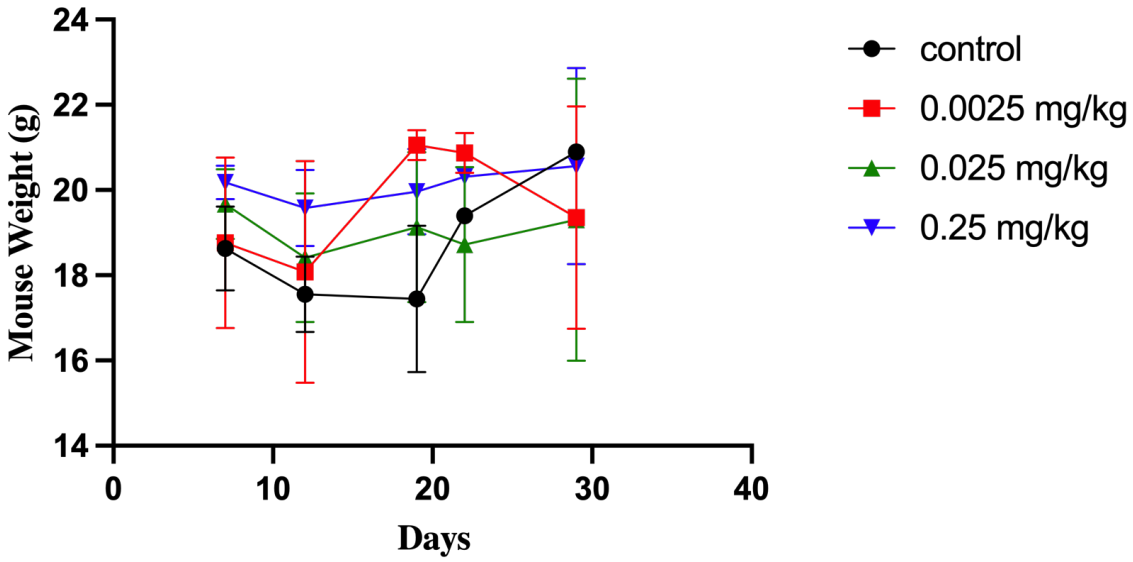

Figure 42: ANXA5-DM1 effects mice weight for BALB/cJ mice bearing 4T1 tumors

Treatment began on day 7 when mice tumors were 3-5 mm in diameter. Mice were treated IP with 0-0.25 mg/kg of DM1 of the ANXA5-DM1 conjugate once every 7 days for 21 days Mice weight was not affected by ANXA5-DM1 treatment (n = 4-6).

ANXA5-DM1 not only targets tumor cells and induces ICD, but also targets the tumor vasculature by cutting off the tumor's nutrient supply. This can promote growth in the presence of hypoxia because of the activation of HIF1-α. Previous *in vivo* analysis using ANXA5-purine nucleoside phosphorylase (ANXA5-PNP) and ANXA5-methionine-γ-lyase (ANXA5-mCGL) fusion proteins (FP), found that the FPs had incomplete tumor killing that resulted in a regrowth of a viable rim of cells around a necrotic core, which coincided with a steep increase in tumor volume, as seen with the 0.25 mg/kg dose of ANXA5-DM1 conjugate after two doses [238]. Additionally, protein affinity for the biomarkers impacts tumor distribution. Antibody-drug conjugates with higher dissociation constants or lower affinity for the ligand of interest can penetrate the whole tumor, whereas antibody-drug conjugates with low dissociation constants or

high affinity for the ligand of interest are mainly localized to the tumor vasculature with lower tumor penetration [239]. The ANXA5-DM1 conjugate was most likely localized to the tumor vasculature, depleting nutrient delivery, and inducing a hypoxic tumor response. But by cutting off the tumor blood supply, the delivery of the ANXA5-DM1 conjugate to the TME would be reduced and renders the therapy ineffective. To combat this, it is necessary to explore a holistic dosing regimen that will counter the hypoxic response (i.e., rapamycin), and aid the activation of the adaptive immune system (i.e., checkpoint inhibiting antibodies) for a multifaceted killing approach (**Figure 43**).

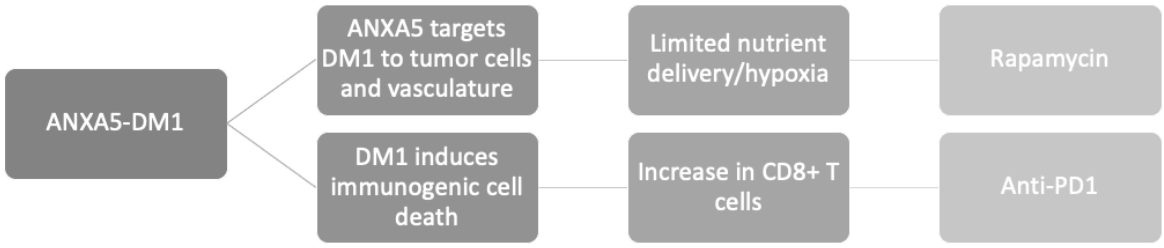

Figure 43: Design rationale for holistic dosing regimen.

ANXA5-DM1 impacts tumor growth in two unique ways. The top branch shows that ANXA5 targets DM1 to both tumor vasculature and tumor cells, which limits nutrient delivery and can induce hypoxia. The growth in the presence of hypoxia can cause activation of hypoxia-inducible factor-1 (HIF-1). Mammalian target of rapamycin (mTOR) inhibitors (i.e., rapamycin,) are thought to reduce angiogenesis by indirectly reducing the synthesis of HIF-1 subunits. The bottom branch shows DM1's ability to activate the adaptive immune system. On top of DM1 being an attractive cytotoxic agent, it has been shown to induce immunogenic cell death (ICD), which leads to the activation of professional antigen-presenting cells and T-cells causing antitumoral immunity. ANXA5-DM1 increases the therapeutic potential for checkpoint inhibitors such as anti-PD-1.

ANXA5-DM1 Holistic Dosing Regimen

To holistically treat murine TNBC, Balb/cJ mice were inoculated with syngenetic EMT6 or 4T1 orthotopic tumors. Mice were treated intraperitoneally with 0.025 mg/kg ANXA5-DM1 once every seven days, 5 mg/kg rapamycin daily, and/or 5 mg/kg anti-PD-1 antibody on days 1, 5, and 9 after tumors reached 3-5 mm in diameter to ensure the tumor was vascularized. When examining tumor volumes for ANXA5-DM1, rapamycin, and/or anti-PD1 treatments, in 4T1 (**Figure 44**) and EMT6 (**Figure 45**) tumor models, it is evident the combination therapies have an added therapeutic benefit, but no treatment group benefited survival (**Table 5**). Survival curves can be viewed in appendix A (**Figures 73 and 74**).

Mice bearing 4T1 tumors and treated with the holistic treatment of ANXA5-DM1, rapamycin, and anti-PD-1 had significantly smaller tumors than untreated mice throughout the treatment (**Figure 46**). On day 31 (3 days after treatment had ended), the holistic treatment had 2.2 times smaller tumor volumes than the untreated control, ANXA5-DM1, anti-PD-1, and ANXA5-DM1 with anti-PD-1 groups (**Figure 46 d**). Interestingly, rapamycin seems to have more therapeutic benefits when combined with ANXA5-DM1 than anti-PD-1 for murine TNBC.

Over the course of the treatment, ANXA5-DM1 and rapamycin showed similar tumor response to the holistic treatment, and when tumors reach over 150 mm^3, rapamycin alone significantly decreases tumor volume **(Figure 46 c and d**). Anti-PD-1 alone or in combination with ANXA5-DM1 did not show significant benefit when compared to untreated mice, but the addition of anti-PD-1 to ANXA5-DM1 with rapamycin does not negatively impact treatment. Rapamycin and anti-PD-1 together also significantly decreased tumor volume during the treatment, but once treatment ended did not have any therapeutic benefit.

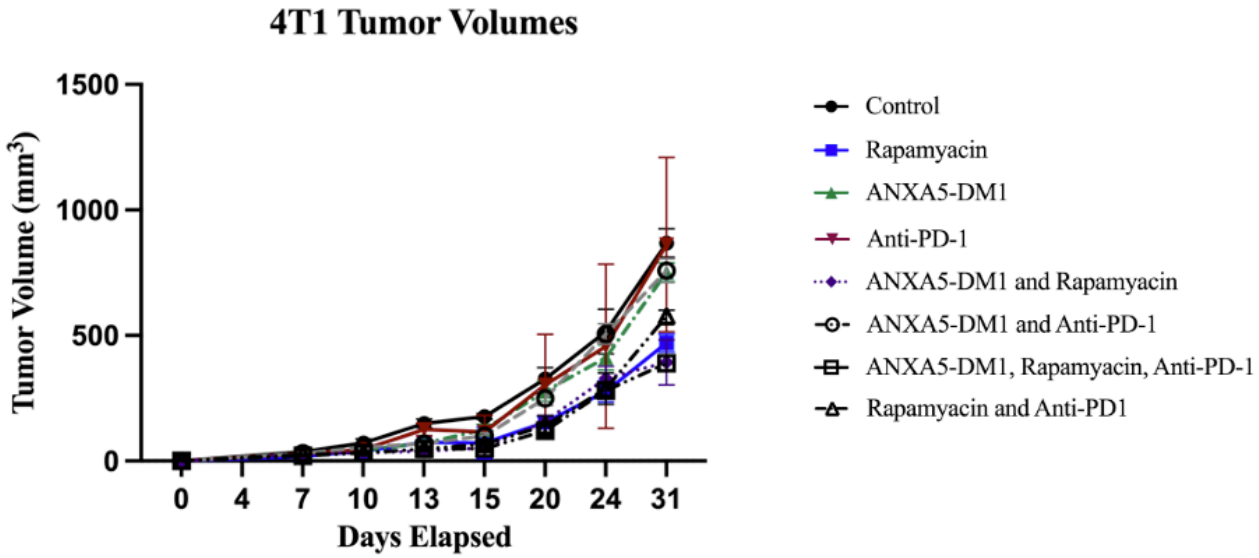

Figure 44: Effect of ANXA5-DM1, rapamycin and/or anti-PD-1 on tumor volume for BALB/cJ mice bearing 4T1 tumors

Treatment began on day 7 when mice tumors were 3-5 mm in diameter. Mice were treated with 0.025 mg/kg of DM1 in the ANXA5-DM1 conjugate IP once every 7 days, 5 mg/kg rapamycin IP daily, and/or 5 mg/kg anti-PD-1 IP on days 1, 5, 9 of treatment. Data presented as mean ± SEM (n = 6).

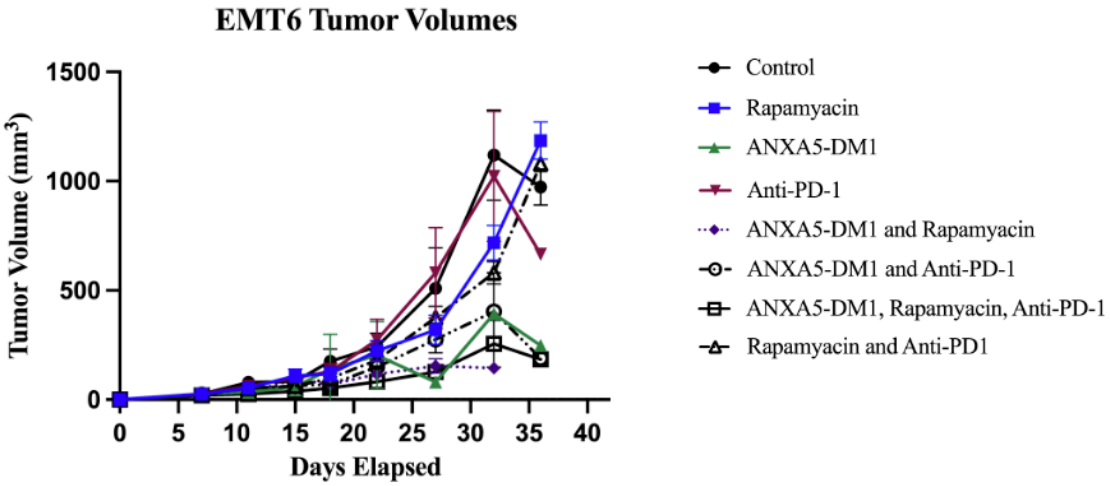

Figure 45: Effect of ANXA5-DM1, rapamycin and/or anti-PD-1 on tumor volume for BALB/cJ mice bearing EMT6 tumors

Treatment began on day 7 when mice tumors were 3-5 mm in diameter. Mice were treated with 0.025 mg/kg of DM1 in the ANXA5-DM1 conjugate IP once every 7 days, and/or 5 mg/kg rapamycin IP daily, and/or 5 mg/kg anti-PD-1 IP on days 1, 5, and 9 of treatment. No statistical significance was observed due to high standard deviations. Data presented as mean ± SEM (n = 6).

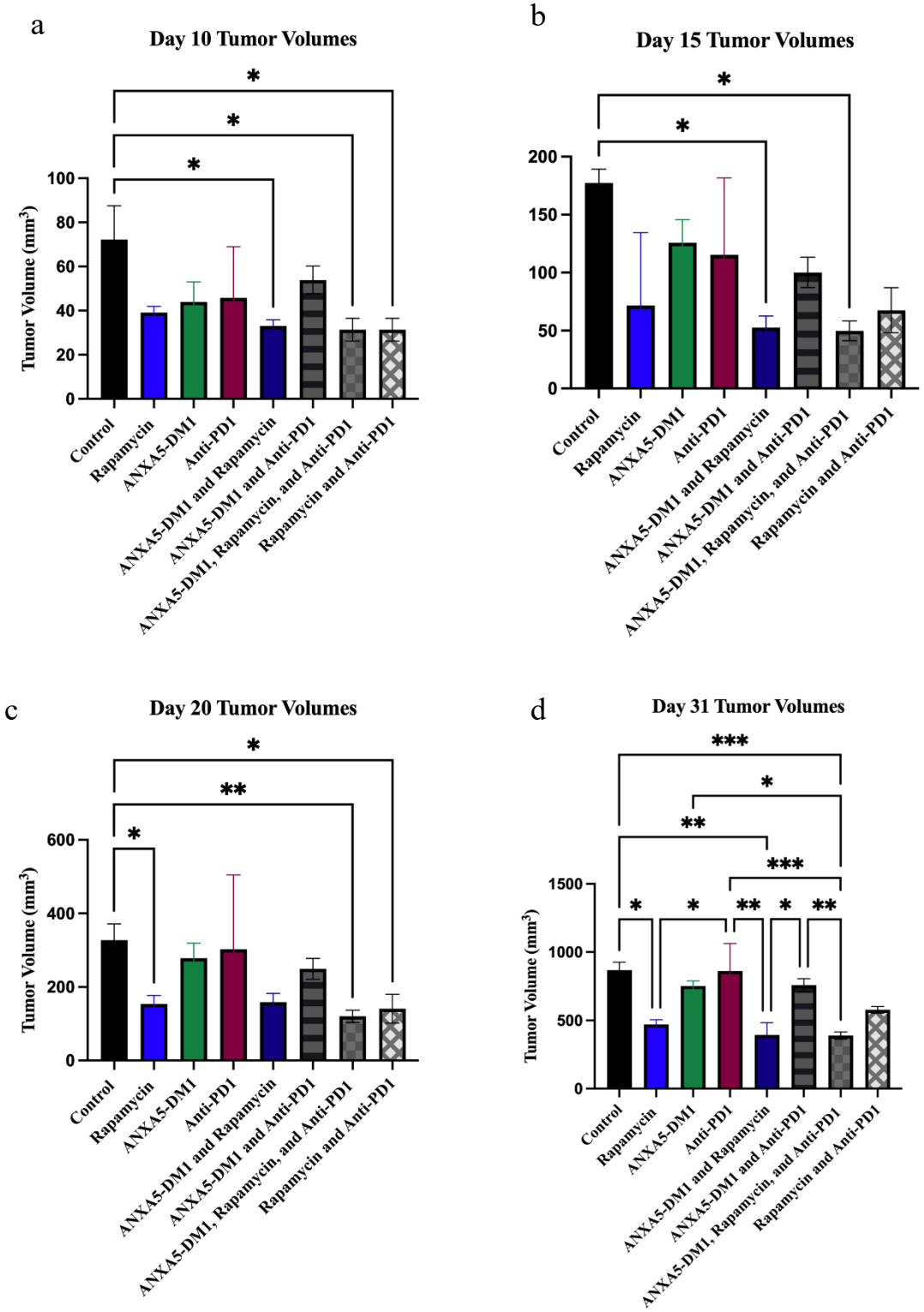
a
Day 10 Tumor Volumes
Tumor Volume (mm3)
0
20
40
60
80
100
*
*
*
Control
Rapamycin
ANXA5-DM1
Anti-PD1
ANXA5-DM1 and Rapamycin
ANXA5-DM1 and Anti-PD1
ANXA5-DM1, Rapamycin, and Anti-PD1
Rapamycin and Anti-PD1
b
Day 15 Tumor Volumes
0
50
100
150
200
*
*
c
Day 20 Tumor Volumes
0
200
400
600
*
**
*
d
Day 31 Tumor Volumes
0
500
1000
1500
***
*
**
***
*
*
**
*
**

Figure 46: Daily effects of ANXA5-DM1, rapamycin and/or anti-PD-1 on tumor volume for BALB/cJ mice bearing 4T1 tumors

ANXA5-DM1 in combination with rapamycin and anti-PD-1 show excellent tumor control. Treatment began on day 7 when mice tumors were 3-5 mm in diameter. Mice were treated with 0.025 mg/kg of DM1 in the ANXA5-DM1 conjugate IP once every 7 days, and/or 5 mg/kg rapamycin IP daily, and/or 5 mg/kg anti-PD-1 IP on days 1, 5, and 9 of treatment. Statistical analysis was performed with a one-way ANOVA with Tukey's multiple comparisons. Statistical significance indicated by *($p < 0.0332$), **($p < 0.0021$), ***($p < 0.0002$) ($n = 6$). Data presented as mean ± SEM ($n = 6$).

EMT6 tumors also responded to the holistic treatment. The ANXA5-DM1, rapamycin, and anti-PD-1 treatment group only significantly decreased tumor volume 4 days after the first ANXA5-DM1 dose (day 11) in comparison to the control, and on day 27 in comparison to the anti-PD-1 group (**Figure 47 a and c**). This is due to the large standard deviations and uneven sample sizes throughout the treatment. But it is important to note that the groups that received ANXA5-DM1 alone or in combination with rapamycin and/or anti-PD-1 maintained tumor volumes under 450 mm^3 throughout the entire treatment (**Figure 47 a-d**). Furthermore, on day 32 (4 days after treatment ended) the average tumor volume for the holistic treatment group was 4.4 times smaller than the control (**Figure 47 d**).

a

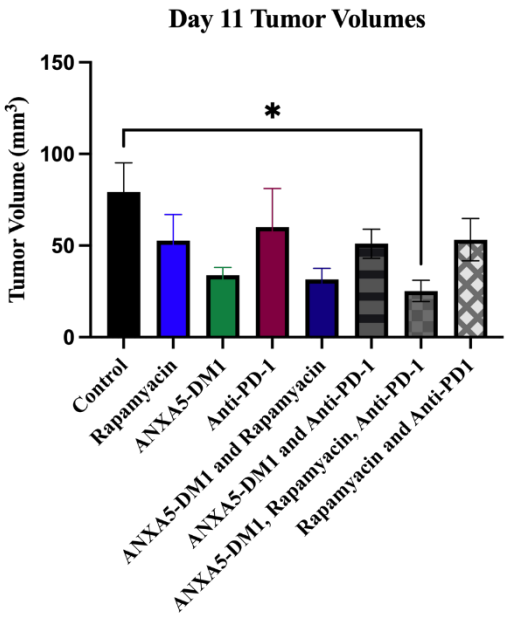
Day 11 Tumor Volumes
Tumor Volume (mm3)
150
100
50
0
*
Control
Rapamycin
ANXA5-DM1
Anti-PD-1
ANXA5-DM1 and Rapamycin
ANXA5-DM1 and Anti-PD-1
ANXA5-DM1, Rapamycin, Anti-PD-1
Rapamycin and Anti-PD1

b

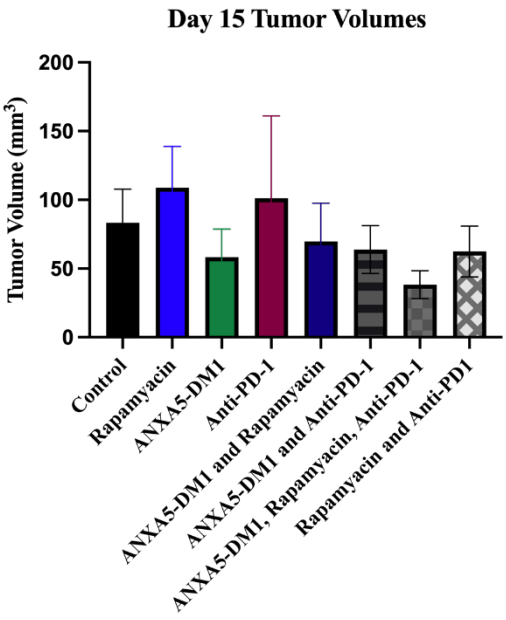
Day 15 Tumor Volumes
Tumor Volume (mm3)
200
150
100
50
0
Control
Rapamycin
ANXA5-DM1
Anti-PD-1
ANXA5-DM1 and Rapamycin
ANXA5-DM1 and Anti-PD-1
ANXA5-DM1, Rapamycin, Anti-PD-1
Rapamycin and Anti-PD1

c

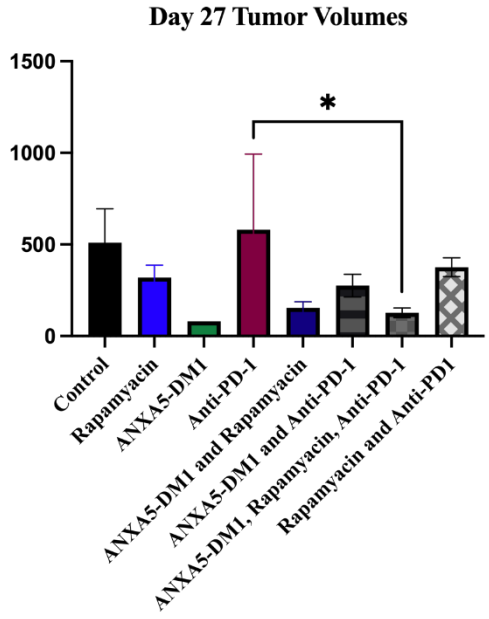
Day 27 Tumor Volumes
1500
1000
500
0
*
Control
Rapamycin
ANXA5-DM1
Anti-PD-1
ANXA5-DM1 and Rapamycin
ANXA5-DM1 and Anti-PD-1
ANXA5-DM1, Rapamycin, Anti-PD-1
Rapamycin and Anti-PD1

d

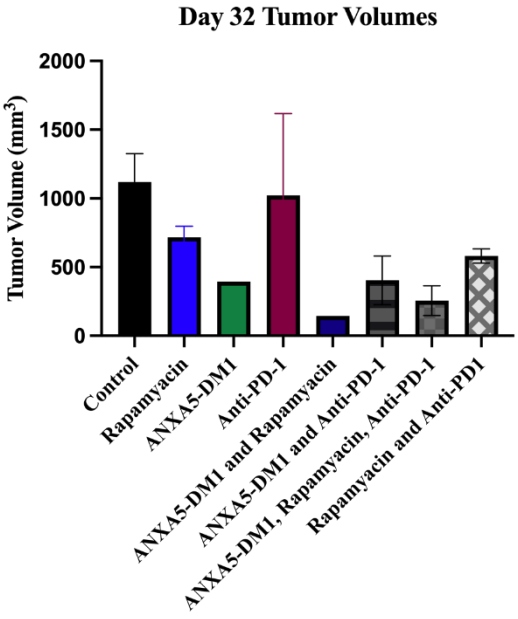
Day 32 Tumor Volumes
Tumor Volume (mm3)
2000
1500
1000
500
0
Control
Rapamycin
ANXA5-DM1
Anti-PD-1
ANXA5-DM1 and Rapamycin
ANXA5-DM1 and Anti-PD-1
ANXA5-DM1, Rapamycin, Anti-PD-1
Rapamycin and Anti-PD1

Figure 47: Daily effects of ANXA5-DM1, rapamycin and/or anti-PD-1 on tumor volume for BALB/cJ mice bearing EMT6 tumors

ANXA5-DM1 in combination with rapamycin and anti-PD-1 shows excellent tumor control, but statistical significance was only observed on day 11 due to uneven sample sizes. Treatment began on day 7 when mice tumors were 3-5 mm in diameter. Mice were treated with 0.025 mg/kg of DM1 in the ANXA5-DM1 conjugate IP once every 7 days, 5 mg/kg rapamycin IP daily, and/or 5 mg/kg anti-PD-1 IP on days 1, 5, and 9 of treatment. Data presented as mean ± SEM (n = 6). Statistical analysis was performed with a one-way ANOVA with Tukey's multiple comparisons. Statistical significance indicated by *($p < 0.0332$).

Table 5: Median survival of BALB/cJ mice for ANXA5-DM1, rapamycin and/or anti-PD-1 treatments

Treatment Group	4T1	EMT6
Control	32	34
Rapamycin	26	34
ANXA5-DM1	33.5	21.5
Anti-PD-1	22	32
ANXA5-DM1 and Rapamycin	26	25
ANXA5-DM1 and Anti-PD-1	35	33
ANXA5-DM1, Rapamycin and Anti-PD-1	31	32
Rapamycin and Anti-PD-1	34	30

EMT6 and 4T1 provide two syngenetic murine TNBC models with an inverse in immunogenicity and metastatic properties. EMT6 is considered a highly immunogenic model and weakly metastatic tumor, whereas 4T1 is poorly immunogenic and spontaneously metastases from the primary tumor to the blood, bone, brain, liver, lungs, and lymph nodes [240-242]. For EMT6 tumors, $CD8^+$ T-cells protect the body from lung metastasis. For 4T1 tumors, the infiltration of a granulocytic subset of myeloid-derived suppressor cells blocks the cytotoxic T-cell immunity, promoting metastatic niches in the lungs [240]. EMT6 cells have high expression of MHC-I, and the immune infiltrates have a large M2-like macrophagic component [243, 244]. Interestingly, by blocking PS exposure on tumor cells, macrophages can be repolarized to the M1 phenotype and promote the differentiation of myeloid-derived suppressor cells into the M1 anticancer phenotype [41]. By using ANXA5-DM1, the PS exposure becomes blocked which may aid in the anticancer immunity in the TME for EMT6 cells, which was observed with smaller tumor volumes for mice treated with the ANXA5-DM1 conjugate.

The immune infiltrates in 4T1 tumors have a large population of $CD4^+$ progenitors, T-regulatory cells, and γδ T cells that promote tumor immunity [41]. Although the T-regulatory cells in 4T1 tumor models have high PD-1 expression, treating T-regulatory cells with an anti-PD-1 monoclonal antibody does not decrease the frequency or function of the T-regulatory cells [41, 245]. This could explain why the anti-PD-1 therapy alone did not have a significant improvement for tumor volume [41, 245]. The growth rates of the tumor models are different as well. 4T1 tumor inoculations use one-tenth of the cells needed for EMT6 inculcations, but both tumor models reach 3-5 mm in 7 days. 4T1 cells are fast growing and because of their high proliferation index, these

cells may respond better to DM1-based therapies. But the complex landscape of TNBC also must be considered.

The holistic treatment combines a three-pronged approach to the targeted killing of TNBC that exploits the hypoxic TME. First ANXA5 delivers DM1 to the tumor microenvironment where it can induce apoptosis and ICD on both tumor cells and tumor vasculature. Because ANXA5-DM1 is targeted to tumor vasculature, DM1 can destroy existing vasculature, adding a hypoxic pocket within the TME. This could explain why ANXA5-DM1 alone did not significantly impact tumor volume for both EMT6 and 4T1 tumors. However, if not enough DM1 is delivered to the vasculature, ANXA5 can aid in the delivery of the conjugate and other drugs into the TME. By nature, ANXA5 is an anticoagulant protein. Thrombin generation requires a negative charge, which is mainly attributed to the externalized PS on activated platelets and cancer cells [246]. Thrombin converts fibrinogen to fibrin, creating a clot that increases VEGF expression in many solid tumors [247]. As ANXA5 binds to PS, it blocks the ability of prothrombin and other coagulation factors to bind to PS, resulting in the anticoagulation activity of ANXA5 [212]. ANXA5 may keep vessels open by decreasing platelet aggregation, which could increase drug delivery to the tumor.

The second aspect of the holistic treatment is the addition of rapamycin. Rapamycin binds to the mTORC1 complex on FKBP12 protein to allosterically hinder the complex, decreasing mTOR activity, and ultimately leading to cell death and a decrease in HIF1-α expression [248-252]. Rapamycin alone can control tumor volume for human TNBC, which was also observed in both murine TNBC models tested [252]. Rapamycin also decreases PD-L1 expression, which leads to the third prong of the holistic dosing regimen - immune stimulation with an anti-PD-1 checkpoint inhibitor [253, 254]. While rapamycin can target and downregulate HIF1-α expression,

it does not necessarily reoxygenate the tumor, maintaining the hypoxia/HIF1-α dependent PD-1 expression on $CD8^+$ T-cells [255]. By simultaneously decreasing PD-L1 expression on cancer cells through rapamycin and maintaining PD-1 expression on T-cells through the intrinsic hypoxic TME, combining an anti-PD-1 monoclonal antibody can aid in the activation of the existing tumor-infiltrating lymphocytes.

Additionally, DM1 induces ICD and the DAMPs aid in the activation of the adaptive immune system by recruiting and maturing dendritic cells [256]. ATP acts as a chemoattractant, and once the dendritic cells are in the ICD TME, calreticulin surface exposure and HMGB1 promote dendritic cells' phagocytosis of the dying cells to facilitate antigen presentation to T-cells. Interestingly, the treatments with ANXA5-DM1 and rapamycin had better tumor control than ANXA5-DM1 and anti-PD-1, suggesting that treating the hypoxic TME provides a better anti-tumor response than activating the adaptive immune system. But, by combining all three, there is better tumor control. However, there was no increase in survival, which may be a result of the immunosuppressive properties of rapamycin.

Rapamycin was first approved as an immunosuppressive agent to prevent renal allograph rejection by the body [257, 258]. Rapamycin causes immunosuppression by blocking cytotoxic T-cell proliferation, but more importantly, promotes the expansion of $CD4^+CD25^+FOXP3^+$ regulatory T-cells to favor immunological tolerance [258, 259]. Additionally, rapamycin prevents dendric cell maturation, preventing cross-presentation to T-cells, and therefore limiting immune activation. The addition of rapamycin could be limiting the adaptive immune system response, thus making the addition of the PD-1 checkpoint inhibitor ineffective.

ANXA5-DM1 Intertumoral Injections

Because there was not a significant increase in survival with our holistic treatment, we contemplated how to increase the ANXA5-DM1 dosing without causing serious adverse events. The goal of intertumoral (IT) injections is to increase the bioavailability of the therapy to the tumor while decreasing systemic side effects [260, 261]. Current work by Gabriela Faria (data not shown) using ANXA5-single wall carbon nanotubes provided evidence that treating the tumor intratumorally would enhance the delivery of ANXA5 to the tumor cells when compared to intravenous injections (IV). IT injections provided a larger release in TNF-α in comparison to IV injections. This provided rationale to treat mice intratumorally, and the ANXA5-DM1 therapy was adapted to an IT injection method.

Mice were treated with IT injections of 0, 0.025, or 0.25 mg/kg of DM1 in the ANXA5-DM1 conjugate daily for 21 days after the tumors reached 3-5 mm in diameter to ensure the tumor was vascularized. The free DM1 controls were omitted because DM1 is extremely toxic and can only be administered when linked to a protein or antibody. The daily IT injections did not cause any adverse events such as hair loss or redness around the injection site each day and had good tumor control (**Figure 48**). By using IT injections, both the 0.025 and 0.25 mg/kg doses maintained tumor volumes under 500 mm^3 during the treatment. On day 28 (19 doses), the 0.25 mg/kg dose significantly decreased tumor volume compared to the control (**Figure 49 a**). By day 32 (2 days after treatment ended), both treatment groups had significantly decreased tumor volume when compared to the control (**Figure 49 b**). More importantly, one mouse in the 0.25 mg/kg group had complete tumor regression and was tumor free for 52 days after treatment ended. However, there was still not an increase in median survival (**Figure 50**), which could be a result of the incomplete delivery of ANXA5-DM1 into the tumor. As the tumor increased in size, the tumors became hard

and stiff. The treatment was expelled at the injection site, making it impossible to verify how much of the conjugate entered the tumor and how much escaped (**Figure 51**).

Tumor stiffness, viscosity of the drug formulation, and needle tip design all affect the delivery and accuracy of IT injections [262]. The most advantageous IT delivery method would include a hydrogel to increase tumor retention, a multi-hole needle to disperse the drug throughout the tumor, and a soft tumor stoma to aid in drug dispersion. In our study, we used the least advantageous IT delivery method by delivering a non-viscous PBS solution in a single-hole needle into a cancer model with a hard stroma, all of which hinder IT drug delivery. Antibody neutralization of ANXA5 may also hinder the complete delivery of the conjugate to the tumor.

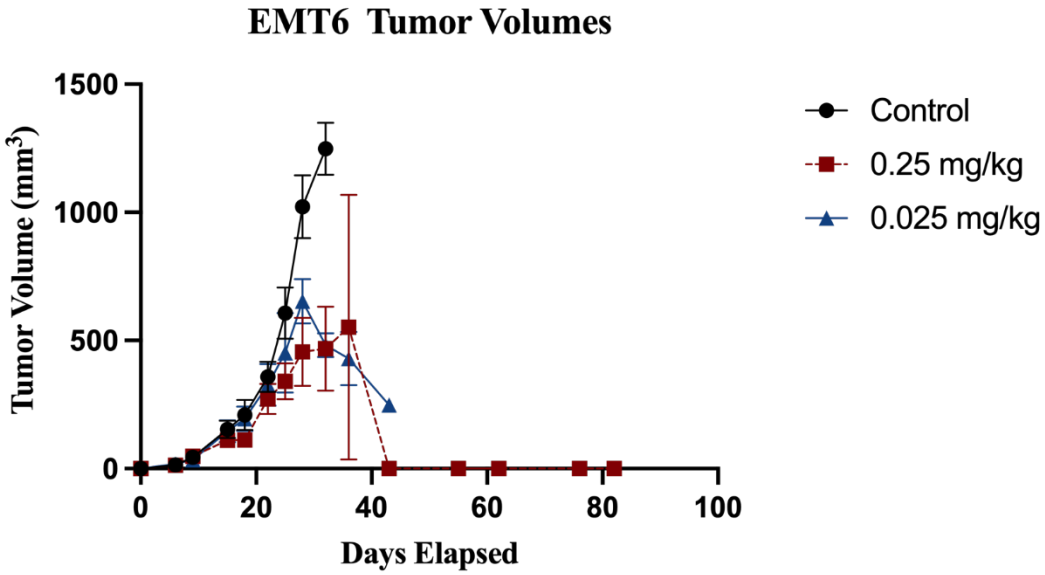

Figure 48: Effects of ANXA5-DM1 IT treatment on tumor volumes for BALB/cJ mice bearing EMT6 tumors

Treatment began on day 9 when mice tumors were 3-5 mm in diameter. Mice were treated with 0.025 mg/kg of DM1 in the ANXA5-DM1 conjugate IT once daily for 21 days. Data presented as mean ± SEM (n = 7).

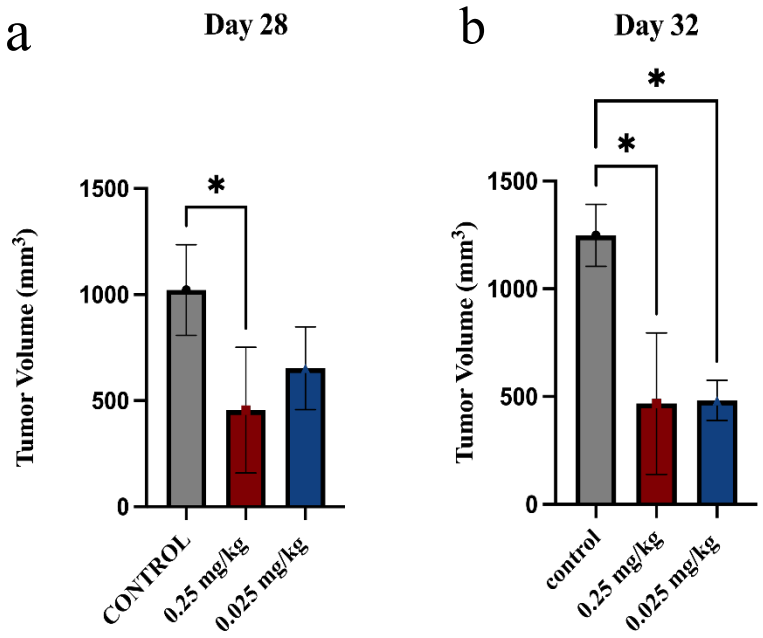

Figure 49: Day 28 and day 38 tumor volumes for ANXA5-DM1 IT treatment for BALB/cJ mice bearing EMT6 tumors

The dosage of 0.25 mg/kg IT injections of ANXA5-DM1 treatment significantly decreased tumor volumes at a) day 28 and b) day 32. The 0.025 mg/kg treatment group significantly decreased tumor volume on b) day 32. Treatment began on day 9 when mice tumors were 3-5 mm in diameter. Data presented as mean ± SEM (n = 7). Statistical analysis was completed with a one-way ANOVA with Tukey's multiple comparisons. Statistical significance is indicated by *($p < 0.0332$).

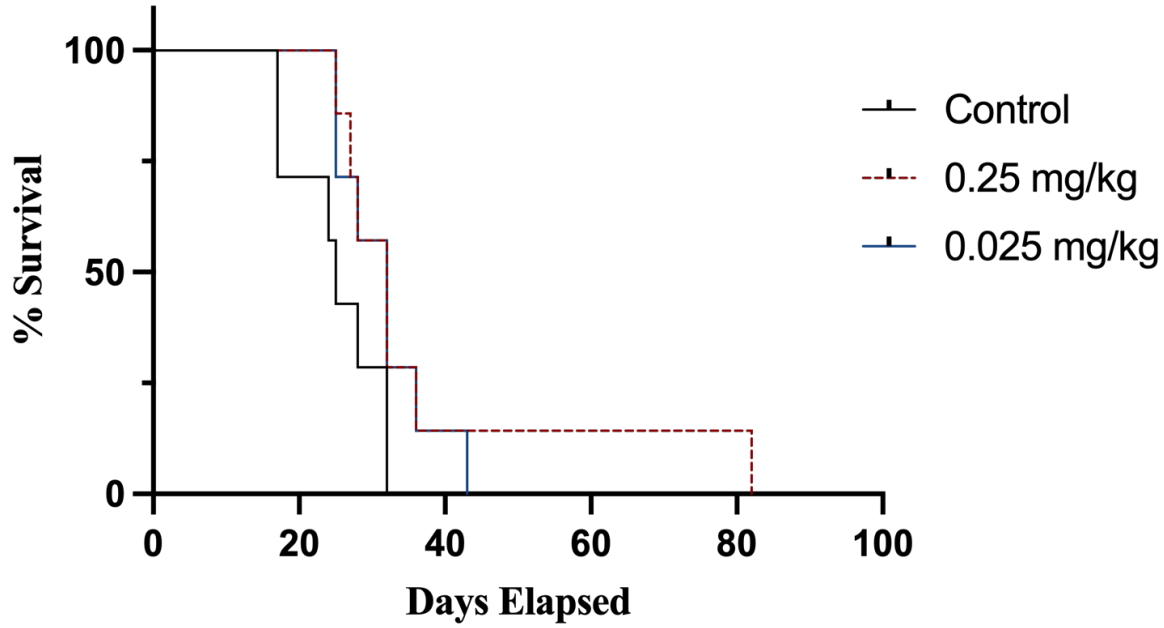

Figure 50: Survival curve for ANXA5-DM1 IT injections for BALB/cJ mice bearing EMT6 tumors

Treatment began on day 9 when mice tumors were 3-5 mm in diameter. Mice were treated with 0.025 mg/kg of DM1 in the ANXA5-DM1 conjugate IT once daily for 21 days Daily IT injections of ANXA5-DM1 did not increase survival. One mouse in the 0.25 mg/kg group survived for 52 days after treatment ended.

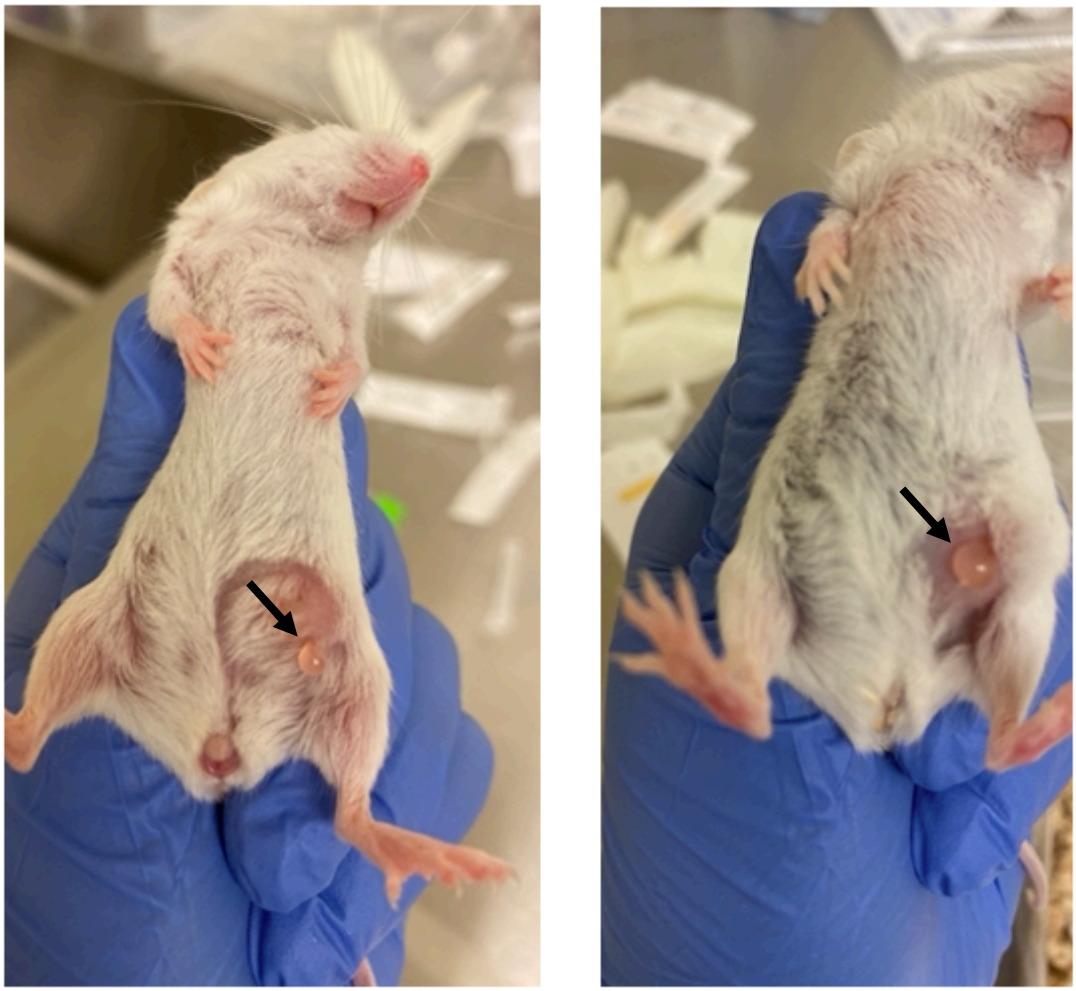

Figure 51: Examples of ANXA5-DM1 IT injection expulsion in BALB/cj mice bearing EMT6 tumors

Immediate ANXA5-DM1 leakage (arrows) was observed in mice with different sized throughout the course of the treatment.

ANXA5 immunogenicity

To assess the immune response against ANXA5 healthy Balb/cJ mice were injected with 3 mg/kg of ANXA5 IP daily for 21 days, which is the equivalent dose of ANXA5 in the 0.25 mg/kg ANXA5-DM1 conjugate. One mouse was euthanized at days 0, 10, and 21 and the blood was collected to examine ANXA5-specific antibody titers.

While it was anticipated that the ANXA5 would not elicit an immune response, there was a very weak presence of ANXA5-specific IgG and/or IgM antibodies by day 10, and by day 21 a 100-fold increase was observed (**Figure 52**). However, none of the mice showed signs of anaphylactic response, autoimmune response (hair loss, dry mouth, dry eyes), or weight loss over the course of the treatment (**Figure 54**). The most probable explanation for this is the use of a human ANXA5 protein in a mouse model. Previous work in our lab by John Krais found that using murine ANXA5 in an ANXA5-mCGL fusion protein did not elicit an immune response in a BALB/cJ murine model [198].

Through a pairwise alignment of Homo sapiens ANNXA5 (Accession: NP_001145) and M. musculus ANXA5 (Accession: NP_033803), the proteins have a percent identity match of 93.65%. Additionally, the Query Cover (how long the sequences are to each other) was 98% and only varied by 1 amino acid. Because the proteins are not completely identical, this could prompt an immune response, but the immune response in nonhuman primates such as mice cannot be a predictive model for translation into humans [263]. While mice are considered an invaluable model organism for examining the immunogenicity of human proteins, the differences in the mouse and human immune systems limit the translatability of the therapies [264-266]. The injection method and frequency also impact the immunogenicity of the protein.

IP injections are not considered the most immunogenic delivery method, but this delivery method can create a pocket of protein deposits inside the peritoneal cavity that allows for the slow release of the protein into a close lymph node, eliciting an immune response [267, 268]. Because the weak immune response was reported on day 10 of repeated IP ANXA5 injections, it is unlikely that the once-a-week IP ANXA5-DM1 treatment was neutralized or caused an immune response. IT injections have been shown to reduce antibody-mediated protein neutralization and decrease systemic side effects, and the IT injections of ANXA5-DM1 would not induce an immunogenic response [269].

It is also important to note that nearly every FDA-approved monoclonal antibody and protein have a rate of immunogenicity on the FDA-licensed package inserts, indicating that an immune response to an antibody or biologic-based therapies is not a criterion that prevents approval [267]. The ultimate test for immunogenicity would be a clinical trial. The first phase I, first in human clinical trial (ClinicalTrails.gov identifier: NCT04850339) to evaluate the safety, tolerability, and pharmacokinetics of single and multiple IV dosing of ANXA5 is currently ongoing. Even with the incomplete delivery and potential immunogenicity of the protein, the IT injections proved to be a better delivery method than IP injections.

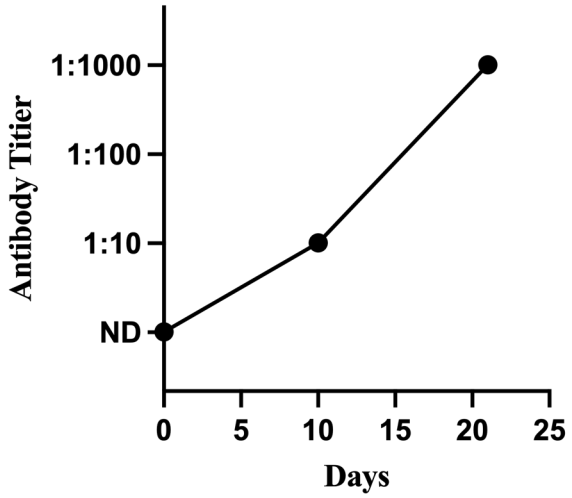

Figure 52: Immunogenicity of ANXA5 daily IP injections in healthy BALB/cJ mice

A weak immune response to ANA5 was observed on day 10, and by day 21, a 100-fold increase was observed. Blood samples were collected on days 0, 10, and 21 during the treatment period and analyzed for the presence of antibodies specific to the administered protein. Antibody detection was performed via ELISA of diluted serum samples with a positive detection reported as a maximum serum dilution factor (antibody titer) (n = 1).

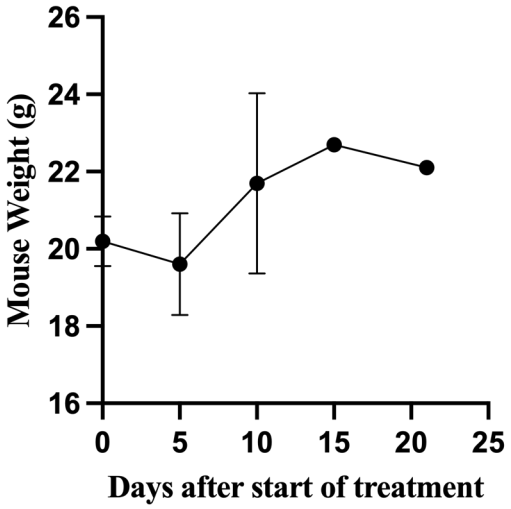

Figure 53: ANXA5 effects on healthy BALB/cJ mice weight

Mice weight was not effected by ANXA5-DM1 treatment (n = 1-3).

Chapter 4: ANXA5-CMB Results and Discussion

ANXA5-CMB Healthy Cell Cytotoxicity

Previously, Dr. Patrick McKernan and Charles Bagarie established that the ANXA5-CMB conjugate had enhanced cytotoxicity against murine TNBC cells when compared to free CMB [152, 153]. The IC50 values of the TNBC cells are summarized in **Table 6**. By conjugating CMB to ANXA5, the conjugate was 57 to 241 times more effective at inducing cell death than the free drug after 24 hours. While the cytotoxic activity of the ANXA5-CMB conjugate is excellent against TNBC cells, the cytotoxicity of the conjugate must be tested against healthy vascular and mammary cells.

Table 6: Summary of ANXA5-CMB and free CMB IC50 on murine TNBC cells

Cell line	ANXA5- CMB IC50	CMB IC50	IC50 Ratio
4T1	2.7 μM	156 μM	57
EMT6	0.42 μM	102 μM	241

ANXA5-CMB cytotoxicity studies were carried out on healthy vascular (HUVEC) and mammary (MCF10A) cells with varying concentrations of ANXA5-CMB. Cells were treated with 0-10 μM of DM1 in the ANXA5-DM1 conjugate. Cells were treated on day 0 and incubated with the conjugate for 24 hours. After 24 hours, cell viability was analyzed via a fluorescent Alamar Blue assay. Percent viability was determined by normalizing the control (0 μM DM1) to 100% and comparing each treatment group to the control (n = 4-8).

Cytotoxicity of ANXA5-CMB on HUVEC and MCF10A cells is shown in **Figures 54 and 55** respectively. The ANXA5-CMB conjugate exhibited 100% cytotoxicity at 1 μM for TNBC cells. The presence of ANXA5-CMB for HUVEC cells did not impact viability with a dose of up to 100 μM (**Figure 54**). While the presence of ANXA5-CMB did induce cell death for the MCF10A cells (**Figure 55**). The IC50 of ANXA5-CMB for the MCF10A cells was 6.0 μM. When comparing the IC50 for the TNBC cells and that of MCF10A, it takes 2.2 to 14.2 more ANXA5-CMB to induce the same amount of cell death for the healthy MCF10A cells. This indicates ANXA5-CMB uptake is limited in the healthy cell lines, and less cytotoxicity is observed. Ideally, ANXA5-CMB would not have impacted MCF10A viability, but cell death is most likely due to a positive feedback loop as discussed in the ANXA5-DM1 healthy cell cytotoxicity section.

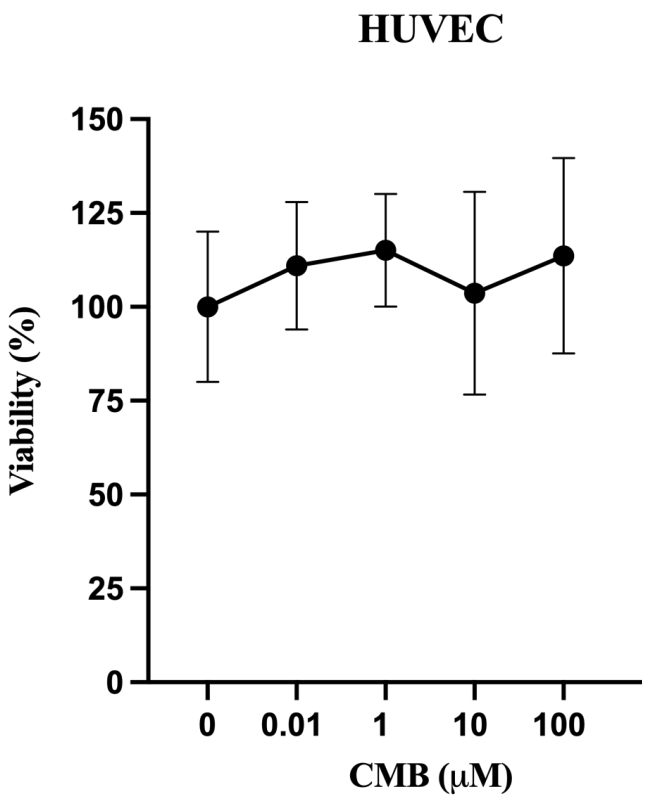

Figure 54: 24-hour effects of ANXA5-CMB on HUVEC cell viability

Cells were treated with 0-100 μM CMB in the ANXA5-CMB conjugate in fully supplemented growth medium with 2 mM calcium. Cells were grown to 90-100% confluency. ANXA5-CMB did not impact cell viability of HUVEC cells. Cell viability was measured via an Alamar Blue assay and viability was compared to the control (0 μM) after 24 hours. Data is presented as mean ± SD (n = 4-8).

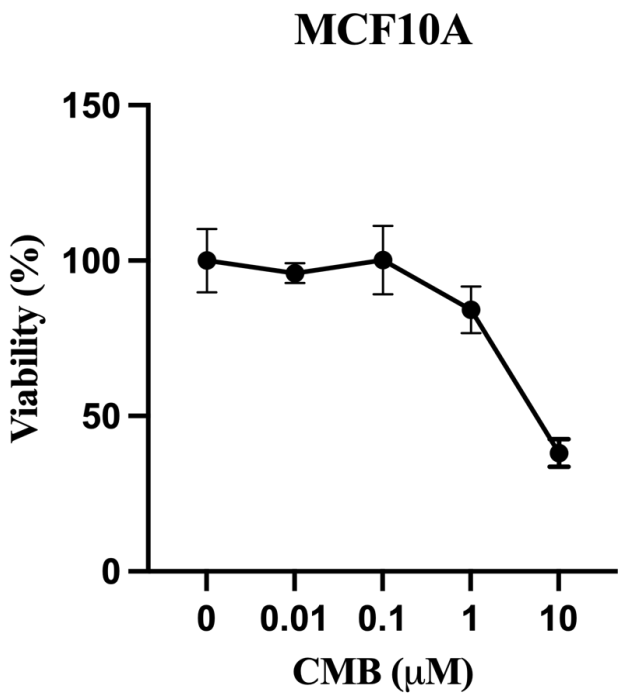

Figure 55: 24-hour effects of ANXA5-CMB on MCF10A cell viability

Cells were treated with 0-100 μM CMB in the ANXA5-CMB conjugate in fully supplemented growth medium with 2 mM calcium. Cells were grown to 90-100% confluency. The IC50 of ANXA5-CMB on MCF10A cells was 6.0 μM. Cell viability was measured via an Alamar Blue assay and viability was compared to the control (μM) after 24 hours. Data is presented as mean ± SD (n = 4-8).

ANXA5-CMB *in Vivo* Dosing Optimization

Daily ANXA5-CMB IP treatment

Previous work by Dr. Patrick McKernan laid the foundation for *in vivo* ANXA5-CMB therapy [152]. In this work, mice were inoculated with 4T1 TNBC on day zero, and one day after tumor inoculation, treatment began. Mice were treated with 0.5 mg/kg CMB in the ANXA5-CMB conjugate for 21 days. The ANXA5-CMB conjugate inhibited tumor growth over the entire 21 days treatment period. However, this study began before the tumor had been established and only one dosage was analyzed for the ANXA5-CMB antitumor effects.

In the current study, Balb/cJ mice were inoculated with syngeneic 4T1 orthotopic tumors. Mice were treated with intraperitoneal (IP) injections of 0, 0.5, 1, 2.5, and 5 mg/kg of CMB in the ANXA5-CMB conjugate daily for 20 days after tumors reached 3-5 mm in diameter to ensure the tumor was vascularized. The free CMB controls were omitted because this was an exploratory study examining dosage escalation and the safety of the ANXA5-CMB conjugate.

On day 11 (6 days after treatment began), mice in the 2.5 and 5 mg/kg treatment groups had significantly smaller tumor volumes than the control (**Figure 56**). Mice treated with over 1 mg/kg maintained tumor volume under 100 mm^3 during the entire treatment. Interestingly, the 0.5 mg/kg treatment group did not have the same therapeutic benefit when the starting tumor size was increased to 3-5 mm in diameter [152]. In the McKernan study, the treatment began one day after tumor inoculation, and the 0.5 mg/kg dose was able to suppress tumor growth over the 21-day period, however; when treatment began 5 days after inoculation, the 0.5 mg/kg dose behaved more like the untreated control. This indicates that the size of the starting tumor dictates how well the ANXA5-CMB conjugate will work.

When TNBC tumors are found below 1 cm in diameter, systemic chemotherapy can provide a good prognosis and patients have a low reoccurrence risk. However, one study in China found that 60% of patients have a tumor diameter between 2-5 cm with an average of 3.1 cm [270, 271]. Similar trends were found with Ghanaian, African American, and white American women with average tumor diameters of 3.2 cm, 2.3 cm, and 2.0 cm, respectively [271]. This suggests, that treating mice one day after tumor inoculation is not clinically relevant, and the 0.5 mg/kg dosage is ineffective. More importantly, the daily treatment schedule proved to be extremely toxic and resulted in fatalities (**Figure 57**). All mice treated with the 5 mg/kg group died by day 15 and had a median survival of only 11.5 days, much less than the 29-day median survival of the untreated control. The 2.5 mg/kg dosage rendered similar results, with a median survival of 13.5 days. Mice treated with a 1 mg/kg dosage fared better, but the median survival was still 6.5 days less than the untreated control. Additionally, the IP daily injections of the protein may be inducing an immune response as discussed in the ANXA5 immunogenicity section, further limiting the therapeutic benefit of the conjugate. While an autopsy was not performed, it is hypothesized that the ANXA5-CMB conjugate could have caused high fatalities in one of two ways. First, the daily injections of the ANXA5-CMB caused leukopenia and severely depressed the bone marrow function, resulting in death. Second, excess ANXA5 is excreted through the kidneys, potentially causing nephrotoxicity, and leading to death. Although fatalities were observed, the 1 and 2.5 mg/kg dosages provided good tumor control, prompting a reexamination of the dosing timeline.

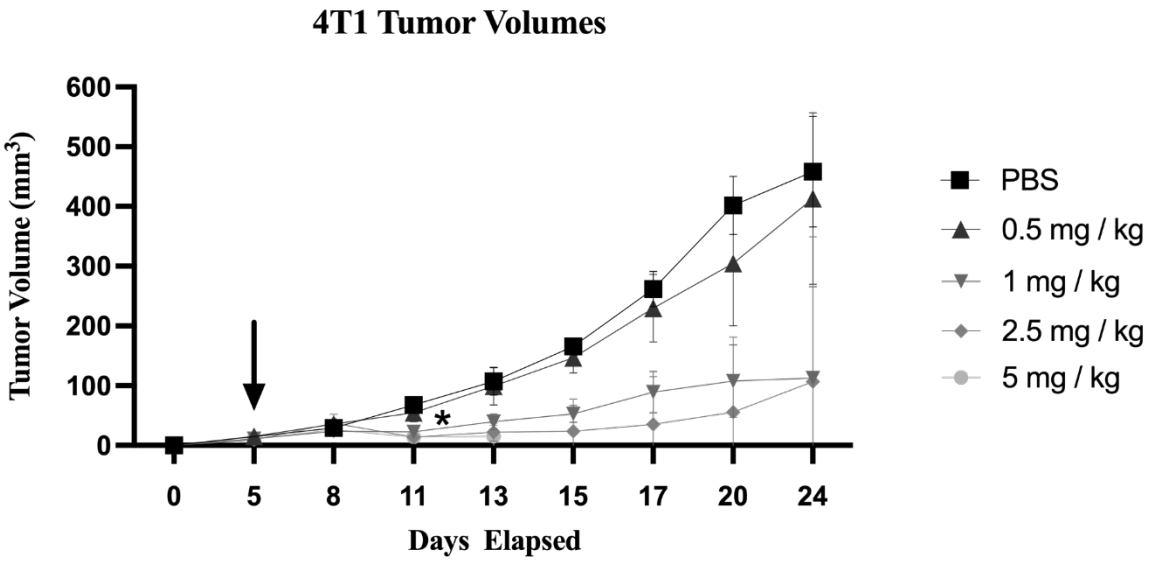

Figure 56: Effect of daily ANXA5-CMB IP injections on 4T1 tumors volumes

Treatment began with mice tumors were 3-5 mm in diameter. Mice were treated with 0-5 mg/kg of CMB in the ANXA5-CMB conjugate daily for 20 days, starting on day 5 (indicated by arrow). Mice in the 2.5 and 5 mg/kg ANXA5-CMB dosage had significantly smaller tumor volumes than the control. Statistical analysis was performed with an one-way ANOVA with Tukey multiple comparisons. Data is represented as mean ± SEM (n = 6). Statistical significance is denoted by * ($p < 0.0332$).

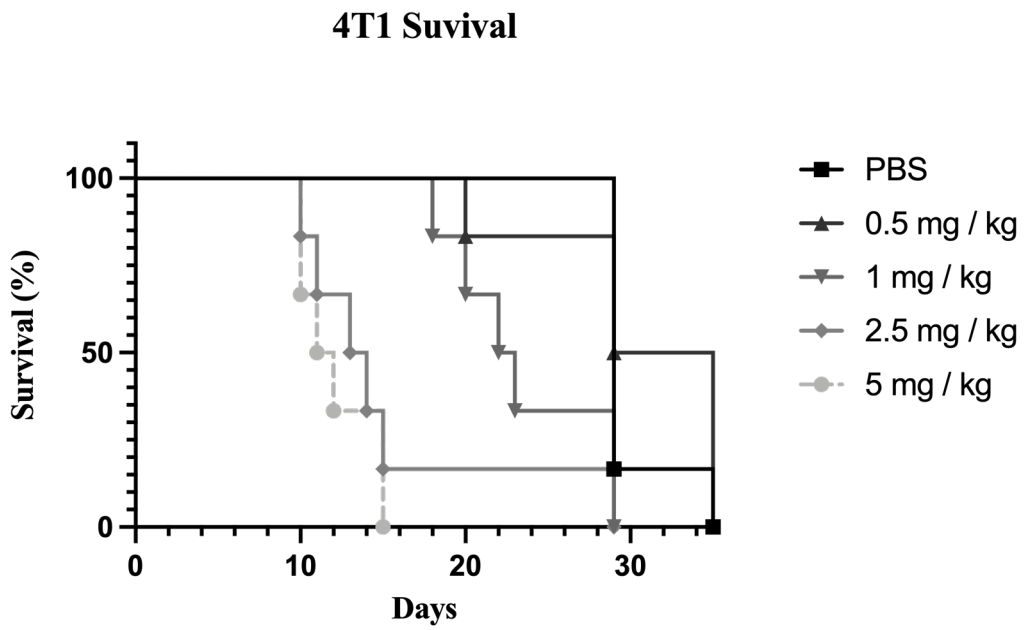

Figure 57: Effect of daily ANXA5-CMB IP injections on mice bearing 4T1 tumors survival

Treatment began with mice tumors were 3-5 mm in diameter. Mice treated with 2.5 and 5 mg/kg ANXA5-CMB daily significantly reduced survival and daily dosing at these dosages are too high. Statistical analysis was performed with a log-rank (Mantel-Cox) curve comparison.

Five-day cycle of ANXA5-CMB IP treatments

To optimize the treatment schedule, mice were treated on a cycle of 5 consecutive days of treatment followed by a 2-day break [272]. Mice were treated for 21 days, which equates to 3 cycles of 15 doses. Balb/cJ mice were treated IP with 1 or 2.5 mg/kg of CMB in the ANXA5-CMB conjugate, and because the treatment is below the 3 mg/kg maximum tolerated dose for free CMB, the 1 and 2.5 mg/kg free CMB drug controls were added [272].

By decreasing the dosing schedule to 5 consecutive days followed by a 2-day break, tumor volumes compared to the untreated control and lethality of the ANXA5-CMB conjugates

decreased (**Figures 58 and 59**). Mice treated with 1 mg/kg ANXA5-CMB maintained tumor volumes under 500 mm^3 during the 21-day treatment period and significantly increased survival by 5.5 days. After two cycles of treatment (day 20), the 1 mg/kg ANXA5-CMB dosage significantly decreased tumor volumes in comparison to the control and both free drug dosages. The 2.5 mg/kg ANXA5-CMB maintained tumor volumes under 550 mm^3 during the 21-day treatment period and after two cycles of treatment (day 20), this dosage significantly decreased tumor volume in comparison to the control (**Figure 58**). But the 2.5 mg/kg ANXA5-CMB dose did not significantly increase survival. However, when comparing the 5 days on and 2 days off schedule to daily injections, the-5 day cycle increased median survival by 5.5 days, indicating that the daily treatments are too lethal. The 1 and 2.5 mg/kg of free CMB behaved similarly to the control, which is not surprising because CMB was discontinued as breast cancer chemotherapy in the 1970s because of the limited therapeutic benefit [272].

Although CMB is not traditionally used for solid cancers, the ANXA5-CMB conjugate provides a targeted delivery of a DNA alkylating agent to the TME. DNA alkylating agents remain a front-line treatment for TNBC, but the double-stranded repair mechanism in TNBC prevents sufficient DNA adducts caused by CBM, rendering the cells resistant to the drug [273]. Additionally, the poor aqueous solubility, short half-life, and covalent interactions with proteins and phospholipids leave only 10% of the original dose available, hindering its effectiveness [273, 274]. By conjugating CMB to ANXA5 a soluble targeted delivery of CMB is achieved.

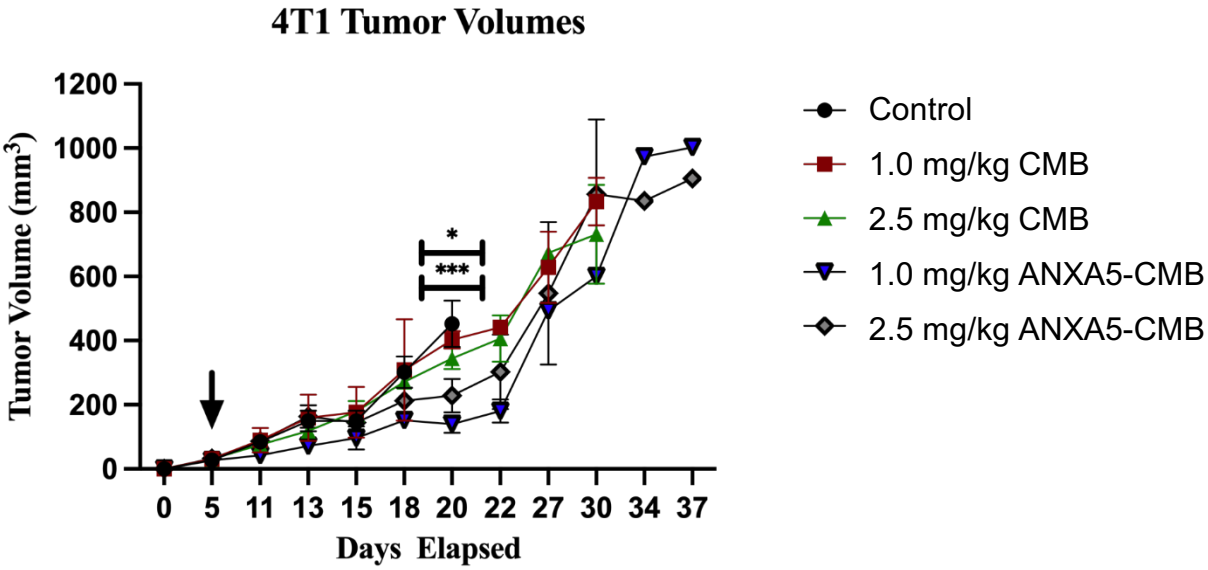

Figure 58: Effect of 5 days on 2 days off ANXA5-CMB IP injections on 4T1 tumors volumes

Treatment began with mice tumors were 3-5 mm in diameter. Mice were treated with 0-2.5 mg/kg of CMB in the ANXA5-CMB conjugate daily for 21 days, starting on day 5 (indicated by arrow). Mice in the 1 and 2.5 mg/kg ANXA5-CMB dosage had significantly smaller tumor volumes than the control on day 20. Statistical analysis was performed with a one-way ANOVA with Tukey multiple comparisons. Data is represented as mean ± SEM (n=6). Statistical significance is denoted by * ($p < 0.0332$) and *** ($p < 0.002$).

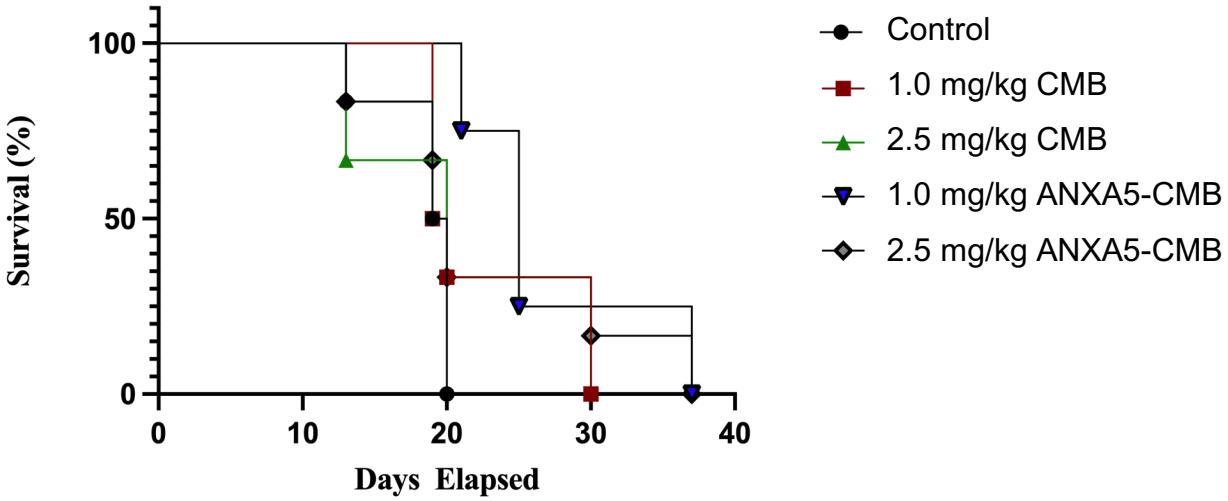

Figure 59: Effect of 5 days on and 2 days off of ANXA5-CMB IP injections on BALB/cJ mice bearing 4T1 tumors survival

Treatment began with mice tumors were 3-5 mm in diameter. Mice treated with 1.0 mg/kg ANXA5-CMB daily significantly increased survival by 5.5 days ($p < 0.0021$). Statistical analysis was performed with a log-rank (Mantel-Cox) curve comparison.

ANXA5-CMB intact denaturing mass analysis

The ANXA5-CMB conjugate was analyzed with denaturing mass analysis by Dr. Aaron Bailey at the University of Texas Medical Branch. By deconvoluting the ANXA5-DM1 conjugate in the mass range of 35-37 kDa, a left-shifted bell curve distribution is observed (**Figure 60**). The ANXA5-CMB conjugate had a drug-to-protein ratio of less than one molecule of CMB to one molecule of ANXA5. The increase in mass was a result of the EDC linker and not CMB, as

indicated by the light pink pastel boxes. EDC added 155 Da to the protein when the linker was added. If a CMB molecule was added to the protein, it was still connected to the linker (purple pastel boxes). This means EDC was not acting as a leaving group after the addition of the primary amines on ANXA5, and this phenomenon has not been reported in the literature to the best of my knowledge.

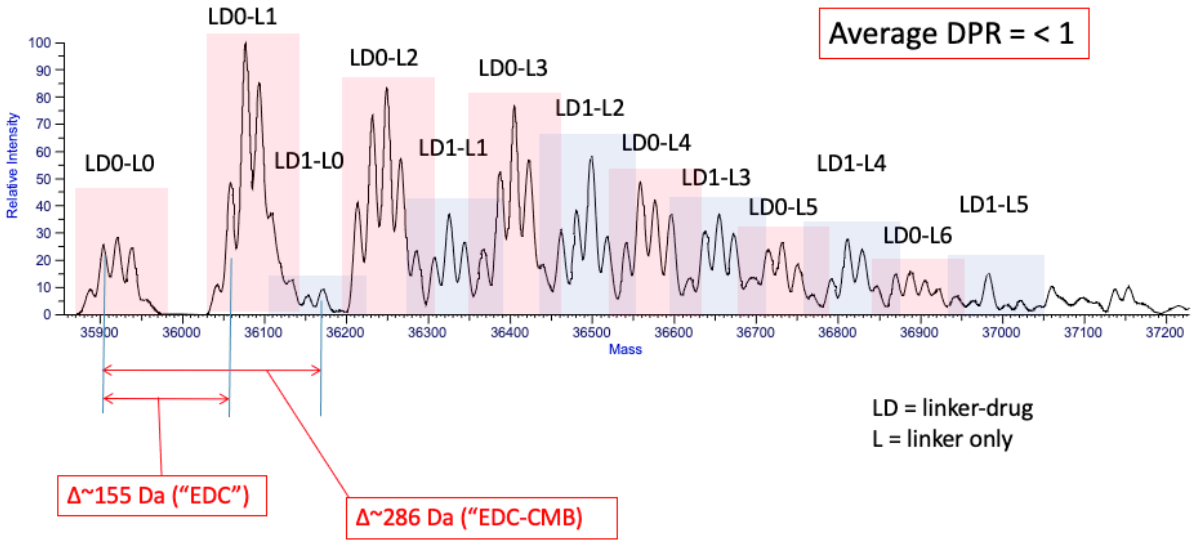

Figure 60: Denaturing intact mass analysis of ANXA5-CMB

ANXA5-CMB mass analysis shows a left-shifted bell curve, with a weighted drug to protein ratio of an average of less than 1 molecule of CMB to 1 molecule of ANXA5. Drug-to-protein ratio was calculated as weighted average of deconvoluted spectra using ReSpect and sliding windows algorithms.

It is hypothesized that the poor solubility of CMB in aqueous solutions is the limiting factor in creating the conjugate. Nearly every conjugation resulted in CMB precipitating out of solution during the addition of the drug, as pH increased before ECD addition, or during EDC addition as indicated by a cloudy white/yellow solution. This means that the free CMB was not available for EDC activation. When ANXA5 was added, the free EDC was able to react with 1 of the 52 carboxylic acids moieties on ANXA5 (aspartate and glutamate residues) (**Figure 61**). The activated protein was then able to react with 1 of the 22 primary amines (lysine residues) (**Figure 62**) on a neighboring ANXA5, and an ANXA5-ANXA5 biproduct was created, as indicated by mass analysis (**Figure 63**). The ANXA5-ANXA5 dimer byproduct was the most abundant species of the conjugate and due to the complexity of the dimer and limitations to protein mass analysis, the dimer product makeup could not be resolved further. The presence of a dimer was not present in previous SDS-PAGE analysis [152, 153]. This demonstrates the ANXA5-CMB conjugation is highly variable and not reliably reproducible.

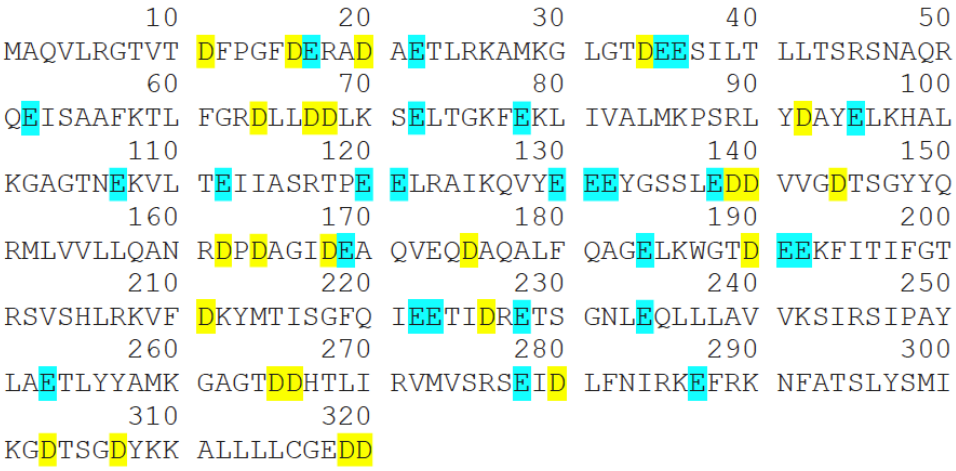

Figure 61: Locations of carbocyclic acid moieties on ANXA5 for EDC activation

Aspartate (blue) and glutamate (yellow) residues are possible EDC activation sites leading to ANXA5-ANXA5 crosslinking.

```
        10         20         30         40         50
MAQVLRGTVT DFPGFDERAD AETLRKAMKG LGTDEESILT LLTSRSNAQR
        60         70         80         90        100
QEISAAFKTL FGRDLLDDLK SELTGKFEKL IVALMKPSRL YDAYELKHAL
       110        120        130        140        150
KGAGTNEKVL TEIIASRTPE ELRAIKQVYE EEYGSSLEDD VVGDTSGYYQ
       160        170        180        190        200
RMLVVLLQAN RDPDAGIDEA QVEQDAQALF QAGELKWGTD EEKFITIFGT
       210        220        230        240        250
RSVSHLRKVF DKYMTISGFQ IEETIDRETS GNLEQLLLAV VKSIRSIPAY
       260        270        280        290        300
LAETLYYAMK GAGTDDHTLI RVMVSRSEID LFNIRKEFRK NFATSLYSMI
       310        320
KGDTSGDYKK ALLLLCGEDD
```

Figure 62: Location of primary amine moieties on ANXA5 for EDC cross linking

Lysine (yellow) residues are possible locations for ANXA5-ANXA5 crosslinking.

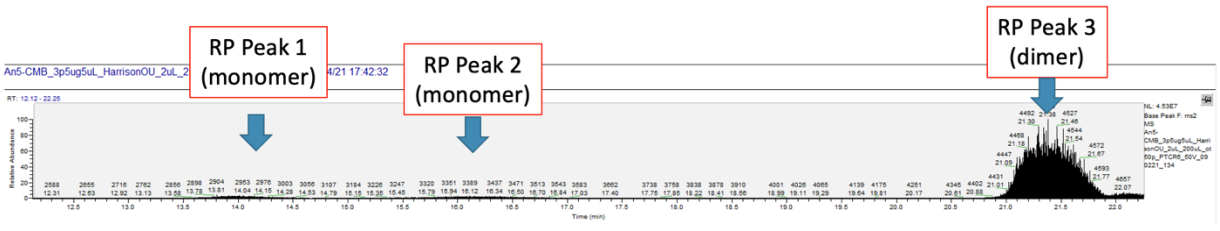

Figure 63: Denaturing intact mass analysis of ANXA5-CMB.

ANXA5-CMB exists as a dimer. The loading of the drug is extremely hindered, and the EDC is activating ANXA5, not CMB, during conjugation.

Although ANXA5-ANXA5 was the most abundant species in the ANXA5-CMB conjugate, the *in vitro* and *in vivo* data suggest that the addition of a CMB molecule could be the only reason for the observed cytotoxicity. ANXA5 is not cytotoxic (**Figure 29**) and the presence of an ANXA5-ANXA5 dimer would only aid in ANXA5 internalization into the cell. Although EDC has shown to be an interchain DNA crosslinking agent, the EDC-activated protein would react with a neighboring ANXA5 and form a dimer [275]. *In vivo*, ANXA5 alone has been shown to suppress tumor growth in a dose-dependent manner at 5 and 10 mg/kg of protein [203]. For *in vivo* dosing, the ANXA5 protein equivalent is only 1 μg/kg of ANXA5 in the 2.5 mg/kg ANXA5-CMB conjugate, and this dose would not have a therapeutic benefit if no drugs were loaded. Because of these uncertainties, it brings to question the reproducibility of this conjugate. Because of this, the ANXA5-CMB project ended.

Chapter 5: ANXA5-Valproic Acid Results and Discussion

Synthesis of ANXA5-VPA

The chemical makeup of ANXA5 and valproic acid (VPA) make them excellent candidates to be linked together through 1-ethyl-3-(3-dimethylamino)propylcarbodiimide, hydrochloride (EDC) crosslinking chemistry (**Figure 64**). EDC provides a zero-length linker that reacts carboxylic acids to amines through an addition-elimination reaction. First EDC activates the lone carboxylic acid on VPA creating an unstable o-acylisourea active ester. Next, ANXA5 is introduced, and 1 of the 22 primary amines (lysine residues) displaces the EDC crosslinker, generating a stable amide bond between ANXA5 and VPA [192]. Synthesis of ANXA5-VPA was confirmed with SDS-PAGE analysis (**Figure 65**).

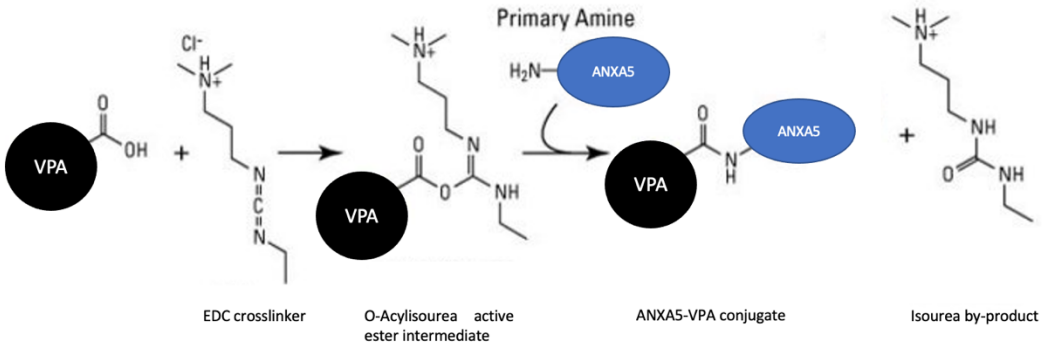

Figure 64: ANAX5-CMB crosslinking scheme

First VPA is activated with EDC. The VPA-EDC reaction generates a reactive O-acylisourea ester intermediate, and once a primary amine (lysine reside) is introduced, the EDC is displaced generating an isourea by-product and the ANXA5-VPA conjugate. Image adapted from https://www.thermofisher.com/order/catalog/product/22980.

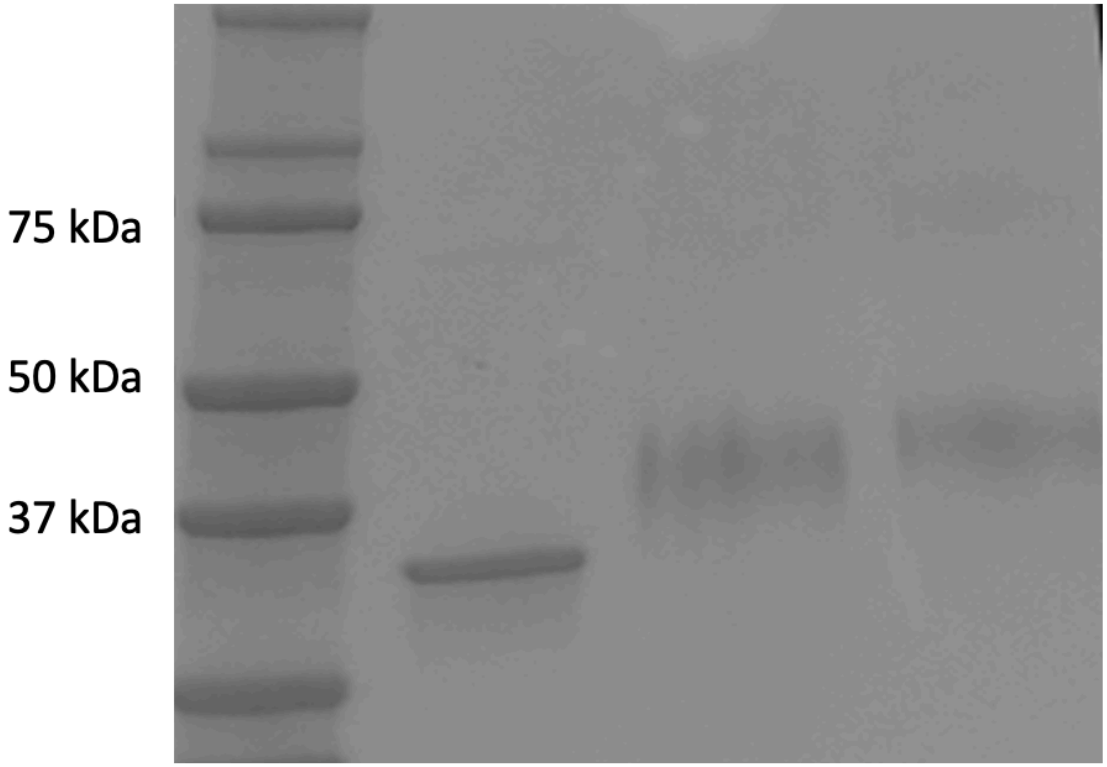

Figure 65: SDS page of ANXA5-VPA conjugate

ANXA5-DM1 shows a mass increase consistent with 10 molecules of VPA added to each protein in lanes 3 and 4. Lane 2 has unconjugated ANXA5 as a control.

EDC crosslinking does not contribute to the molecular weight of the ANXA5-VPA conjugate, and any increase in weight is a result of the addition of a VPA drug molecule. For every VPA molecule added, a shift upward of 144 da will be observed. Using gel electrophoresis, we observe a mass increase from 36 kDa of ANXA5 to about 38 kDa which indicates the addition of

14 molecules of VPA to 1 ANXA5 for two separate conjugations (**Figure 66**). After quantifying four separate conjugations, the average drug-to-protein ratio of VPA to ANXA5 is 10:1 (**Table 7**).

The current FDA-approved antibody-drug conjugates have an antibody-to-drug ratio of less than 4:1, due to the highly cytotoxic payloads that cannot be administered as a free drug [276]. VPA is already FDA-approved as an antiepileptic drug and can be administered as a free drug. The ANXA5-VPA can carry over two times more drugs and would possibly not be limited by severe side effects (hair loss, weight loss, nausea, vomiting, etc.) as seen with current chemotherapies and antibody-drug conjugates. The ANXA5-VPA conjugate was relatively pure, with very little ANXA5-ANXA5 crosslinking as indicated by the absence of band smear at approximately 75 kDa. While SDS-PAGE has proven to be an efficient method in quantifying ANXA5-drug conjugates, it is the only method available for the ANXA5-VPA conjugate [152, 153, 192, 206, 277]. VPA lacks a chromophore and has poor UV absorption, so fluorescent excitation or UV absorption techniques (i.e., plate reader, UV-Vis, etc.) cannot be utilized [278]. While quantitation limitations exist, the simple chemistry for the ANXA5-VPA is advantageous for yield and cost.

Table 7: Average molecules of VPA added to ANXA5

ANXA5-VPA sample	Molecules of VPA
1	15.1
2	13.8
3	4.5
4	5.6
Average	9.7 ± 5.4

Many chemotherapeutic agents have low aqueous solubility and complex structures that involve multiple carboxylic acids and/or primary amines, making them incompatible with EDC crosslinking [279]. The complex chemistries needed to create unwanted byproducts that decrease the final yield and ultimately lead to an increase in cost. However, the simple structure of VPA makes it an ideal molecule to link to ANXA5. VPA is a short-chain fatty acid with only one carboxylic acid and does not contain any primary amines, meaning unwanted VPA-VPA bioproducts will not be formed. Another advantage of VPA is that it is water soluble, unlike CMB. The ANXA5-VPA conjugation protocol utilizes over 10 times more EDC than the ANXA5-CMB conjugation protocol, and the presence of ANXA5-ANXA5 dimers was not observed with the VPA conjugation. This further validating solubility of activated drug limits drug loading.

ANXA5-VPA Cytotoxicity

After confirming the conjugation of VPA to ANXA5, the cytotoxicity of the ANXA5-VPA conjugate was tested in two murine TNBC cell lines. EMT6 and 4T1 cells were incubated with 0-10 mM of VPA in the ANXA5-VPA conjugate or free VPA for 48 hours. After 48 hours, cell viability was analyzed via a fluorescent Alamar Blue assay. Percent viability was determined by normalizing the control (0 mM VPA) to 100% and comparing each treatment group to the control ($n = 3$).

For both murine TNBC cell lines, the ANXA5-VPA conjugate showed superior cytotoxic activity when compared to free VPA after 48 hours (**Figures 68 and 67**). The ANXA5-VPA conjugate significantly increased cell death at doses as low as 97 nM when compared to the free drug control. The IC50 after 48 hours for both cell lines was approximately 10 μM, but the IC50 value for free VPA could not be obtained with a dose of up to 10 mM. This finding for free VPA

is unsurprising, given the fact that VPA requires over 1 mM and 72-96 hours to achieve an IC50 value [280, 281]. The ANXA5-VPA conjugate not only decreases the concentration of VPA needed to induce cell death but also decreases time. While this is the first protein-VPA conjugate to be developed, a tumor-homing peptide-VPA conjugate has also been created. (iRGD-GFLG-VPA) [282].

The iRGD-GFLG-VPA consists of three parts. The first part consists of the tumor-homing peptide iRGD. iRGD is a cell-penetrating peptide that is localized at integrins expressed on tumor vasculature [282, 283]. The second part consists of a lysosomal degrading tetrapeptide spacer (GFLG) which allows the drug to be released into the cell. The third part is the drug VPA. The iRGD-GFLG-VPA was linked together through a six-step reaction involving solid-phase peptide synthesis and purified via semi-preparative HPLC [282]. In comparison, the ANXA5-VPA conjugate requires only two steps and has a high overall yield. The iRGD-GFLG-VPA has been tested on prostate cancer cells, but the peptide conjugate still requires a full 72 hours and a VPA dose above 1 mM. More importantly, the covalent addition of VPA did not affect cytotoxicity differently than a mixture of VPA with iRGD-GFLG. The cytotoxic action of the ANXA5-VPA conjugate is a result of the covalent addition of VPA and not the protein (**Figure 32**). Additionally, the ANXA5-VPA conjugate delivers nearly 10 times more VPA than the iRGD-GFLG-VPA conjugate, and internalization is nonreceptor mediated, unlike iRGD.

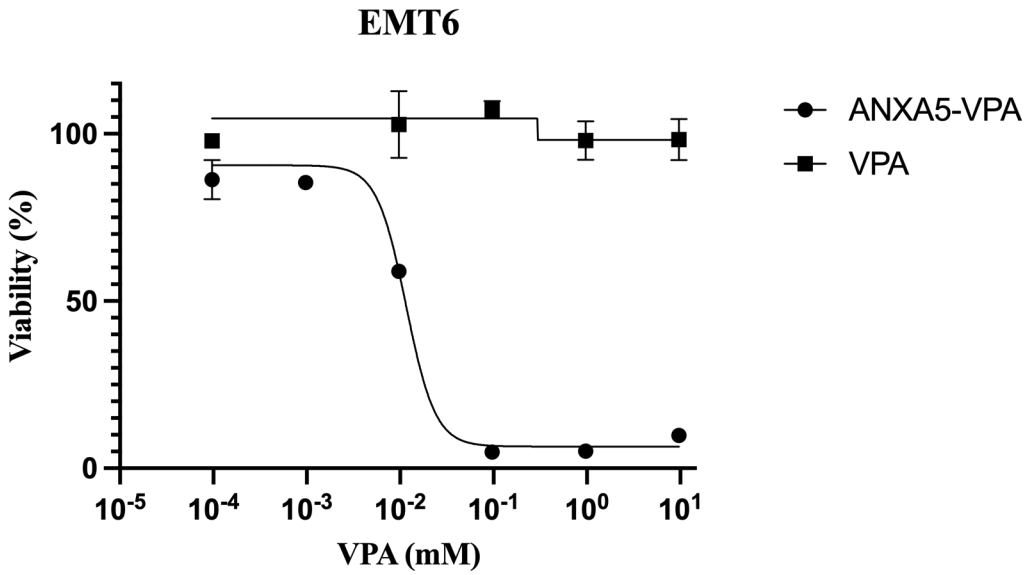

Figure 66: 48-hour effects of ANXA5-VPA and free VPA on 4T1 cell viability

Cells were treated with 0-10 mM VPA in the ANXA5-VPA conjugate or free VPA in fully supplemented growth medium. The IC50 concentration for ANXA5-VPA was .009 mM, while the IC50 concentration of free VPA could not be calculated. Cell viability was measured via an Alamar Blue assay, and each sample was represented as a percentage of the untreated control (0 mM) and viability was compared to the control (0 mM) after 48 hours. Statistical analysis at each dose was performed with a student's T-test with data represented as mean ± SD (n = 3)

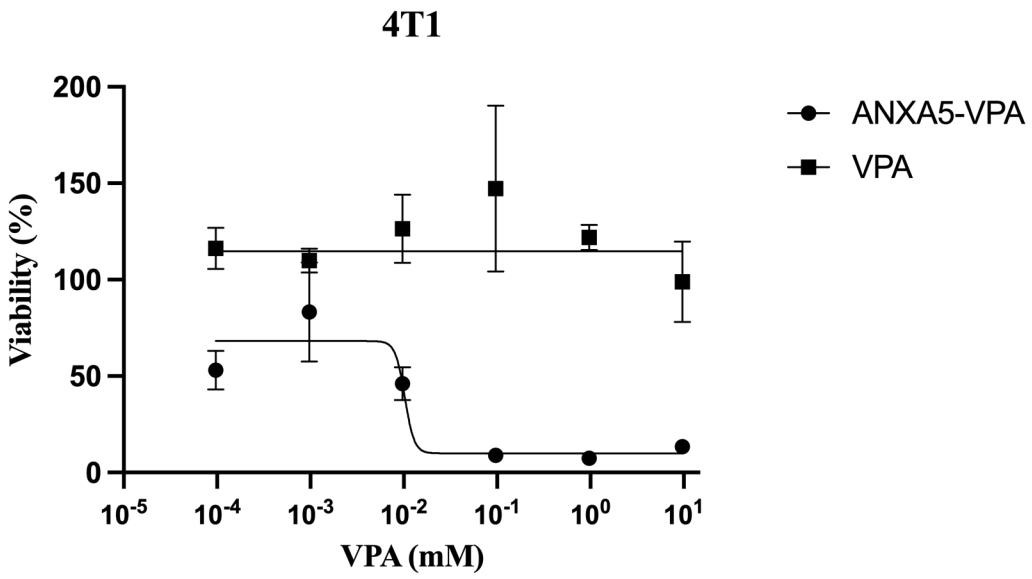

Figure 67: 48-hour effects of ANXA5-VPA and free VPA on 4T1 cell viability

Cells were treated with 0-10 mM VPA in the ANXA5-VPA conjugate or free VPA in fully supplemented growth medium. The IC50 concentration for ANXA5-VPA was .010 mM, while the IC50 concentration of free VPA could not be calculated. Cell viability was measured via an Alamar Blue assay, and each sample was represented as a percentage of the untreated control (0 mM) and viability was compared to the control (0 mM) after 48 hours. Statistical analysis at each dose was performed with a student's T-test with data represented as mean ± SD (n = 3)

Chapter 6: Conclusions and Future Directions

Three ANXA5-protein drug conjugates with different mechanisms of action have been created for the treatment of TNBC. The ANXA5-drug conjugates have profound anticancer effects both *in vitro* and in *vivo*.

The novel ANXA5-DM1 conjugate is highly reproducible and has an average drug-to-protein ratio of 4:1. ANXA5 has a high specificity to external PS exposure and can bind to PS-expressing cells in as little as 5 minutes and has a preference to TNBC over healthy vasculature and epithelium. The conjugate readily reproduces an IC50 value under 1 nM for TNBC cells, and healthy vasculature and epithelial cells require 4-190 times more drugs in the conjugate to induce 50% cell death. The ANXA5-DM1 conjugate has increased ATP release and calreticulin surface exposure, which are hallmarks of ICD. ANXA5-DM1 may be classified as an ICD inducer. When translated *in vivo*, 0.025 mg/kg maintains tumor volumes under 500 mm^3 when treated once a week for 21 days. When combining the ANXA5-DM1 with the mTOR inhibitor, rapamycin, and the checkpoint inhibitor, anti-PD-1, tumor volumes were 2.2-4.4 times smaller at the end of the treatment than the untreated control in two syngeneic murine TNBC models. When changing the administration from IP to IT, the frequency and dosage of ANXA5-DM1 were increased, and one mouse had complete tumor regression. This work provided fundamental *in vitro* characterization and *in vivo* translation of the ANXA5-DM1 conjugate.

ANXA5-CMB does not induce cell death on HUVEC cells, and for MCF10A cells, 2.2-14 times more conjugate is needed to induce cell death in comparison to TNBC cells. When translated *in vivo*, daily IP injections of ANXA5-CMB over 1 mg/kg resulted in tumor volumes below 100 mm^3; however, daily IP injections of the ANXA5-CMB conjugate resulted in high fatalities. When the dosing schedule was optimized to a continuous 5-day treatment period followed by 2

consecutive days of rest, 1 mg/kg of ANXA5-CMB significantly increased survival while maintaining tumor volumes under 500 mm^3 during a 21-day treatment period. The ANXA5-CMB conjugate was quantified through mass analysis, but a drug-to-protein ratio of <1:1 was observed. The limited reproducibility due to the aqueous solubility limitation of CMB brings uncertainties to the actual composition of the conjugate.

The ANXA5-VPA conjugate was created through EDC crosslinking and had an average protein-to-drug ratio of 10:1 as quantified by SDS-PAGE analysis. The ANXA5-VPA conjugate showed superior cytotoxicity over the free drug. The conjugate also decreased the amount of time needed to induce cell death. This work provided the first-ever protein-VPA conjugate for the treatment of TNBC.

Moving forward, there are many opportunities to optimize the ANXA5-protein drug conjugates for cancer therapies. First and foremost, the ANXA5-protein drug conjugates could be translated to another cancer type because PS externalization is a fundamental characteristic of cancer. ANXA5-based therapies have proven to be successful in treating bladder, prostate, and pancreatic cancer, suggesting the ANXA5-protein drug conjugates could be utilized to treat these cancers as well.

For the ANXA5-DM1 conjugate, further dosage optimization of IT injections would be needed. Daily injections of the ANXA5-DM1 provided great tumor control, but treatment expulsion was a huge limitation of the therapy. By creating a hydrogel-based system, a sustained release of the ANXA5-DM1 conjugate could be achieved [284]. This would provide for less frequent injections and prevent the escape of the conjugate from the tumor. An additional IT immunogenicity study would also be beneficial to determine the difference between IT and IP injection methods. To expand on the holistic treatment, I would recommend the same study

performed but with ANXA5-DM1 IT injections. In addition to an anti-PD-1 monoclonal antibody, an anti-cytotoxic T-lymphocyte-associated protein 4 (CTLA-4) monoclonal antibody could be used as a combination immunotherapy [285].

For the ANXA5-VPA conjugate, it would be necessary to explore mass analysis to be able to fully quantify the conjugates drug to protein ratio. For *in vitro* analysis, the cytotoxic activity of the conjugate should be tested against healthy cell lines (MCF10A, HUVEC, HAAE-1). The cytotoxic effects of ANXA5-VPA could also be assessed for caspase regulation, pro-/anti-apoptotic molecule regulation, HDAC activity, and chromatin acetylation patterns of histones H3 and H4. For *in vivo* analysis, a dosage optimization study would be needed to explore the therapeutic effects of the conjugate. It would also be interesting to explore how the ANXA5-DM1 and ANXA5-VPA conjugate could be used as a dual-targeted treatment. VPA has been shown to enhance the anti-cancer activity of microtubule inhibitors by regulating tubulin acylation [286]. Although competitive inhibition may occur because both conjugates are fighting for PS binding sites, it is unlikely that both conjugates will completely saturate the cell surface.

This dissertation has provided valuable data for the translation of the ANXA5-DM1 and ANXA5-CMB conjugates as well as designing and testing the anticancer activity of the novel ANXA5-VPA conjugate. The three conjugates exhibit different anticancer effects, but reliably deliver chemotherapeutic agents to the tumor surfaced for internalization. ANXA5-protein drug conjugates provide an exciting and promising future for cancer treatment.

References

[1] H. Sung, J. Ferlay, R.L. Siegel, M. Laversanne, I. Soerjomataram, A. Jemal, F. Bray, Global Cancer Statistics 2020: GLOBOCAN Estimates of Incidence and Mortality Worldwide for 36 Cancers in 185 Countries, CA Cancer J Clin, 71 (2021) 209-249.

[2] S. Senapati, A.K. Mahanta, S. Kumar, P. Maiti, Controlled drug delivery vehicles for cancer treatment and their performance, Signal Transduct Target Ther, 3 (2018) 7.

[3] T. Lammers, F. Kiessling, W.E. Hennink, G. Storm, Drug targeting to tumors: principles, pitfalls and (pre-) clinical progress, J Control Release, 161 (2012) 175-187.

[4] R.A. Kudgus, C.A. Walden, R.M. McGovern, J.M. Reid, J.D. Robertson, P. Mukherjee, Tuning pharmacokinetics and biodistribution of a targeted drug delivery system through incorporation of a passive targeting component, Sci Rep, 4 (2014) 5669.

[5] N.D. Donahue, H. Acar, S. Wilhelm, Concepts of nanoparticle cellular uptake, intracellular trafficking, and kinetics in nanomedicine, Adv Drug Deliv Rev, 143 (2019) 68-96.

[6] R.L. Siegel, K.D. Miller, H.E. Fuchs, A. Jemal, Cancer statistics, 2022, CA Cancer J Clin, 72 (2022) 7-33.

[7] A. Srivastava, D.J. Creek, Discovery and Validation of Clinical Biomarkers of Cancer: A Review Combining Metabolomics and Proteomics, 2019.

[8] Targeted Cancer Therapies, 2021.

[9] J.G. Kay, M. Koivusalo, X. Ma, T. Wohland, S. Grinstein, Phosphatidylserine dynamics in cellular membranes, Molecular Biology of the Cell, (2012).

[10] J.E. Vance, Phosphatidylserine and phosphatidylethanolamine in mammalian cells: Two metabolically related aminophospholipids, 2008.

[11] J.G. Kay, S. Grinstein, Sensing phosphatidylserine in cellular membranes, 2011.

[12] S. Nagata, T. Sakuragi, K. Segawa, Flippase and scramblase for phosphatidylserine exposure, Current Opinion in Immunology, 62 (2020) 31-38.

[13] K.F. N'Guessan, P.H. Patel, X. Qi, SapC-DOPS - A Phosphatidylserine-targeted Nanovesicle for selective Cancer therapy, 2020.

[14] S.D. Vallabhapurapu, V.M. Blanco, M.K. Sulaiman, S.L. Vallabhapurapu, Z. Chu, R.S. Franco, X. Qi, Variation in human cancer cell external phosphatidylserine is regulated by flippase activity and intracellular calcium, Oncotarget, (2015).

[15] S. Riedl, B. Rinner, M. Asslaber, H. Schaider, S. Walzer, A. Novak, K. Lohner, D. Zweytick, In search of a novel target - Phosphatidylserine exposed by non-apoptotic tumor cells and

metastases of malignancies with poor treatment efficacy, Biochimica et Biophysica Acta - Biomembranes, 1808 (2011) 2638-2645.

[16] S. Ran, P.E. Thorpe, Phosphatidylserine is a marker of tumor vasculature and a potential target for cancer imaging and therapy.

[17] S. Ran, A. Downes, P.E. Thorpe, Increased exposure of anionic phospholipids on the surface of tumor blood vessels, Cancer Research, (2002).

[18] K. Clodi, K.O. Kliche, S. Zhao, D. Weidner, T. Schenk, U. Consoli, S. Jiang, V. Snell, M. Andreeff, Cell-surface exposure of phosphatidylserine correlates with the stage of fludarabine-induced apoptosis chronic lymphocytic leukemia and expression of apoptosis-regulating genes, Cytometry, (2000).

[19] I.J. Fidler, A.J. Schroit, J. Connor, C.D. Bucana, I.J. Fidler, Elevated Expression of Phosphatidylserine in the Outer Membrane Leaflet of Human Tumor Cells and Recognition by Activated Human Blood Monocytes, Cancer Research, (1991).

[20] J. Xu, S.M. Su, X. Zhang, U.I. Chan, R. Adhav, X. Shu, J. Liu, J. Li, L. Mo, Y. Wang, T. An, J.H. Lei, K. Miao, C.X. Deng, X. Xu, ATP11B inhibits breast cancer metastasis in a mouse model by suppressing externalization of nonapoptotic phosphatidylserine, J Clin Invest, 132 (2022).

[21] Y. Song, W.T. Barry, D.S. Seah, N.M. Tung, J.E. Garber, N.U. Lin, Patterns of recurrence and metastasis in BRCA1/BRCA2-associated breast cancers, Cancer, 126 (2020) 271-280.

[22] H.J. Chang, U.C. Yang, M.Y. Lai, C.H. Chen, Y.C. Fann, High BRCA1 gene expression increases the risk of early distant metastasis in ER(+) breast cancers, Sci Rep, 12 (2022) 77.

[23] K.I. Savage, D.P. Harkin, BRCA1, a 'complex' protein involved in the maintenance of genomic stability, FEBS J, 282 (2015) 630-646.

[24] P. Liang, H. Yang, Molecular underpinning of intracellular pH regulation on TMEM16F, J Gen Physiol, 153 (2021).

[25] B.A. Webb, M. Chimenti, M.P. Jacobson, D.L. Barber, Dysregulated pH: a perfect storm for cancer progression, Nat Rev Cancer, 11 (2011) 671-677.

[26] T. Sakuragi, H. Kosako, S. Nagata, Phosphorylation-mediated activation of mouse Xkr8 scramblase for phosphatidylserine exposure, Proceedings of the National Academy of Sciences of the United States of America, (2019).

[27] J.H. Chung, D.H. Kim, Y.S. Kim, B.S. Son, D. Kim, C. Hwang, D. Shin, S.G. Noh, J.H. Han, D.K. Kim, J.H. Kim, J.S. Koo, H.Y. Chung, S.H. Yoon, Upregulation of P21-Activated Kinase 1 (PAK1)/CREB Axis in Squamous Non-Small Cell Lung Carcinoma, Cell Physiol Biochem, 50 (2018) 304-316.

[28] H. Takatsu, M. Takayama, T. Naito, N. Takada, K. Tsumagari, Y. Ishihama, K. Nakayama, H.W. Shin, Phospholipid flippase ATP11C is endocytosed and downregulated following Ca(2+)-mediated protein kinase C activation, Nat Commun, 8 (2017) 1423.

[29] E. Silva-Pavez, J.C. Tapia, Protein Kinase CK2 in Cancer Energetics, Front Oncol, 10 (2020) 893.

[30] Y. Sang, P. Kong, S. Zhang, L. Zhang, Y. Cao, X. Duan, T. Sun, Z. Tao, W. Liu, SGK1 in Human Cancer: Emerging Roles and Mechanisms, Front Oncol, 10 (2020) 608722.

[31] J. Suzuki, D.P. Denning, E. Imanishi, H.R. Horvitz, S. Nagata, Xk-related protein 8 and CED-8 promote phosphatidylserine exposure in apoptotic cells, Science, 341 (2013) 403-406.

[32] T. Dittmar, J. Weiler, T. Luo, R. Hass, Cell-Cell Fusion Mediated by Viruses and HERV-Derived Fusogens in Cancer Initiation and Progression, Cancers (Basel), 13 (2021).

[33] J.M. Whitlock, L.V. Chernomordik, Flagging fusion: Phosphatidylserine signaling in cell-cell fusion, J Biol Chem, 296 (2021) 100411.

[34] G.W. Kim, G.H. Nam, I.S. Kim, S.Y. Park, Xk-related protein 8 regulates myoblast differentiation and survival, FEBS J, 284 (2017) 3575-3588.

[35] R. Audo, C. Hua, M. Hahne, B. Combe, J. Morel, C.I. Daien, Phosphatidylserine Outer Layer Translocation Is Implicated in IL-10 Secretion by Human Regulatory B Cells, PLoS One, 12 (2017) e0169755.

[36] F.K. Noubissi, T. Harkness, C.M. Alexander, B.M. Ogle, Apoptosis-induced cancer cell fusion: a mechanism of breast cancer metastasis, Faseb J, 29 (2015) 4036-4045.

[37] R.B. Birge, S. Boeltz, S. Kumar, J. Carlson, J. Wanderley, D. Calianese, M. Barcinski, R.A. Brekken, X. Huang, J.T. Hutchins, B. Freimark, C. Empig, J. Mercer, A.J. Schroit, G. Schett, M. Herrmann, Phosphatidylserine is a global immunosuppressive signal in efferocytosis, infectious disease, and cancer, 2016.

[38] T. Burstyn-Cohen, A. Maimon, TAM receptors, Phosphatidylserine, inflammation, and Cancer, Cell Commun Signal, 17 (2019) 156.

[39] K.V. Myers, S.R. Amend, K.J. Pienta, Targeting Tyro3, Axl and MerTK (TAM receptors): implications for macrophages in the tumor microenvironment, Mol Cancer, 18 (2019) 94.

[40] X. Liang, M. Luo, B. Shao, J.Y. Yang, A. Tong, R.B. Wang, Y.T. Liu, R. Jun, T. Liu, T. Yi, X. Zhao, Y.Q. Wei, X.W. Wei, Phosphatidylserine released from apoptotic cells in tumor induces M2-like macrophage polarization through the PSR-STAT3-JMJD3 axis, Cancer Commun (Lond), 42 (2022) 205-222.

[41] S. Budhu, R. Giese, A. Gupta, K. Fitzgerald, R. Zappasodi, S. Schad, D. Hirschhorn, L.F. Campesato, O. De Henau, M. Gigoux, C. Liu, G. Mazo, L. Deng, C.A. Barker, J.D. Wolchok, T.

Merghoub, Targeting Phosphatidylserine Enhances the Anti-tumor Response to Tumor-Directed Radiation Therapy in a Preclinical Model of Melanoma, Cell Rep, 34 (2021) 108620.

[42] F. Bakar, Annexin Proteins: Novel Promising Targets for Anticancer Drug Development, in: M.L. Jolanta Natalia Latosińska (Ed.) Unique Aspects of Anti-cancer Drug Development, IntechOpen, London, United Kingdom 2017.

[43] M.A. Lizarbe, J.I. Barrasa, N. Olmo, F. Gavilanes, J. Turnay, Annexin-phospholipid interactions. Functional implications, Int J Mol Sci, 14 (2013) 2652-2683.

[44] Y. Xi, R. Ju, Y. Wang, Roles of Annexin A protein family in autophagy regulation and therapy, Biomed Pharmacother, 130 (2020) 110591.

[45] J. Wang, J. Liu, Y. Cao, M. Hu, Z. Hua, Domain IV of Annexin A5 Is Critical for Binding Calcium and Guarantees Its Maximum Binding to the Phosphatidylserine Membrane, Molecules, 22 (2017).

[46] I. Vermes, C. Haanen, H. Steffens-Nakken, C. Reutellingsperger, A novel assay for apoptosis Flow cytometric detection of phosphatidylserine expression on early apoptotic cells using fluorescein labelled Annexin V, Journal of Immunological Methods, (1995).

[47] D.R. Patel, J.M. Isas, A.S. Ladokhin, C.C. Jao, Y.E. Kim, T. Kirsch, R. Langen, H.T. Haigler, The conserved core domains of annexins A1, A2, A5, and B12 can be divided into two groups with different Ca2+-dependent membrane-binding properties, Biochemistry, 44 (2005) 2833-2844.

[48] H.O. van Genderen, H. Kenis, L. Hofstra, J. Narula, C.P. Reutelingsperger, Extracellular annexin A5: functions of phosphatidylserine-binding and two-dimensional crystallization, Biochim Biophys Acta, 1783 (2008) 953-963.

[49] K. Schutters, C. Reutelingsperger, Phosphatidylserine targeting for diagnosis and treatment of human diseases, Apoptosis, 15 (2010) 1072-1082.

[50] Y.C. Lin, C. Chipot, S. Scheuring, Annexin-V stabilizes membrane defects by inducing lipid phase transition, Nat Commun, 11 (2020) 230.

[51] H. Kenisi, H. Van Genderen, A. Bennaghmouch, H.A. Riniaj, P. Frederik, J. Narula, L. Hofstra, C.P.M. Reutelingsperger, Cell surface-expressed phosphatidylserine and annexin A5 open a novel portal of cell entry, Journal of Biological Chemistry, (2004).

[52] L. Ungethum, M. Chatrou, D. Kusters, L. Schurgers, C.P. Reutelingsperger, Molecular imaging of cell death in tumors. Increasing annexin A5 size reduces contribution of phosphatidylserine-targeting function to tumor uptake, PLoS One, 9 (2014) e96749.

[53] H. Maeda, H. Nakamura, J. Fang, The EPR effect for macromolecular drug delivery to solid tumors: Improvement of tumor uptake, lowering of systemic toxicity, and distinct tumor imaging in vivo, Adv Drug Deliv Rev, 65 (2013) 71-79.

[54] A. Woodward, G.N.F. Faria, R.G. Harrison, Annexin A5 as a targeting agent for cancer treatment, Cancer Lett, 547 (2022) 215857.

[55] W.H. Organization, World Cancer Report: Cancer Research for Cancer Prevention, 2020.

[56] M. Zubair, S. Wang, N. Ali, Advanced Approaches to Breast Cancer Classification and Diagnosis, Front Pharmacol, 11 (2020) 632079.

[57] K.A. Won, C. Spruck, Triplenegative breast cancer therapy: Current and future perspectives (Review), Int J Oncol, 57 (2020) 1245-1261.

[58] S.M. Ilie, X.E. Bacinschi, I. Botnariuc, R.M. Anghel, Potential clinically useful prognostic biomarkers in triple-negative breast cancer: preliminary results of a retrospective analysis, Breast Cancer (Dove Med Press), 10 (2018) 177-194.

[59] Z. Wang, H. Wang, X. Sun, Y. Fang, S.S. Lu, S.N. Ding, X.S. Chen, K.W. Shen, A Risk Stratification Model for Predicting Overall Survival and Surgical Benefit in Triple-Negative Breast Cancer Patients With de novo Distant Metastasis, Front Oncol, 10 (2020) 14.

[60] J.Y. Hsu, C.J. Chang, J.S. Cheng, Survival, treatment regimens and medical costs of women newly diagnosed with metastatic triple-negative breast cancer, Sci Rep, 12 (2022) 729.

[61] D. O'Reilly, M.A. Sendi, C.M. Kelly, Overview of recent advances in metastatic triple negative breast cancer, World J Clin Oncol, 12 (2021) 164-182.

[62] F. Carlino, A. Diana, A. Piccolo, A. Ventriglia, V. Bruno, I. De Santo, O. Letizia, F. De Vita, B. Daniele, F. Ciardiello, M. Orditura, Immune-Based Therapy in Triple-Negative Breast Cancer: From Molecular Biology to Clinical Practice, Cancers (Basel), 14 (2022).

[63] W.M.C. van den Boogaard, D.S.J. Komninos, W.P. Vermeij, Chemotherapy Side-Effects: Not All DNA Damage Is Equal, Cancers (Basel), 14 (2022).

[64] G. Bedoschi, P.A. Navarro, K. Oktay, Chemotherapy-induced damage to ovary: mechanisms and clinical impact, Future Oncol, 12 (2016) 2333-2344.

[65] D. Albano, M. Benenati, A. Bruno, F. Bruno, M. Calandri, D. Caruso, D. Cozzi, R. De Robertis, F. Gentili, I. Grazzini, G. Micci, A. Palmisano, C. Pessina, P. Scalise, F. Vernuccio, A. Barile, V. Miele, R. Grassi, C. Messina, S.W.G. Young, Imaging side effects and complications of chemotherapy and radiation therapy: a pictorial review from head to toe, Insights Imaging, 12 (2021) 76.

[66] S. Mancuso, D. Scaturro, M. Santoro, G. Di Gaetano, F. Vitagliani, V. Falco, S. Siragusa, S. Gonnelli, G.L. Mauro, Bone damage after chemotherapy for lymphoma: a real-world experience, BMC Musculoskelet Disord, 22 (2021) 1024.

[67] X. Bai, J. Ni, J. Beretov, P. Graham, Y. Li, Triple-negative breast cancer therapeutic resistance: Where is the Achilles' heel?, Cancer Lett, 497 (2021) 100-111.

[68] R.M. Layman, B. Arun, PARP Inhibitors in Triple-Negative Breast Cancer Including Those With BRCA Mutations, Cancer J, 27 (2021) 67-75.

[69] N. D'Abreo, S. Adams, Immune-checkpoint inhibition for metastatic triple-negative breast cancer: safety first?, Nat Rev Clin Oncol, 16 (2019) 399-400.

[70] P. Tarantino, C. Corti, P. Schmid, J. Cortes, E.A. Mittendorf, H. Rugo, S.M. Tolaney, G. Bianchini, F. Andre, G. Curigliano, Immunotherapy for early triple negative breast cancer: research agenda for the next decade, NPJ Breast Cancer, 8 (2022) 23.

[71] N. Tung, J.E. Garber, PARP inhibition in breast cancer: progress made and future hopes, NPJ Breast Cancer, 8 (2022) 47.

[72] S.M. Noordermeer, H. van Attikum, PARP Inhibitor Resistance: A Tug-of-War in BRCA-Mutated Cells, Trends Cell Biol, 29 (2019) 820-834.

[73] H. Li, Z.Y. Liu, N. Wu, Y.C. Chen, Q. Cheng, J. Wang, PARP inhibitor resistance: the underlying mechanisms and clinical implications, Mol Cancer, 19 (2020) 107.

[74] X. Liu, K. Wu, D. Zheng, C. Luo, Y. Fan, X. Zhong, H. Zheng, Efficacy and Safety of PARP Inhibitors in Advanced or Metastatic Triple-Negative Breast Cancer: A Systematic Review and Meta-Analysis, Front Oncol, 11 (2021) 742139.

[75] M. Althobiti, M.A. Aleskandarany, C. Joseph, M. Toss, N. Mongan, M. Diez-Rodriguez, C.C. Nolan, I. Ashankyty, I.O. Ellis, A.R. Green, E.A. Rakha, Heterogeneity of tumour-infiltrating lymphocytes in breast cancer and its prognostic significance, Histopathology, 73 (2018) 887-896.

[76] H. Yi, Y. Li, Y. Tan, S. Fu, F. Tang, X. Deng, Immune Checkpoint Inhibition for Triple-Negative Breast Cancer: Current Landscape and Future Perspectives, Front Oncol, 11 (2021) 648139.

[77] Z. Liu, M. Li, Z. Jiang, X. Wang, A Comprehensive Immunologic Portrait of Triple-Negative Breast Cancer, Transl Oncol, 11 (2018) 311-329.

[78] R. Nanda, L.Q. Chow, E.C. Dees, R. Berger, S. Gupta, R. Geva, L. Pusztai, K. Pathiraja, G. Aktan, J.D. Cheng, V. Karantza, L. Buisseret, Pembrolizumab in Patients With Advanced Triple-Negative Breast Cancer: Phase Ib KEYNOTE-012 Study, J Clin Oncol, 34 (2016) 2460-2467.

[79] O. Shahzad, N. Thompson, G. Clare, S. Welsh, E. Damato, P. Corrie, Ocular adverse events associated with immune checkpoint inhibitors: a novel multidisciplinary management algorithm, Ther Adv Med Oncol, 13 (2021) 1758835921992989.

[80] K.M. Fenn, K. Kalinsky, Sacituzumab govitecan: antibody-drug conjugate in triple-negative breast cancer and other solid tumors, Drugs Today (Barc), 55 (2019) 575-585.

[81] L.A. Carey, D. Loirat, K. Punie, A. Bardia, V. Dieras, F. Dalenc, J.R. Diamond, C. Fontaine, G. Wang, H.S. Rugo, S.A. Hurvitz, K. Kalinsky, J. O'Shaughnessy, S. Loibl, L. Gianni, M. Piccart, Y. Zhu, R. Delaney, S. Phan, J. Cortes, Sacituzumab govitecan as second-line treatment for

metastatic triple-negative breast cancer-phase 3 ASCENT study subanalysis, NPJ Breast Cancer, 8 (2022) 72.

[82] D.M. Goldenberg, T.M. Cardillo, S.V. Govindan, E.A. Rossi, R.M. Sharkey, Trop-2 is a novel target for solid cancer therapy with sacituzumab govitecan (IMMU-132), an antibody-drug conjugate (ADC), Oncotarget, 6 (2015) 22496-22512.

[83] D.V. Santi, L. Cabel, F.C. Bidard, Does sacituzumab-govitecan act as a conventional antibody drug conjugate (ADC), a prodrug of SN-38 or both?, Ann Transl Med, 9 (2021) 1113.

[84] A.J. Ocean, A.N. Starodub, A. Bardia, L.T. Vahdat, S.J. Isakoff, M. Guarino, W.A. Messersmith, V.J. Picozzi, I.A. Mayer, W.A. Wegener, P. Maliakal, S.V. Govindan, R.M. Sharkey, D.M. Goldenberg, Sacituzumab govitecan (IMMU-132), an anti-Trop-2-SN-38 antibody-drug conjugate for the treatment of diverse epithelial cancers: Safety and pharmacokinetics, Cancer, 123 (2017) 3843-3854.

[85] A. Bardia, S.A. Hurvitz, S.M. Tolaney, D. Loirat, K. Punie, M. Oliveira, A. Brufsky, S.D. Sardesai, K. Kalinsky, A.B. Zelnak, R. Weaver, T. Traina, F. Dalenc, P. Aftimos, F. Lynce, S. Diab, J. Cortes, J. O'Shaughnessy, V. Dieras, C. Ferrario, P. Schmid, L.A. Carey, L. Gianni, M.J. Piccart, S. Loibl, D.M. Goldenberg, Q. Hong, M.S. Olivo, L.M. Itri, H.S. Rugo, A.C.T. Investigators, Sacituzumab Govitecan in Metastatic Triple-Negative Breast Cancer, N Engl J Med, 384 (2021) 1529-1541.

[86] G.L. Rosano, E.A. Ceccarelli, Recombinant protein expression in Escherichia coli: advances and challenges, Front Microbiol, 5 (2014) 172.

[87] E. Doevendans, H. Schellekens, Immunogenicity of Innovative and Biosimilar Monoclonal Antibodies, Antibodies (Basel), 8 (2019).

[88] A. Juan, F.J. Cimas, I. Bravo, A. Pandiella, A. Ocana, C. Alonso-Moreno, Antibody Conjugation of Nanoparticles as Therapeutics for Breast Cancer Treatment, Int J Mol Sci, 21 (2020).

[89] S.M. Kupchan, Y. Komoda, W.A. Court, G.J. Thomas, R.M. Smith, A. Karim, C.J. Gilmore, R.C. Haltiwanger, R.F. Bryan, Maytansine, a novel antileukemic ansa macrolide from Maytenus ovatus, J Am Chem Soc, 94 (1972) 1354-1356.

[90] S. Wasantapruek, M. Kruatrachue, A. Piankijagum, K. Limpongs, Letter: Novel maytansinoids. Structural interrelations and requirements for antileukemic activity, J Am Chem Soc, 96 (1974) 3706-3708.

[91] B. Bhattacharyya, J. Wolff, Maytansine binding to the vinblastine sites of tubulin, FEBS Letters, 75 (1977) 159-162.

[92] R.H. Blum, T. Kahlert, Maytansine: a phase I study of an ansa macrolide with antitumor activity, Cancer Treat Rep, 62 (1978) 435-438.

[93] B.F. Issell, S.T. Crooke, Maytansine, Cancer Treat Rev, 5 (1978) 199-207.

[94] B.A. Chabner, A.S. Levine, B.L. Johnson, R.C. Young, Initial clinical trials of maytansine, an antitumor plant alkaloid, Cancer Treat Rep, 62 (1978) 429-433.

[95] F. Cabanillas, V. Rodriguez, S.W. Hall, M.A. Burgess, G.P. Bodey, E.J. Freireich, Phase I study of maytansine using a 3-day schedule, Cancer Treat Rep, 62 (1978) 425-428.

[96] R.V. Chari, B.A. Martell, J.L. Gross, S.B. Cook, S.A. Shah, W.A. Blättler, S.J. McKenzie, V.S. Goldmacher, Immunoconjugates containing novel maytansinoids: promising anticancer drugs, Cancer Res, 52 (1992) 127-131.

[97] V.S. Goldmacher, W.A. Blättler, J.M. Lambert, R.V.J. Chari, Immunotoxins and Antibody-Drug Conjugates for Cancer Treatment, in: V. Muzykantov, V. Torchilin (Eds.) Biomedical Aspects of Drug Targeting, Springer US, Boston, MA, 2002, pp. 291-309.

[98] M. Lopus, Antibody-DM1 conjugates as cancer therapeutics, Cancer Lett, 307 (2011) 113-118.

[99] A.W. Tolcher, L. Ochoa, L.A. Hammond, A. Patnaik, T. Edwards, C. Takimoto, L. Smith, J. de Bono, G. Schwartz, T. Mays, Z.L. Jonak, R. Johnson, M. DeWitte, H. Martino, C. Audette, K. Maes, R.V. Chari, J.M. Lambert, E.K. Rowinsky, Cantuzumab mertansine, a maytansinoid immunoconjugate directed to the CanAg antigen: a phase I, pharmacokinetic, and biologic correlative study, J Clin Oncol, 21 (2003) 211-222.

[100] A. Kumar, J. White, R. James Christie, N. Dimasi, C. Gao, Chapter Twelve - Antibody-Drug Conjugates, in: R.A. Goodnow (Ed.) Annual Reports in Medicinal Chemistry, Academic Press2017, pp. 441-480.

[101] S. Wedam, L. Fashoyin-Aje, X. Gao, E. Bloomquist, S. Tang, R. Sridhara, K.B. Goldberg, B.L. King-Kallimanis, M.R. Theoret, A. Ibrahim, L. Amiri-Kordestani, R. Pazdur, J.A. Beaver, FDA Approval Summary: Ado-Trastuzumab Emtansine for the Adjuvant Treatment of HER2-positive Early Breast Cancer, Clin Cancer Res, 26 (2020) 4180-4185.

[102] F. Borys, E. Joachimiak, H. Krawczyk, H. Fabczak, Intrinsic and Extrinsic Factors Affecting Microtubule Dynamics in Normal and Cancer Cells, Molecules, 25 (2020).

[103] W. Shuai, G. Wang, Y. Zhang, F. Bu, S. Zhang, D.D. Miller, W. Li, L. Ouyang, Y. Wang, Recent Progress on Tubulin Inhibitors with Dual Targeting Capabilities for Cancer Therapy, J Med Chem, 64 (2021) 7963-7990.

[104] A.E. Prota, K. Bargsten, J.F. Diaz, M. Marsh, C. Cuevas, M. Liniger, C. Neuhaus, J.M. Andreu, K.H. Altmann, M.O. Steinmetz, A new tubulin-binding site and pharmacophore for microtubule-destabilizing anticancer drugs, Proc Natl Acad Sci U S A, 111 (2014) 13817-13821.

[105] F.W. Hunter, H.R. Barker, B. Lipert, F. Rothé, G. Gebhart, M.J. Piccart-Gebhart, C. Sotiriou, S.M.F. Jamieson, Mechanisms of resistance to trastuzumab emtansine (T-DM1) in HER2-positive breast cancer, 2020.

[106] Z. Wu, S. Li, X. Zhu, The Mechanism of Stimulating and Mobilizing the Immune System Enhancing the Anti-Tumor Immunity, Front Immunol, 12 (2021) 682435.

[107] X. Zhu, S. Li, B. Xu, H. Luo, Cancer evolution: A means by which tumors evade treatment, Biomed Pharmacother, 133 (2021) 111016.

[108] K. Dhatchinamoorthy, J.D. Colbert, K.L. Rock, Cancer Immune Evasion Through Loss of MHC Class I Antigen Presentation, Front Immunol, 12 (2021) 636568.

[109] S. Ostrand-Rosenberg, L.A. Horn, S.T. Haile, The programmed death-1 immune-suppressive pathway: barrier to antitumor immunity, J Immunol, 193 (2014) 3835-3841.

[110] B.T. Fife, K.E. Pauken, T.N. Eagar, T. Obu, J. Wu, Q. Tang, M. Azuma, M.F. Krummel, J.A. Bluestone, Interactions between PD-1 and PD-L1 promote tolerance by blocking the TCR-induced stop signal, Nat Immunol, 10 (2009) 1185-1192.

[111] T. Azuma, S. Yao, G. Zhu, A.S. Flies, S.J. Flies, L. Chen, B7-H1 is a ubiquitous antiapoptotic receptor on cancer cells, Blood, 111 (2008) 3635-3643.

[112] S. Ma, Y. Zhao, W.C. Lee, L.T. Ong, P.L. Lee, Z. Jiang, G. Oguz, Z. Niu, M. Liu, J.Y. Goh, W. Wang, M.A. Bustos, S. Ehmsen, A. Ramasamy, D.S.B. Hoon, H.J. Ditzel, E.Y. Tan, Q. Chen, Q. Yu, Hypoxia induces HIF1alpha-dependent epigenetic vulnerability in triple negative breast cancer to confer immune effector dysfunction and resistance to anti-PD-1 immunotherapy, Nat Commun, 13 (2022) 4118.

[113] L.F. Neves, J.J. Krais, B.D. Van Rite, R. Ramesh, D.E. Resasco, R.G. Harrison, Targeting single-walled carbon nanotubes for the treatment of breast cancer using photothermal therapy, Nanotechnology, 24 (2013) 375104.

[114] A.J. Majmundar, W.J. Wong, M.C. Simon, Hypoxia-inducible factors and the response to hypoxic stress, Mol Cell, 40 (2010) 294-309.

[115] H. Ikeda, H. Kakeya, Targeting hypoxia-inducible factor 1 (HIF-1) signaling with natural products toward cancer chemotherapy, J Antibiot (Tokyo), 74 (2021) 687-695.

[116] G. Yang, D. Francis, J.R. Krycer, M. Larance, Z. Zhang, C.J. Novotny, A. Diaz-Vegas, K.M. Shokat, D.E. James, Dissecting the biology of mTORC1 beyond rapamycin, Sci Signal, 14 (2021) eabe0161.

[117] B. Kramer, M. Polit, R. Birk, N. Rotter, C. Aderhold, HIF-1alpha and mTOR - Possible Novel Strategies of Targeted Therapies in p16-positive and -negative HNSCC, Cancer Genomics Proteomics, 15 (2018) 175-184.

[118] T. Tian, X. Li, J. Zhang, mTOR Signaling in Cancer and mTOR Inhibitors in Solid Tumor Targeting Therapy, Int J Mol Sci, 20 (2019).

[119] M. Prvanovic, M. Nedeljkovic, N. Tanic, T. Tomic, T. Terzic, Z. Milovanovic, Z. Maksimovic, N. Tanic, Role of PTEN, PI3K, and mTOR in Triple-Negative Breast Cancer, Life (Basel), 11 (2021).

[120] K.M. Dodd, J. Yang, M.H. Shen, J.R. Sampson, A.R. Tee, mTORC1 drives HIF-1alpha and VEGF-A signalling via multiple mechanisms involving 4E-BP1, S6K1 and STAT3, Oncogene, 34 (2015) 2239-2250.

[121] B. Wang, Q. Zhao, Y. Zhang, Z. Liu, Z. Zheng, S. Liu, L. Meng, Y. Xin, X. Jiang, Targeting hypoxia in the tumor microenvironment: a potential strategy to improve cancer immunotherapy, J Exp Clin Cancer Res, 40 (2021) 24.

[122] L. Galluzzi, I. Vitale, S.A. Aaronson, et al., Molecular mechanisms of cell death: recommendations of the Nomenclature Committee on Cell Death 2018, Cell Death Differ, 25 (2018) 486-541.

[123] K.P. Fabian, B. Wolfson, J.W. Hodge, From Immunogenic Cell Death to Immunogenic Modulation: Select Chemotherapy Regimens Induce a Spectrum of Immune-Enhancing Activities in the Tumor Microenvironment, Front Oncol, 11 (2021) 728018.

[124] A. Ahmed, S.W.G. Tait, Targeting immunogenic cell death in cancer, Mol Oncol, 14 (2020) 2994-3006.

[125] J. Fucikova, O. Kepp, L. Kasikova, G. Petroni, T. Yamazaki, P. Liu, L. Zhao, R. Spisek, G. Kroemer, L. Galluzzi, Detection of immunogenic cell death and its relevance for cancer therapy, Cell Death Dis, 11 (2020) 1013.

[126] F. Ghiringhelli, L. Apetoh, A. Tesniere, L. Aymeric, Y. Ma, C. Ortiz, K. Vermaelen, T. Panaretakis, G. Mignot, E. Ullrich, J.L. Perfettini, F. Schlemmer, E. Tasdemir, M. Uhl, P. Genin, A. Civas, B. Ryffel, J. Kanellopoulos, J. Tschopp, F. Andre, R. Lidereau, N.M. McLaughlin, N.M. Haynes, M.J. Smyth, G. Kroemer, L. Zitvogel, Activation of the NLRP3 inflammasome in dendritic cells induces IL-1beta-dependent adaptive immunity against tumors, Nat Med, 15 (2009) 1170-1178.

[127] M. Zhu, M. Yang, J. Zhang, Y. Yin, X. Fan, Y. Zhang, S. Qin, H. Zhang, F. Yu, Immunogenic Cell Death Induction by Ionizing Radiation, Front Immunol, 12 (2021) 705361.

[128] S. Pawaria, R.J. Binder, CD91-dependent programming of T-helper cell responses following heat shock protein immunization, Nat Commun, 2 (2011) 521.

[129] S. Yuan, Z. Liu, Z. Xu, J. Liu, J. Zhang, High mobility group box 1 (HMGB1): a pivotal regulator of hematopoietic malignancies, J Hematol Oncol, 13 (2020) 91.

[130] M. Jiang, J. Zeng, L. Zhao, M. Zhang, J. Ma, X. Guan, W. Zhang, Chemotherapeutic drug-induced immunogenic cell death for nanomedicine-based cancer chemo-immunotherapy, Nanoscale, 13 (2021) 17218-17235.

[131] M. Bauzon, P.M. Drake, R.M. Barfield, B.M. Cornali, I. Rupniewski, D. Rabuka, Maytansine-bearing antibody-drug conjugates induce in vitro hallmarks of immunogenic cell death selectively in antigen-positive target cells, OncoImmunology, (2019).

[132] P. Müller, M. Kreuzaler, T. Khan, D.S. Thommen, K. Martin, K. Glatz, S. Savic, N. Harbeck, U. Nitz, O. Gluz, M. Von Bergwelt-Baildon, H. Kreipe, S. Reddy, M. Christgen, A. Zippelius, Trastuzumab emtansine (T-DM1) renders HER2+ breast cancer highly susceptible to CTLA-4/PD-1 blockade, Science Translational Medicine, (2015).

[133] B. Southard, Novel Targeted Annexin V: Drug Conjugate for Cancer Chemotherapeutic Treatment, University of Oklahoma2019.

[134] M. Huhe, J. Lou, Y. Zhu, Y. Zhao, Y. Shi, B. Wang, X. Sun, X. Zhang, Y. Zhang, Z.N. Chen, A novel antibody-drug conjugate, HcHAb18-DM1, has potent anti-tumor activity against human non-small cell lung cancer, Biochem Biophys Res Commun, 513 (2019) 1083-1091.

[135] H. Donaghy, Effects of antibody, drug and linker on the preclinical and clinical toxicities of antibody-drug conjugates, MAbs, 8 (2016) 659-671.

[136] J. Lu, F. Jiang, A. Lu, G. Zhang, Linkers Having a Crucial Role in Antibody-Drug Conjugates, Int J Mol Sci, 17 (2016) 561.

[137] H.K. Erickson, P.U. Park, W.C. Widdison, Y.V. Kovtun, L.M. Garrett, K. Hoffman, R.J. Lutz, V.S. Goldmacher, W.A. Blattler, Antibody-maytansinoid conjugates are activated in targeted cancer cells by lysosomal degradation and linker-dependent intracellular processing, Cancer Res, 66 (2006) 4426-4433.

[138] A. Gilman, The initial clinical trial of nitrogen mustard, Am J Surg, 105 (1963) 574-578.

[139] J.L. Everett, J.J. Roberts, W.C.J. Ross, 486. Aryl-2-halogenoalkylamines. Part XII. Some carboxylic derivatives of NN-di-2-chloroethylaniline, Journal of the Chemical Society (Resumed), (1953) 2386-2392.

[140] M.J. Geraci, Mustard gas: imminent danger or eminent threat?, Ann Pharmacother, 42 (2008) 237-246.

[141] R.K. Singh, S. Kumar, D.N. Prasad, T.R. Bhardwaj, Therapeutic journery of nitrogen mustard as alkylating anticancer agents: Historic to future perspectives, Eur J Med Chem, 151 (2018) 401-433.

[142] S.L. Smith, War! What is it good for? Mustard gas medicine, CMAJ, 189 (2017) E321-E322.

[143] E.B. Krumbhaar, H.D. Krumbhaar, The Blood and Bone Marrow in Yelloe Cross Gas (Mustard Gas) Poisoning: Changes produced in the Bone Marrow of Fatal Cases, J Med Res, 40 (1919) 497-508.493.

[144] F. Lehmann, J. Wennerberg, Evolution of Nitrogen-Based Alkylating Anticancer Agents, Processes, 9 (2021) 377.

[145] S. Neidle, D.E. Thurston, Chemical approaches to the discovery and development of cancer therapies, Nat Rev Cancer, 5 (2005) 285-296.

[146] M. Di Antonio, K.I. McLuckie, S. Balasubramanian, Reprogramming the mechanism of action of chlorambucil by coupling to a G-quadruplex ligand, J Am Chem Soc, 136 (2014) 5860-5863.

[147] M.J. Reese, D.W. Knapp, K.M. Anderson, J.A. Mund, J. Case, D.R. Jones, R.A. Packer, In vitro effect of chlorambucil on human glioma cell lines (SF767 and U87-MG), and human microvascular endothelial cell (HMVEC) and endothelial progenitor cells (ECFCs), in the context of plasma chlorambucil concentrations in tumor-bearing dogs, PLoS One, 13 (2018) e0203517.

[148] E.Z. Ezdinli, L. Stutzman, Chlorambucil Therapy for Lymphomas and Chronic Lymphocytic Leukemia, JAMA, 191 (1965) 444-450.

[149] L. Wang, W. Qin, Y.J. Huo, X. Li, Q. Shi, J.E.J. Rasko, A. Janin, W.L. Zhao, Advances in targeted therapy for malignant lymphoma, Signal Transduct Target Ther, 5 (2020) 15.

[150] A. Polavarapu, J.A. Stillabower, S.G. Stubblefield, W.M. Taylor, M.H. Baik, The mechanism of guanine alkylation by nitrogen mustards: a computational study, J Org Chem, 77 (2012) 5914-5921.

[151] M. Clinic, Chlorambucil (Oral Route) 2022.

[152] P. McKernan, Therapeutic applications of bioconjugates in human disease, Ph.D Dissertation, University of Oklahoma, Norman Oklahoma, 2018, pp. 251.

[153] C. Bagarie, Annexin a5 - chlorambucil: a targeted theraptuic drug agasint leukemia and breast cancer, M.S. Thesis, The University of Oklahoma, Norman Oklahoma, 2018, pp. 92.

[154] B.S. Burton, On the propyl derivatives and decomposition products of ethylacetoacetate, Am Chem J, 3 (1882) 385-395.

[155] H. Meunier, G. Carraz, Y. Neunier, P. Eymard, M. Aimard, [Pharmacodynamic properties of N-dipropylacetic acid], Therapie, 18 (1963) 435-438.

[156] S. Lunke, S. Maxwell, I. Khurana, N.H. K, J. Okabe, K. Al-Hasani, A. El-Osta, Epigenetic evidence of an Ac/Dc axis by VPA and SAHA, Clin Epigenetics, 13 (2021) 58.

[157] M. Göttlicher, S. Minucci, P. Zhu, O.H. Krämer, A. Schimpf, S. Giavara, J.P. Sleeman, F. Lo Coco, C. Nervi, P.G. Pelicci, T. Heinzel, Valproic acid defines a novel class of HDAC inhibitors inducing differentiation of transformed cells, EMBO Journal, (2001).

[158] N. Darwiche, Epigenetic mechanisms and the hallmarks of cancer: an intimate affair, Am J Cancer Res, 10 (2020) 1954-1978.

[159] W.A. Flavahan, E. Gaskell, B.E. Bernstein, Epigenetic plasticity and the hallmarks of cancer, Science, 357 (2017).

[160] L. Hontecillas-Prieto, R. Flores-Campos, A. Silver, E. de Alava, N. Hajji, D.J. Garcia-Dominguez, Synergistic Enhancement of Cancer Therapy Using HDAC Inhibitors: Opportunity for Clinical Trials, Front Genet, 11 (2020) 578011.

[161] V. Kumar, J.K. Thakur, M. Prasad, Histone acetylation dynamics regulating plant development and stress responses, Cell Mol Life Sci, 78 (2021) 4467-4486.

[162] D. Wu, Y. Qiu, Y. Jiao, Z. Qiu, D. Liu, Small Molecules Targeting HATs, HDACs, and BRDs in Cancer Therapy, Front Oncol, 10 (2020) 560487.

[163] P. Guo, W. Chen, H. Li, M. Li, L. Li, The Histone Acetylation Modifications of Breast Cancer and their Therapeutic Implications, Pathol Oncol Res, 24 (2018) 807-813.

[164] R. Hai, L. He, G. Shu, G. Yin, Characterization of Histone Deacetylase Mechanisms in Cancer Development, Front Oncol, 11 (2021) 700947.

[165] K. Zhang, Z. Liu, Y. Yao, Y. Qiu, F. Li, D. Chen, D.J. Hamilton, Z. Li, S. Jiang, Structure-Based Design of a Selective Class I Histone Deacetylase (HDAC) Near-Infrared (NIR) Probe for Epigenetic Regulation Detection in Triple-Negative Breast Cancer (TNBC), J Med Chem, 64 (2021) 4020-4033.

[166] A. Suraweera, K.J. O'Byrne, D.J. Richard, Combination Therapy With Histone Deacetylase Inhibitors (HDACi) for the Treatment of Cancer: Achieving the Full Therapeutic Potential of HDACi, Front Oncol, 8 (2018) 92.

[167] J.J. McClure, X. Li, C.J. Chou, Advances and Challenges of HDAC Inhibitors in Cancer Therapeutics, Adv Cancer Res, 138 (2018) 183-211.

[168] C. Cianferotti, V. Faltoni, E. Cini, E. Ermini, F. Migliorini, E. Petricci, M. Taddei, L. Salvini, G. Battistuzzi, F.M. Milazzo, A.M. Anastasi, C. Chiapparino, R. De Santis, G. Giannini, Antibody drug conjugates with hydroxamic acid cargos for histone deacetylase (HDAC) inhibition, Chem Commun (Camb), 57 (2021) 867-870.

[169] F.M. Milazzo, L. Vesci, A.M. Anastasi, C. Chiapparino, A. Rosi, G. Giannini, M. Taddei, E. Cini, V. Faltoni, E. Petricci, G. Battistuzzi, L. Salvini, V. Carollo, R. De Santis, ErbB2 Targeted Epigenetic Modulation: Anti-tumor Efficacy of the ADC Trastuzumab-HDACi ST8176AA1, Front Oncol, 9 (2019) 1534.

[170] E. Cini, V. Faltoni, E. Petricci, M. Taddei, L. Salvini, G. Giannini, L. Vesci, F.M. Milazzo, A.M. Anastasi, G. Battistuzzi, R. De Santis, Antibody drug conjugates (ADCs) charged with HDAC inhibitor for targeted epigenetic modulation, Chem Sci, 9 (2018) 6490-6496.

[171] L. Travaglini, L. Vian, M. Billi, F. Grignani, C. Nervi, Epigenetic reprogramming of breast cancer cells by valproic acid occurs regardless of estrogen receptor status, Int J Biochem Cell Biol, 41 (2009) 225-234.

[172] A.L. Cohen, L. Neumayer, K. Boucher, R.E. Factor, G. Shrestha, M. Wade, J.G. Lamb, K. Arbogast, S.R. Piccolo, J. Riegert, M. Schabel, A.H. Bild, T.L. Werner, Window-of-Opportunity

Study of Valproic Acid in Breast Cancer Testing a Gene Expression Biomarker, JCO Precis Oncol, 1 (2017).

[173] D.C. Marchion, E. Bicaku, A.I. Daud, D.M. Sullivan, P.N. Munster, Valproic acid alters chromatin structure by regulation of chromatin modulation proteins, Cancer Res, 65 (2005) 3815-3822.

[174] M.L.S. Mello, Sodium Valproate-Induced Chromatin Remodeling, Front Cell Dev Biol, 9 (2021) 645518.

[175] W. Li, Z. Sun, Mechanism of Action for HDAC Inhibitors-Insights from Omics Approaches, Int J Mol Sci, 20 (2019).

[176] Y. Sixto-Lopez, M. Bello, J. Correa-Basurto, Exploring the inhibitory activity of valproic acid against the HDAC family using an MMGBSA approach, J Comput Aided Mol Des, 34 (2020) 857-878.

[177] M.A. Elbadawi, M.K. Awadalla, M.M. Hamid, M.A. Mohamed, T.A. Awad, Valproic acid as a potential inhibitor of Plasmodium falciparum histone deacetylase 1 (PfHDAC1): an in silico approach, Int J Mol Sci, 16 (2015) 3915-3931.

[178] M. Dejligbjerg, M. Grauslund, T. Litman, L. Collins, X. Qian, M. Jeffers, H. Lichenstein, P.B. Jensen, M. Sehested, Differential effects of class I isoform histone deacetylase depletion and enzymatic inhibition by belinostat or valproic acid in HeLa cells, Mol Cancer, 7 (2008) 70.

[179] N. Fortunati, S. Bertino, L. Costantino, O. Bosco, I. Vercellinatto, M.G. Catalano, G. Boccuzzi, Valproic acid is a selective antiproliferative agent in estrogen-sensitive breast cancer cells, Cancer Lett, 259 (2008) 156-164.

[180] N. Aztopal, M. Erkisa, E. Erturk, E. Ulukaya, A.H. Tokullugil, F. Ari, Valproic acid, a histone deacetylase inhibitor, induces apoptosis in breast cancer stem cells, Chem Biol Interact, 280 (2018) 51-58.

[181] T. Mawatari, I. Ninomiya, M. Inokuchi, S. Harada, H. Hayashi, K. Oyama, I. Makino, H. Nakagawara, T. Miyashita, H. Tajima, H. Takamura, S. Fushida, T. Ohta, Valproic acid inhibits proliferation of HER2-expressing breast cancer cells by inducing cell cycle arrest and apoptosis through Hsp70 acetylation, Int J Oncol, 47 (2015) 2073-2081.

[182] Z. Ozman, B. Ozbek Iptec, E. Sahin, G. Guney Eskiler, A. Deveci Ozkan, S. Kaleli, Regulation of valproic acid induced EMT by AKT/GSK3beta/beta-catenin signaling pathway in triple negative breast cancer, Mol Biol Rep, 48 (2021) 1335-1343.

[183] A. Wawruszak, J.J. Luszczki, J. Kalafut, K. Okla, M. Halasa, A. Rivero-Muller, A. Stepulak, Additive Pharmacological Interaction between Cisplatin (CDDP) and Histone Deacetylase Inhibitors (HDIs) in MDA-MB-231 Triple Negative Breast Cancer (TNBC) Cells with Altered Notch1 Activity-An Isobolographic Analysis, Int J Mol Sci, 20 (2019).

[184] N. Fortunati, S. Bertino, L. Costantino, M. De Bortoli, A. Compagnone, A. Bandino, M.G. Catalano, G. Boccuzzi, Valproic acid restores ER alpha and antiestrogen sensitivity to ER alpha-negative breast cancer cells, Mol Cell Endocrinol, 314 (2010) 17-22.

[185] S.K. Saha, Y. Yin, K. Kim, G.M. Yang, A.A. Dayem, H.Y. Choi, S.G. Cho, Valproic Acid Induces Endocytosis-Mediated Doxorubicin Internalization and Shows Synergistic Cytotoxic Effects in Hepatocellular Carcinoma Cells, Int J Mol Sci, 18 (2017).

[186] M.G. Catalano, N. Fortunati, M. Pugliese, R. Poli, O. Bosco, R. Mastrocola, M. Aragno, G. Boccuzzi, Valproic acid, a histone deacetylase inhibitor, enhances sensitivity to doxorubicin in anaplastic thyroid cancer cells, J Endocrinol, 191 (2006) 465-472.

[187] X.H. Tong, C. Zheng, G.J. Jiang, S.Y. Dong, [Sodium valproate enhances doxorubicin cytotoxicity in breast cancer cells in vitro], Nan Fang Yi Ke Da Xue Xue Bao, 35 (2015) 62-65.

[188] Y.J. Seo, Y. Kang, L. Muench, A. Reid, S. Caesar, L. Jean, F. Wagner, E. Holson, S.J. Haggarty, P. Weiss, P. King, P. Carter, N.D. Volkow, J.S. Fowler, J.M. Hooker, S.W. Kim, Image-guided synthesis reveals potent blood-brain barrier permeable histone deacetylase inhibitors, ACS Chemical Neuroscience, (2014).

[189] L. Akbarzadeh, T. Moini Zanjani, M. Sabetkasaei, Comparison of Anticancer Effects of Carbamazepine and Valproic Acid, Iran Red Crescent Med J, 18 (2016) e37230.

[190] A. Duenas-Gonzalez, M. Candelaria, C. Perez-Plascencia, E. Perez-Cardenas, E. de la Cruz-Hernandez, L.A. Herrera, Valproic acid as epigenetic cancer drug: Preclinical, clinical and transcriptional effects on solid tumors, 2008.

[191] C. Killick-Cole, A. Bienemann, D. Asby, W. Singleton, M. Wyatt, L. Boulter, N. Barua, S. Gill, Preclinical Analysis of Sodium Valproate for the Treatment of Dipg by Convection Enhanced Delivery, Neuro-Oncology, 19 (2017) 55-55.

[192] P. McKernan, B. Cassidy, A. Woodward, J. Battiste, D. Drevets, R. Harrison, Anionic phospholipid expression as a molecular target in Listeria monocytogenes and Escherichia coli, Int J Antimicrob Agents, 56 (2020) 106183.

[193] W. Yang, A.N. Frickenstein, V. Sheth, A. Holden, E.M. Mettenbrink, L. Wang, A.A. Woodward, B.S. Joo, S.K. Butterfield, N.D. Donahue, D.E. Green, A.G. Thomas, T. Harcourt, H. Young, M. Tang, Z.A. Malik, R.G. Harrison, P. Mukherjee, P.L. DeAngelis, S. Wilhelm, Controlling Nanoparticle Uptake in Innate Immune Cells with Heparosan Polysaccharides, Nano Lett, 22 (2022) 7119-7128.

[194] W.R. Algar, A brief introduction to traditional bioconjugate chemistry, in: W.R. Algar, P.E. Dawson, I.L. Medintz (Eds.) Chemoselective and Bioorthogonal Ligations Reactions Wiley-VCH Verlag GmbH, Weinhem, Germany, 2017, pp. 1-36.

[195] A.O. Bailey, G. Han, W. Phung, P. Gazis, J. Sutton, J.L. Josephs, W. Sandoval, Charge variant native mass spectrometry benefits mass precision and dynamic range of monoclonal antibody intact mass analysis, MAbs, 10 (2018) 1214-1225.

[196] M.M. Jensen, J.T. Jorgensen, T. Binderup, A. Kjaer, Tumor volume in subcutaneous mouse xenografts measured by microCT is more accurate and reproducible than determined by 18F-FDG-microPET or external caliper, BMC Med Imaging, 8 (2008) 16.

[197] D.M. Euhus, C. Hudd, M.C. LaRegina, F.E. Johnson, Tumor measurement in the nude mouse, J Surg Oncol, 31 (1986) 229-234.

[198] J.J. Krais, N. Virani, P.H. McKernan, Q. Nguyen, K.M. Fung, V.I. Sikavitsas, C. Kurkjian, R.G. Harrison, Antitumor synergism and enhanced survival with a tumor vasculature–targeted enzyme prodrug system, rapamycin, and cyclophosphamide, Molecular Cancer Therapeutics, (2017).

[199] J.A. Lunn, R. Lee, J. Smaller, B.M. MacKay, T. King, G.B. Hunt, P. Martin, M.B. Krockenberger, D. Spielman, R. Malik, Twenty two cases of canine neural angiostrongylosis in eastern Australia (2002-2005) and a review of the literature, Parasit Vectors, 5 (2012) 70.

[200] N.R. Palwai, Targeting fusion proteins containing L-methioninase to cancer cells School of Chemical, Biological, and Materials Engineering University of Oklahoma Norman Oklahoma USA 2007.

[201] J.C. Lessard, Growth media for E. coli, Methods Enzymol, 533 (2013) 181-189.

[202] K.E. Kram, S.E. Finkel, Rich Medium Composition Affects Escherichia coli Survival, Glycation, and Mutation Frequency during Long-Term Batch Culture, Appl Environ Microbiol, 81 (2015) 4442-4450.

[203] X. Zhang, L. Huo, H. Jin, Y. Han, J. Wang, Y. Zhang, X. Lai, Z. Le, J. Zhang, Z. Hua, Anti-cancer activity of Annexin V in murine melanoma model by suppressing tumor angiogenesis, Oncotarget, 8 (2017) 42602-42612.

[204] F. Qiu, M. Hu, B. Tang, X. Liu, H. Zhuang, J. Yang, Z.C. Hua, Annexin v-trail fusion protein is a more sensitive and potent apoptotic inducer for cancer therapy, Scientific Reports, (2013).

[205] M. Losen, B. Frölich, M. Pohl, J. Büchs, Effect of oxygen limitation and medium composition on Escherichia coli fermentation in shake-flask cultures, Biotechnol Prog, 20 (2004) 1062-1068.

[206] B. Southard, Novel targted annexin V - drug conjugates for cancer chemotherapeutic treatment, M.S. Thesis, The University of Oklahoma, Norman, OKlahoma, 2019.

[207] V.E. Gray, R.J. Hause, D.M. Fowler, Analysis of Large-Scale Mutagenesis Data To Assess the Impact of Single Amino Acid Substitutions, Genetics, 207 (2017) 53-61.

[208] K.P. Guillen, E.A. Ruben, N. Virani, R.G. Harrison, Annexin-directed beta-glucuronidase for the targeted treatment of solid tumors, Protein Eng Des Sel, 30 (2017) 85-94.

[209] J.J. Krais, O. de Crescenzo, R.G. Harrison, Purine Nucleoside Phosphorylase Targeted by Annexin V to Breast Cancer Vasculature for Enzyme Prodrug Therapy, PLoS ONE, (2013).

[210] B.D. Van Rite, R.G. Harrison, Annexin V-targeted enzyme prodrug therapy using cytosine deaminase in combination with 5-fluorocytosine, Cancer Letters, (2011).

[211] H. Matsubayashi, T. Arai, S. Izumi, T. Sugi, J.A. McIntyre, T. Makino, Anti-annexin V antibodies in patients with early pregnancy loss or implantation failures, Fertil Steril, 76 (2001) 694-699.

[212] L. Mui, C.M. Martin, B.J. Tschirhart, Q. Feng, Therapeutic Potential of Annexins in Sepsis and COVID-19, Front Pharmacol, 12 (2021) 735472.

[213] G. Krikun, C.J. Lockwood, X.X. Wu, X.D. Zhou, S. Guller, C. Calandri, A. Guha, Y. Nemerson, J.H. Rand, The expression of the placental anticoagulant protein, annexin V, by villous trophoblasts: immunolocalization and in vitro regulation, Placenta, 15 (1994) 601-612.

[214] J.E. Salmon, G. Girardi, V.M. Holers, Activation of complement mediates antiphospholipid antibody-induced pregnancy loss, Lupus, 12 (2003) 535-538.

[215] M.M. Ewing, M.R. de Vries, M. Nordzell, K. Pettersson, H.C. de Boer, A.J. van Zonneveld, J. Frostegard, J.W. Jukema, P.H. Quax, Annexin A5 therapy attenuates vascular inflammation and remodeling and improves endothelial function in mice, Arterioscler Thromb Vasc Biol, 31 (2011) 95-101.

[216] B. Peng, C. Guo, H. Guan, S. Liu, M.Z. Sun, Annexin A5 as a potential marker in tumors, Clin Chim Acta, 427 (2014) 42-48.

[217] H. Sato, H. Ogata, L.M. De Luca, Annexin V inhibits the 12-O-tetradecanoylphorbol-13-acetate-induced activation of Ras/extracellular signal-regulated kinase (ERK) signaling pathway upstream of Shc in MCF-7 cells, Oncogene, 19 (2000) 2904-2912.

[218] G. Xue, L.Q. Hao, F.X. Ding, Q. Mei, J.J. Huang, C.G. Fu, H.L. Yan, S.H. Sun, Expression of annexin a5 is associated with higher tumor stage and poor prognosis in colorectal adenocarcinomas, J Clin Gastroenterol, 43 (2009) 831-837.

[219] X. Sun, B. Wei, S. Liu, C. Guo, N. Wu, Q. Liu, M.Z. Sun, Anxa5 mediates the in vitro malignant behaviours of murine hepatocarcinoma Hca-F cells with high lymph node metastasis potential preferentially via ERK2/p-ERK2/c-Jun/p-c-Jun(Ser73) and E-cadherin, Biomed Pharmacother, 84 (2016) 645-654.

[220] J. Tang, Z. Qin, P. Han, W. Wang, C. Yang, Z. Xu, R. Li, B. Liu, C. Qin, Z. Wang, M. Tang, W. Zhang, High Annexin A5 expression promotes tumor progression and poor prognosis in renal cell carcinoma, Int J Oncol, 50 (2017) 1839-1847.

[221] X. Li, L. Chen, X.J. Liang, Y.F. Gao, X.J. Wang, Q. Xu, Y. Yan, F.L. Gao, Annexin A5 protein expression is associated with the histological differentiation of uterine cervical squamous cell carcinoma in patients with an increased serum concentration, Mol Med Rep, 6 (2012) 1249-1254.

[222] G.D. Lewis Phillips, G. Li, D.L. Dugger, L.M. Crocker, K.L. Parsons, E. Mai, W.A. Blattler, J.M. Lambert, R.V. Chari, R.J. Lutz, W.L. Wong, F.S. Jacobson, H. Koeppen, R.H. Schwall, S.R. Kenkare-Mitra, S.D. Spencer, M.X. Sliwkowski, Targeting HER2-positive breast cancer with trastuzumab-DM1, an antibody-cytotoxic drug conjugate, Cancer Res, 68 (2008) 9280-9290.

[223] C.A. Hudis, Trastuzumab--mechanism of action and use in clinical practice, N Engl J Med, 357 (2007) 39-51.

[224] I.E. Krop, S.B. Kim, A.G. Martin, P.M. LoRusso, J.M. Ferrero, T. Badovinac-Crnjevic, S. Hoersch, M. Smitt, H. Wildiers, Trastuzumab emtansine versus treatment of physician's choice in patients with previously treated HER2-positive metastatic breast cancer (TH3RESA): final overall survival results from a randomised open-label phase 3 trial, Lancet Oncol, 18 (2017) 743-754.

[225] R. Nicoletti, S. Lopez, S. Bellone, E. Cocco, C.L. Schwab, J.D. Black, F. Centritto, L. Zhu, E. Bonazzoli, N. Buza, P. Hui, D. Mezzanzanica, S. Canevari, P.E. Schwartz, T.J. Rutherford, A.D. Santin, T-DM1, a novel antibody-drug conjugate, is highly effective against uterine and ovarian carcinosarcomas overexpressing HER2, Clin Exp Metastasis, 32 (2015) 29-38.

[226] M. Cavaco, M. Castanho, V. Neves, Peptibodies: An elegant solution for a long-standing problem, Biopolymers, (2017).

[227] G.M. Sharif, A. Wellstein, Cell density regulates cancer metastasis via the Hippo pathway, Future Oncol, 11 (2015) 3253-3260.

[228] G.M. Sharif, M.O. Schmidt, C. Yi, Z. Hu, B.R. Haddad, E. Glasgow, A.T. Riegel, A. Wellstein, Cell growth density modulates cancer cell vascular invasion via Hippo pathway activity and CXCR2 signaling, Oncogene, 34 (2015) 5879-5889.

[229] A.C. Gregorio, N.A. Fonseca, V. Moura, M. Lacerda, P. Figueiredo, S. Simoes, S. Dias, J.N. Moreira, Inoculated Cell Density as a Determinant Factor of the Growth Dynamics and Metastatic Efficiency of a Breast Cancer Murine Model, PLoS One, 11 (2016) e0165817.

[230] P.C. Bailey, R.M. Lee, M.I. Vitolo, S.J.P. Pratt, E. Ory, K. Chakrabarti, C.J. Lee, K.N. Thompson, S.S. Martin, Single-Cell Tracking of Breast Cancer Cells Enables Prediction of Sphere Formation from Early Cell Divisions, iScience, 8 (2018) 29-39.

[231] J.S. Brown, J.J. Cunningham, R.A. Gatenby, Aggregation Effects and Population-Based Dynamics as a Source of Therapy Resistance in Cancer, IEEE Trans Biomed Eng, 64 (2017) 512-518.

[232] K. Trajkovic, C. Valdez, D. Ysselstein, D. Krainc, Fluctuations in cell density alter protein markers of multiple cellular compartments, confounding experimental outcomes, PLoS One, 14 (2019) e0211727.

[233] C.W. Yun, S.H. Lee, The Roles of Autophagy in Cancer, Int J Mol Sci, 19 (2018).

[234] S.G. Mathiassen, D. De Zio, F. Cecconi, Autophagy and the Cell Cycle: A Complex Landscape, Front Oncol, 7 (2017) 51.

[235] C. Enrico Bena, M. Del Giudice, A. Grob, T. Gueudre, M. Miotto, D. Gialama, M. Osella, E. Turco, F. Ceroni, A. De Martino, C. Bosia, Initial cell density encodes proliferative potential in cancer cell populations, Sci Rep, 11 (2021) 6101.

[236] P. Liu, L. Zhao, O. Kepp, G. Kroemer, Quantitation of calreticulin exposure associated with immunogenic cell death, Methods Enzymol, 632 (2020) 1-13.

[237] I. Martins, Y. Wang, M. Michaud, Y. Ma, A.Q. Sukkurwala, S. Shen, O. Kepp, D. Metivier, L. Galluzzi, J.L. Perfettini, L. Zitvogel, G. Kroemer, Molecular mechanisms of ATP secretion during immunogenic cell death, Cell Death Differ, 21 (2014) 79-91.

[238] J.J. KRAIS, DEVELOPMENT AND PRECLINICAL EVALUATION OF ENZYME PRODRUG THERAPIES TARGETED TO THE TUMOR VASCULATURE, Biomedical Engineering Univeristy of Oklahoma 2014.

[239] R. Tsumura, S. Manabe, H. Takashima, Y. Koga, M. Yasunaga, Y. Matsumura, Influence of the dissociation rate constant on the intra-tumor distribution of antibody-drug conjugate against tissue factor, J Control Release, 284 (2018) 49-56.

[240] R. Piranlioglu, E. Lee, M. Ouzounova, R.J. Bollag, A.H. Vinyard, A.S. Arbab, D. Marasco, M. Guzel, J.K. Cowell, M. Thangaraju, A. Chadli, K.A. Hassan, M.S. Wicha, E. Celis, H. Korkaya, Primary tumor-induced immunity eradicates disseminated tumor cells in syngeneic mouse model, Nat Commun, 10 (2019) 1430.

[241] S. Ravindranathan, K.G. Nguyen, S.L. Kurtz, H.N. Frazier, S.G. Smith, B.P. Koppolu, N. Rajaram, D.A. Zaharoff, Tumor-derived granulocyte colony-stimulating factor diminishes efficacy of breast tumor cell vaccines, Breast Cancer Res, 20 (2018) 126.

[242] B.A. Pulaski, S. Ostrand-Rosenberg, Mouse 4T1 breast tumor model, Curr Protoc Immunol, Chapter 20 (2001) Unit 20 22.

[243] J.W. Yu, S. Bhattacharya, N. Yanamandra, D. Kilian, H. Shi, S. Yadavilli, Y. Katlinskaya, H. Kaczynski, M. Conner, W. Benson, A. Hahn, L. Seestaller-Wehr, M. Bi, N.J. Vitali, L. Tsvetkov, W. Halsey, A. Hughes, C. Traini, H. Zhou, J. Jing, T. Lee, D.J. Figueroa, S. Brett, C.B. Hopson, J.F. Smothers, A. Hoos, R. Srinivasan, Tumor-immune profiling of murine syngeneic tumor models as a framework to guide mechanistic studies and predict therapy response in distinct tumor microenvironments, PLoS One, 13 (2018) e0206223.

[244] L. Carpen, P. Falvo, S. Orecchioni, G. Mitola, R. Hillje, S. Mazzara, P. Mancuso, S. Pileri, A. Raveane, F. Bertolini, A single-cell transcriptomic landscape of innate and adaptive intratumoral immunity in triple negative breast cancer during chemo- and immunotherapies, Cell Death Discov, 8 (2022) 106.

[245] T.L. Whiteside, FOXP3+ Treg as a therapeutic target for promoting anti-tumor immunity, Expert Opin Ther Targets, 22 (2018) 353-363.

[246] C.J. Reddel, C.W. Tan, V.M. Chen, Thrombin Generation and Cancer: Contributors and Consequences, Cancers (Basel), 11 (2019).

[247] M.Z. Wojtukiewicz, M. Mysliwiec, E. Sierko, M. Sobierska, J. Kruszewska, A. Lipska, P. Radziwon, S.C. Tucker, K.V. Honn, Elevated Microparticles, Thrombin-antithrombin and VEGF Levels in Colorectal Cancer Patients Undergoing Chemotherapy, Pathol Oncol Res, 26 (2020) 2499-2507.

[248] K.G. Foster, D.C. Fingar, Mammalian target of rapamycin (mTOR): conducting the cellular signaling symphony, J Biol Chem, 285 (2010) 14071-14077.

[249] H.X. Yuan, K.L. Guan, Structural insights of mTOR complex 1, Cell Res, 26 (2016) 267-268.

[250] J. Xie, X. Wang, C.G. Proud, mTOR inhibitors in cancer therapy, F1000Res, 5 (2016).

[251] E. Seront, R. Boidot, C. Bouzin, O. Karroum, B.F. Jordan, B. Gallez, J.P. Machiels, O. Feron, Tumour hypoxia determines the potential of combining mTOR and autophagy inhibitors to treat mammary tumours, Br J Cancer, 109 (2013) 2597-2606.

[252] S.C. Land, A.R. Tee, Hypoxia-inducible factor 1alpha is regulated by the mammalian target of rapamycin (mTOR) via an mTOR signaling motif, J Biol Chem, 282 (2007) 20534-20543.

[253] K.J. Lastwika, W. Wilson, 3rd, Q.K. Li, J. Norris, H. Xu, S.R. Ghazarian, H. Kitagawa, S. Kawabata, J.M. Taube, S. Yao, L.N. Liu, J.J. Gills, P.A. Dennis, Control of PD-L1 Expression by Oncogenic Activation of the AKT-mTOR Pathway in Non-Small Cell Lung Cancer, Cancer Res, 76 (2016) 227-238.

[254] A. Zheng, F. Li, F. Chen, J. Zuo, L. Wang, Y. Wang, S. Chen, B. Xiao, Z. Tao, PDL1 promotes head and neck squamous cell carcinoma cell growth through mTOR signaling, Oncol Rep, 41 (2019) 2833-2843.

[255] A. Palazon, P.A. Tyrakis, D. Macias, P. Velica, H. Rundqvist, S. Fitzpatrick, N. Vojnovic, A.T. Phan, N. Loman, I. Hedenfalk, T. Hatschek, J. Lovrot, T. Foukakis, A.W. Goldrath, J. Bergh, R.S. Johnson, An HIF-1alpha/VEGF-A Axis in Cytotoxic T Cells Regulates Tumor Progression, Cancer Cell, 32 (2017) 669-683 e665.

[256] J. Zhou, G. Wang, Y. Chen, H. Wang, Y. Hua, Z. Cai, Immunogenic cell death in cancer therapy: Present and emerging inducers, J Cell Mol Med, 23 (2019) 4854-4865.

[257] J. Li, S.G. Kim, J. Blenis, Rapamycin: one drug, many effects, Cell Metab, 19 (2014) 373-379.

[258] A. Baroja-Mazo, B. Revilla-Nuin, P. Ramirez, J.A. Pons, Immunosuppressive potency of mechanistic target of rapamycin inhibitors in solid-organ transplantation, World J Transplant, 6 (2016) 183-192.

[259] A. Mondino, D.L. Mueller, mTOR at the crossroads of T cell proliferation and tolerance, Semin Immunol, 19 (2007) 162-172.

[260] N. Momin, J.R. Palmeri, E.A. Lutz, N. Jailkhani, H. Mak, A. Tabet, M.M. Chinn, B.H. Kang, V. Spanoudaki, R.O. Hynes, K.D. Wittrup, Maximizing response to intratumoral immunotherapy in mice by tuning local retention, Nat Commun, 13 (2022) 109.

[261] L.H. Bender, F. Abbate, I.B. Walters, Intratumoral Administration of a Novel Cytotoxic Formulation with Strong Tissue Dispersive Properties Regresses Tumor Growth and Elicits Systemic Adaptive Immunity in In Vivo Models, Int J Mol Sci, 21 (2020).

[262] N.M. Munoz, M. Williams, K. Dixon, C. Dupuis, A. McWatters, R. Avritscher, S.Z. Manrique, K. McHugh, R. Murthy, A. Tam, A. Naing, S.P. Patel, D. Leach, J.D. Hartgerink, S. Young, P. Prakash, P. Hwu, R.A. Sheth, Influence of injection technique, drug formulation and tumor microenvironment on intratumoral immunotherapy delivery and efficacy, J Immunother Cancer, 9 (2021).

[263] P.J. van Meer, M. Kooijman, V. Brinks, C.C. Gispen-de Wied, B. Silva-Lima, E.H. Moors, H. Schellekens, Immunogenicity of mAbs in non-human primates during nonclinical safety assessment, MAbs, 5 (2013) 810-816.

[264] V. Brinks, W. Jiskoot, H. Schellekens, Immunogenicity of therapeutic proteins: the use of animal models, Pharm Res, 28 (2011) 2379-2385.

[265] L. Tao, T.A. Reese, Making Mouse Models That Reflect Human Immune Responses, Trends Immunol, 38 (2017) 181-193.

[266] F. Faraji, Z. Karjoo, M.V. Moghaddam, S. Heidari, R.Z. Emameh, R. Falak, Challenges related to the immunogenicity of parenteral recombinant proteins: Underlying mechanisms and new approaches to overcome it, Int Rev Immunol, 37 (2018) 301-315.

[267] R. Dingman, S.V. Balu-Iyer, Immunogenicity of Protein Pharmaceuticals, J Pharm Sci, 108 (2019) 1637-1654.

[268] G. Kijanka, W. Jiskoot, H. Schellekens, V. Brinks, Effect of treatment regimen on the immunogenicity of human interferon Beta in immune tolerant mice, Pharm Res, 30 (2013) 1553-1560.

[269] C.C. Baniel, E.G. Sumiec, J.A. Hank, A.M. Bates, A.K. Erbe, A.A. Pieper, A.G. Hoefges, R.B. Patel, A.L. Rakhmilevich, Z.S. Morris, P.M. Sondel, Intratumoral injection reduces toxicity and antibody-mediated neutralization of immunocytokine in a mouse melanoma model, J Immunother Cancer, 8 (2020).

[270] L.N. Chaudhary, Early stage triple negative breast cancer: Management and future directions, Semin Oncol, 47 (2020) 201-208.

[271] N. Yuan, M. Meng, C. Liu, L. Feng, L. Hou, Q. Ning, G. Xin, L. Pei, S. Gu, X. Li, X. Zhao, Clinical characteristics and prognostic analysis of triple-negative breast cancer patients, Mol Clin Oncol, 2 (2014) 245-251.

[272] E.M. Tacconi, S. Badie, G. De Gregoriis, T. Reislander, X. Lai, M. Porru, C. Folio, J. Moore, A. Kopp, J. Baguna Torres, D. Sneddon, M. Green, S. Dedic, J.W. Lee, A.S. Batra, O.M. Rueda, A. Bruna, C. Leonetti, C. Caldas, B. Cornelissen, L. Brino, A. Ryan, A. Biroccio, M. Tarsounas, Chlorambucil targets BRCA1/2-deficient tumours and counteracts PARP inhibitor resistance, EMBO Mol Med, 11 (2019) e9982.

[273] M. Millard, J.D. Gallagher, B.Z. Olenyuk, N. Neamati, A selective mitochondrial-targeted chlorambucil with remarkable cytotoxicity in breast and pancreatic cancers, J Med Chem, 56 (2013) 9170-9179.

[274] P. Pocasap, N. Weerapreeyakul, J. Timonen, J. Järvinen, J. Leppänen, J. Kärkkäinen, J. Rautio, Tyrosine–chlorambucil conjugates facilitate cellular uptake through L-type amino acid transporter 1 (LAT1) in human breast cancer cell line MCF-7, International Journal of Molecular Sciences, (2020).

[275] A.B. Moshnikova, V.N. Afanasyev, O.V. Proussakova, S. Chernyshov, V. Gogvadze, I.P. Beletsky, Cytotoxic activity of 1-ethyl-3-(3-dimethylaminopropyl)-carbodiimide is underlain by DNA interchain cross-linking, Cell Mol Life Sci, 63 (2006) 229-234.

[276] A.Q. Dean, S. Luo, J.D. Twomey, B. Zhang, Targeting cancer with antibody-drug conjugates: Promises and challenges, MAbs, 13 (2021) 1951427.

[277] A. Aissanou, Annexin A5-methotrexate: a novel targeted theraputic against breast cancer and leukemia, M.S. thesis, The University of Oklahoma Norman, Oklahoma 2020.

[278] M. Abualhasan, N.W. Odeh, G.N. Younis, O.F. Zeidan, Analytical Method Development for Sodium Valproate through Chemical Derivatization, Int J Anal Chem, 2020 (2020) 5672183.

[279] M. Narvekar, H.Y. Xue, J.Y. Eoh, H.L. Wong, Nanocarrier for poorly water-soluble anticancer drugs--barriers of translation and solutions, AAPS PharmSciTech, 15 (2014) 822-833.

[280] M. Terranova-Barberio, S. Thomas, N. Ali, N. Pawlowska, J. Park, G. Krings, M.D. Rosenblum, A. Budillon, P.N. Munster, HDAC inhibition potentiates immunotherapy in triple negative breast cancer, Oncotarget, 8 (2017) 114156-114172.

[281] M. Terranova-Barberio, M.S. Roca, A.I. Zotti, A. Leone, F. Bruzzese, C. Vitagliano, G. Scogliamiglio, D. Russo, G. D'Angelo, R. Franco, A. Budillon, E. Di Gennaro, Valproic acid potentiates the anticancer activity of capecitabine in vitro and in vivo in breast cancer models via induction of thymidine phosphorylase expression, Oncotarget, 7 (2016) 7715-7731.

[282] Z.H. Peng, J. Kopecek, Synthesis and activity of tumor-homing peptide iRGD and histone deacetylase inhibitor valproic acid conjugate, Bioorg Med Chem Lett, 24 (2014) 1928-1933.

[283] K.N. Sugahara, T. Teesalu, P.P. Karmali, V.R. Kotamraju, L. Agemy, D.R. Greenwald, E. Ruoslahti, Coadministration of a tumor-penetrating peptide enhances the efficacy of cancer drugs, Science, 328 (2010) 1031-1035.

[284] D.Y. Fan, Y. Tian, Z.J. Liu, Injectable Hydrogels for Localized Cancer Therapy, Front Chem, 7 (2019) 675.

[285] A. Rotte, Combination of CTLA-4 and PD-1 blockers for treatment of cancer, 2019.

[286] M.G. Catalano, R. Poli, M. Pugliese, N. Fortunati, G. Boccuzzi, Valproic acid enhances tubulin acetylation and apoptotic activity of paclitaxel on anaplastic thyroid cancer cell lines, Endocr Relat Cancer, 14 (2007) 839-845.

[287] S.C. Rockwell, R.F. Kallman, L.F. Fajardo, Characteristics of a serially transplanted mouse mammary tumor and its tissue-culture-adapted derivative, J Natl Cancer Inst, 49 (1972) 735-749.

[288] I. Holen, L. Saleh, P.D. Ottewell, M.A. Lawson, Chapter 4 - In vivo models used in studies of bone metastases, in: D. Heymann (Ed.) Bone Sarcomas and Bone Metastases - From Bench to Bedside (Third Edition), Academic Press2022, pp. 35-53.

[289] B. Schrors, S. Boegel, C. Albrecht, T. Bukur, V. Bukur, C. Holtstrater, C. Ritzel, K. Manninen, A.D. Tadmor, M. Vormehr, U. Sahin, M. Lower, Multi-Omics Characterization of the 4T1 Murine Mammary Gland Tumor Model, Front Oncol, 10 (2020) 1195.

[290] H.D. Soule, T.M. Maloney, S.R. Wolman, W.D. Peterson, Jr., R. Brenz, C.M. McGrath, J. Russo, R.J. Pauley, R.F. Jones, S.C. Brooks, Isolation and characterization of a spontaneously immortalized human breast epithelial cell line, MCF-10, Cancer Res, 50 (1990) 6075-6086.

[291] Y. Qu, B. Han, Y. Yu, W. Yao, S. Bose, B.Y. Karlan, A.E. Giuliano, X. Cui, Evaluation of MCF10A as a Reliable Model for Normal Human Mammary Epithelial Cells, PLoS One, 10 (2015) e0131285.

[292] G. Kremmidiotis, A.F. Leske, T.C. Lavranos, D. Beaumont, J. Gasic, A. Hall, M. O'Callaghan, C.A. Matthews, B. Flynn, BNC105: a novel tubulin polymerization inhibitor that selectively disrupts tumor vasculature and displays single-agent antitumor efficacy, Mol Cancer Ther, 9 (2010) 1562-1573.

[293] B.D. Van Rite, Y.A. Lazrak, M.L. Pagnon, N.R. Palwai, L.F.F. Neves, P.S. McFetridge, R.G. Harrison, Enzyme prodrug therapy designed to target l-methioninase to the tumor vasculature, Cancer Letters, (2011).

Appendix A: Supplementary Data

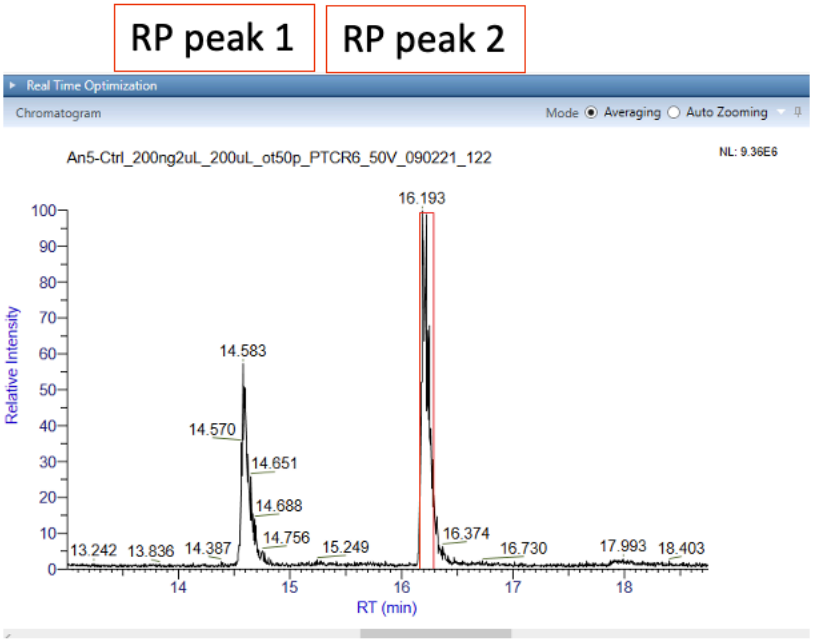

Figure 68: ANXA5 retention time

ANXA5 exists as isobaric isomers. Peak one of ANXA5 eluted after 14.5 minutes. Peak two of ANXA5 eluted after 16.1 minutes. Retention time was obtained on Vanquish Horizon UHPLC system (Thermo Scientific) through a SEC UHPLC column (BEH200 SEC 4.6 x 50 mm, Waters), at a flow rate of 20 µL/min.

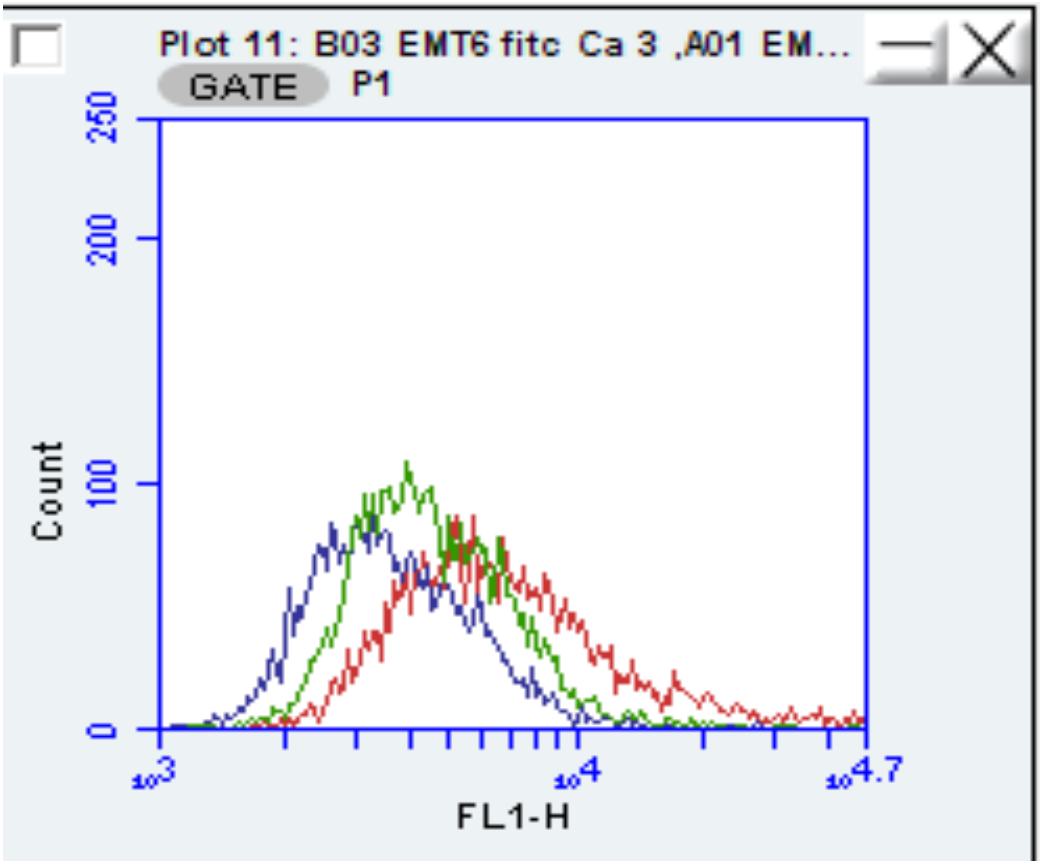

Figure 69: EMT6 ANXA5-FITC histogram curves

Calcium supplemented (red curve) medium increases median fluorescent intensity in FL-1 of ANXA5-FITC binding in comparison to EDTA supplemented (green curve) medium and unstained control cells (blue curve) for EMT6 cells. EDTA supplemented medium (green curve) behaves more like unstained EMT6 cells indicated ANXA5 binding is calcium dependent. Cells were stained with ANXA5-FITC for 15 minutes at room temperature in the dark. Cells were analyzed on a BD Biosciences Accuri C6 flow cytometer, with an excitation at 488 nm and a 533/30 band pass filter, which was used to capture 5,000 gated events per sample. Data was collected and analyzed with BD C6 Accuri software (n = 3).

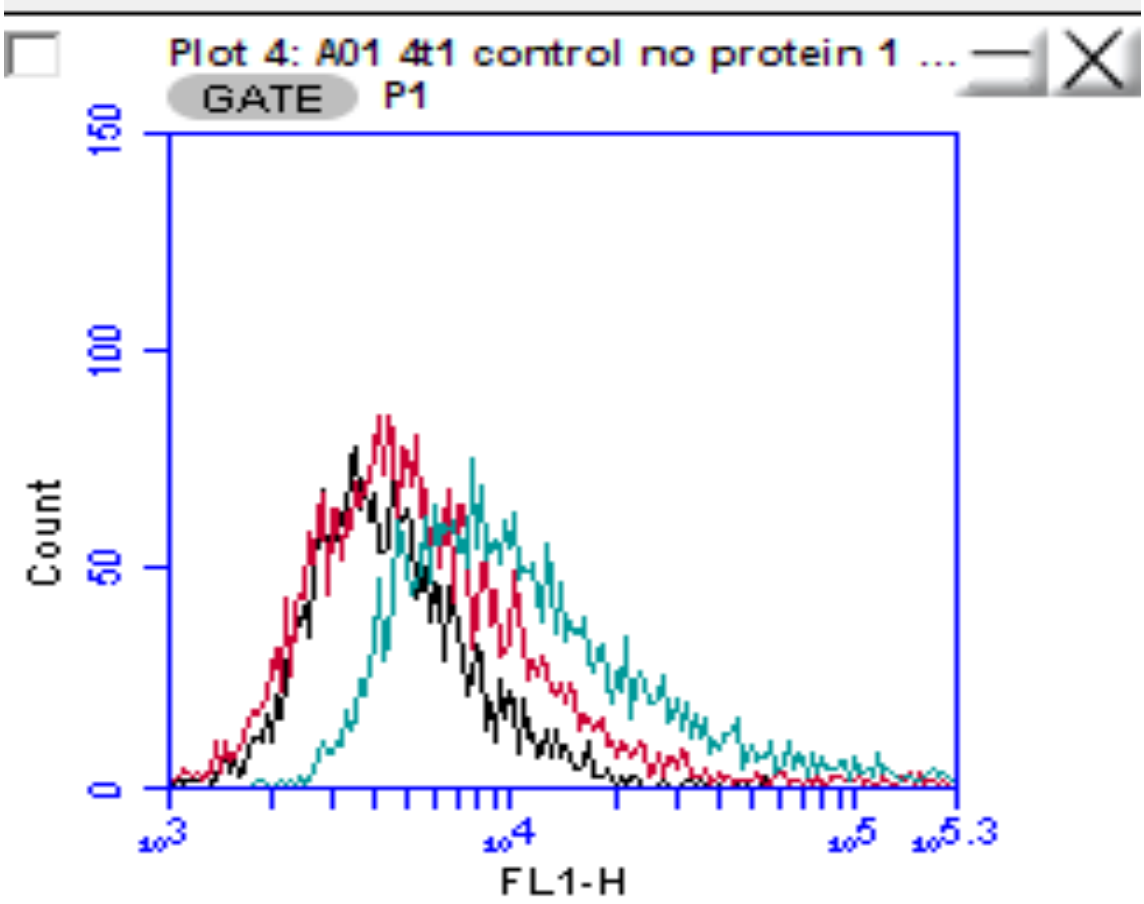

Figure 70: 4T1 ANXA5-FITC histogram curves

Calcium supplemented (teal curve) medium increases median fluorescent intensity in FL-1 of ANXA5-FITC binding in comparison to EDTA supplemented (red curve) medium and unstained control cells (black curve) for 4T1 cells. EDTA supplemented medium (red curve) behaves more like unstained 4T1 cells indicated ANXA5 binding is calcium dependent. Cells were stained with ANXA5-FITC for 15 minutes at room temperature in the dark. Cells were analyzed on a BD Biosciences Accuri C6 flow cytometer, with an excitation at 488 nm and a 533/30 band pass filter, which was used to capture 5,000 gated events per sample. Data was collected and analyzed with BD C6 Accuri software (n = 3).

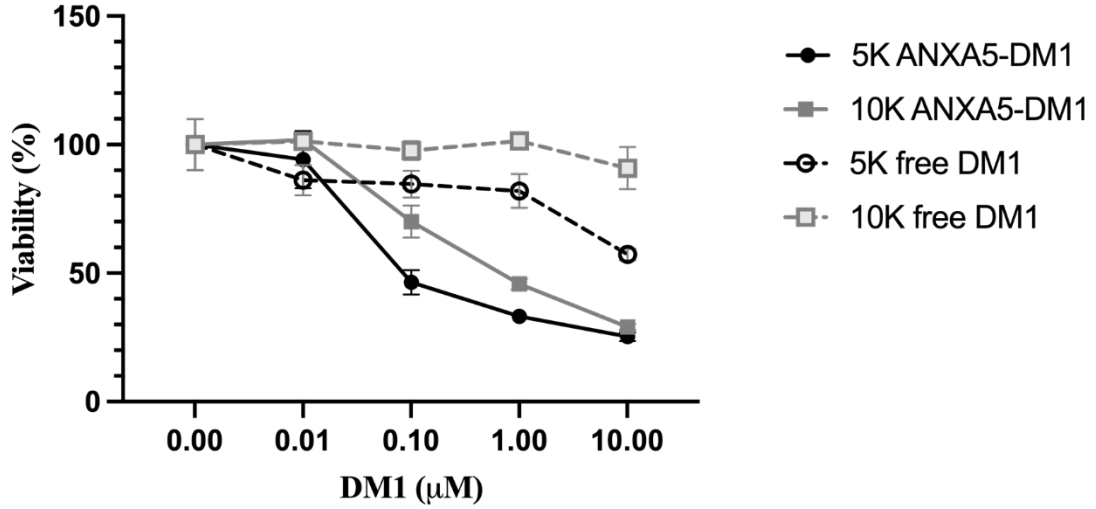

Figure 71: Seeding density effects for ANXA5-DM1 and free DM1 for EMT6 cells

The IC50 for cells seeded with 5k cells per well was 0.033 nM for ANXA5-DM1, and the IC50 for cells seeded at 10k cells per well was 0.15 nM for ANXA5-DM1. The IC50 value for free DM1 could not be obtained. EMT6 cells were seeded at 5k or 10k cells per well and treated with 0-10 nM DM1 in the ANXA5-DM1 or free DM1in fully supplemented growth medium with 2 mM calcium. Cell viability was measured via an Alamar Blue assay, and each sample was represented as a percentage compared to the untreated control (0 nM) after 24 hours. Statistical analysis at each dose was performed with a student's T-test with data represented as mean ± SD (n = 3). Statistical significance is denoted by *($p < 0.033$), **($p < 0.0021$), and *** ($p < 0.0002$).

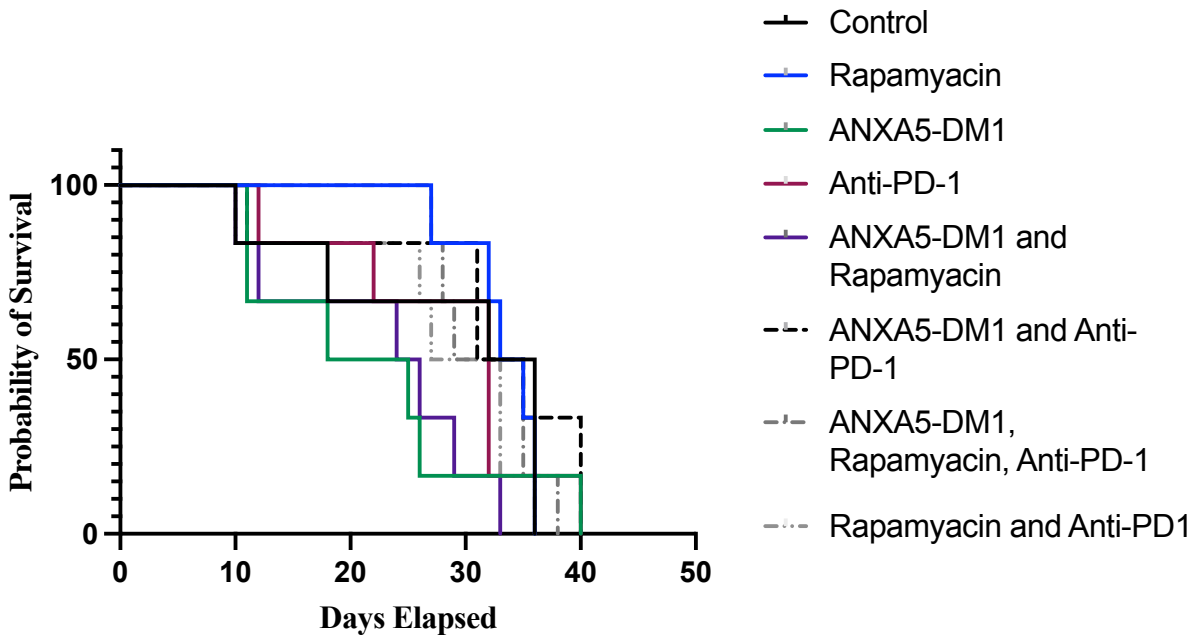

Figure 72: Holistic treatment survival curves for BALB/cJ mice bearing EMT6 tumors

Treatment began on day 7 when mice tumors were 3-5 mm in diameter. Mice were treated with 0.025 mg/kg of DM1 in the ANXA5-DM1 conjugate IP once every 7 days, 5 mg/kg rapamycin IP daily, and/or 5 mg/kg anti-PD-1 IP on days 1, 5, 9 of treatment (n = 6). No statistical significance was found.

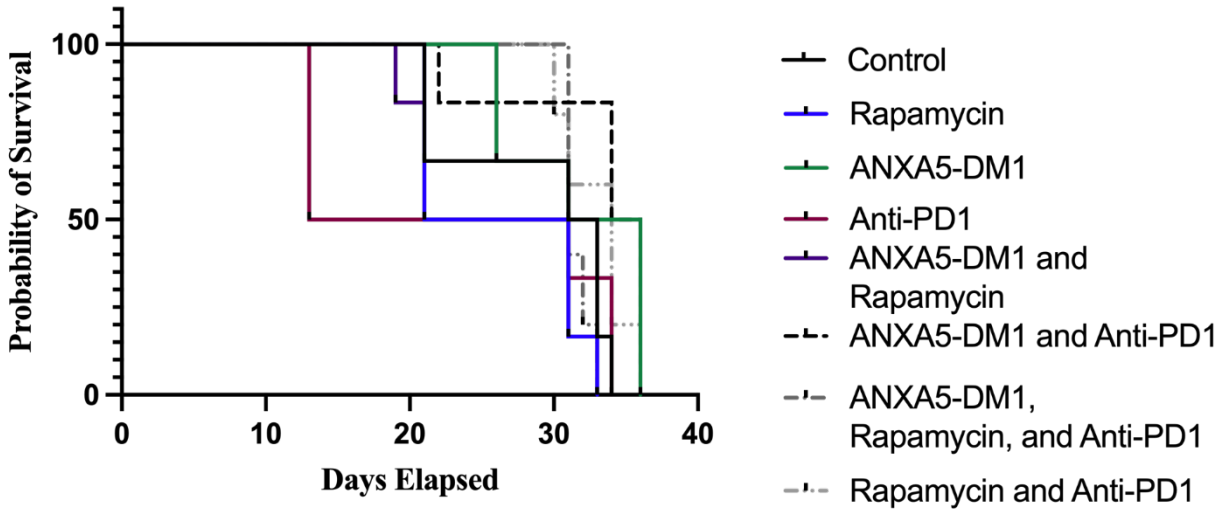

Figure 73: Holistic treatment survival curves for BALB/cJ mice bearing 4T1 tumors

Treatment began on day 7 when mice tumors were 3-5 mm in diameter. Mice were treated with 0.025 mg/kg of DM1 in the ANXA5-DM1 conjugate IP once every 7 days, 5 mg/kg rapamycin IP daily, and/or 5 mg/kg anti-PD-1 IP on days 1, 5, 9 of treatment (n = 6). No statistical significance was found.

Appendix B: Protocols

B1: Protein Production

Protein Expression & Purification of ANXA5

- Day before starting, autoclave the following items:
- 900 ml TB medium
- 100 ml TB buffer
- 4 1 liter Erlenmeyer flask (with aluminum foil on top)
- 125 ml Erlenmeyer flask (with aluminum foil on top)
- 100 ml beaker (with aluminum foil on top)
- All sizes of tips
- 1.5 ml centrifuge tubes (like 100)
- Freezing solution (10 ml glycerol, 10 ml DI H2O)

Day 1:

1. Culture 5 µl of E. coli BL21(DE3) harboring pET303CT with the fusion gene AV in10 ml of Terrific Broth (TB) medium containing 35 mg/ml kanamycin in a 125 ml Erlenmeyer flask overnight at 37 °C with shaking at 200 rpm.

- TB medium: 12 g Tryptone, 24 g yeast extract, 4 ml glycerol, 900 ml DI H2O
- TB buffer: 2.31 g KH_2PO4, 12.54 g K_2HPO4, 100 ml DI H_2O
- Add 35 mg kanamycin to the 1 L of TB medium before taking out the 10 ml for the initial culture.
    - Add after autoclaving
- Incubate overnight.

If expanding:

- Add 20 mL freezing solution to overnight bacterial growth.
- Final glycerol concentration is 25%.
- Aliquot bacterial into cryo-vials at volume preferred.
- Our lab typically does 1 ml increments but if the students need less do that.

Day 2:

2. Add 10 ml of the cell culture to 1 liter of fresh culture medium + kanamycin and incubate at 37 C with shaking (200 rpm). Take 1.5 mL of medium before adding the bacteria, as a blank. This cell culture was grown to mid-log phase => OD600 = 0.5.

- Transfer 10 mL of bacteria to 1 L TB medium.
- Transfer entire volume of medium to four 1 L flasks.
- Put in shaker at 37C at 200 rpm.
- After 1.5 h of shaking, measure optical density at 600 nm (absorbance). When OD600nm = 1.2, then proceed to next step.

Day 2:

3. Add isopropyl β-D-thiogalactopyranoside (IPTG - stored @ -20ºC top shelf) to a final concentration of 0.4 mM (96 mg IPTG total – 24 mg per flask) to solutions in four 1 L flasks and incubate at 25 °C with shaking (180 rpm) for 8 h to induce protein expression.

- Take 750 ml sample of solution before adding IPTG. Label it 'BI.'
- Add 24 mg IPTG to each flask.
- Put back in shaker at 25 °C for 8 hours.

- IPTG stimulates the production of fusion protein. (IPTG activates the promoter in the plasmid that will start the transcription of the gene that follows the promoter =>Annexin A5 gene.)

Day 2:

4. Harvest the cells by centrifugation for 10 min at 1000 x g, at 4ºC.

- Take 750 ml sample before centrifuge. Label sample 'BC.'
- Centrifuge at 1000xg = ~3000 rpm (centrifuge uses rpm – consult table on machine). Only 4 – 50 ml centrifuge tubes at a time, temp 4ºC, 10 mins.
- After first centrifuge, pour out supernatant, add more culture to same 4 tubes. Bacteria will be stuck to side of tubes, so inverting to pour out is not a problem.
- Place the 4 tubes in -20ºC freezer for overnight storage.

Day 3

5. Resuspend the cell pellet in 40 ml of sonication buffer.

- Add ~10 ml to each of the 4 centrifuge tubes.
- Vortex to resuspend cell pellets.
- Pour contents of the 4 tubes back into the 100 ml beaker.
- Sonication Buffer Recipe
  - TPCK - 0.704 mg.
  - PMSF - 6.968 mg.
  - HPLC EtOH - 400 µl.
  - β-mercaptoethanol - 4 µl.
  - sodium phosphate dibasic – 113.6 mg.
  - 40 mL DI H_2O.
  - Dissolve TPCK and PMSF in EtOH
  - Mix remaining ingredients in a beaker

- Correct solution to pH 7.4 – using HCl

6. Lyse the cells by sonication on ice for 30 sec at 5 watts, and then allow it to cool for 30 sec on ice. Repeat this cycle 4 more times.
7. Centrifuge the lysate obtained at 4,000 x g for 2 hours min to remove the cell debris and take the supernatant.

Day 3:

8. Add to lysed cells:

- imidazole - 0.0817 g
- NaCl - 1.168 g

9. Equilibrate a 5 ml HisTrap chromatography column with Wash Buffer 1.

- WASH BUFFER 1 Recipe
  - 500 mL of diH_2O
  - sodium phosphate dibasic - 1.42 g
  - imidazole - 1.362 g
  - 500 mM NaCl - 14.61 g
  - Correct this to pH 7.4.

10. Feed the soluble protein fraction into the column.
11. Remove endotoxin with 350 mL of wash buffer 2

- WASH BUFFER 2 (300 mL)
  - sodium phosphate dibasic - 0.8517 g
  - imidazole - 0.817 g
  - NaCl - 8.766 g

    - Trition X-114 - 3 ml
    - Correct this to pH 7.4.

12. Remove wash buffer 2 with 100 mL of wash buffer 1.
    - Wash buffer 2 interferes with Bradford reagent

13. Elute the protein using elution buffer and collect the elution.
    - ELUTION BUFFER (300 mL)
        - sodium phosphate dibasic - 0.8517 g
        - imidazole - 10.212 g
        - NaCl - 8.766 g
        - Correct this to pH 7.0.

14. Dialyze eluted protein for 3 hours against 2 liters of dialysis buffer.
    - DIALYSIS BUFFER
        - 2 L of diH_2O
        - sodium phosphate dibasic - 5.678 g
        - Adjust to pH 7.4

15. Regenerate the column with 25 mL each of:
    - KCl (14.91 g in 200 mL diH_2O)
    - NaOH (8.0 g in 200 mL of diH_2O)
    - diH_2O
    - HPLC Grade EtOH (1.46 mL EtOH in 23.5 mL diH_2O)

16. Measure the concentration of protein

17. Cleave the C-terminal His-tag
    - Acro Biosystems HRV-3C protease cleavage enzyme, GSt Tag

- Resuspend lyophilized protease in 1 ml of sterile 50% glycerol and DI H_2O (may vary based on lot, check certificate of analysis from company).
-

Day 4

18. Equilibrate the HisTrap column with wash buffer 1.
19. Add imidazole (40 mM) and NaCl (500 mM) to the cleaved protein solution.
20. Feed the solution to theHisTrap column.
    - The protein is in the flowthrough of this stage.
21. Feed wash buffer 1 into column to pull out all cleaved protein before proceeding forward.
22. Elute uncleaved protein with elution buffer.
23. Dialyze purified protein for 3 hours against 2 liters of dialysis buffer.
    - DIALYSIS 2 BUFFER
        - sodium phosphate dibasic - 5.5678 g
        - NaCl - 11.688 g
        - Adjust to pH 7.4.
24. Regenerate the column as in step 15.
25. Sterile filter the protein with a 0.22 uM filter
27. Aliquot purified protein into cryovials and flash freeze in liquid nitrogen and store at -80 °C.
28. Perform Bradford assay for protein concentration, annexin binding, and SDS-PAGE.

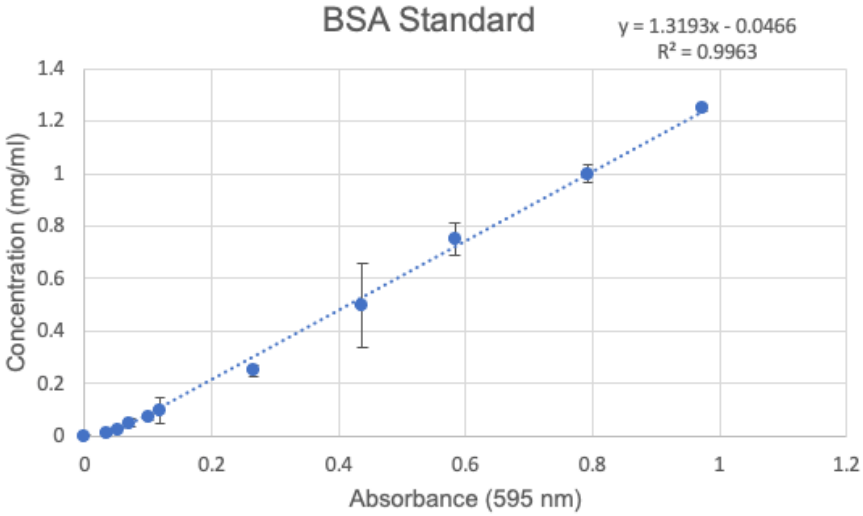

Figure 74: BSA standard for protein quantification

B2: ANXA5-DM1 Conjugation

1. Dissolve 1.2 mg of sulfo-SMCC in 200 ul of DI water.
2. Add dropwise sulfo-SMCC mixture to 1 mg/ml of ANXA5 and react for 1 hour at 4 °C.
3. Dialysis over night with 10 kDa MWCO dialysis tube in 2 liters PBS.
    - 5.678 g sodium phosphate dibasic (20 mM)
    - 11.688 g NaCl(100 mM)
4. Dissolve 1.0 mg DM1 in 150 uL DMSO.
5. Add DM1 solution drop wise to ANXA5-SMCC mixture.
    - Place on orbital shaker for 2 hours in 4 °C.

6. Dialysis for 8 hours with 10 kDa MWC dialysis tube in 2 liters of PBS.
    - 5.678 g sodium phosphate dibasic (20 mM)
    - 11.688 g NaCl(100 mM)
7. Determine protein concentration via Bradford assay.
8. Characterize conjugation via SDS-PAGE.
9. Read absorbance of conjugate at 288 nm and compare to standard curve.
    - To calculate the number of drugs loaded onto one ANXA5
        - Read the absorbance of the conjugate and a protein control (an equal amount of protein as found in the conjugate) at 288 nm.
        - Subtract the absorbance of the ANXA5 control from the ANXA5-DM1 conjugate (ab(ANXA5-DM1) – ab(ANXA5).
        - With the difference use the standard curve to calculate the amount of drug found in the conjugate
        - Solve for molecules of DM1 to molecules of ANXA5 from the mg/ml of DM1 from the standard curve and mg/ml of ANXA5 the Bradford assay.
            - Example calculation: (x mg / ml DM1 / x mg /ml ANXA5) * (1/738.3 mg DM1/ 1 mole DM1) * (36,000 mg ANXA5 / 1 mole ANXA5) = mole DM1/mole ANXA5

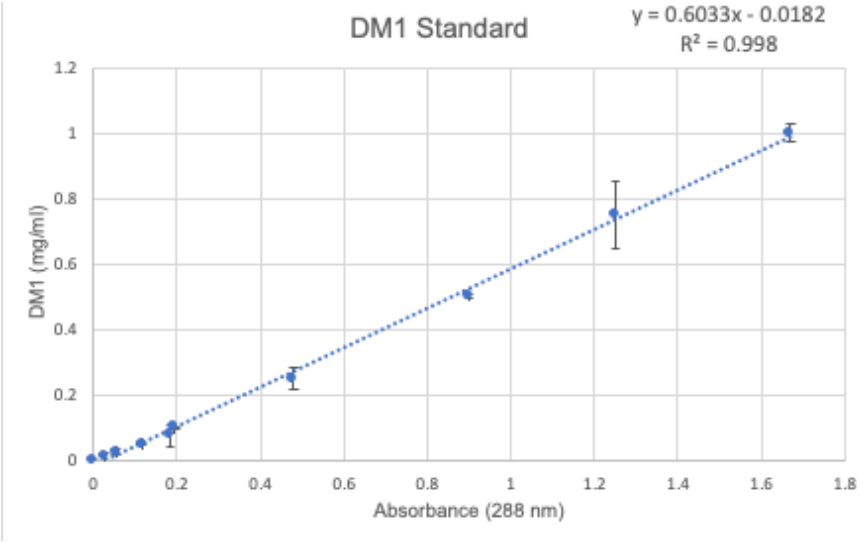

Figure 75: DM1 concentration standard

B3: ANXA5-CMB Conjugation

1) Dissolve 100 µg of chlorambucil in 50 µL of 12 M HCl (Chlorambucil is insoluble at neutral pH, but dissolves readily at pHs below 5. However, chlorambucil is unstable in acidic solutions and should not be stored for long periods of time in acidic solutions.)

2) Dilute the mixture in 1 mL of phosphate buffer. (This provides a larger working volume of chlorambucil to continue downstream production.)

3) Add 10 mg of EDC. (The EDC will bind the carboxylic groups of chlorambucil increasing their chemical reactivity towards primary amines.)

4) Add 7 mg of suflo-NHS. (Sulfo-NHS stabilizes the EDC activated carboxylic groups, increasing the efficiency of the chlorambucil-annexin reaction.)

5) Stir vigorously for 15 minutes.

6) Add 2 µL of β-mercaptoethanol. (β-mercaptoethanol neutralizes the excess EDC and NHS preventing their interference in downstream reactions.)

7) Immediately titrate the solution to a pH of 7.4. (Raising the pH stabilizes the sensitive chlorambucil functional groups.)

8) Add 2.33 mL of a 1 mg/ml solution of annexin in phosphate buffer. (The annexin is kept at a low concentration to prevent precipitation and crosslinking.

The dilute mixture also serves to further neutralize some of the acid from step.)

9) Stir gently for 12 hours,

10) Centrifuge for 10 minutes at 7,000 RCF (Chlorambucil is not stable in neutral pH solutions and will precipitate. The precipitate is easily removed by centrifugation.)

11) Retain the supernatant and discard the pellet.

12) Dialyze the supernatant against 2 L of phosphate buffered saline for 8 hours.

(This step removes the rest of the unbound chlorambucil as well as other upstream contaminants such as β-mercaptoethanol.)

13) Filter the dialysate using a 0.2 μm filter.

14) Immediately flash freeze under liquid nitrogen and store at -80 °C until immediately before use.

B4: ANXA5-VPA Conjugation

1. Dissolve 10 mg of VPA in 1 mL of PBS.

2. Add 132 mg of EDC to the 10 mg/mL VPA-PBS mixture.

3. Incubate at room temperature for 30 minutes on orbital shaker.

4. Add 5 uL of BME to deactivate EDC for 10 minutes on orbital shaker at room temperature.

- Keep BME in fume hood

5. Add 1 ml of 1 mg/ml ANXA5 to VPA mixture.

6. Incubate at room temperature for 2 hours.

7. Dialysis for 8 hours with 10 kDa MWC dialysis tube in 2 liters of PBS. Change dialysis at least once.

- 5.678 g sodium phosphate dibasic (20 mM)
- 11.688 g NaCl(100 mM)

8. Determine protein concentration via Bradford assay.

9. Characterize conjugation via SDS-PAGE.

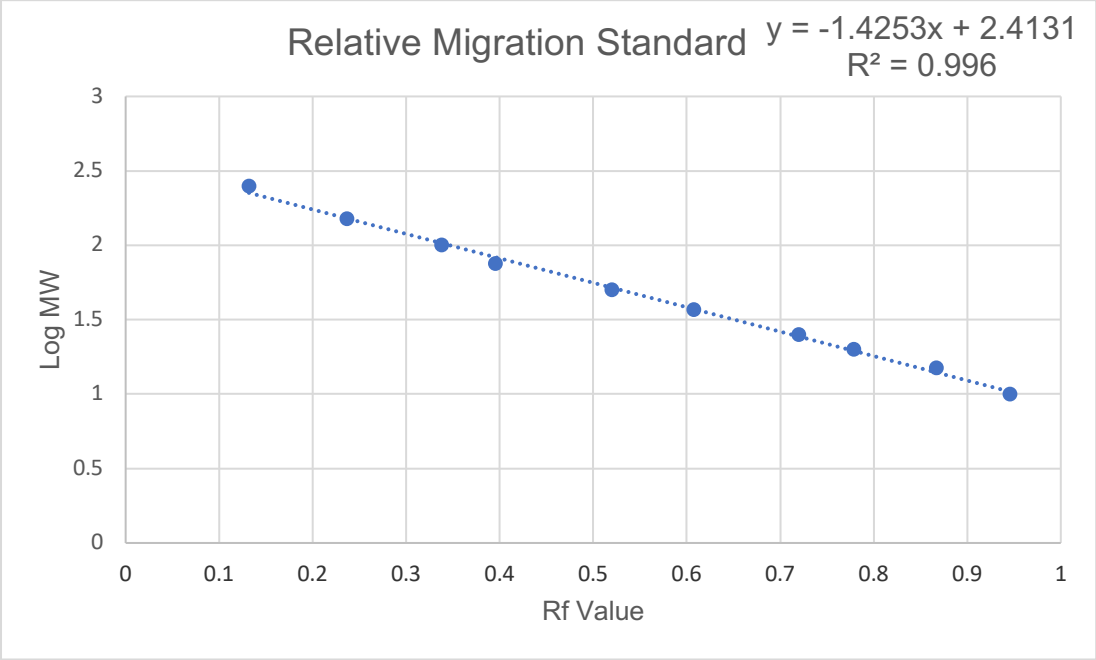

Figure 76: SDS-PAGE relative migration standard

B5: Cell Culture

EMT6

EMT6 cells (ATCC, Manassas, VA, USA) are a murine breast carcinoma that are triple negative for estrogen receptor (ER), progesterone receptor (PR), and human epidermal growth factor receptor 2 (HER2) and derived from hyperplastic alveolar nodule in BALB/c mice [287]. EMT6 provide a syngeneic TNBC breast cancer model and is highly immunogenic. EMT6 cells have high innate expression of MHC-I and high expression of immunostimulatory chemokines making it a valuable model to explore immune profile changes after chemotherapy [243].

4T1

4T1 cells (ATCC, Manassas, VA, USA) are a murine breast carcinoma that are triple negative for ER, PR and HER2 receptors and derived from spontaneous generation in BALB/cfC3H mice [288]. When implanted into BALB/c mice, 4T1 cells provide a syngeneic breast cancer model that mimics stage IV of human breast cancer that spontaneously metastases from the primary tumor to the blood, bone, brain, liver, lungs and lymph nodes [242]. Unlike EMT6 cells, 4T1 is poorly immunogenic, but 4T1 does resemble human TNBC at the transcriptional level, making it a valuable model to explore chemotherapy for TNBC [242, 289].

HUVEC

Human umbilical venule endothelial (HUVEC) cells (ATCC, Manassas, VA, USA) are human primary cells derived from the veins of umbilical cord tissue. HUVECs are one of the most widely cell types used study healthy vasculature.

MCF10A

MCF10A (ATCC, Manassas, VA, USA) is a healthy, breast mammary epithelial cell line originated from a healthy 36-year-old female. The MCF10A cells are non-tumorigenic, immortal, and do not express estrogen receptor on the surface, and is one the most widely used cell line when studying healthy breast epithelium [290, 291].

HAAE-1

Human Abdominal Aorta Endothelial (HAAE-1) cells (Coriell Institute for Medical Research, Camden, NJ; AG09799) are healthy vascular cell line originated from a healthy 20-year-old male. HAAE-1 is an accepted cell line for healthy vasculature endothelium [292]. What makes HAAE-1 cells unique is their ability to mimic healthy or cancerous vasculature based upon confluency. Pervious work in our lab has shown when HAAE-1 cells are grown below 100% confluency, PS expression is externalized mimicking tumor epithelium; however when confluency reaches 100%, PS expression is decreased mimicking healthy vascular epithelium [208, 210, 293].

Table 8: Cell Culture Conditions

Cell Line	Cell Type	Base Media	Supplements	Notes	Freezing Media
4T1	Metastatic Mouse TNBC	RPMI with glutamine	10% FBS and 1 % antibiotic-antimycotic		Complete media with 10% DMSO
EMT6	Mouse TNBC	Waymouths	15% FBS and 1 % antibiotic-antimycotic		Complete media with 10% DMSO

L1210	Mouse Lymphocytic Leukemia	Dulbecco's Modified Eagle's Medium (DMEM)	10% Horse Serum and 1 % antibiotic-antimycotic	Renew media every 2-4 days by adding fresh media	Complete media with 5% DMSO
HUVEC	Human Umbilical Vein Endothelial cells	Vascular Cell Basal Medium	Endothelial Cell Growth Kit-BBE and 1 % antibiotic-antimycotic		Complete media with 10% DMSO
MCF10A	Human Healthy Mammary Gland Epithelial cells	Mammary Epithelial Cell Growth Medium (MEGM)	MEGM Bullet Kit: 1 x Orange Cap Vial with BPE 2.00 mL 1 x Green Cap Vial with hEGF 0.50 mL 1 x Lilac Cap Vial with Insulin 0.50 mL 1 x Natural Cap Vial with Hydrocortisone 0.50 mL 1 x Red Cap Vial with GA-1000 0.50	ATCC does not use the Red GA in MEGM bullet kit. Must use Soybean Trypsin Inhibitor for subculturing. FBS is not in media.	Complete media with 7.5% DMSO

			ml and 100 ng/ml Cholera Toxin and 1 % antibiotic-antimycotic		
HAAE-1	Human Abdominal Aorta Endothelial cells	Ham F12	30 ug/ml endothelial cell growth supplement (15 mg/500 ml media), 17.5 U/ml heparin (8750 U/500 mL or 17.5 mg heparin / 500 ml) , 10% FBS, and 1 % antibiotic-antimycotic	Coat plates and flasks with 0.1% gelatin before seeding	Complete media with 5% DMSO

B6: Biotinylating ANXA5

ROCHE Biotin protein labeling kit (Cat. No. 11 418 165 001)

Contents:

1. **Blocking reagent** (green screw cap) One vial powder; it serves for saturation of the Sephadex G-25 columns to avoid unspecific binding of the `protein to the column material thereby avoiding loss of yield.
2. **Phosphate buffered saline** (PBS) (blue screw cap) One vial, powder; it is used in equilibration of the Sephadex G-25 columns after blocking, for dissolving reagents, diluting of the protein, and for elution of the labeled protein from the column.
3. D**-Biotinoyl--aminocaproic acid-N-hydroxysuccinimide ester** (Biotin-7-NHS) Five reaction vials with 5 mg each, Lyophilizate; biotin-7-NHS reacts with free amino groups of the proteins forming stable amide bonds (molecular weight: 454.5).
4. **Dimethylsulfoxide (DMSO**) (red screw cap) Two vials with 2.5 ml solution each; it serves as solvent for the biotin-7-NHS and if necessary for further dilutions.
5. **Sephadex G-25 columns**. The five columns serve for separation of non reacted biotin-7-NHS. The columns are preswollen. The volume of the column is 9.1 ml, the filling height is 5 cm. The maximal sample volume is 2.5 ml. The columns are fitted with a stopper on the top and with a cap on the bottom. Before use the column's outlet has to be opened with a scissor.

Solution Preparations:

1. **Blocking solution:** Dissolve the contents of the bottle blocking reagent (green screw cap) in 300 ml DI H_2O.

2**. PBS solution:** Dissolve the contents of the bottle PBS (blue screw cap) in 1 I redist. water.

3. **Biotin-7-NHS solution**: The solution should be freshly prepared before labeling. Add to the contents of the reaction vial which includes biotin-7-NHS 250 ul DMSO and vortex the solution several times.

- The resulting concentration of the biotin-7-NHS solution is 20 mg/ml.
- For the labeling mix the volume of the biotin-7-NHS solution should not exceed 5% of the total reaction volume (e.g. add maximal 50 l biotin-7-NHS solution to 1 ml protein solution).

Column Preparation:

- Not more than 10 mg protein (in a maximum of 2.5 ml) should be purified by each column.
- Care should be taken that the volume of the labeling mix does not exceed 2.5 ml since correct separation in the column cannot be guaranteed.
- Fix the column with a clamp at a stand (if clamps and stand or adequate equipment is not available, the column can also be held in a hand) and place an at least 100 ml containing beaker under the column.
- Open outlet of the column with scissors, remove the cap from the top of the column, and let the content flow out. Add 5 ml blocking solution to the column and let run through. Rinse the column afterwards with 30 ml PBS solution in total (6 × 5 ml) and let it flow through.
    - The column should not run dry! The Sephadex G-25 column is now ready to use. If the column is not immediately used, fix the stopper on the top and the cap at the bottom and store the column at +2 to +8°C.

Biotin Calculations (from online protocol):

- Protein of ~40,000 Da
    - 1 mg protein /1 mL PBS
    - Stock biotin solution: 20 mg/ml in DMSO
    - Molar Ratio of 10 molecules of biotin to 1 molecule of protein (~40,000 Da)
        - 0.114 mg biotin/1 mg of protein ➔5.7 uL biotin to 1 ml RXN
            - 20 mg/ml biotin (X ml) = 0.114 mg biotin/ 1 ml RXN (1 ml RXN)
                - X = 5.7 uL stock biotin to RXN
    - Molar Ratio of 20 molecules of biotin to 1 molecule of protein (~40,000 Da)
        - 0.227 mg of biotin/1 mg of protein ➔11.35 uL biotin to 1 ml RNX
            - 20 mg/ml biotin (X ml) = 0.227 mg biotin / 1 ml RXN * (1 ml RXN)
                - X =11.35 uL stock biotin to RXN

- Incubate at 15-25 °C for 2 hours gentle stirring.

B7: Quantify Biotin on Protein

Pierce Biotin Quantification Kit (28005)

Kit Contents:

- HABA/avidin premix, no-weigh format
- Biotinylated horseradish peroxidase (40 kDa) 5 mg

Important Product Information

• Following any biotin-labeling reaction, the biotinylated protein sample to be assayed must be dialyzed or desalted to remove nonreacted and hydrolyzed biotinylation reagent.

• Samples must be in one of the recommended buffers (PBS or TBS, see Reagent Preparation Section) for the assay. Avoid buffers containing potassium (such as Modified Dulbecco's PBS), which will cause precipitation in the assay. Other buffers may interfere and should not be used unless first validated by comparison to results using PBS or TBS.

• Slight color variation between the HABA/avidin premix microtubes does not affect product performance.

Reagent Preparations:

Procedure for quantitation of moles of biotin per mole of protein – Microplate Format Note: The Biotinylated HRP may be used as a positive control to verify assay performance. See the product label for the biotinylation level.

1 mg/ml

1. Equilibrate the HABA/avidin premix to room temperature.

2. Add 100µL of ultrapure water to one microtube of the HABA/avidin premix. Mix with pipette tip.

3. Pipette 160µL of PBS into a microplate well.

4. Add 20 µL of the HABA/avidin premix solution from step 2 to the PBS in the well. Place microplate on an orbital shaker or equivalent to mix.

5. Measure the absorbance of the solution in the well at 500 nm and record the value as A500 HABA/avidin.

6. Add 20 µL of biotinylated sample or biotinylated HRP (positive control) to the well containing the HABA/avidin reaction mixture. Mix as described above.

7. Measure the absorbance of the solution in the well at 500nm and record the value as A500 HABA/avidin/biotin sample once the value remains constant for at least 15 seconds.

8. Proceed to the calculation of moles of biotin per mole of protein at https://www.thermofisher.com/us/en/home/life-science/protein-biology/protein-labeling-crosslinking/biotinylation/biotin-quantitation-kits/haba-calculator.htm

B8: Colorimetric Adherent Cell Binding Strength

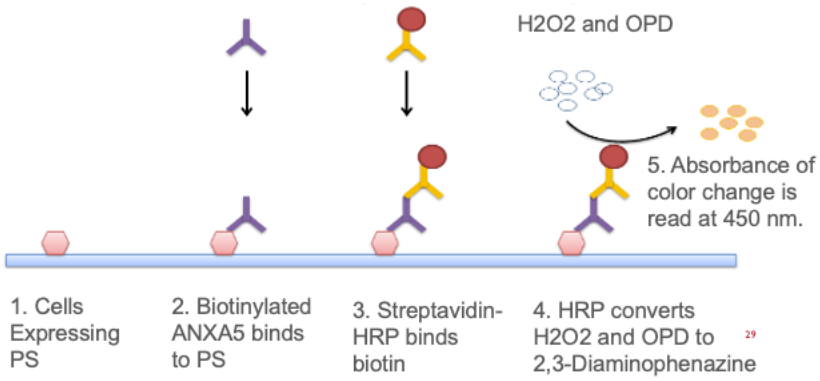

Figure 77: Colorimetric binding strength protocol

Image adapted from: https://www.sinobiological.com/category/indirect-elisa

Materials:

- 0.25% Glutaraldehyde (GA)
    - Take 100 ul of 25% GA and put into 9.90 ml of PBS
- 50 mM NH_4Cl
    - 40.1175 mg NH_4Cl into 15 ml of PBS
- 0.5% BSA
    - 2.5 g BSA into 500 ml PBS
- 2 mM CaCl2
    - Make 0.01 g/ml $CaCl_2$ stock in DI H_2O.
    - Add 1.47 ml of $CaCl_2$ stock to 50 ml of 0.5% BSA PBS.
    - Add protein dilutions to Ca supplemented PBS for specific binding.
- 5 mM EDTA
    - Dissolve 73.06 mg EDTA into 50 ml 0.5% BSA PBS.
        - May have to raise pH to around 8 to get EDTA to dissolve.
    - Add protein dilutions to EDTA supplemented media for non-specific binding.

1. Grow cancerous or healthy cells in respective media in T-75 flasks u until they reach 80-85% confluence.
    - *4T1 TNBC*: RMPI 1640 with glutamate, 10% FBS and 1% anti-anti
    - *EMT6 TNBC:* Waymouths, 10% FBS and 1 % anti-anti
    - *L1210 leukemia:* DMEM, 10% horse serum and 1% anti-anti
    - *MCF10A healthy breast epithelial:* MEGM with MEGM bullet kit 1 x orange cap vial with BPE 2.00 mL, 1 x green cap vial with hEGF 0.50 mL, 1 x lilac cap vial with

Insulin 0.50 mL, 1 x natural cap vial with Hydrocortisone 0.50 mL (omitting red cap according to ATCC recommendation) 0.50 ml and 100 ng/ml Cholera Toxin and 1% anti-anti

- *HUVEC,* vascular cells basal medium, endothelial cell growth kit-BBE and 1% anti-anti

2. Transfer 50,000 cells/well to two 24-well plates.
3. (OPTIONAL FOR HEALTHY CELLS) Expose phosphatidylserine (PS) on surface of endothelial cells by adding 1 mM H_2O_2 for one hour with 100 uL complete media.
    - Add 2 uL of 30% H_2O_2 to 20 ml of complete cell media.
4. Fix the cells in all 48 wells by adding 100 µl/well PBS buffer containing 0.25% glutaraldehyde. Remove before proceeding.
5. Quench excess aldehyde groups by incubating with 100 µl/well of 50 mM NH_4Cl, diluted in PBS buffer, for 5 min. Remove after incubation period.
6. For cancer cells, perform a 1 hr pre-treatment with 300 ul 0.5% BSA diluted in PBS at 37 °C.
7. Dilute biotinylated ANXA5 in 0.5% BSA diluted in PBS buffer, with concentrations of 20 nM, 12 nM, 8 nM, 4 nM, 2 nM, 0.5 nM, and 0.05 nM. Add 300 µl to wells in Sets 1 and 2, using triplicates of each concentration. The blank for each set will receive no FP.

    1. Set 2 (21 wells) gets PBS + BSA + 2 mM Ca + ANXA5
    2. Blank (3 wells) gets PBS + BSA + 2 mM Ca
    3. Set 1 (21 wells) gets PBS + BSA + 5 mM EDTA + ANXA5
    4. Blank (3 wells) gets PBS + BSA + 5 mM EDTA

8. Incubate for 2 hours at 37 °C, 5% CO_2.
9. Wash 4 times with 300 µl of 0.5% BSA diluted in PBS buffer.
10. Add 300 µl of Streptavidin-HRP (2 µg/ml) and incubate for 1 hour at room temperature. (Streptavidin-HRP is in 4 °C glass fridge)
11. Wash 4 times with 300 µl of PBS buffer.
12. Add 300 µl of the chromogenic substrate O-phenylenediamine (OPD) to each well. (OPD is in 4 C). The OPD solution is made with phosphate citrate buffer (1 capsule in 100 ml DI water). Prior to use, add 40 µl of 30% H_2O_2. Weigh out the desired amount of OPD with a concentration of 0.4 mg/ml.
    - HRP reacts with H_2O_2 to induce yellow color change.
13. Incubate for 30 minutes at room temperature and in the dark to minimize OPD color change.
14. Transfer 100 µl of the supernatant to 96-well plates.
15. Measure absorbance at 450 nm.

B9: Flow Cytometry ANXA5-FITC Binding

Abcam Annexin V-Fitc Apoptosis staining / detection kit (ab14085)

ANXA5-FITC concentration is 50 ug/ml

1. Grow cancerous or healthy cells in respective media in T-75 flasks u until they reach 80-85% confluence.

    - *4T1 TNBC*: RMPI 1640 with glutamate, 10% FBS and 1% antibiotic-antimycotic

- *EMT6 TNBC:* Waymouths, 10% FBS and 1 % antibiotic-antimycotic
- *MCF10A healthy breast epithelial:* MEGM with MEGM bullet kit 1 x orange cap vial with BPE 2.00 mL, 1 x green cap vial with hEGF 0.50 mL, 1 x lilac cap vial with insulin 0.50 mL, 1 x natural cap vial with hydrocortisone 0.50 mL (omitting red cap according to ATCC recommendation) 0.50 ml and 100 ng/ml cholera toxin and 1% antibiotic-antimycotic

2. Transfer 50,000 cells/well to two 24-well plates. Let cells incubate for 24 hours at 37 °C and 5% CO_2.

- For confluency effects: have a plate for confluent and nonconfluent cells
- For calcium binding effects: have a plates for calcium supplemented and EDTA supplemented plates

3. Add 100 uL of trypsin to each well and let set until 90% cells are detached from the plate (~ 2 minutes).

4. Add 300 uL of fresh media and add to microcentrifuge tube and centrifuge at 500 x g for 5 minutes.

5. Count cells and resuspend at 1-5 x 10^5 cells in 500 uL binding buffer supplied in the kit

- For calcium dependence: Add 5 mM of EDTA to binding buffer for resuspending cells.

6. Add 5 uL of ANXA5-FITC to each tube and incubate in the dark for 15 minutes.

7. Analyze cells using the BD Biosciences Accuri C6.

- FL 1: excitation at 488 and a 533/30 band pass filter.
- Gate on at least 5,000 events.

B10: Plate Reader ANXA5-FITC Binding

1. Grow cancerous or healthy cells in respective media in T-75 flasks u until they reach 80-85% confluence.

- *4T1 TNBC*: RMPI 1640 with glutamate, 10% FBS and 1% anti-anti
- *EMT6 TNBC:* waymouths, 10% FBS and 1 % anti-anti
- *MCF10A healthy breast epithelial:* MEGM with MEGM bullet kit 1 x orange cap vial with BPE 2.00 mL, 1 x green cap vial with hEGF 0.50 mL, 1 x lilac cap vial with insulin 0.50 mL, 1 x natural cap vial with hydrocortisone 0.50 mL (omitting red cap according to ATCC recommendation) 0.50 ml and 100 ng/ml cholera toxin and 1% antibiotic-antimycotic

2. Add 2 mL of trypsin to each T75 flask, and incubate until 90% of the cells become detached (~5-10 minutes).

3. Count cells 2 mL of fresh media and add to 15 mL tube and centrifuge at 500 x g for 5 minutes.

4. Count cells to have 500,000 cells/0.1 mL binding buffer (supplied by the kit).

- When cells are resuspended, transfer 0.1 mL of cells in binding buffer to microcentrifuge tube.

5. Add 1 uL of ANXA5-FITC to each tube and incubate in the dark for 5 minutes at room temperature.

6. Wash cells at 500 x g for 5 minutes to remove unbound ANXA5-FITC.

7. Resuspend cells in 100 uL of binding buffer.

8. Transfer 100 uL of ANXA5-FITC cell mixture to a black 96 well plate.

9. Read cells on plate reader

- Fluorescent ex/em: 486/528 nM
- Sensitivity 100

B11: ANXA5 Conjugate Cytotoxicity

1. After treatment ends, remove cells from incubator and place in sterile laminar flow hood.
2. To each well, add complete media supplemented with 10% Alamar Blue dye.
    a. Add 1000 uL of Alamar Blue dye to 9 mL complete media.
        i. For 24 well plates: each well gets 300 uL
        ii. For 96 well plates: each well gets 100 uL
    b. Incubate Alamar Blue and media without cells for negative control.
3. Place plates into incubator (37 C, 5% CO2) for 2-4 hours.
    a. Depends on cell type
    b. Do not let pink color saturate control wells.
4. Measure samples on microtiter plate reader though fluorescence (excitation: 560 nm, emission: 590 nm).
    a. Example calculation: (fluorescence of treated control/fluorescence of untreated control) * 100%

B12: ATP Release

Molecular Probes ATP determination kit

Kit Contents

- D-Luciferin (Component A, MW 302, blue cap), 5 vials, each containing 3 mg of lyophilized powder
- Luciferase, firefly recombinant (Component B, red cap) 40 µL of a 5 mg/mL solution in 25 mM Tris-acetate, pH 7.8, 0.2 M ammonium sulfate, 15% (v/v) glycerol and 30% (v/v) ethylene glycol
- Dithiothreitol (DTT) (Component C, MW 154, black cap) 25 mg
- Adenosine 5′-triphosphate (ATP) (Component D, green cap), 400 µL of a 5 mM solution in TE buffer
- 20X reaction buffer (Component E) 10 mL of 500 mM Tricine buffer, pH 7.8, 100 mM $MgSO_4$, 2 mM EDTA and 2 mM sodium azide
-
    - The ATP Determination Kit provides sufficient reagents to perform 200 ATP assays using 500 µL sample volumes or 1000 ATP assays using 100 µL sample volumes. The contents of this kit are sufficient to make at least 100 mL of a standard reaction solution (see step 2.1 below) containing 0.5 mM D-luciferin, 1.25 µg/mL firefly luciferase, 25 mM Tricine buffer, pH 7.8, 5 mM $MgSO_4$, 100 µM EDTA and 1 mM DTT

Storage and handling upon receipt: this kit should be stored at ≤–20°C, protected from light. For long term storage and infrequent use, store the firefly luciferase frozen at –80°C. Avoid repeated freezing (at –80°C) and thawing. When properly stored, these reagents are stable for six months to one year.

The following protocol has been developed as a generalized procedure suitable for many experimental applications. Optimal reaction conditions for specific experimental circumstances may be determined empirically by adjusting the amounts of D-luciferin and firefly luciferase added to the reaction. In the protocol below, a 10 mL "standard reaction solution" is prepared. This volume of standard reaction solution is sufficient for about twenty of 500 µL reactions or about one hundred of 100 µL reactions, depending upon luminometer requirements. For fewer or more assays, modify the protocol accordingly.

Special Precautions: Because of the high sensitivity of the luciferin–luciferase reaction, avoid contamination with ATP from exogenous biological sources, such as bacteria or fingerprints.

- Protect the D-luciferin and firefly luciferase reagents from light as much as possible.
- Mix solutions containing firefly luciferase gently, for example, by inversion; vortex mixing may denature the enzyme.
- Arsenate compounds may inhibit the reaction.
- The optimum temperature for the reaction is 28°C. At higher temperatures, the reaction is slower.
- Reagent Preparation

1.1 Make 1.0 mL of 1X reaction buffer by adding 50 µL of 20X reaction buffer (Component E) to 950 µL of deionized water (dH2 O). This volume will be sufficient to make 1 mL of 10 mM D-luciferin stock solution.

1.2 Make 1 mL of a 10 mM D-luciferin stock solution by adding 1 mL of 1X reaction buffer (prepared in step 1.1) to one vial of D-luciferin (Component A, blue cap). Protect from light until use. The D-luciferin stock solution is reasonably stable for several weeks if stored at ≤–20°C, protected from light.

1.3 Prepare a 100 mM DTT stock solution by adding 1.62 mL of di H_2O to the bottle containing 25 mg of DTT (Component C, black cap). Aliquot into ten 160 µL volumes and store frozen at ≤–20°C. Stock solutions of DTT stored properly are stable for six months to one year. Thawed aliquots should be kept on ice or at 4°C until ready for use.

1.4 Prepare low-concentration ATP standard solutions by diluting the 5 mM ATP solution (Component D, green cap) in di H_2O. The concentrations and volumes to make depend upon the sensitivity and design of the luminometer to be used. Typically, ATP concentrations ranging from 1 nM to 1 µM are appropriate. These dilute solutions are stable for several weeks when stored at ≤ –20 °C.

Standard Reaction Solution

2.1 We suggest combining the components of the reaction as follows to make 10 mL of a standard reaction solution. Adjust the volumes according to requirements.

- 8.9 mL dH2 O • 0.5 mL 20X reaction buffer (Component E)
- 0.1 mL 0.1 M DTT (from step 1.3)
- 0.5 mL of 10 mM D-luciferin (from step 1.2, store the remaining 0.5 mL at ≤–20°C for up to several weeks)

- 2.5 µL of firefly luciferase 5 mg/mL stock solution
- Add 10% of fresh cell media (without it the blank with read higher than the samples)

2.2 Gently invert the tube to mix, do not vortex; the firefly luciferase enzyme is easily denatured. Keep the reaction solution protected from light until use. Although the solution may be stored at 2–6°C protected from light for several days, assay sensitivity will diminish with time

Standard Curve

3.1 Place an appropriate volume of the standard reaction solution (prepared in steps 2.1 and 2.2) in the luminometer and measure the background luminescence.

3.2 Start the reaction by adding the desired amount of dilute ATP standard solution (prepared in step 1.4) and read the luminescence. The volume of the dilute ATP standard solution that is added to the standard assay solution (prepared in step 2.1) should be no more than 10% of the total assay volume. For example, a 100 µL total assay volume should contain 10 µL or less of the ATP standard solution.

3.3 Subtract the background luminescence. 3.4 Generate a standard curve for a series of ATP concentrations. Be sure to always add a constant sample volume of the ATP containing solution.

Sample Analysis

4.1 Follow the directions given in Standard Curve, substituting ATP-containing samples for the ATP standard solutions. Please note that the total volume of the experimental sample assays should be equal to that of the ATP standard assays, with the amount of sample added amounting to no more than 10% of the total assay volume.

4.2 Calculate the amount of ATP in the experimental samples from the standard curve.

SPEICAL NOTE: If the absorbance readings of treated samples are below the absorbance in the standard curve, remake the reaction solution with 10% of cell media to have same background absorbance.

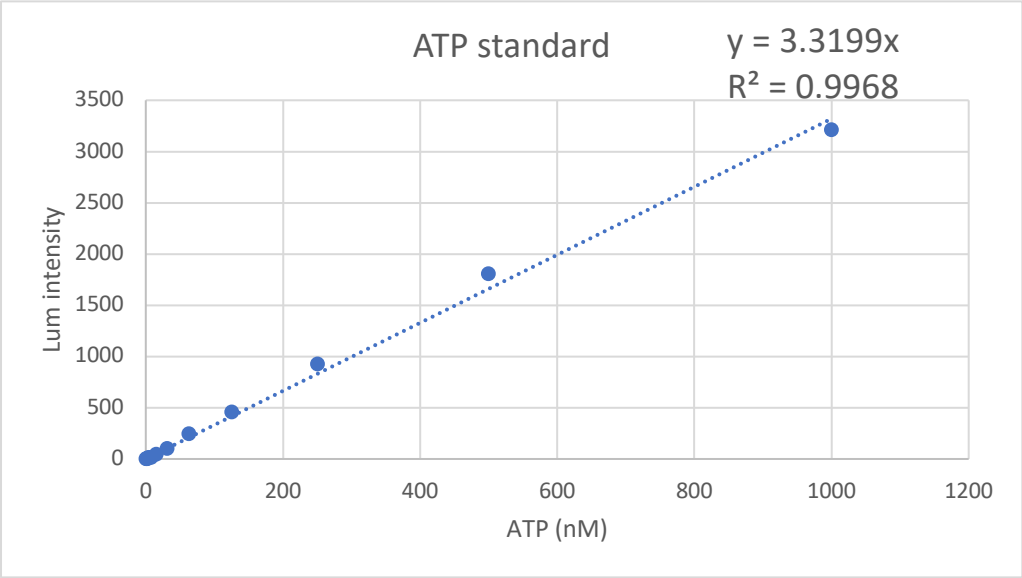

Figure 78: ATP standard

B13: Calretinin Surface Expression

1. Plate EMT6 or 4T1 cells at 25,000 cells/well in 24 well plates.

2. After 24 hours, treat cells with 10 nM of DM1 in the ANXA5-DM1 conjugate or free DM1 in fully supplemented media supplemented with 2 mM CaCl2 for 24 hours (300 uL).

3. Collect media of cells to collect dead cells and place in microcentrifuge tubes.

4. Wash cells with PBS and add 100 µL of trypsin to each well for 1-2 minutes.

5. Quench trypsin with 100 µL and add to microcentrifuge tube with dead cell media.

6. Configure at 500 x g for 5 minutes and count cells.

- 100,000 cells per sample
- Combine 3 wells into one to have enough cells.

7. Resuspend cells in 4% PFA to fix cells at 4 °C for 20 minutes.

8. Wash cells 2 times with 500 µl of 0.5% BSA-PBS at 500 x g for 5 minutes.

9. Resuspend cells in 100 µl of 0.5% BSA-PBS solution and add 1 µl of CD16/CD32 Fc Block (eBioscience, San Diego, CA, USA) to each sample and incubate for 20 minutes 4 °C.

10. Add 1 µl of FITC labeled calreticulin (Novus Biologicals, Centennial, CO, USA) and incubate for 30 minutes in the dark at 4 °C.

11. Analyze cells on BD Biosciences Accuri C6 (Franklin Lakes, New Jersey, USA), with excitation at 488 nm and a 533/30 band pass filter, capture 10,000 gated events per sample. Collect the data and analyze with BD C6 Accuri software. To have enough cells, one sample has three wells, and each sample is analyzed 3 times. All experiments are conducted in triplicate.

B14: Tumor Inoculations

If using Matrigel, take Matrigel out of – 20 °C freezer 24 hours before tumor inoculations. Place Matrigel in 4 °C to thaw overnight. Matrigel hardens and is unusable at room temperature.

1. Culture cells in respective cell media.
2. Once cells reach 75% confluence, discard culture medium.
3. Wash cells with 5 ml of fresh PBS 1 times.

4. Add 2 ml of .25% trypsin/ mM EDTA solution. Let sit for 5 minutes or until all cells have been lifted from the plate.
5. Add 6 ml of fresh RMPI media and transfer to 15 ml conical tube.
6. Centrifuge cells at 1100 X G for 5 minutes at room temperature.
7. Count cells with hemocytometer.
8. Wash cells with ice cold PBS in the centrifuge at 1100 X G for 5 minutes.
    a. Remove any media from the cells so there is not an immune reaction.
9. Discard supernatant and resuspend cells so that in 50 uL of 50% PBS and 50% Matrigel (if not using Matrigel, only use PBS).
    a. 50,000 cells in 50 uL needed per mice.
    b. Keep cells on ice (Matrigel hardens at room temp).
    c. Estimated calculation: 50,000 cells /(50 ul) = 2,000,000 cell /(X uL)

       X = 2000 uL or 2 mL
10. Load cells into 1 ml syringe without needle to prevent shearing.
    a. Remove air bubbles.
11. Add 30-gauge needle.
12. Secure a 6-week-old female BALB/c mouse with one hand by grasping behind the ears using the index finger and thumb. Stretch the mouse body across the hand to expose the abdomen. Secure the tail against the hand using the last two digits of the same hand that secures the neck.

13. Inoculate the mouse tumor cells subcutaneously (s.c.) in the 4th mammary fat pad by gently penetrating the skin, with the bevel of the needle facing up, and depressing the syringe to the appropriate volume

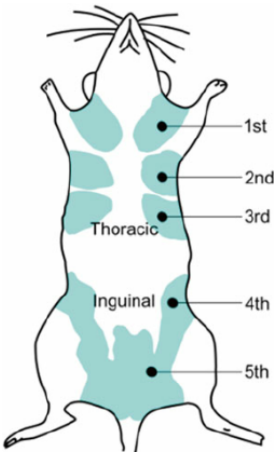

Figure 79: Mouse mammary fat pads

B15: Blood Collection

Day before collection autoclave microcentrifuge tubes (least 1 per mouse) and surgery equipment (forceps, scissors ect.).

1. Euthanize mice.
    a. Put mice under 2% isoflurane.
    b. Bilateral thoracotomy.
2. Collect blood
    a. Puncture heart with 30 gauge needed on 3 ml syringe to aspirate blood. If needed, use pipet to collect blood in the abdominal cavity.
3. Allow blood to clot at room temperature for 15-20 minutes.
4. Centrifuge blood at 15,000 x g for 20 minutes.
    a. Keep supernatant.

B15: ANXA5 Protein Specific Antibody Titers

Sandwich ELISA

1. Add 100 µl of 20 ug/ml of ANXA5 in 0.1 M carbonate coating buffer and incubate overnight at 4 °C with plate cover.

- Carbonate coating buffer
  - 0.08 g Na_2CO_3
  - 0.15 g $NaHCO_3$
  - 25 mL DI H_2O
  - Adjust pH to 9.6.

2. Wash plate 2 times with 200 µl PBS.

3. Block for 2 hours at room temperature with 200 µl of blocking buffer.

- Blocking buffer
  - PBS
  - 10% FBS
  - Adjust pH to 7.4.

4. Wash plate 2 times with 200 µl PBS.

5. Add 100 µl of plasma dilution samples and incubate overnight at 4 °C.

- Serum dilutions range from 1:10-1:10,000,000

6. Wash plate 4 times with 200 µl PBS.

7. Add 100 µl of diluted rabbit anti-mouse IgG IgM conjugated to HRP and incubate at room temp for 1 hour.

- HPR conjugated rabbit anti-mouse IgG IgM (Jackson Immuno 315-035-044).
- Reconstitute antibody with 1.5 mL DI H_2O.
    - Centrifuge if not clear.
- Dilute to 1:25,000 for assay (2 µl into 50 ml PBS).

8. Wash plate 4 times with 200 µl PBS.

9. Add 100 µl of OPD H2O2 solution (make within 5 minutes of use).

- Add one capsule of phosphate-citrate tablet to 100 mL DI in beaker and stir.
    - Make no more than 30 minutes before OPD use.
- Weigh 0.4 mg/ml OPD and place in foil coated tube.
    - 6.4 mg for 16 mL phosphate citrate buffer
- Add 40 µl for 30% H2O2 to 16 mL of OPD solution.
    - Mix for 30 seconds.

10. Transfer 100 µl of supernatant to 96-well plate.

11. Measure absorbance at 450 nm on plate reader.